Ollscoil Chathair Bhaile Átha Cliath

Dublin City University

Novel Heterocyclic Functionalised Ferrocenyl Derivatives as Potential Anti-Cancer Agents

Karen Guadalupe Ontiveros Castillo, M.Sc.

PhD thesis

Assoc. Prof. Andrew Kellett **Assoc. Prof. Kieran Nolan**

School of Chemical Sciences

Faculty of Science and Health

Dublin City University

Ireland

September 2019

Dedicated to my family,

and to people touched by cancer.

“We won’t stop until cancer does!”

DECLARATION

I hereby certify that this material, which I now submit for assessment on the programme of study leading to the award of Ph.D. is entirely my own work, that I have exercised reasonable care to ensure that the work is original, and does not to the best of my knowledge breach any law of copyright, and has not been taken from the work of others save and to the extent that such work has been cited and acknowledged within the text of my work.

Signed: _____ ID No. 14212132

Karen Guadalupe Ontiveros Castillo

Date: _____

ACKNOWLEDGEMENTS

First and foremost, I would like to thank GOD. *"For all things are from Him, by Him, and for Him. Glory belongs to Him forever! Amen."* - Romans 11:36

I would like also to thank:

Dr. Peter Kenny for initially accepting me as his PhD student, and Dr. Andrew Kellett for later adopting me in his research group. Your wisdom and mentorship have been crucial for the success in my postgraduate studies.

National Council of Science and Technology (CONACYT), and the Institute of Innovation and Transference of Technology (I^2T^2) from the government of the state of Nuevo León (Mexico), for sponsoring my studies abroad (grant #399856).

Dr. Lingli Lu (PKRG) and Nicolò Fantoni (AKRG), who managed to be mentors for me. And all the rest of the postgraduates who shared this road with me.

All the academic and technical staff of the School of Chemical Sciences at DCU, especially Dr. Kieran Nolan, Prof. Apryll Stalcup, Dr. Emma Coyle, Prof. Vickie McKee, Julie McArthur, Veronica Dobbin, Damien McGuirk, John McLoughlin, Ambrose May, Vinny Hooper, and Catherine Keogh.

Laboratory of Genomics and Genetic Engineering from Faculty of Chemical Sciences at Universidad Autónoma de Nuevo León (Mexico), specially Dr. Mónica Ramírez, Dr. Patricia González, Dr. Eder Arredondo and M.Sc. Jorge Zacatecas.

My dearest friends who always cheer me up no matter the distance, specially Brenda, Priscy, Lilo, Misael, Mino, Mayra, Luis and Iván.

And finally and most importantly, my beloved family: My soulmate Oscar Castro, you have followed and supported me in every way possible, I love you to infinity and beyond (*"we were just meant to be"*); daddy Jesús and mommy Gloria, for all your sacrifices, constant support, care and guidance; I owe everything to you; my siblings Jesús Jr., Edwin, Abbie and my lovely niece Kaori and nephew Mateo, the shared time with you has been the best because you are marvellous people, your existence inspires me to be the best big sister, I couldn't have done it without you; and grandpa Tacho, grandma Reyna, aunts, uncles, cousins… I hope I've made all of you proud!

POSTER PRESENTATIONS

- **A biological evaluation of novel ferrocenyl dipeptide bioconjugates as anticancer agents.**

  Karen G. Ontiveros-Castillo, Áine Mooney, Andrew Kellett, Rachel Tiedt, James Murphy, Norman O'Donovan, Peter T. M. Kenny

  8th International Symposium on Bioorganometallic Chemistry (2016)

  Moscow, Russia

- **Biological evaluation of *N*-(1'-alkyl-6-ferrocenyl-2-naphthoyl) amino acid and dipeptide derivatives.**

  Ontiveros-Castillo, K.G.; Lu, L.; Kenny, P.T.M.; González-Barranco, P. and Ramírez-Cabrera, M.A.

  II Medicinal Chemistry Ireland Conference (2018)

  Dublin City University – Dublin, Ireland

- **Synthesis, characterisation and biological activity of novel heterocyclic functionalised ferrocenyl derivatives.**

  Karen G. Ontiveros-Castillo, Mónica A. Ramírez-Cabrera, Eder Arredondo-Espinoza, Vickie McKee, Peter T. M. Kenny and Andrew Kellett

  Royal Society of Chemistry - Organic Division Ireland Regional Meeting (2019)

  University College Dublin – Dublin, Ireland

SCIENTIFIC TALKS

- **A biological evaluation of novel ferrocenyl dipeptide bioconjugates as anticancer agents.**
  8th International Symposium on Bioorganometallic Chemistry (2016)
  Moscow, Russia

- **Synthesis, characterisation and biological evaluation of novel ferrocenyl derivatives as potential anti-cancer agents**
  DCU Chemistry Day (2018) *Runner-up winner*
  Dublin City University – Dublin, Ireland

- **Synthesis, characterisation and biological evaluation of novel ferrocenyl derivatives as potential anti-cancer agents**
  70th Irish Universities Chemistry Research Colloquium (2018)
  Queen's University Belfast – Belfast, United Kingdom

- **Recent advances in the synthesis and biological application of ferrocenyl derivatives**
  DCU Chemistry Day (2019)
  Dublin City University – Dublin, Ireland

- **Recent advances in the synthesis and biological application of ferrocenyl derivatives**
  71th Irish Universities Chemistry Research Colloquium (2019)
  RCSI and Technological University Dublin – Dublin, Ireland

TABLE OF CONTENTS

LIST OF TABLES

LIST OF FIGURES

LIST OF SCHEMES

ABBREVIATIONS

A549	human lung carcinoma
ACE	angiotensin-converting enzyme
AcOEt	ethyl acetate
ADCs	antibody-drug conjugates
ALL	acute lymphocytic leukaemia
ATCC	American Type Culture Collection
ATP	adenosine triphosphate
br	broad (spectral)
CAR	chimeric antigen receptor
CML	chronic myelogenous leukaemia
Cp	C_5H_5, cyclopentadienyl ring ligand
CP	cyclophosphamide
CSCs	cancer stem cells
ctDNA	calf thymus DNA
d	doublet (spectral)
D-Ala	D-alanine
dd	doublet of doublets (spectral)
dq	doublet of quartets (spectral)
dt	doublet of triplets (spectral)
ddd	doublet of doublet of doublets (spectral)
decomp.	decomposition
DEMFc+	decamethylferricenium tetrafluoroborate
DHFR	enzyme dihydrofolate reductase
DMSO-d_6	deuterated dimethylsulfoxide
DNA	deoxyribonucleic acid
EDC	*N*-(3-dimethylaminopropyl)-*N*'-ethylcarbodiimide hydrochloride
EDTA	ethylenediaminetetraacetic acid
EMEM	Eagle's Minimum Essential Medium
Et	ethyl group
EtBr	3,8-diamino-5-ethyl-6-phenylphenanthridinium bromide
EtOH	ethanol
FBS	foetal bovine serum
Fc	ferrocene
FDA	U.S. Food and Drug Administration
5-FU	5-fluorouracil
GABA	γ-aminobutyric acid
Gly	glycine
^{1}H NMR	proton nuclear magnetic resonance
H1299	human non-small cell lung cancer cell line
H_{ar}	aromatic hydrogens (spectral)
Hex	hexane
HBV	hepatitis B virus
HCV	hepatitis C virus
HeLa	human epithelioid cervical carcinoma cell line
HIV	human immunodeficiency virus
HPV	human papillomavirus
HT144	human malignant melanoma cell line

IC_{50}	half maximal inhibitory concentration
IR	infra-red spectroscopy
J	coupling constant (spectral)
K_{app}	apparent binding constants
L	linear DNA
L-Ala	L-alanine
LOX-IMVI	human malignant amelanotic melanoma cell line
m	*meta* position
m	multiplet (spectral)
Malme-3M	human lung malignant melanoma cell line
MCF-7	human breast adenocarcinoma cell line
MDA-MB-231	human breast adenocarcinoma cell line
MDA-MB-435S	human breast melanoma cell line
MDR	multiple drug resistance
Me	methyl group
MeOH	methanol
MLCT	metal to ligand charge transfer
m. p.	melting point
6-MP	6-mercaptopurine
MTS	3-(4,5-dimethylthiazol-2-yl)-5-(3-carboxymethoxyphenyl)-2-(4-sulfophenyl)-2H-tetrazolium
MTT	3-(4,5-dimethylthiazol-2-yl)-2,5-diphenyltetrazolium bromide
NAD^+	oxidized form of nicotinamide adenine dinucleotide
NADH	reduced form of nicotinamide adenine dinucleotide
NHS	*N*-hydroxysuccinimide (1-hydroxy-2,5-pyrrolidinedione)
NIH 3T3	murine embryonic fibroblast cell line
NMR	nuclear magnetic resonance
NSCLC	non-small cell lung cancer
o	ortho position
OC	open-circular DNA
OEt	ethoxy group
OH	hydroxyl functional group
OMe	methoxy group
p	*para* position
PARP	poly ADP ribose polymerase
PBS	phosphate-buffered saline
PC-3	prostate adenocarcinoma cell line
Pen-Strep	Penicillin-Streptomycin
pH	potential of hydrogen
q	quartet (spectral)
qd	quartet of doublets (spectral)
qt	quartet of triplets (spectral)
quint	quintet (spectral)
RNA	ribonucleic acid
ROS	reactive oxygen species
rt	room temperature
s	singlet (spectral)
SAR	structure-activity relationship
SC	supercoiled DNA
SCLC	small cell lung cancer

SiHa	human cervical carcinoma cell line
SK-MEL-28	human skin melanoma cell line
t	time
t	triplet (spectral)
T	temperature
td	triplet of doublets (spectral)
tt	triplet of triplets (spectral)
thioTEPA	*N*,*N*′,*N*″-triethylenethiophosphoramide
TLC	thin layer chromatography
UV-Vis	ultraviolet–visible spectroscopy
WHO	World Health Organisation
WST	water-soluble tetrazolium salt
WST-1	2-(4-iodophenyl)-3-(4-nitrophenyl)-5-(2,4-disulfophenyl)-2H-tetrazolium, monosodium salt
XTT	2,3-bis-(2-methoxy-4-nitro-5-sulfophenyl)-2H-tetrazolium-5-carboxanilide
η^5-C_5H_4	substituted cyclopentadienyl ring
η^5-C_5H_5	unsubstituted cyclopentadienyl ring

UNITS

Å	Angstrom
bp	base pair
C_{50}	concentration required to reduce 50% fluorescence
cm	centimetre
cm^{-1}	reciprocal wavelength
eq	equivalent
g	gram
h	hour
Hz	hertz
IC_{50}	half maximal inhibitory concentration
K_{app}	apparent binding constant on DNA
L	litre
M	molar
MHz	megahertz
mg	milligram
min	minute
mL	millilitre
mm	millimetre
mM	millimolar
mmol	millimole
mol	mole
mV	millivolt
ng	nanogram
nm	nanometre
nM	nanomolar
pH	potential hydrogen
ppm	part(s) per million
s	second
V	volt
δ	chemical shift (ppm)
ε	molar absorption coefficient
μg	microgram
$\mu g\ mL^{-1}$	microgram per millilitre
μL	microlitre
μM	micromolar
°	degrees
°C	degrees Celsius
%	percentage

ABSTRACT

Novel Heterocyclic Functionalised Ferrocenyl Derivatives as Potential Anti-Cancer Agents

Karen Guadalupe Ontiveros Castillo, M.Sc.

Earlier *in vitro* studies have shown that ferrocenyl amino acid and dipeptide bioconjugates exhibit anti-proliferative activity against the lung cancer cell lines H1299 and A549, the melanoma cell lines SK-MEL-28, HT-144, MalMe-3M and Lox-IMVI, and the breast cancer cell line MCF-7. The aim of this research was to further explore the structure-activity relationship (SAR) of ferrocenyl compounds other than amino acid bioconjugates. Thus, a series of novel heterocyclic functionalised ferrocenyl derivatives has been synthesized, characterized and biologically evaluated for their anti-proliferative activity and interaction with DNA. The synthesis was achieved by the conventional *N*-(3-dimethylaminopropyl)-*N*′-ethylcarbodiimide hydrochloride (EDC) and *N*-hydroxysuccinimide (NHS) coupling protocol. Characterisation was completed by a range of techniques including NMR (^{1}H, ^{13}C, DEPT-135, COSY, HSQC, HMBC), IR, UV-Vis, MS, elemental analysis and X-rays crystallography. For the *in vitro* anti-proliferative evaluation, compounds were tested against the human cervical carcinoma cell line SiHa (ATCC® HTB-35™) and the human liver cell line Chang (ATCC® CCL-13™) via the WST-1 assay. Suitable candidates were then examined for potential DNA binding and damaging properties. The anti-proliferative activity of additional derivatives previously developed by this group is also reported; these compounds belong to the series of *N*-(1′-alkyl-6-ferrocenyl-2-naphthoyl) amino acid and dipeptide esters and *N*-(ferrocenylmethylamino acid) fluorinated benzene carboxamides. Compounds *N*-(1′-ethyl-6-ferrocenyl-2-naphthoyl)-glycine-D-alanine ethyl ester, *N*-(ferrocenylmethyl-L-norleucine)-3,4,5-trifluorobenzene carboxamide and *N*-(ferrocenylmethyl-L-(+)-α-phenylglycine)-2,3,4,5,6-pentafluorobenzene carboxamide have shown to be significantly more cytotoxic against SiHa cells than chemotherapeutic control drugs vincristine and cisplatin, whilst maintaining a moderate percentage of viability on Chang cells. The overall results suggest that some ferrocenyl derivatives analysed are promising anticancer agents worthy of future therapeutic analysis.

CHAPTER 1

1 Cancer and bioorganometallic chemistry

This Chapter details the background to cancer and cancer treatments. The description of problems associated with current chemotherapy then leads to the focus on metal-based drugs and bioorganometallic chemistry, where an overview of ferrocene and ferrocene-based drugs is outlined.
My contribution to this chapter was the literature review of the state-of-the-art of the topics mentioned, summarising the biological results obtained from the family of ferrocene bioconjugates to date. The analysis of the structure-activity relationship of these compounds allowed me to set up the aims for the present project.

1.1 Cancer

1.1.1 Definition

The World Health Organisation (WHO) defines cancer as a generic term for a collection of diseases which can affect any part of the body. It starts when abnormal cells divide without stopping, forming tumour masses. These cells can invade adjoining tissues, and hence disseminate to distant sites where they settle to form a new cluster. This feature, which distinguish malign from benign tumours, is known as metastasis: Tumour cells grow in new tissue causing organ dysfunction, leading next to death. Metastases are a major cause of death from cancer.[1–4]

1.1.2 Types

The distinct categories of cancers are based on the cell type which originates the tumours. This classification is shown in Figure 1.1.[2,5–7]

Carcinoma is the most common type of cancer; it is initiated by epithelial cells, which overcoat the surfaces of the skin and organs. According with the diverse types of epithelial cells, carcinomas can be: (i) adenocarcinoma, formed in cells which produce mucus or fluids, such as breast, prostate, and colon cancers; (ii) basal cell carcinoma, originated in the basal layer of the epidermis; (iii) epidermoid cell carcinoma, started in the squamous cells which form the surface of the skin, organs and both respiratory and digestive tracts, for example cervix, vagina, neck and anus cancers; and (iv) transitional cell carcinoma, commenced in the urothelium, a tissue conformed by different-size layers of epithelial cells (kidney, bladder and ureter cancers).[2,5–7]

Sarcoma is begun in bone and soft tissues, like cartilage, fat, muscle, tendons and ligaments. According with the diverse types of tissue, sarcomas can be: (i) osteosarcoma, also called osteogenic sarcoma, the most common cancer of the bone often affecting large bones of the arm or leg; (ii) leiomyosarcoma, formed by smooth muscle cells, for example abdomen, uterus or pelvis cancers; (iii) Kaposi sarcoma, growing as purple lesions in the nose, mouth and/or throat; (iv) malignant fibrous histiocytoma, fast growing cancer habitually originated in arms, legs or back of the abdomen; (v) liposarcoma, infrequent cancer started in the fat cells; and (vi) dermatofibrosarcoma protuberans, slow growing cancer commenced as a hard knob, generally in the limbs or trunk of the body.[2,5–7]

Leukaemia is started in the blood-forming tissue, which is situated in the bone marrow. It can be acute or chronic, depending on the speed of the disease; depending on the type of blood cell where it is initiated, it can be lymphoblastic or myeloid.[2,5–7]

Lymphoma is built in lymphocytes, which are part of the immune system. The two major forms are Hodgkin and non-Hodgkin lymphoma. Hodgkin lymphoma is regularly formed from B cells and can be categorized as: (i) classical Hodgkin lymphoma, characterized by Reed-Sternberg cells, which are unnatural lymphocytes containing more than one nucleus; according with the diverse presences of the lymphoma cells, it can be nodular sclerosing, mixed cellularity, lymphocyte-rich or lymphocyte-depleted; and (ii) nodular lymphocyte-predominant Hodgkin lymphoma, an uncommon type which is attributed to popcorn-shaped Reed-Sternberg cell. Non-Hodgkin lymphoma is a cancer started from B-cells or T-cells; according with the speed of growth, it can be either indolent or aggressive.[2,5–7]

Myeloma is initiated in plasma cells, which are white blood cells producing antibodies. Melanoma is started in melanocytes, which are cells making melanin. It is mostly formed on the skin but can also be present in other pigmented tissues, for example the eye.[2,5–7]

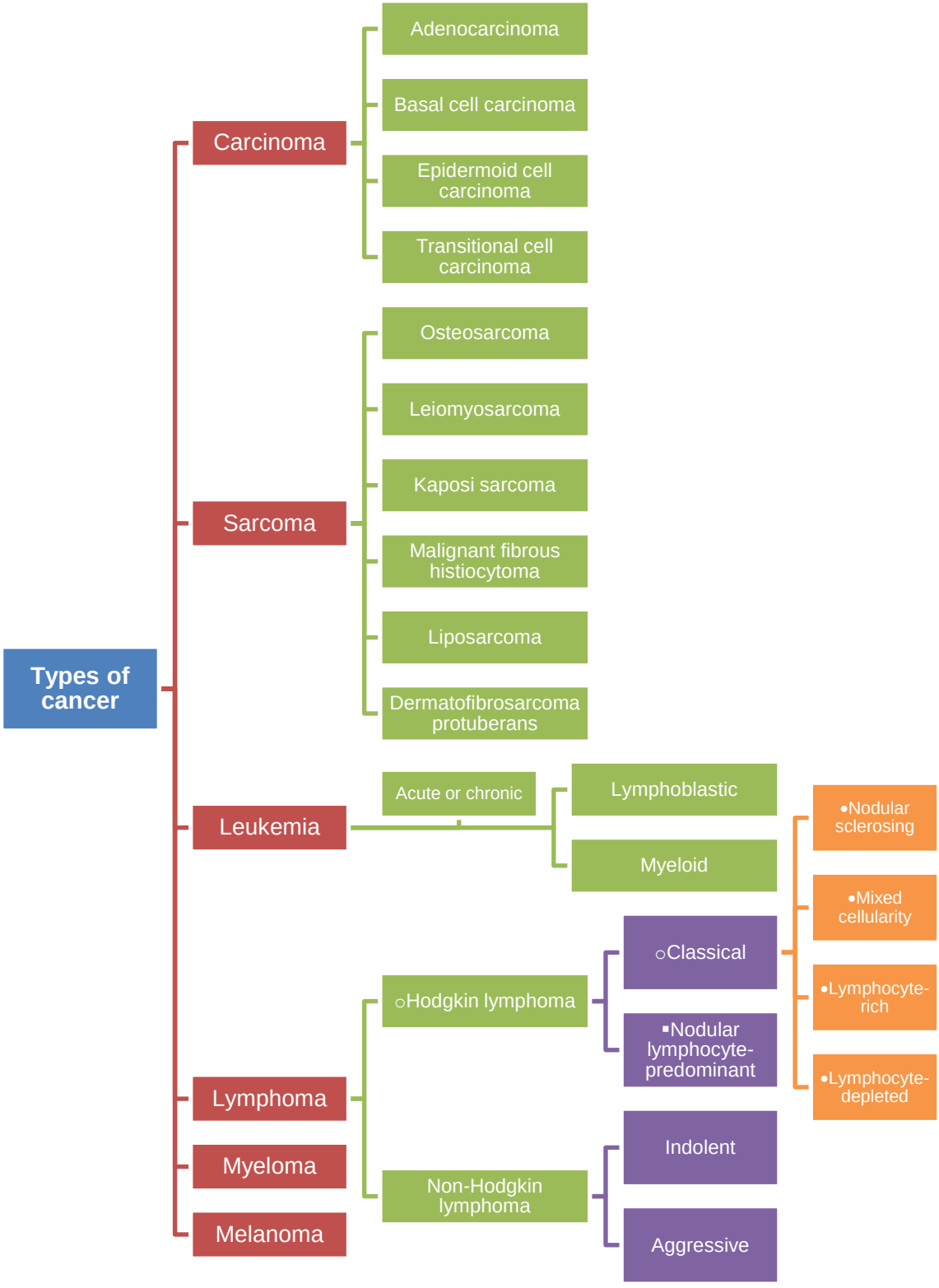

Figure 1.1. Types of cancer based on cell type.

1.1.3 Mortality

Cancer is a leading cause of death worldwide. In 2012, 14.1 million new cancer cases were reported; from these, 8.2 million were mortal. In 2018, this number increased to 9.6 million individuals who died from cancer.[8] The most common types of cancer death and their frequencies are enlisted in Figure 1.2. It is thought that the number of cases will increment ~70% over the next two decades.[1]

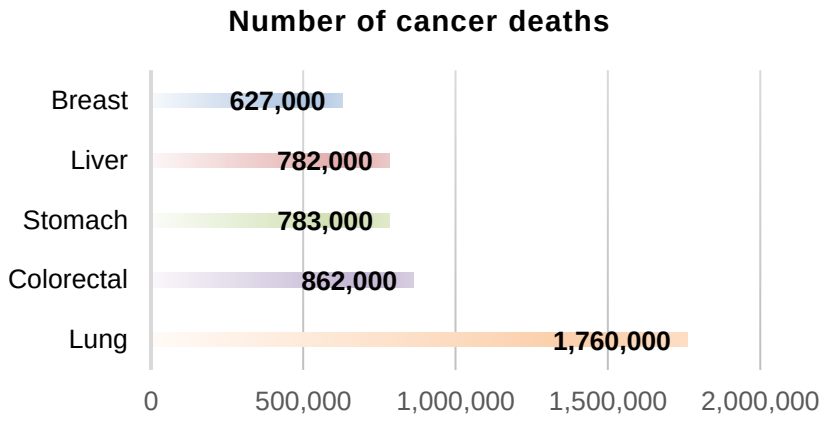

Figure 1.2. Mortality attributed to cancer in 2018, WHO.

1.1.4 Causes

Cancer is the result of a complex process which includes the metamorphosis of normal cells into tumoral cells. This transformation can be caused by agents which damage the genes involved in the control of cell proliferation (proto-oncogenes), which act in conjunction with agents that do not damage genes but selectively boost the tumour cells growth. Therefore, cancer rise is determined by the interface between the genetic factors of a person and external agents, whose types are enlisted in Table 1.1.[1,9]

Table 1.1. Types of carcinogens.

Carcinogen	Example
Physical	Ultraviolet[10] and ionizing radiation[11].
Chemical	Asbestos[12,13], tobacco smoke[14,15], arsenic[16,17].
Biological	Infections from certain bacteria (as *Helicobacter pylori*[18] or *Chlamydia trachomatis*[19]), parasites (as *Schistosoma haematobium*[20], *Opisthorchis viverrini* and *Clonorchis sinensis*[21]), or viruses[22] (as HIV[23–25], HPV[26–28], HBV and HCV[29–31]).

In addition to these agents, there are another risk factors for cancers such as ageing, tobacco and/or alcohol use, unhealthy diet, and lack of physical activity, which for example are related with the lung cancer incidence in patients who never smoked tobacco. [1,11,32,33]

1.1.5 Mechanisms of cell death

Cancer occurs when a single cell accumulates several mutations, usually for some years, escaping from the proliferation and death processes.[34] A cell can die in two ways: necrosis or apoptosis. Necrosis is a disordered process based in the autolysis of the cell; it is caused by external factors (trauma, infection, or toxins) which induce a swelling of the cell, generating inflammation and lysis of the membrane. Apoptosis is a type of programmed cell death, or "cell suicide", it is an organized process where the cell content is packed into small membranous units to be "collected" by the immunity cells; it removes cells during growth, deletes cells infected by virus and also the potentially cancerogenic cells, maintaining the equilibrium in the body. The differences between both processes can be found in Table 1.2.[35–38] When cancer arises, the human body generates its own defences to naturally destroy abnormal cells through the immunological system; in most cases, however, this is not enough. Therefore, other methods (and their combinations) are required to eradicate this problem.[39]

Table 1.2. Comparison between necrosis and apoptosis.

Feature	Necrosis	Apoptosis
Stimulus	Massive aggression, toxins, anoxia, ATP drop	Physiological and pathological conditions without ATP drop
Energy requirements	Any	ATP dependent
Histology	Lysis of the cytoplasm and organelles	Condensation of chromatin, apoptotic bodies (chromatin residues surrounded by membrane)
Zone	Tissue areas	Isolated cells
Patent of DNA rupture	Irregular sizes	Fragments of 185 base pairs or multiples
Plasmatic membrane	Lysis	Intact, with molecular alterations
Phagocytosis of dead cells	Immigrant phagocytes	Neighbouring cells
Tissue reaction	Inflammation	No inflammation
Initiation phase	Inflamed cell, damaged organelles, altered chromatin	Wrinkled cell with bubbles, loss of intercellular junctions, intact organelles, margin chromatin
Effector phase	Plasmatic membrane alteration, loss of mitochondrial homeostasis, cell lysis, organelles and chromatin destroyed, content release	Failures in repair and homeostasis mechanisms, condensed chromatin, activation of endonucleases, DNA fragmentation, apoptotic bodies, intact organelles, content unreleased
Degrading phase	Phagocytosis with inflammation	Phagocytosis without inflammation

1.1.6 Treatments

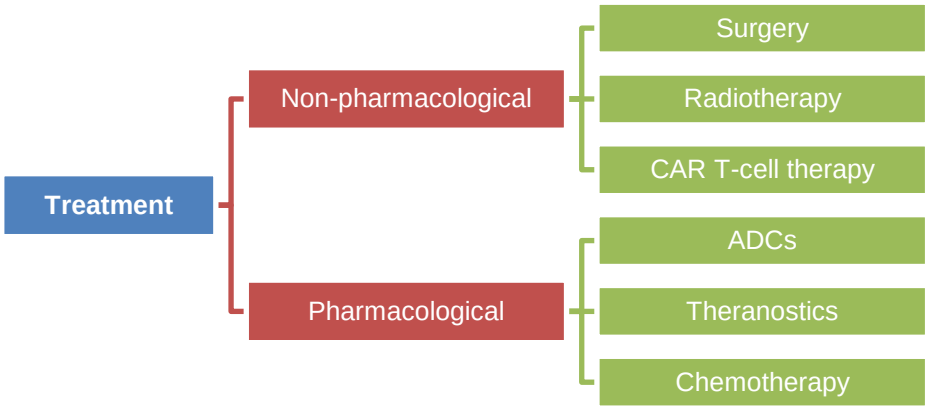

Figure 1.3. Some types of cancer treatments.

1.1.6.1 Surgery

Surgery can be used to prevent, diagnose, determine the stage, cure or reduce cancer. Curative surgery is only performed when cancer is localized in a specific part of the body, which could be partially or totally removed.[40,41]

1.1.6.2 Radiotherapy

Also known as radiation therapy, it is a local treatment which uses particles or high energy waves such as gamma, electron, proton or X-rays to delete or damage cancer cells. Radiation acts on DNA inside cells producing small breakages which avoid growth and division of cancer cells, causing their death. However, most radiotherapies cannot reach all parts of the body, rendering them useless against metastatic cancer.[42–44]

1.1.6.3 CAR T-cell therapy

In this type of treatment, the gene for the chimeric antigen receptor (CAR) is added to T-cells isolated from the patient's blood. This activates and stimulates T-cell proliferation, differentiation and cytotoxic activities for tumour cell elimination. The potency of this therapy has been proved against various B cell malignancies such as lymphomas and leukaemias. Nevertheless, CAR-T therapy is far from a curative therapy if used alone. Combination with other treatments is essential to mitigate the drawbacks of this therapy, such as immunogenicity, loss of target antigens, cytokine release syndrome and neurological toxicities.[45,46]

1.1.6.4 ADCs

Antibody-drug conjugates (ADCs) are an emerging class of complex drugs for cancer treatment. They are composed of cytotoxic drugs attached to an antibody, providing selective delivery of the cytotoxic drug to cancer cells via the specific binding of the antibody moiety to cancer-selective cell surface molecules. However, the efficacy, stability and pharmacokinetics of the ADCs are significantly affected by the drug-antibody ratio; this is important because the degradation of the antibody fragment will result in free drug leading to undesirable toxicity.[47–49]

1.1.6.5 Theranostics

By combining both therapeutic and imaging functions in one delivery formulation, theranostic nanomedicines enable diagnosis, therapy, and monitoring of treatment progress and efficacy. This aims to eliminate multi-step procedures, reducing delays in treatment and improving patient care. It offers various advantages like improved diagnosis, tumour specific delivery of drugs, and reduced lethal effects to normal tissues. Still, some drawbacks include long imaging times, relatively low sensitivity and high costs.[50,51]

1.1.6.6 Chemotherapy

Chemotherapy involves the use of drugs to treat any disease. Whilst no pharmacological treatments extract, eradicate or damage only localized cancer cells, chemotherapy can also destroy cancer cells that have metastasized to other parts of the body. It is often used in combination with surgery or radiotherapy: before, to reduce the tumour size; or after, to destroy remnant cancer cells.[44,52,53] Most conventional anti-neoplastic drugs fall into the following mechanisms of action (Figure 1.4):

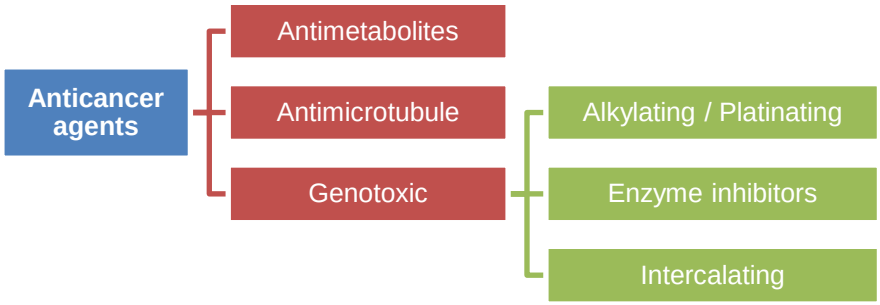

Figure 1.4. Mechanism of action of most anticancer drugs.

1.1.6.6.1 Antimetabolite agents

Antimetabolite drugs interfere with the formation of key biomolecules such as nucleotides, which are DNA building blocks; they inhibit DNA replication and, hence, cell division. For example, the drug methotrexate **1** impedes the enzyme dihydrofolate reductase (DHFR), which uses dihydrofolic acid to produce tetrahydrofolic acid; tetrahydrofolic acid is essential for the synthesis of thymidylate and purine nucleotides, and both are necessary for DNA synthesis and cell division. Other antimetabolite drugs are 5-fluorouracil (5-FU) **2**, gemcitabine (Gemzar®) **3** and 6-mercaptopurine (6-MP) **4**; they have been used in the

treatment of lymphoblastic leukaemia and pancreatic, bladder, breast, ovarian and non-small cell lung cancers (Figure 1.5).[54–57]

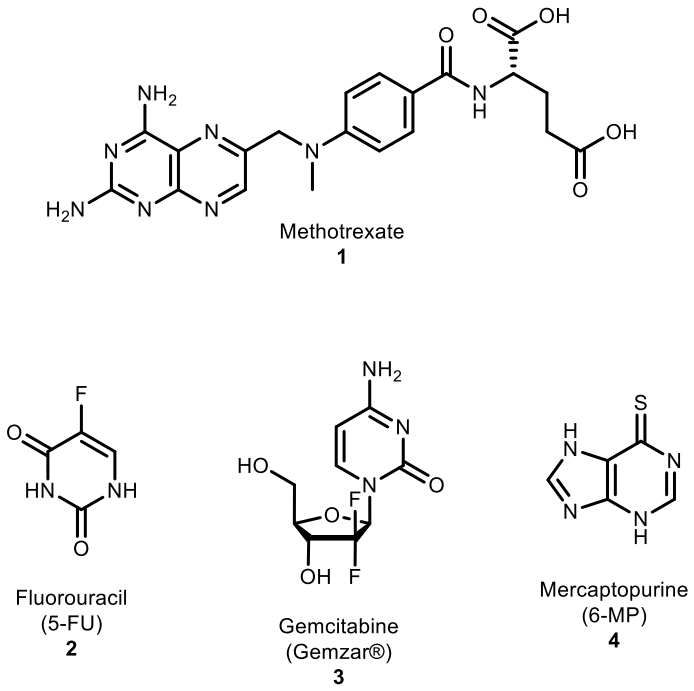

Figure 1.5. Examples of clinical antimetabolite agents.

1.1.6.6.2 Antimicrotubule agents

Antimicrotubule drugs prevent cell division by interfering with microtubules function, which are dynamic cellular structures found throughout the cytoplasm forming the cytoskeleton. Microtubules are conformed by α-tubulin and β-tubulin, whose polymerization (assembly) forms the mitotic spindle in the cell.[58] Two of the most popular antimicrotubule agents are vincristine **5** and paclitaxel (Taxol®) **6**; their structures are shown in Figure 1.6. Vincristine **5** binds to tubulin, interfering with its assembly into microtubules. On the other hand, paclitaxel (Taxol®) **6** stabilizes the microtubule, preventing their disassembly. They have been used in the treatment of acute lymphocytic leukaemia, neuroblastoma, acute myeloid leukaemia, and small and non-small cell lung, cervical, pancreatic, ovarian and breast cancers.[59–64]

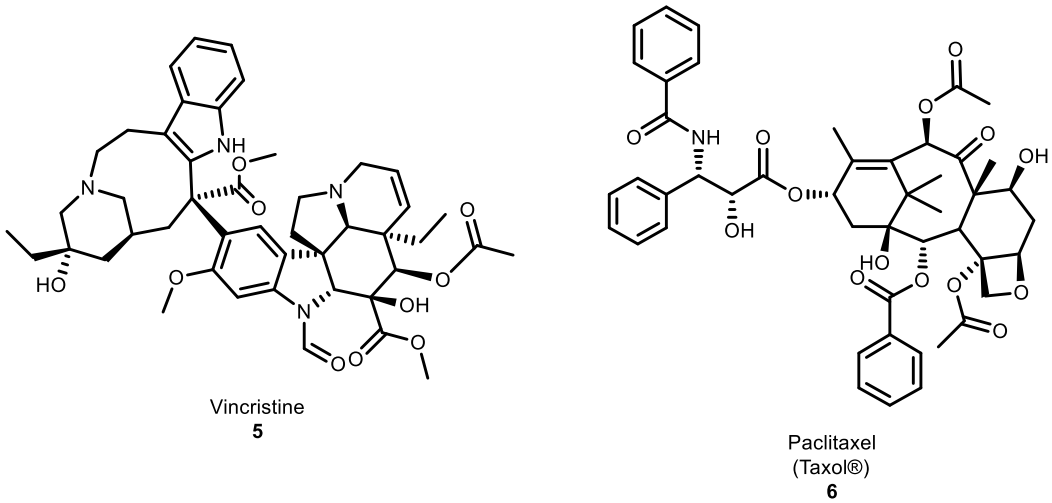

Figure 1.6. Examples of antimicrotubule agents.

1.1.6.6.3 Genotoxic agents

Genotoxicity refers to damage to the DNA.[65] These drugs deteriorate genetic information within a cell by interfering with replication and cell division processes. They can be categorized into:

Alkylating agents. They show the ability to bind alkyl groups to DNA via covalent bonds, modifying DNA bases and hence leading to replication and transcription interferences, causing further mutations. Some examples are 1,4-butanediol dimethanesulfonate (busulfan) **7**, cyclophosphamide (CP) **8**, lomustine **9** and *N*,*N*′,*N*″-triethylenethiophosphoramide (thioTEPA) **10**, which have been used against retinoblastoma, ovarian and breast cancers (Figure 1.7).[66–69]

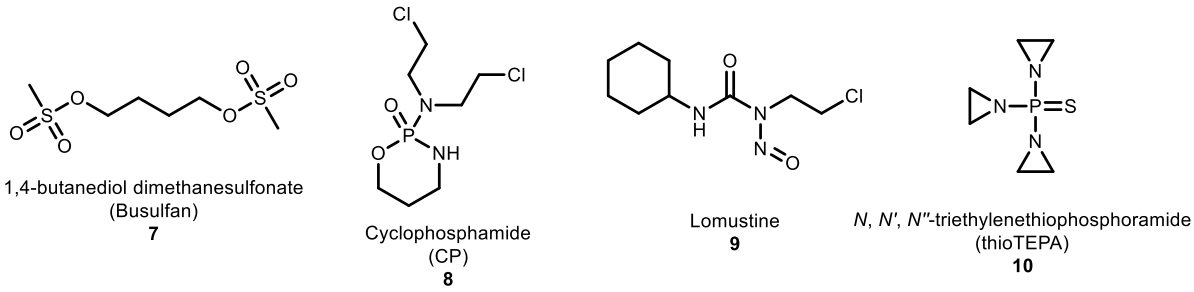

Figure 1.7. Examples of alkylating agents.

Enzyme inhibitors. These drugs damage key enzymes such as topoisomerases, which are directly related to DNA replication; examples include etoposide **11**, which has been used against testicular, cervical, small and non-small cell lung cancers (Figure 1.8).[70–74] Another important class are PARP inhibitors, which are drugs that block repair of DNA by inhibiting the enzyme poly ADP ribose polymerase (PARP); niraparib **12** is a drug with this mechanism of action, and it was recently approved for treatment of epithelial ovarian, fallopian tube, and primary peritoneal cancer.[75–77]

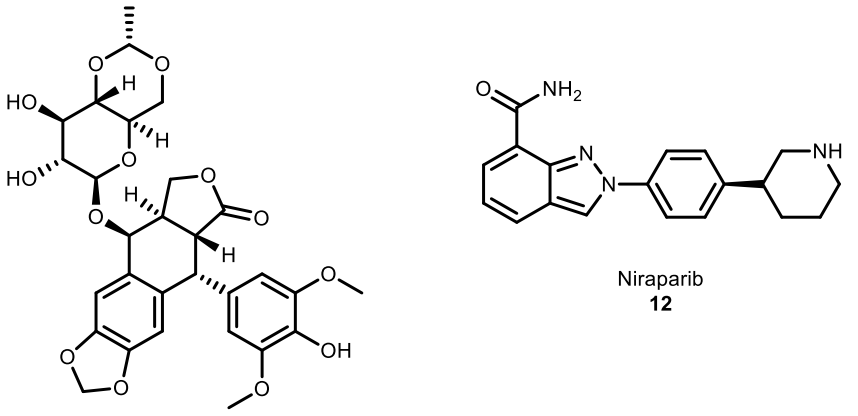

Figure 1.8. Examples of enzyme inhibitor agents.

Intercalating agents. These compounds insert into the DNA strands and bind to them, causing structural distortions that stop cell division. Examples of them are doxorubicin (Adriamycin®) **13** and dactinomycin **14**, which have been used in the treatment of ovarian, breast, bladder and small cell lung cancers (Figure 1.9).[78–82]

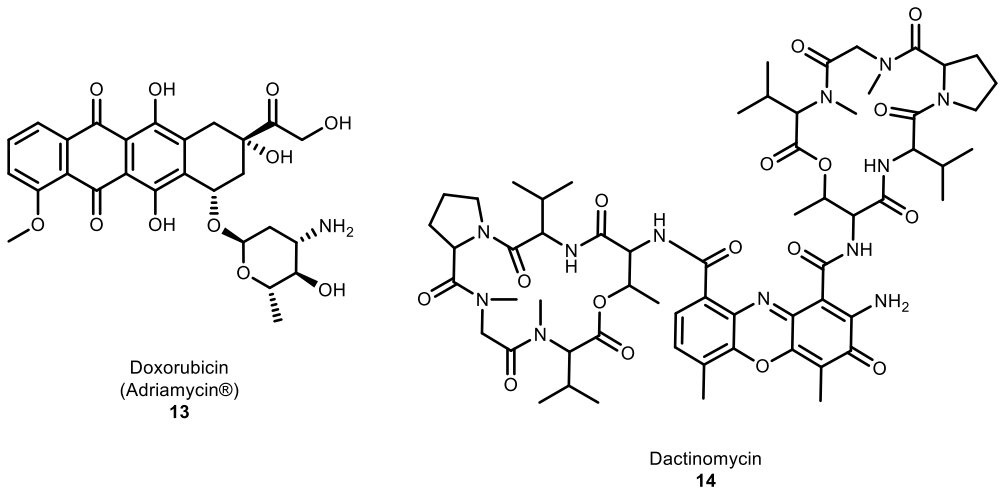

Figure 1.9. Examples of intercalating agents.

1.1.6.6.4 Problems associated with current chemotherapy

Chemotherapy involves the use of agents which are cytotoxic, i.e. they kill or damage cells. Their selectivity is based on the cell's rate of growth: cancer cells tend to divide faster than normal cells; therefore, antineoplastic drugs show preference by targeting fast-dividing cells. However, as these compounds travel throughout the body in the bloodstream, they can find and affect normal cells that are constantly growing and dividing too, like the examples enlisted in Table 1.3. Other side effects include nausea, fatigue, sickness, constipation, diarrhoea, vomiting, sleep disturbance, and appetite changes.[83–87]

Table 1.3. Side effects of cancer chemotherapy in normal cells.

Type of normal cell damaged	Consequence
Bone marrow	Petechiae, infections, anaemia, myelosuppression
Hair follicles	Alopecia, including eyelashes and eyebrows
Skin	Dry and sensitive skin, easy bruising and bleeding
Nerves	Numbness or tingling in hands and feet
Gastrointestinal tract	Sores in mouth, tongue and throat; pain with swallowing, infections
Reproductive system	Changes in libido and sexual function, infertility

Another major problem regarding to chemotherapy treatment is drug resistance, which is considered its main reason for failure. The types of resistance to antineoplastic drugs are shown in Figure 1.10.[88,89] Moreover, some cancer cells have developed the ability to survive and grow despite different chemotherapy agents; this is known as multiple drug resistance (MDR) of cancer cells. MDR constitutes a problem with vast clinical implications, as it obligates further research and development of new chemotherapeutic agents.[90] In addition, the persistence of cancer stem cells (CSCs) is a primary cause of tumour relapse and metastasis, as CSCs are highly resistant to chemotherapy and are uniquely capable of seeding new tumours.[91,92] All these inconveniences have attracted the attention of the scientific community, expanding the design and synthesis of varied organic molecules which incorporate diverse functional groups in their structure, conferring antineoplastic activity on them.

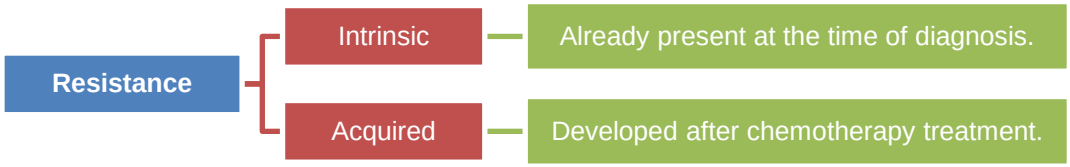

Figure 1.10. Types of cancer resistance.

1.2 Metal based drugs

1.2.1 Introduction

In an attempt to find new drugs that can solve the current problems of cancer chemotherapy, research in the synthesis and application of compounds containing metals in their structures is currently considered a growing area in medicinal chemistry. The use of metal based compounds has increased dramatically as a result of their excellent potential to bind to negatively charged biomolecules (such as nucleic acids or proteins), due to their positively charged centres.[93] In the case of anticancer compounds, a categorization of metal antineoplastic drugs has been proposed by Gianferrara *et al.*, according to their mechanism of action (Figure 1.11).[94]

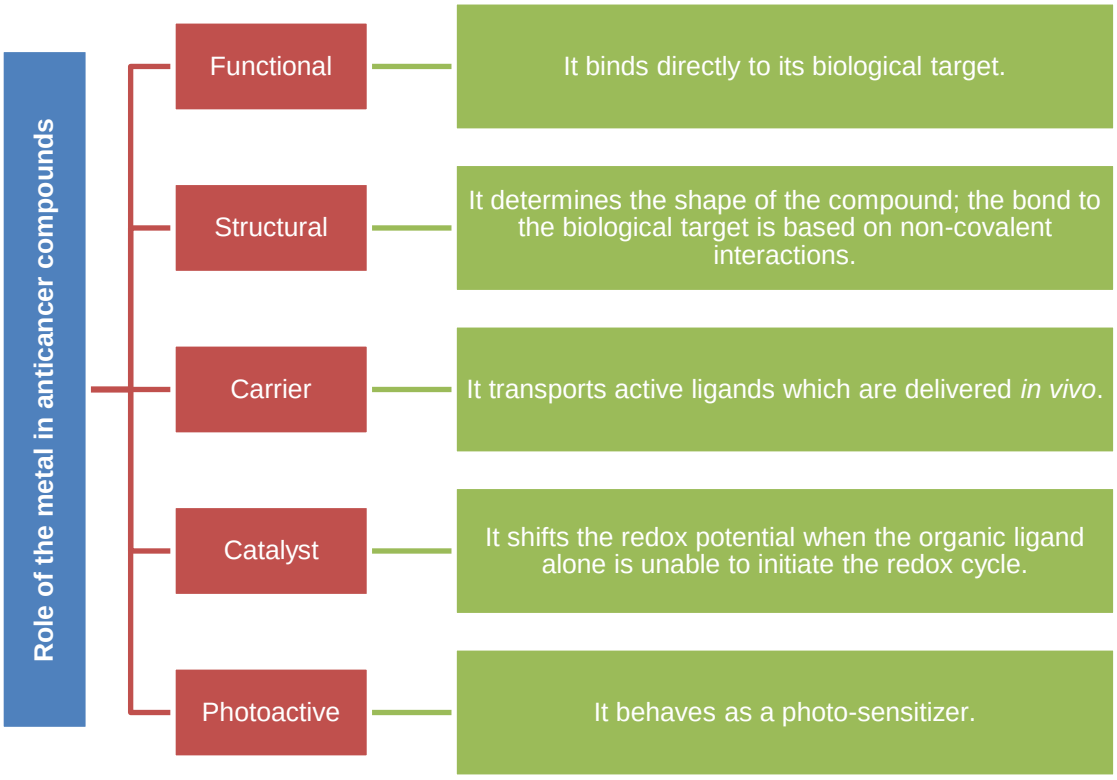

Figure 1.11. The different roles of metals in anticancer compounds.

1.2.2 Platinum agents

Platinum agents play a considerable role in cancer chemotherapy nowadays. Cisplatin **15**, or *cis*-diaminedichloroplatinum(II), one of the most widely used anticancer metal complexes today, was first synthesized by Italian chemist Michele Peyrone in 1844, and it was initially known as Peyrone's chloride. It is a square-planar complex composed of two labile chloride ions and two ammonia groups coordinated in a *cis* configuration to the central Pt(II) atom, as shown in Figure 1.12.[95,96]

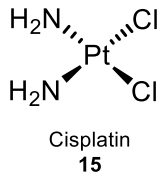

Figure 1.12. Structure of cisplatin **15**.

However, the success of cisplatin **15** as one of the most important drugs started more than 100 years after, when its anticancer properties were accidentally discovered in 1965 by Barnett Rosenberg, while studying the effect of electric field on bacterial growth. They noticed that cell division was inhibited and tracked this as a consequence of the platinum plates used during the experiment; hence suggesting that this discovery may also be used against tumour growth.[97]

The unique mechanism of action of cisplatin **15** is based on its facility to replace the chloride groups by neutral water molecules following uptake of the drug into the nucleus of cells (Figure 13).[98] This process is facilitated within the cell by the relatively low concentration of chloride ions in the cytoplasm.[99,100] The platinum core of these positively charged species form then intra-strand cross-links DNA adducts via a covalent bond with the adenine and guanine residues in the position N-7. Consequently, this change in DNA structure leads to a disruption in its replication and transcription processes, affecting cell viability and inducing apoptosis.[101–104]

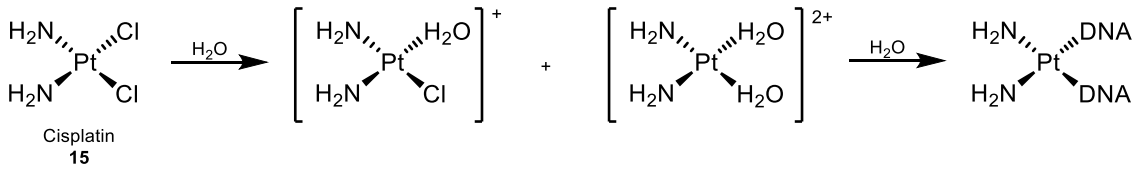

Figure 1.13. Cellular activation of cisplatin **15**.

Cisplatin **15** is currently used in the treatment of breast, testicular, ovarian, head, neck, colorectal, bladder and lung cancers.[105,106] Nevertheless, the many severe toxic side effects associated to cisplatin **15** due to its non-specific targeting have led to the design and synthesis of analogues, such as the 2nd and 3rd generation platinum drugs carboplatin **16** and oxaliplatin **17** (Figure 1.14).[107]

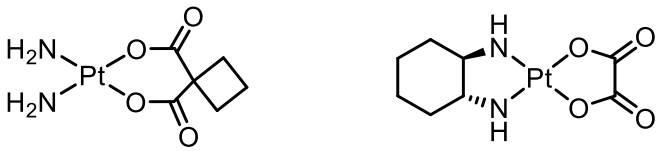

Carboplatin **16** Oxaliplatin **17**

Figure 1.14. Structures of cisplatin analogues: carboplatin **16** and oxaliplatin **17**.

These derivatives contain different leaving groups compared to the chloride ions of cisplatin **15**: carboplatin **16** is composed by a cyclobutane-1,1-dicarboxylate ligand, and oxaliplatin **17** has an oxalate group. These modifications improved the solubility, increased the stability and reduced the toxicity of the complexes.[108,109]

Despite its success in the treatment of tumours, the singular chemical structure of cisplatin **15** does not offer a wider possibility for further rational improvements to increase its selectivity towards cancer cells. Another important restriction associated with these platinum drugs is their limited effectiveness as a result of their intrinsic and acquired resistance, which includes increased DNA repair, decreased influx, increased efflux, among others.[110–112]

1.2.3 Bioorganometallic chemistry

New generations of metal-based compounds have been developed to overcome the side effects, drug resistance and limited spectrum of activity of platinum drugs. In this context, bioorganometallic compounds represent a strongly emerging area of research in the seeking of alternative metal-based drug design. Bioorganometallic chemistry is a field dedicated to the study of biomolecules or biologically active molecules that contain at least one direct bond between a carbon and a metal.[113]

The antitumor activity of a range of organometallic complexes of transition metals (Au, Co, Cu, Fe, Ga, Ge, Hf, Mo, Nb, Pt, Sn, Rh, Ru, Ti, V, Zr) has been reported.[114–120] Some of these complexes belong to a special group of called metallocenes, which are organometallic compounds where the metal cation (denoted as M) is π-bonded to two aromatic ring structures, typically two cyclopentadienyl (Cp) anions (Figure 1.15).[121]

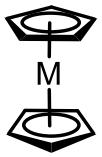

Figure 1.15. General chemical structure of a metallocene compound.

1.2.3.1 Titanium

The first metallocene described with anticancer activity was titanocene dichloride **18** (Figure 1.16) by Köpf and Köpf-Maier in 1979. It was the first non-platinum organometallic compound to enter clinical trials as an anticancer drug in 1993, but its efficacy against breast cancer and renal-cell carcinoma (both metastatic) was too low to be pursued, thus Phase II clinical trials were aborted.[122–124]

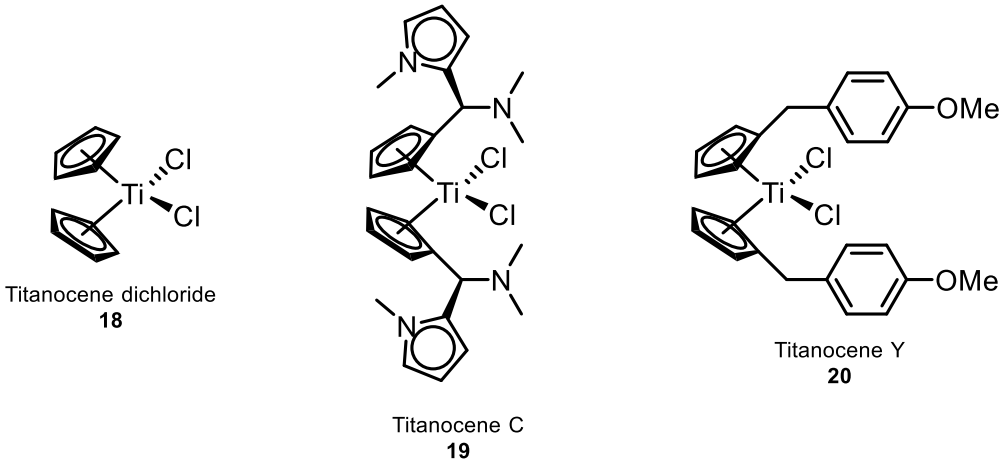

Figure 1.16. Structures of titanocene dichloride **18**, titanocene C **19** and titanocene Y **20**

Tacke *et al.* have focused in the synthesis of enhanced derivatives of **18** showing anticancer activity both *in vitro* and *in vivo*. Their studies have shown that compound *bis*-(*N*,*N*-dimethylamino-2-(*N*-methylpyrrolyl)-methyl-cyclopentadienyl) titanium(IV) dichloride, also known as titanocene C **19**, exhibited antiproliferative effect against pig

kidney carcinoma (LLC-PK) cell line with an IC_{50} value of 5.5 μM. On the other hand, compound *bis*-[(*p*-methoxybenzyl)cyclopentadienyl] titanium(IV) dichloride, namely titanocene Y **20**, had an IC_{50} value of 21 μM, plus it was found to be active against a panel of other 36 human tumour cell lines. In addition, titanocene dichloride **18** showed an IC_{50} value of 2000 μM against the same cell line. These results suggest that the functionalized cyclopentadienyl rings improved remarkably the cytotoxicity, and also increased the water solubility compared to **18** itself. Moreover, cross-resistance to cisplatin or oxoplatin was low for **19** and absent for **20**, respectively, in human promyelocytic leukaemia HL-60 cell line.[125–132]

1.2.3.2 Ruthenium

The first investigations regarding to ruthenium complexes showing anti-proliferative activity began in the 1980s with the synthesis of cisplatin-inspired structures. Compound *fac*-triamminetrichlororuthenium(III), or *fac*-$Ru(NH_3)_3Cl_3$ **21**, displayed great activity against the P388 mouse leukaemia cell line, but its application in clinical studies was unfortunately abandoned due to its poor aqueous solubility. To overcome this obstacle, its analogue *cis*-dichlorotetrakis(dimethylsulfoxide)ruthenium(II), or *cis*-$Ru(DMSO)_4Cl_2$ **22**, was developed and found to be easy to dissolve in water but exhibited only minimal activity against the same cell line, although it is highly active in some other tumour systems such as the Lewis lung carcinoma.[133–138] Nevertheless, the actual success of ruthenium complexes as anticancer agents started with the synthesis of KP418 [imidazolium-bis-imidazole tetrachlororuthenate(III)] **23** by Keppler *et al.* in 1986, which had a tumour inhibition effect in the range or better than the controls 5-fluorouracil (5-FU) **2**, cyclophosphamide (CP) **8**, or cisplatin **15** against both P388 leukaemia and B16 melanoma cell lines. Subsequent research were conducted on KP1019 **24** (the indazole analogue of **23**), and on NAMI-A **25**. They were found to have superior anticancer activity to their predecessor **23** and are currently still under study as they have been admitted into human clinical testing (Figure 1.17).[139–147]

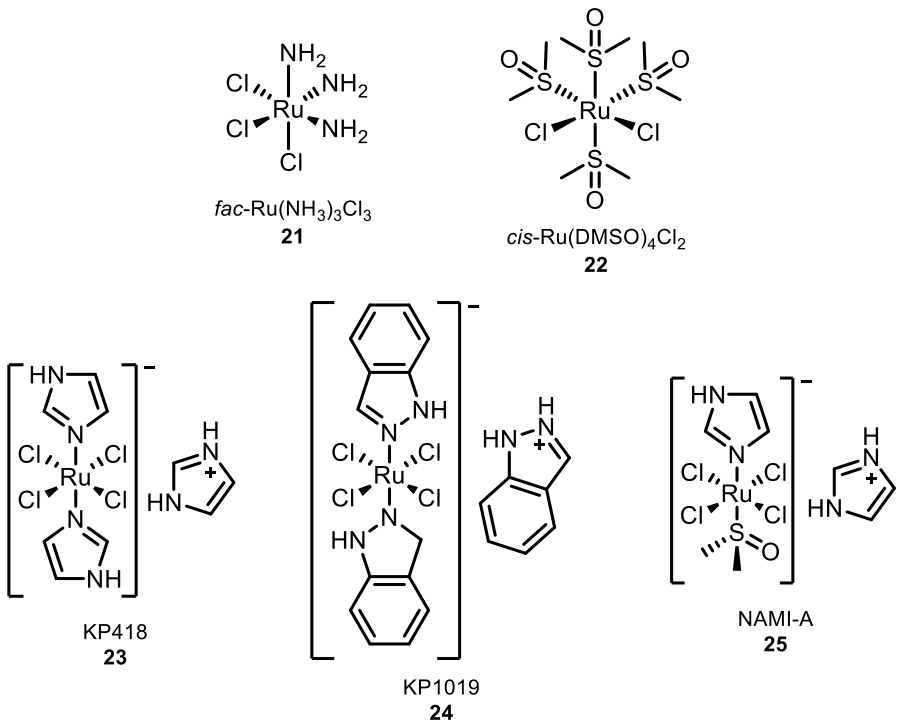

Figure 1.17. Structures of ruthenium complexes **21**-**25**.

1.2.3.3 Ferrocene

Jaouen *et al.* describe ferrocene **26** (Figure 1.18) as the quintessential organometallic compound.[148] It was one of the first metallocene compounds discovered in the early 1950s,[149–151] and it is still a leading focus of research due to its unique properties, for example aromaticity, easy preparation, kinetic stability, low toxicity, redox activity, relative lipophilicity, and easy derivatization into ferricenium salts.[152,153] Ferrocene is the most stable metallocene, as a result of the perfect electron-pairing in the valence shells of its three moieties, obeying the 18-electron rule: the two electron-rich, aromatic cyclopentadienyl anions contains six π-electron each, and are bonded with the six valence *d*-electrons of the Fe^{2+} ion.[152]

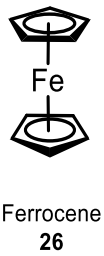

Figure 1.18. Structure of ferrocene **26**.

The reversible oxidation/reduction process of ferrocene to yield the ferrocenium cation (Fc → Fc^+) constitutes one of its main features (Scheme 1.1). This process is favoured by electron-donating substituents in ferrocene (such as alkyl groups), while it is impeded by electron-withdrawing substituents (for example, aryl groups); therefore, the oxidation potential of ferrocene is susceptible to the nature of its substituents. These redox properties of ferrocene have often been implicated in its cytotoxicity.[121,152]

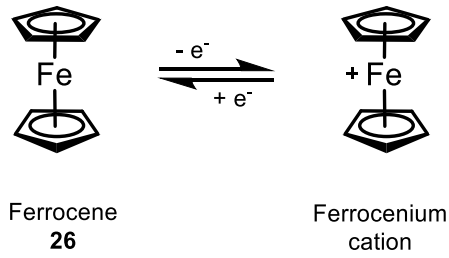

Scheme 1.1. Oxidation/reduction process of ferrocene **26**.

Ferrocene derivatives have shown diverse biological activities such as antibacterial, antifungal, antimicrobial, antiviral, and of course anticancer activity.[153–164] The first ferrocene compounds to show anti-proliferative effects were ferrocenium salts. Köpf-Maier *et al.* were the pioneers on report the cytotoxic activity of salt-like ferrocenium complexes against Ehrlich ascites tumours in 1984. The most active compounds were both picrate and trichloroacetate salts, with an optimum cure rate of 100% at a dose of 220-300 mg/kg (Figure 1.19).[165,166]

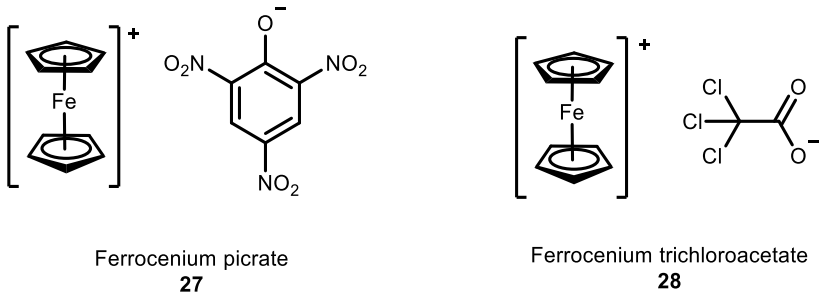

Figure 1.19. Structures of ferrocenium picrate **27** and ferrocenium trichloroacetate **28**.

More recently, Osella *et al.* reported that only ferrocenium salts could inhibit the growth of Ehrlich ascites tumour cells *in vivo*, compared to Fe^{2+} complexes which were unable to show this anticancer activity; this demonstrates that the oxidation state of the iron in the ferrocene is a significant feature to biological activity. Decamethylferricenium

tetrafluoroborate (DEMFc+) **29** was the most active compound showing antineoplastic activity against the human breast cancer cell line MCF-7, displaying an IC_{50} value of 35 μM (Figure 1.20). It has been proposed that the activity of ferrocenium salts is not based on their direct intercalation with DNA, but on their capability to generate reactive oxygen species (ROS) which cause oxidative DNA damage; this was concluded based on ^{1}H and ^{13}C NMR studies which suggest that interaction with DNA occurs mainly via an electrostatic interaction with the phosphate backbone.[167,168]

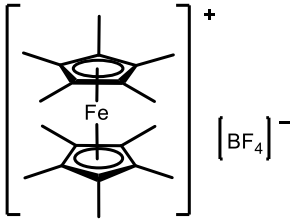

Decamethylferricenium tetrafluoroborate
(DEMFc+)
29

Figure 1.20. Structure of decamethylferricenium tetrafluoroborate (DEMFc+) **29**.

In subsequent studies, Tabbì *et al.* confirmed that DEMFc+ **29** was forming a reactive oxygenated species (ROS) as a result of its degradation in water. They suggested that a hydroxyl radical ($^{\bullet}OH$) was being generated as part of the iron-catalysed Haber-Weiss reaction followed by a Fenton reaction (Scheme 1.2). Additionally, the cytotoxic synergic effect between **29** and bleomycin **30** (Figure 1.21) was demonstrated. Bleomycin **30** is an FDA-approved antitumor drug of natural origin, usually complementary to cisplatin in chemotherapy; its mechanism of action starts with the chelation of metal ions, primarily iron. Therefore, the bleomycin activation was increased by the Fe^{2+}/Fe^{3+} species available from DEMFc+ **29** degradation.[169–171]

$$Fe^{3+} + O_2^{\bullet-} \rightarrow Fe^{2+} + O_2$$

$$Fe^{2+} + H_2O_2 \rightarrow Fe^{3+} + OH^- + {}^{\bullet}OH$$

$$\text{Net: } O_2^{\bullet-} + H_2O_2 \rightarrow O_2 + OH^- + {}^{\bullet}OH$$

Scheme 1.2. Haber-Weiss and Fenton reactions.

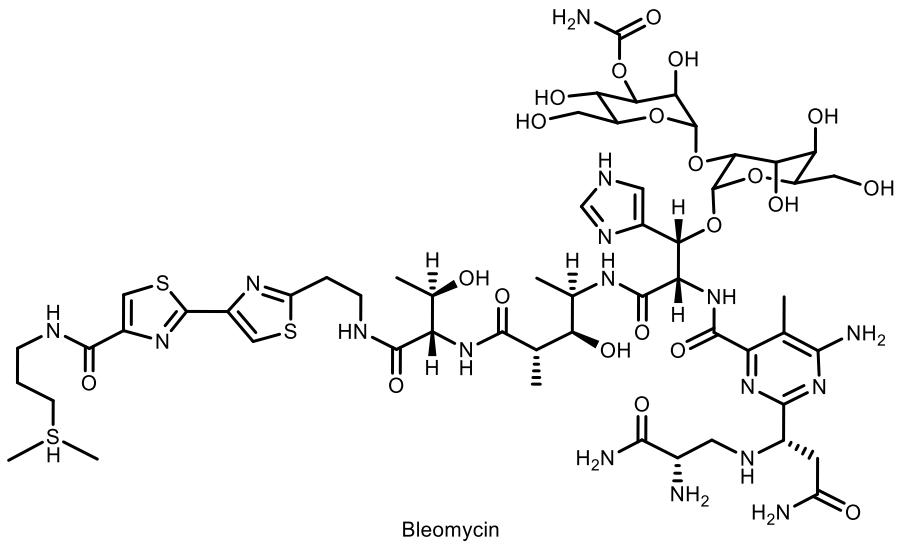

Bleomycin
30

Figure 1.21. Structure of bleomycin **30**.

The synthesis of the first azaferrocene derivatives including phosphonate groups was reported by Kowalski *et al*. These compounds were transformed into their corresponding *N*-methyl iodide salts, and compound (*N*-methyl)-2,5-dimethylazaferrocenyl phosphonate iodide **31** was found to present antimetabolic activity against HeLa human epithelioid cervical carcinoma cell line, and selectivity to this cancerous cell line compared to the non-cancerous NIH 3T3 murine embryonic fibroblast cell line. Later on, they studied the DNA scission activity of these type of compounds, finding that *N*-methyl-azaferrocene iodide **32** can induce a complete degradation *in vitro* of the DNA plasmid at their lowest concentration tested of 6.25 μM (Figure 1.22).[172,173]

(*N*-methyl)-2,5-dimethylazaferrocenyl phosphonate iodide
31

N-methyl-azaferrocene iodide
32

Figure 1.22. Structures of (*N*-methyl)-2,5-dimethylazaferrocenyl phosphonate iodide **31** and *N*-methyl-azaferrocene iodide **32**.

Since 1996, Jaouen *et al.* have published extensively on the preparation of novel functionalized ferrocene derivatives which consist of the linking of the active metabolite of drug tamoxifen **33** and ferrocene; this results in the series of ferrocifen **34**, an innovative class of complexes which combines the antiestrogenic effect of tamoxifen with the cytotoxic properties of ferrocene. The most remarkable compound is the diphenolic [3]ferrocenophane **35** (the [3] indicates the number of bridging atoms) with an IC_{50} of 0.09 μM against hormone-independent MDA-MB-231 breast cancer cell line, being considerably more potent than its non-cyclic analogue **36** (IC_{50} = 0.6 μM). Compound **35** also has an antiproliferative effect on PC-3 prostate cancer cell line, with a IC_{50} of 94 nM (Figure 1.23).[174–180]

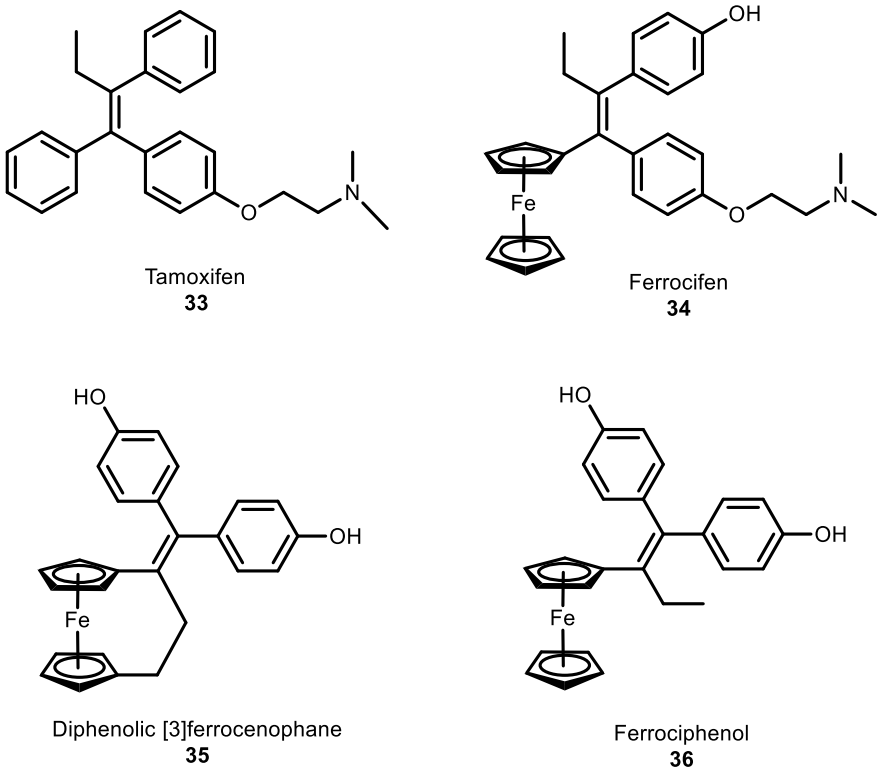

Figure 1.23. Structures of tamoxifen **33** and its ferrocenyl-analogues **34**-**36**.

1.2.3.3.1 Ferrocenyl-peptide bioconjugates

In recent years, Kenny *et al.* have reported the synthesis, characterisation and biological evaluation of several ferrocenyl-peptide bioconjugates, with interesting results as follows.

A series of *N*-(ferrocenylmethyl)benzene-carboxamide derivatives were synthesized by Kelly *et al.*[181] using standard peptide coupling procedures. By replacing hydrogen with fluorine, a well-known strategy in drug-discovery research[182], the 4-fluoro derivative compound **37** exhibited the strongest anti-proliferative activity, with an IC_{50} value of 11-14 μM on the MDA-MB-435S breast cancer cell line. In addition, a dose-dependent relationship was found since the cytotoxic activity increased as the concentration of this compound increased (Figure 1.24).

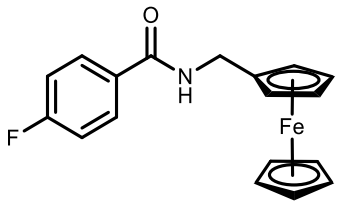

4-fluoro-*N*-(ferrocenylmethyl)benzene carboxamide
37

Figure 1.24. Structure of 4-fluoro-*N*-(ferrocenylmethyl)benzene carboxamide **37**.

Corry *et al.*[183] analysed the compound *N*-{*ortho*-(ferrocenyl)-benzoyl}-glycine ethyl ester **38**, which was tested *in vitro* against H1299 and H1299 carboplatin-resistant variant lung cancer cell lines. This compound was found to be cytotoxic with an IC_{50} value of 48 μM; the starting material, *ortho*-ferrocenyl ethyl benzoate, was totally inactive against this cell line. In this research, they also reported the synthesis of *N*-*ortho*-ferrocenyl benzoyl dipeptide esters; compound *N*-{*ortho*-(ferrocenyl)-benzoyl}-glycine-L-alanine ethyl ester **39** was the most active, with an IC_{50} value of 5.3 μM against H1299 lung cancer cell line. As observed, the addition of a second amino acid into the structure improved significantly the biological activity of the molecule (Figure 1.25).

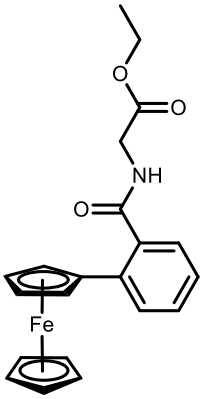

N-{*ortho*-(ferrocenyl)-benzoyl}-glycine ethyl ester
38

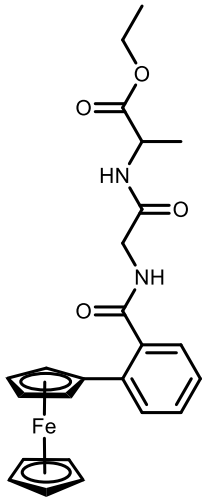

N-{*ortho*-(ferrocenyl)-benzoyl}-glycine-L-alanine ethyl ester
39

Figure 1.25. Structures of *N*-{*ortho*-(ferrocenyl)-benzoyl}-glycine ethyl ester **38** and *N*-{*ortho*-(ferrocenyl)-benzoyl}-glycine-L-alanine ethyl ester **39**.

A series of *N-meta*-ferrocenyl benzoyl dipeptide esters containing L-alanine as the first α-amino acid in the dipeptide chain were synthesized by Goel *et al*.[184] Compound *N*-{*meta*-ferrocenyl)benzoyl}-L-alanine-glycine ethyl ester **40** was found to be the most active, with an IC_{50} value of 26 μM against H1299 lung cancer cell line; whereas its corresponding *ortho*-analogue showed an IC_{50} value of 21 μM. This suggest that the orientation around the central benzoyl moiety is not a decisive aspect for biological activity (Figure 1.26).

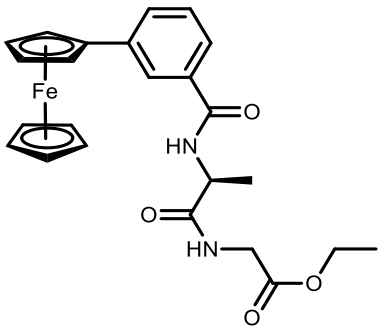

N-{*meta*-ferrocenyl)benzoyl}-L-alanine-glycine ethyl ester
40

Figure 1.26. Structure of *N*-{*meta*-ferrocenyl)benzoyl}-L-alanine-glycine ethyl ester **40**.

Subsequent studies by Corry *et al.*[185] leading to the synthesis of a series of (ferrocenyl)benzoyl dipeptide esters and its cytotoxicity against H1299 lung cancer cell line. It was concluded that an increase in alkyl chain length of the second amino acid also increases the IC_{50} values, as observed with the following examples: compounds *N*-{*meta*-(ferrocenyl)-benzoyl}-glycine-L-alanine ethyl ester **41**, and *N*-{*para*-(ferrocenyl)-benzoyl}-glycine-L-alanine ethyl ester **42** gave IC_{50} values of 4.0 and 6.6 μM against H1299 lung cancer cell line, respectively; whereas compounds *N*-{*meta*-(ferrocenyl)-benzoyl}-glycine-L-2-aminobutyric acid ethyl ester **43**, *N*-{*meta*-(ferrocenyl)-benzoyl}-glycine-L-norvaline ethyl ester **44**, and *N*-{*meta*-(ferrocenyl)-benzoyl}-glycine-L-norleucine ethyl ester **45** showed IC_{50} values of 10.5 μM, 19.1 μM and 18.9 μM, respectively (Figure 1.27).

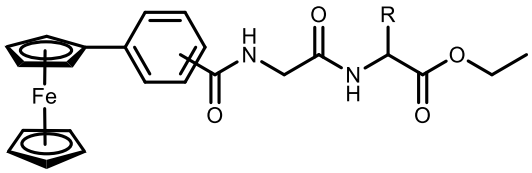

41: *m* position, R = $-CH_3$
42: *p* position, R = $-CH_3$
43: *m* position, R = $-C_2H_5$
44: *m* position, R = $-C_3H_9$
45: *m* position, R = $-C_4H_9$

Figure 1.27. Structures of *N*-(ferrocenyl)benzoyl dipeptide ethyl ester derivatives.

The synthesis of *N*-(ferrocenyl-naphthoyl) dipeptide ethyl esters was reported by Mooney *et al*.[186] In comparison with the corresponding *N*-(ferrocenyl)benzoyl derivatives, it was concluded that the replacement of the benzoyl moiety by a naphthoyl moiety linking the redox active ferrocene group to the peptide chain increased considerably the anti-proliferative effect of the molecule against H1299 cell line. Compound *N*-(6-ferrocenyl-2-naphthoyl)-glycine-L-alanine ethyl ester **46** was found to be the most active derivative of the naphthoyl series, displaying an IC_{50} value of 1.3 μM; this value is slightly lower than that found for the clinically employed anti-cancer drug cisplatin, which showed an IC_{50} value of 1.5 μM against the same cancer cell line (Figure 1.28).

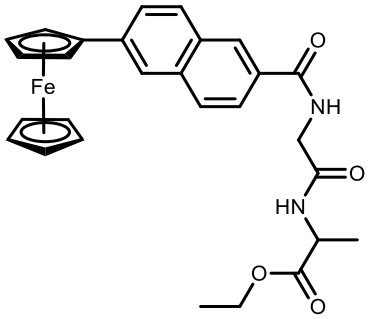

N-(6-ferrocenyl-2-naphthoyl)-glycine-L-alanine ethyl ester
46

Figure 1.28. Structure of *N*-(6-ferrocenyl-2-naphthoyl)-glycine-L-alanine ethyl ester **46**.

A series of *N*-(ferrocenyl)benzoyl tri- and tetrapeptide esters were also synthesized by Corry *et al*.[187] The anti-proliferative effects of compounds *N*-{*ortho*-(ferrocenyl)benzoyl}-glycine-glycine-glycine ethyl ester **47** and *N*-{*ortho*-(ferrocenyl)benzoyl}-glycine-glycine-glycine-glycine ethyl ester **48** were measured *in vitro* against H1299 lung cancer cell line, and both gave IC_{50} values greater than 50 μM. Therefore, it can be concluded that the biological activity decreases when the length of the peptide chain is extended, in comparison with the *N*-(ferrocenyl)benzoyl amino acid and dipeptide derivatives (Figure 1.29).

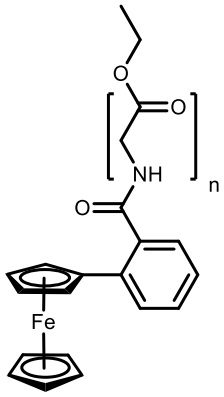

47: n = 3
48: n = 4

Figure 1.29. Structure of *N*-(ferrocenyl)benzoyl tri- and tetrapeptide esters **47** and **48**.

Mooney *et al.*[188] studied the biological activity of novel *N*-(ferrocenyl)naphthoyl amino acid and dipeptide esters and their intermediates against H1299 NSCLC and SK-MEL-28 cell lines. The intermediates failed to produce an effect in either cell line; whilst the synthesized compounds exhibited a strong anti-proliferative effect in the H1299 cell line, whereas the SK-MEL-28 cells were slightly more resistant to them. Compounds *N*-(6-ferrocenyl-2-naphthoyl)-γ-aminobutyric acid ethyl ester **49** and *N*-(6-ferrocenyl-2-naphthoyl)-glycine-D-alanine ethyl ester **50** showed a particularly high activity, with IC_{50} values of 0.62 μM and 0.33 μM on H1299, and 1.41 μM and 1.83 μM on Sk-Mel-28, respectively (Figure 1.30).

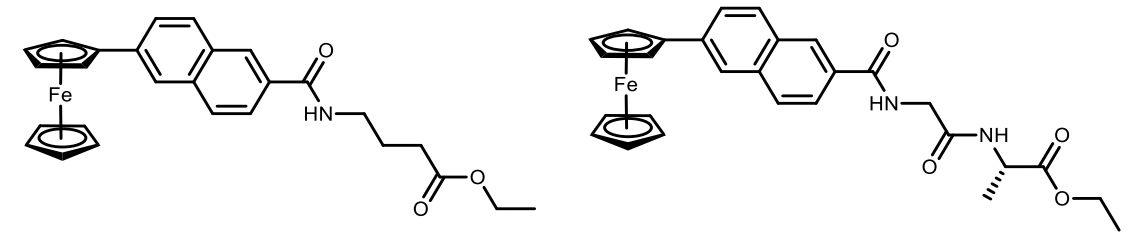

N-(6-ferrocenyl-2-naphthoyl)-γ-aminobutyric acid ethyl ester **49**

N-(6-ferrocenyl-2-naphthoyl)-glycine-D-alanine ethyl ester **50**

Figure 1.30. Structures of *N*-(6-ferrocenyl-2-naphthoyl)-γ-aminobutyric acid ethyl ester **49** and *N*-(6-ferrocenyl-2-naphthoyl)-glycine-D-alanine ethyl ester **50**.

The SAR studies of the *N*-(6-ferrocenyl-2-naphthoyl) derivatives were continued by Mooney[189]. Novel compounds *N*-(6-ferrocenyl-2-naphthoyl)-glycine-glycine ethyl ester **51** and *N*-(6-ferrocenyl-2-naphthoyl)-sarcosine-glycine ethyl ester **52** were found to be the most active, with remarkable IC_{50} values of 0.13 μM and 0.14 μM, respectively, against H1299 cancer cell line; these compounds were also found to have significant activity in the SK-MEL-28 human skin melanoma cell line, with IC_{50} values of 1.10 μM and 1.06 μM, respectively (Figure 1.31).

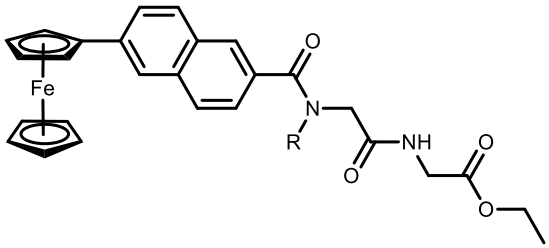

51: R = -H
52: R = -CH_3

Figure 1.31. Structures of *N*-(6-ferrocenyl-2-naphthoyl)-glycine-glycine ethyl ester **51** and *N*-(6-ferrocenyl-2-naphthoyl)-sarcosine-glycine ethyl ester **52**.

A series of *N*-(ferrocenylmethyl amino acid) fluorinated benzene carboxamide derivatives were synthesized by Butler *et al*.[190] Compound *N*-(ferrocenylmethyl-L-alanine)-3,4,5-trifluorobenzene carboxamide **53** was the most active giving an IC_{50} value of 2.4 μM against MCF-7 breast cancer cell line *in vitro* (Figure 1.32).

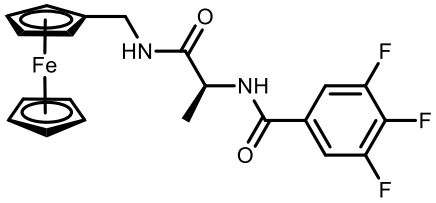

N-(ferrocenylmethyl-L-alanine)-3,4,5-trifluorobenzene carboxamide
53

Figure 1.32. Structure of *N*-(ferrocenylmethyl-L-alanine)-3,4,5-trifluorobenzene carboxamide **53**.

Butler[191] also reported the synthesis of a series of *N*-{(ferrocenyl)-benzoyl}-aminoalkanes, to analyse the substitution pattern around the aromatic benzoyl moiety and the attachment of the various aminoalkanes. The most active derivative synthesised was *N*-{*para*-(ferrocenyl)-benzoyl}-aminooctane **54**, with an IC_{50} of 1.10 μM against MCF-7 breast cancer cell line *in vitro* (Figure 1.33).

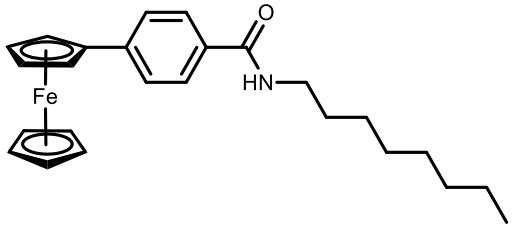

N-{*para*-(ferrocenyl)-benzoyl}-aminooctane
54

Figure 1.33. Structure of *N*-{*para*-(ferrocenyl)-benzoyl}-aminooctane **54**.

A series of *N*-{6-(ferrocenyl)ethynyl-2-naphthoyl} amino acid and dipeptide ethyl esters were prepared by Harry *et al*.[192] Compound *N*-{6-(ferrocenyl)ethynyl-2-naphthoyl}-sarcosine-L-alanine ethyl ester **55** was found to be the most active derivative, with an IC_{50} value of 3.2 μM against H1299 NSCLC cell line. It can be concluded that the incorporation of a multiple bond between the ferrocene and naphthoyl moieties had a negative effect in the biological activity of the molecule (Figure 1.34).

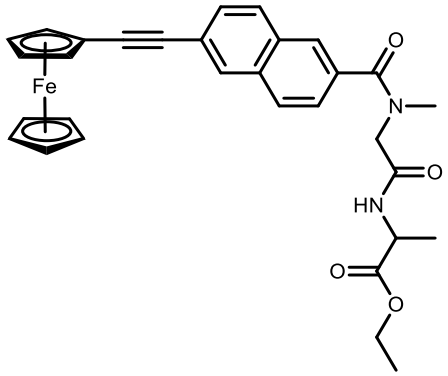

N-{6-(ferrocenyl)ethynyl-2-naphthoyl}-sarcosine-L-alanine ethyl ester
55

Figure 1.34. Structure of *N*-{6-(ferrocenyl)ethynyl-2-naphthoyl}-sarcosine-L-alanine ethyl ester **55**.

Subsequent SAR studies by Harry *et al.*[193] led to the synthesis of 1-alkyl-1′-*N*-*para*-(ferrocenyl) benzoyl dipeptide esters by conventional peptide chemistry. It was observed that the alkylation of the cyclopentadiene ring increases the antineoplastic activity of the molecule, but also this activity decreases with an increase of the alkyl group size (propyl < ethyl < methyl). These derivatives exhibited cytotoxic effects on H1299 human lung carcinoma cell line, being the compound 1-methyl-1′-*N*-{*para*-(ferrocenyl)-benzoyl}-glycine-L-alanine ethyl ester **56** the most active derivative with an IC_{50} of 4.5 μM, more cytotoxic *in vitro* than the clinically employed anticancer drug carboplatin which was found to have an IC_{50} of 10.0 μM (Figure 1.35).

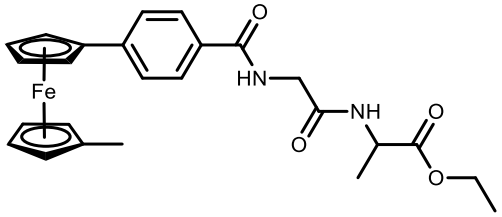

1-methyl-1'-*N*-{*para*-(ferrocenyl)-benzoyl}-glycine-L-alanine ethyl ester
56

Figure 1.35. Structure of 1-methyl-1′-*N*-{*para*-(ferrocenyl)-benzoyl}-glycine-L-alanine ethyl ester **56**.

The synthesis of a series of *N*-{*para*-(ferrocenyl)cinnamoyl} amino acid and dipeptide derivatives was reported by Tiedt[194]; these compounds did not show significant activity at 1 μM on HT144 human malignant melanoma cell line, hence no IC_{50} values were determined. In this research, a series of *N*-(6-ferrocenyl-2-naphthoyl) amino acid and dipeptide derivatives were also synthesized; the compound *N*-(6-ferrocenyl-2-

naphthoyl)-glycine-glycine methyl ester **57** was the most active derivative, showing an IC_{50} value of 0.2 μM on A549, LOX-IMVI and HT-144, and 0.3 μM on H1299 and Malme-3M cell lines. This demonstrated that naphthoyl moiety plays a key role on the antineoplastic activity of the molecule, in comparison with the cinnamoyl linker studied (Figure 1.36).

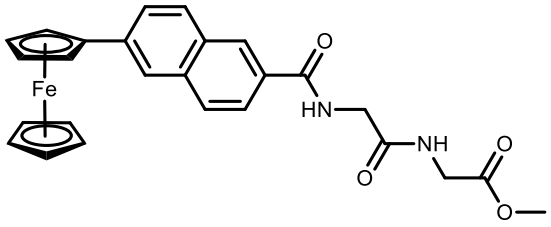

N-(6-ferrocenyl-2-naphthoyl)-glycine-glycine methyl ester
57

Figure 1.36. Structure of *N*-(6-ferrocenyl-2-naphthoyl)-glycine-glycine methyl ester **57**.

The most recent synthesis of ferrocenyl bioconjugates was achieved by Lu[195]; she synthesized two series of compounds: *N*-(1′-alkyl-6-ferrocenyl-2-naphthoyl) amino acid and dipeptide esters **130**-**143**, and *N*-(ferrocenylmethylamino acid)-fluorinated-benzene carboxamide derivatives **144**-**154** (Figure 1.37). The biological evaluation of these products was performed during this research and are presented in Sections 3.4 and 3.5, respectively.

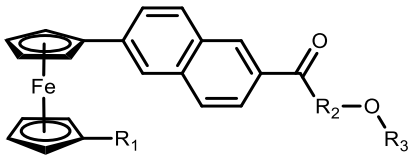

R_1 = CH_3, C_2H_5
R_2 = GABA, Gly-Gly, Gly-L-Ala, Gly-D-Ala
R_3 = CH_3, C_2H_5

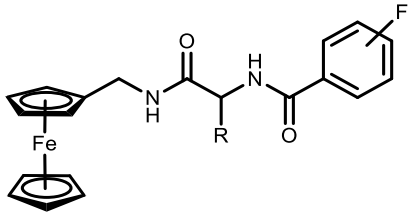

R = -H, -CH_3, -CH_2CH_3, -$CH_2CH_2CH_3$, -$CH_2(CH_2)_2CH_3$, -$CH_2CH(CH_3)_2$, -$CH_2CH_2SCH_3$, -Ph

Figure 1.37. General structures of *N*-(1′-alkyl-6-ferrocenyl-2-naphthoyl) amino acid and dipeptide esters **130**-**143**, and *N*-(ferrocenylmethylamino acid)-fluorinated-benzene carboxamide derivatives **144**-**154**.

1.3 Conclusions

Cancer is a destructive disease that can affect any part of the body, thus being a major cause of death worldwide. The resistance of cancer cells and the presence of side effects are common problems on current conventional therapies; hence further research for treatment development is necessary due to the increasing prevalence of these drug resistant cancers. Platinum coordination compounds, represented by cisplatin and derivatives, are essential agents used in cancer chemotherapy. Due to their proven activity against a variety of tumours, several research initiatives in the field of bioorganometallic chemistry have merged to identify other metallodrugs with possible antineoplastic activity.[116] Consequently, the approach of rational drug design has been extended to the development of non-platinum anticancer drugs, and a large number of such complexes have been developed.

Ferrocene has been extensively used in medicinal chemistry over the last decades, and diverse applications have been proposed mainly because ferrocene is a stable, non-toxic compound with redox properties.[159] The anticancer effectiveness of iron complexes was first reported in ferrocenium salts, and was attributed to their capability to form reactive oxygen species, inducing oxidative DNA damage.[196] In recent years, Kenny *et al.* have reported several series of ferrocene derivatives with antineoplastic activity, researching the SAR by modifying each moiety of their molecules.[181,183–195] These results suggest that ferrocenyl complexes are promising anticancer agents worthy of future therapeutic analysis.

The aim of this research is to develop novel ferrocenyl derivatives for use as potential anticancer agents. The strategy is to analyse the SAR to lead a rational design of novel compounds, based on the preceding studies of ferrocenyl bioconjugates which have been described earlier. Previous *in vitro* experiments by Kenny *et al.* concluded that both *N*-{(ferrocenyl)benzoyl} and *N*-{(ferrocenyl)naphthoyl} derivatives exhibit antineoplastic activity against H1299 and SK-MEL-28 cancer cell lines. In addition, it was determined that the incorporation of a multiple bond between the ferrocene and naphthoyl moieties had a negative effect in the biological activity of the molecule. Furthermore, it was also shown that the biological activity decreases when the length of the peptide chain is extended.[183,185,187–189,192] From all these studies, the most active compounds are summarised in Table 1.4.

Table 1.4. IC_{50} values of the most active ferrocenyl bioconjugates.

Compound name	No.	H1299 [μM]	SK-MEL-28 [μM]
Cisplatin	**15**	1.50 ± 0.10	-
N-(6-ferrocenyl-2-naphthoyl)-glycine-glycine ethyl ester	**51**	0.13 ± 0.02	1.10 ± 0.13
N-(6-ferrocenyl-2-naphthoyl)-sarcosine-glycine ethyl ester	**52**	0.14 ± 0.02	1.06 ± 0.05
N-(6-ferrocenyl-2-naphthoyl)-glycine-D-alanine ethyl ester	**50**	0.33 ± 0.02	1.83 ± 0.04
N-(6-ferrocenyl-2-naphthoyl)-γ-aminobutyric acid ethyl ester	**49**	0.62 ± 0.07	1.41 ± 0.04
N-(6-ferrocenyl-2-naphthoyl)-glycine-L-alanine ethyl ester	**46**	1.30 ± 0.10	3.74 ± 0.37

The primary objective of this work is to continue the exploration of the SAR in the ferrocenyl derivatives to identify potential candidates for biological studies with increased activity and solubility. To help with the identification of specific biological targets, the best strategy is to carry out different series of synthesis to identify the most favourable structural features which enhance both antineoplastic activity and selectivity to cancer cells. This research work proposes to generate a series of analogues of the previously reported ferrocenyl bioconjugates by modification of each moiety, as outlined in Chapter 2.

C H A P T E R 2

2 Synthesis and structural characterisation of novel heterocyclic functionalised ferrocenyl derivatives

My contribution to Chapter 2 was the synthesis of the novel heterocyclic functionalised ferrocenyl derivatives **99**-**120** and their starting materials, following a number of protocols already established within Dr. Peter Kenny's research group at DCU. I then proceeded to characterise them by a range of spectroscopic techniques, such as NMR (^{1}H, ^{13}C, DEPT-135, COSY, HSQC, HMBC), IR and UV-Vis. All these experiments were carried out at Laboratory X249 Organic Research – School of Chemical Sciences – Faculty of Sciences and Health – Dublin City University (Dublin, Ireland) under the supervision of Dr. Peter T. M. Kenny.
Mass spectrometry studies were carried out by Dr. Dilip Rai at Teagasc Food Research Centre Ashtown (Ireland). X-rays crystallography studies were conducted by Prof. Vickie McKee at University of Southern Denmark (Denmark). Elemental analysis were carried out by Dr. Mayra A. Hernández-López at Instituto Tecnológico y de Estudios Superiores de Monterrey (Mexico).

2.1 Project rationale

The main purpose of this work is to continue the exploration of the SAR in the ferrocenyl derivatives to identify potential candidates for biological studies with increased activity and solubility. The ferrocenyl bioconjugates previously reported[181,183–195] consist of three key moieties, as observed in Figure 2.1:

1. A redox-active centre.
2. A conjugated linker.
3. An amino acid or dipeptide ester chain.

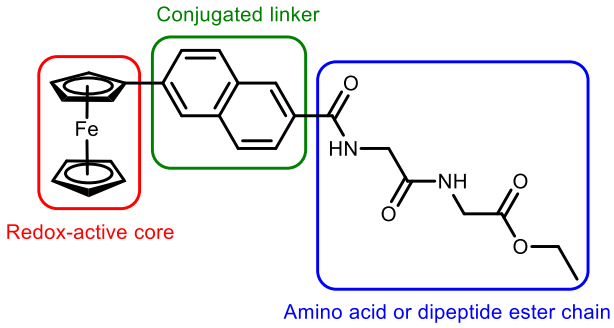

Figure 2.1. General structure of ferrocenyl amino acid or dipeptide derivatives.

To help with the identification of specific biological targets, the best strategy is to carry out different series of synthesis to identify the most favourable structural features which enhance both antineoplastic activity and selectivity to cancer cells. This research work proposes to generate a series of analogues of the previously reported ferrocenyl bioconjugates by modification of each moiety as follows:

2.1.1 Variations on the ferrocene core

The first region for possible modification is the redox active moiety. The incorporation of a metallocene other than ferrocene is an alternative for structural modification. Ruthenium undergoes electrochemical oxidation more readily than ferrocene, thus ruthenocene is a common candidate for replacement as low oxidation potential is considered as an important feature for antiproliferative activity.[152,197] Nevertheless, the oxidation of ruthenocene is a controversial reaction as it has been reported as both a one-electron and a two-electron irreversible process. In fact, a loss of activity against ER(-) breast cancer cell line was reported by Pigeon *et al.* when the ferrocenyl moiety of the previously prepared tamoxifen derivatives was replaced with ruthenocene. The reversible redox

properties exhibited by the previously studied ferrocenyl amino acid and dipeptide derivatives are believed to be crucial in the mode of action of these type of compounds, therefore it was concluded that ruthenocene analogues are unlikely to present the same anticancer activity.[152,198,199]

Furthermore, a study contrasting the anticancer activity of *N*-(6-ferrocenyl-2-naphthoyl)-glycine-glycine ethyl ester **51** and its non-organometallic analogue *N*-(2-naphthoyl)-glycine-glycine ethyl ester **58** (Figure 2.2) against H1299 and SK-MEL-28 cell lines has shown that the ferrocene moiety is key for antiproliferative effect. At a concentration of 1 μM, compound **51** exhibited a strong inhibition of the cell viability whilst **58** failed to produce a significant effect in either cell line. The percentages of cell growth for **58** were 87.6 ± 18.4% for H1299 cell line, and 95.6 ± 10.9% for SK-MEL-28 cell line.[188]

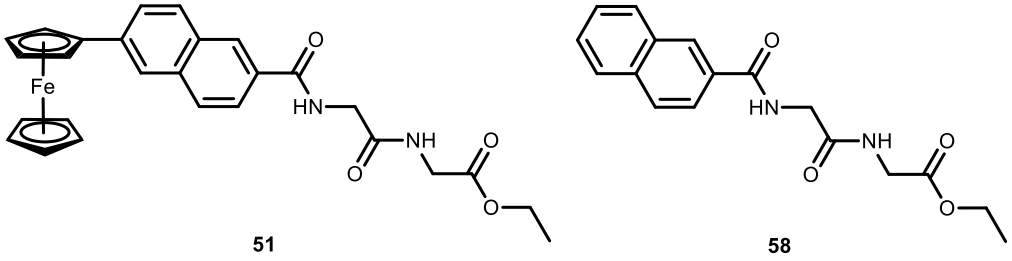

Figure 2.2. Structures of *N*-(6-ferrocenyl-2-naphthoyl)-glycine-glycine ethyl ester **51** and *N*-(2-naphthoyl)-glycine-glycine ethyl ester **58**.

Still, the ferrocene itself allows a further modification by di-substitution. Previous studies have shown that the alkylation of the cyclopentadiene ring increases the antineoplastic activity of the molecule, but also this activity decreases with an increase of the alkyl group size (propyl < ethyl < methyl).[193] In this research, the ethyl group was maintained for a series of derivatives, hence two type of ferrocenyl moieties were studied (Figure 2.3).

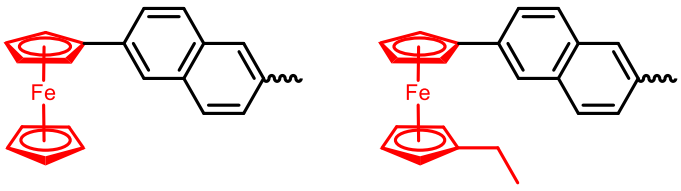

Figure 2.3. Variations on the ferrocene moiety.

2.1.2 Variations on the conjugated linker

Many aromatic conjugated systems could be coupled to the ferrocene core. The degree of conjugation and the orientation represent important structural features that can be varied depending on the choice of linker. In this research, the linkers studied were naphthoyl, benzoyl and cinnamoyl moieties (Figure 2.4).

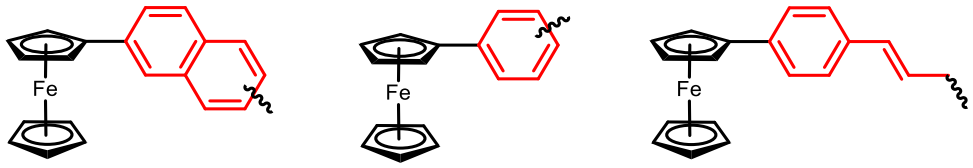

Figure 2.4. Variations on the conjugated linker.

Different orientations were investigated in the above linkers. The *ortho*, *meta* and *para* positions were studied for benzoyl derivatives; and *para* position for cinnamoyl derivatives. In the case of naphthoyl series, a search of commercially available chemicals led to three disubstituted naphthalene starting materials: 6-amino-2-naphthoic acid **59**, 3-amino-2-naphthoic acid **67** and 1,5-diaminonaphthalene **83**.

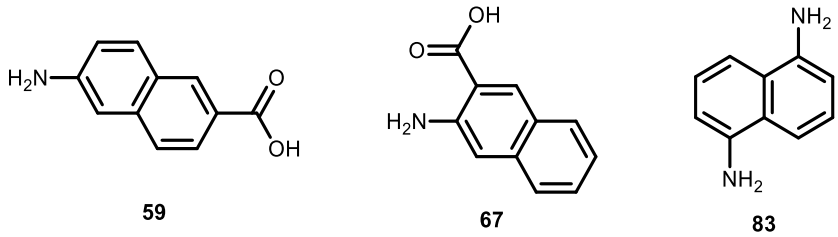

59 **67** **83**

Figure 2.5. Starting materials for naphthoyl series.

2.1.3 Variations on the amino acid or dipeptide chain

The amino acid or dipeptide ester chain moiety offers an excellent option for introducing diversity into this series of ferrocenyl derivatives. As stated before, the biological activity decreases when the length of the peptide chain is extended to tri- or tetrapeptides;[187] hence, longer chains are not an option for SAR analysis.

As most of the 20 essential α-amino acids have been already studied at different stages of the ferrocenyl bioconjugates synthesis,[181,183–195] a further exploration of moieties other than amino acids were considered in this SAR study. Previous research indicated that antineoplastic activity is higher when small α-amino acids such as glycine and L-alanine are used.[197] Therefore, the use of short amino cyclic molecules such as

aminopyridine, benzylamine or cyclohexylamine is an interesting approach never investigated before in ferrocenyl bioconjugates and represents an innovative variety for ferrocenyl derivatives (Figure 2.6).

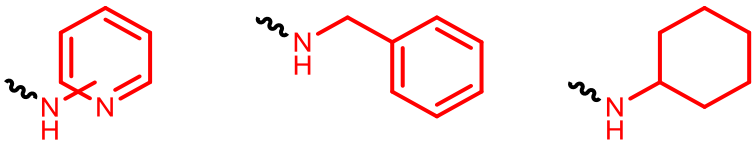

Figure 2.6. Variations on the amino acid or dipeptide ester chain.

2.2 The synthesis of novel heterocyclic functionalised ferrocenyl derivatives

2.2.1 Introduction

Previous studies have shown the importance of a conjugated linker in the molecule, as it is thought it can lower the oxidation potential of the ferrocene core.[152,197] For that reason, three different conjugated moieties (naphthoyl, benzoyl and cinnamoyl) were used in this study to investigate their effects on biological activity. The series of *N*-(6-ferrocenyl-2-naphthoyl) (Scheme 2.1), *N*-(3-ferrocenyl-2-naphthoyl) (Scheme 2.2), *N*-(ferrocenyl)benzoyl (Scheme 2.3) and *N*-{*para*-(ferrocenyl)cinnamoyl} (Scheme 2.4) derivatives were prepared via standard peptide coupling methods using *N*-(3-dimethylaminopropyl)-*N*′-ethylcarbodiimide hydrochloride (EDC) and *N*-hydroxysuccinimide (NHS) coupling protocol. A solution of the appropriate ferrocenyl carboxylic acid in dichloromethane (CH_2Cl_2) at 0 °C was treated with EDC, NHS and triethylamine (Et_3N). An equimolar amount of the required amine reagent was then added to this solution with stirring. The procedure is similar to that used for the synthesis of the previous ferrocenyl dipeptide esters in Dr. Peter Kenny's research group.[181,183–195]

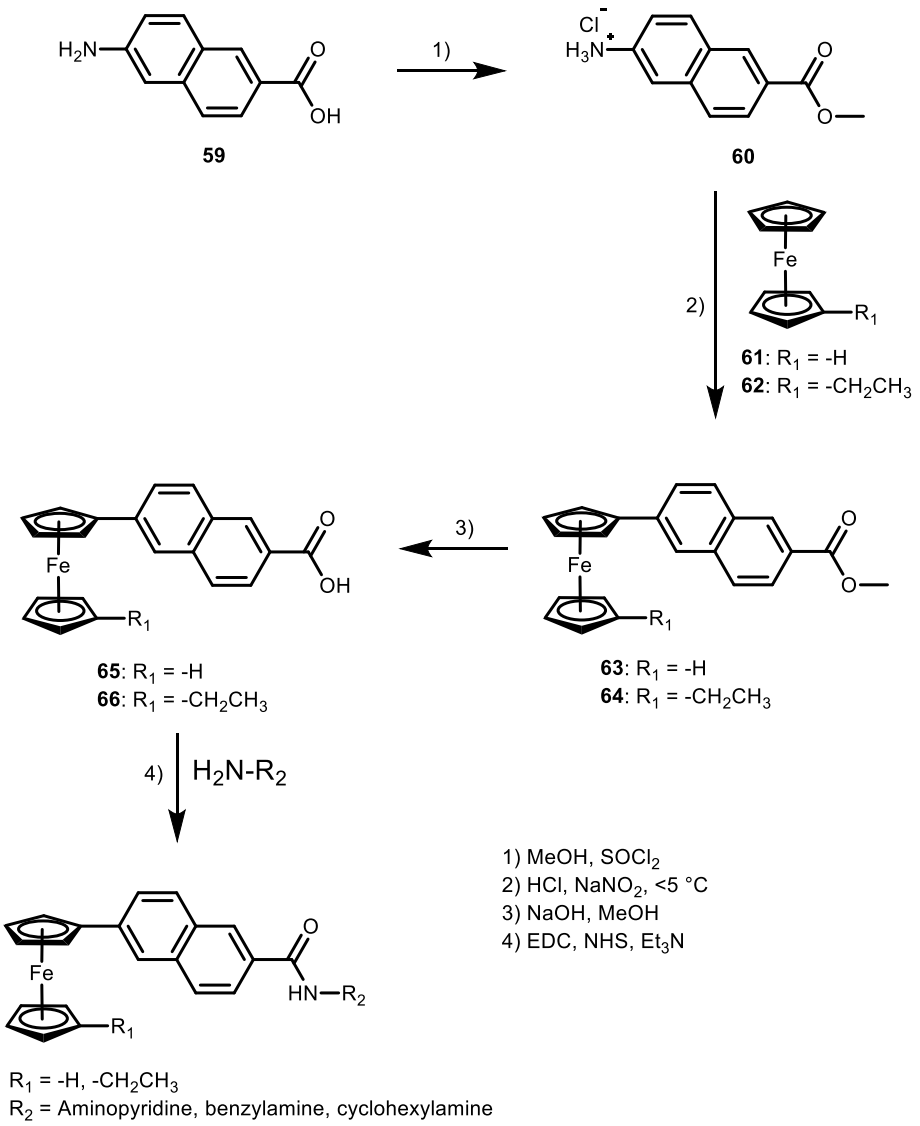

Scheme 2.1. The general reaction scheme for the synthesis of *N*-(6-ferrocenyl-2-naphthoyl) derivatives.

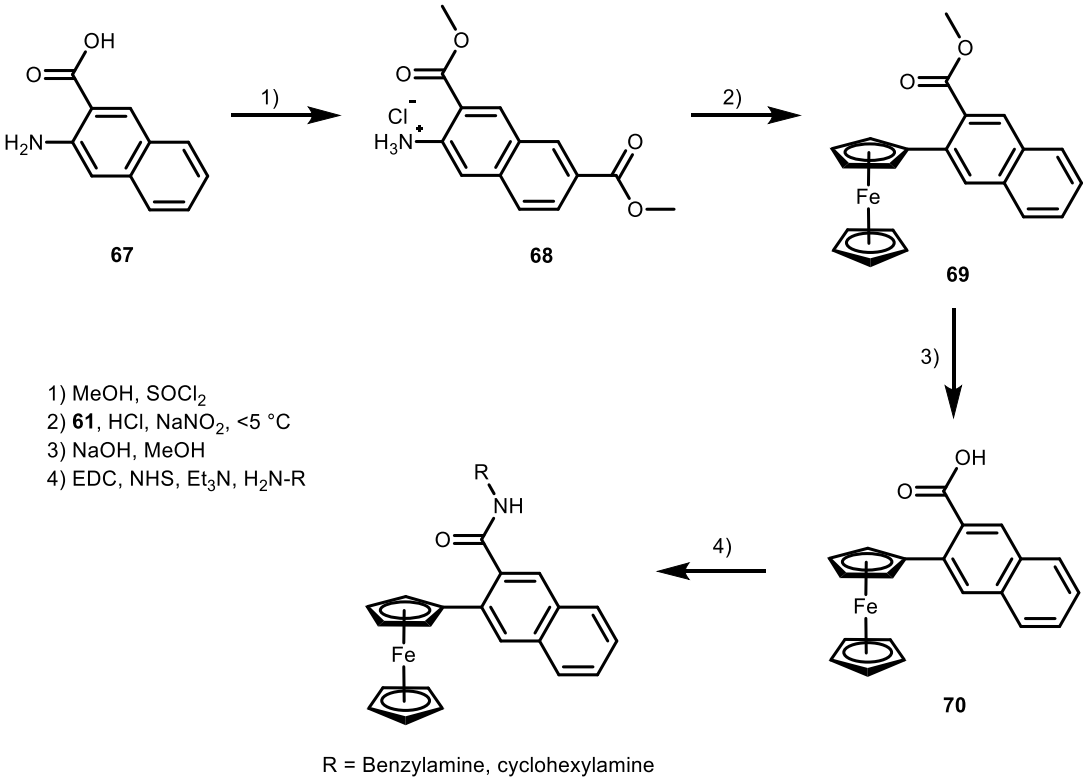

Scheme 2.2. The general reaction scheme for the synthesis of *N*-(3-ferrocenyl-2-naphthoyl) derivatives.

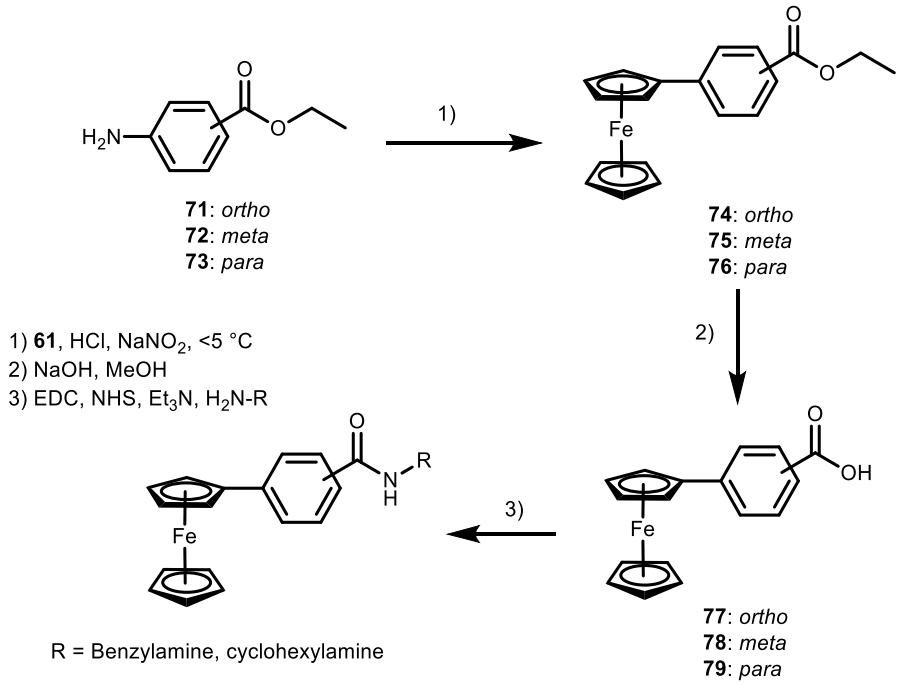

Scheme 2.3. The general reaction scheme for the synthesis of *N*-(ferrocenyl)benzoyl derivatives.

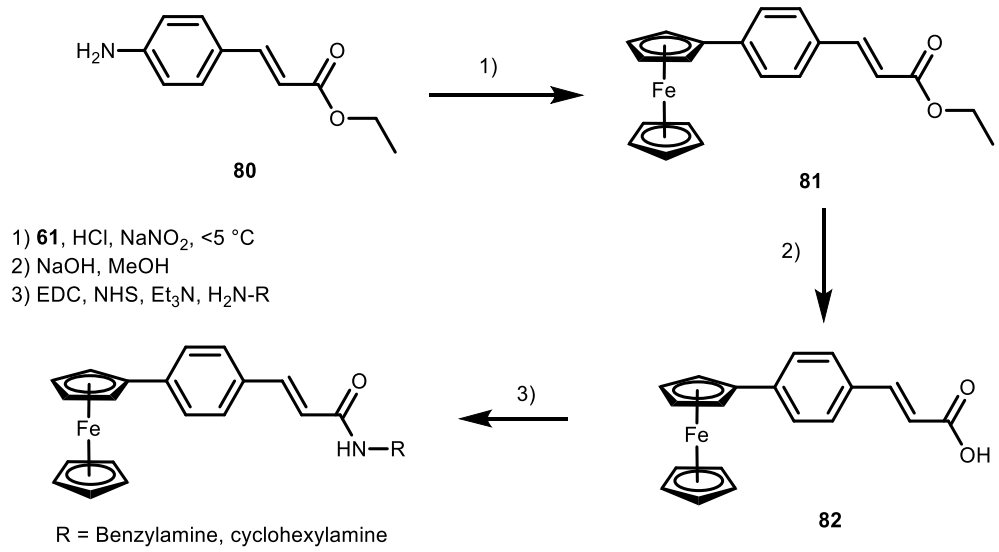

Scheme 2.4. The general reaction scheme for the synthesis of *N*-{*para*-(ferrocenyl)cinnamoyl} derivatives.

2.2.2 Preparation of ethyl ferrocene 62

The synthesis of the starting material ethyl ferrocene **62** was achieved through the reductive deoxygenation of the commercially available acetylferrocene **87** via the combined action of lithium aluminium hydride ($LiAlH_4$) and the use of a strong Lewis acid such as aluminium trichloride ($AlCl_3$) in diethyl ether, as shown in Scheme 2.5. The desired alkylated ferrocene **62** was obtained with a percentage yield of 74%. The procedure is similar to that used for the synthesis of the previous ferrocenyl dipeptide esters in Dr. Peter Kenny's research group.[192,193,195]

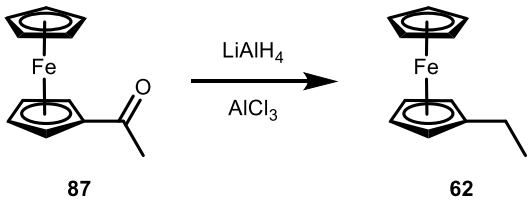

Scheme 2.5. Synthesis of ethyl ferrocene **62**.

2.2.3 Esterification of carboxylic acids

The ester group was proposed to protect the carboxylic acid group present in the starting materials 6-amino-2-naphthoic acid **59** and 3-amino-2-naphthoic acid **67**. Ester group can be formed via methanol (MeOH) and thionyl chloride ($SOCl_2$), yielding compound 6-(methoxycarbonyl)naphthalen-2-aminium chloride **60** or compound 3-(methoxycarbonyl)naphthalen-2-aminium chloride **68** (Scheme 2.6). The procedure is similar to that used for the synthesis of the previous ferrocenyl dipeptide esters in Dr. Peter Kenny's research group.[186,188,189,194,195]

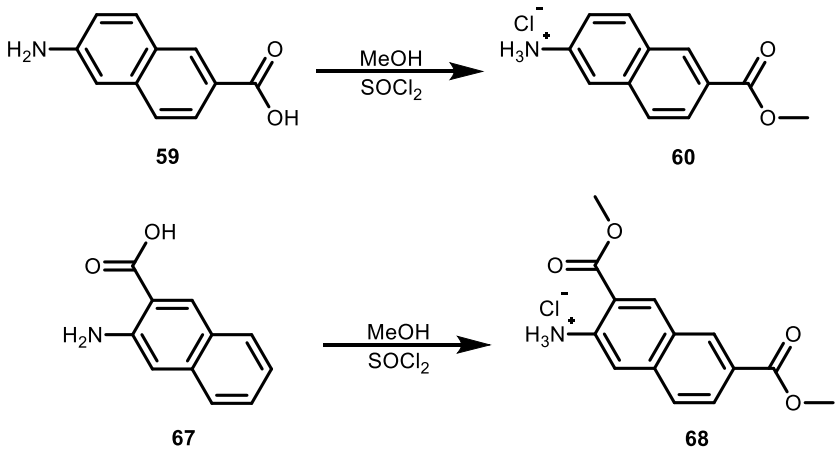

Scheme 2.6. Esterification of carboxylic acids **59** and **67** using methanol and thionyl chloride.

This is a two-step reaction. Firstly, the 6-amino-2-naphthoic acid **59** reacts with thionyl chloride ($SOCl_2$) to generate a carboxylic acyl chloride (Scheme 2.7). This is a useful reaction because the resulting carboxylic acyl chloride is a versatile and very reactive compound; these are not generally synthetic targets, but rather intermediates which are useful in the synthesis of other carboxylic acid derivatives such as the desired ester 6-(methoxycarbonyl)naphthalen-2-aminium chloride **60**.[200]

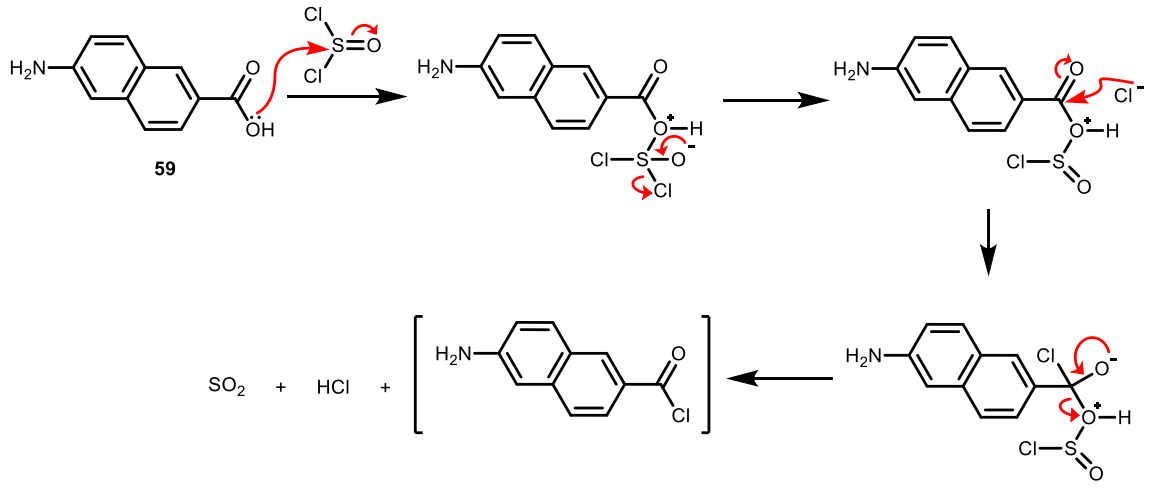

Scheme 2.7. Acid chloride formation from 6-amino-2-naphthoic acid **59**.

Secondly, the acyl chloride reacts instantly with methanol (MeOH) in a very exothermic reaction via nucleophilic addition/elimination reaction (Scheme 2.8). HCl is a subproduct in both reactions, and that is the reason why the amine group appears as its protonated form in the final product 6-(methoxycarbonyl)naphthalen-2-aminium chloride **60**.[201]

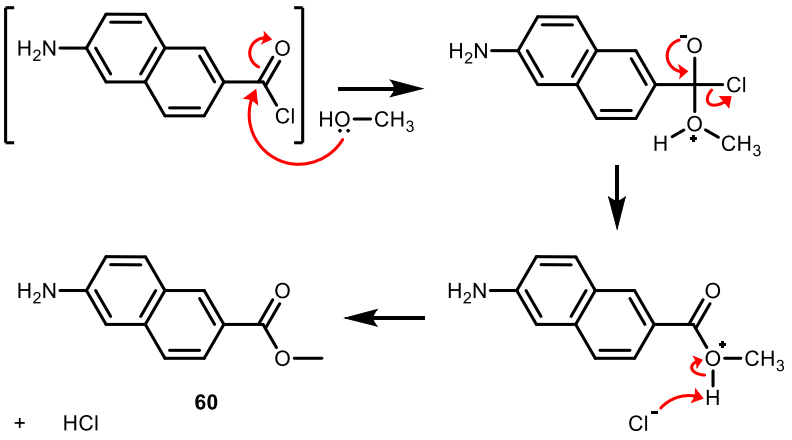

Scheme 2.8. Reaction mechanism between acid chloride and methanol.

The 3-amino-2-naphthoic acid **67** follows the same mechanism to yield the 3-(methoxycarbonyl)naphthalen-2-aminium chloride **68**.

2.2.4 Introduction of the ferrocenyl moiety via diazonium coupling

The appropriate carboxylate ester was treated with sodium nitrite ($NaNO_2$) in presence of hydrochloric acid (HCl) at a temperature below 5 °C to yield the corresponding diazonium salt, which then reacts *in situ* with the ferrocene reagent (**61** or **62**) via electrophilic aromatic substitution to generate the analogous ferrocenyl carboxylate, as shown in Scheme 2.9 for 6,2-naphthoyl series. The procedure is similar to that used for the synthesis of the previous ferrocenyl dipeptide esters in Dr. Peter Kenny's research group.[181,183–195]

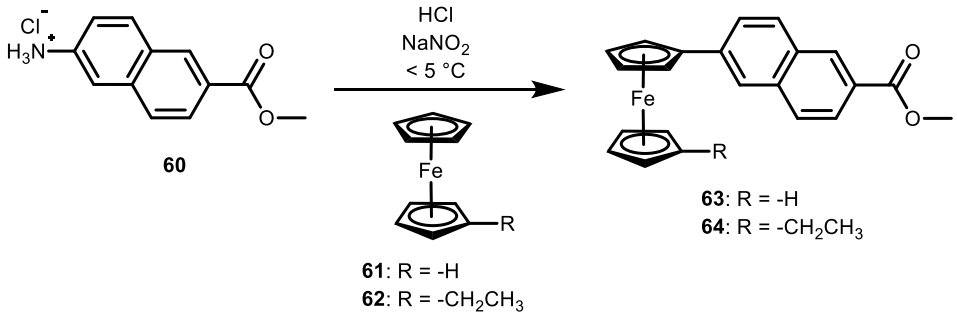

60

61: R = -H
62: R = -CH_2CH_3

63: R = -H
64: R = -CH_2CH_3

Scheme 2.9. Diazonium coupling reaction of 6-(methoxycarbonyl)naphthalen-2-aminium chloride **60** with ferrocene **61** or ethyl ferrocene **62**.

The carboxylate esters **68**, **71**-**73** and **80** were coupled to ferrocene **61** using the same protocol as above, yielding the ferrocenyl carboxylates shown in Figure 2.7.

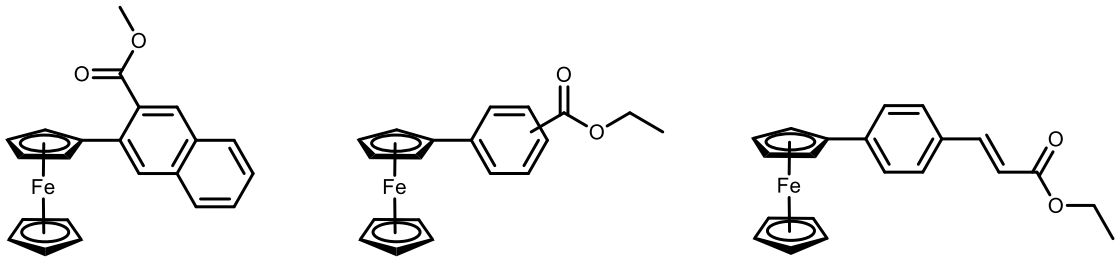

69

74: *ortho*
75: *meta*
76: *para*

81

Figure 2.7. Products of diazonium coupling reaction of carboxylate esters **68**, **71**-**73** and **80** with ferrocene **61**.

The reaction mechanism for the diazonium coupling using 6-(methoxycarbonyl)naphthalen-2-aminium chloride **60** is shown in Scheme 2.10. The diazonium coupling reactions of the other carboxylate esters follow the same mechanism.

The diazotization process starts with the treatment of the anion from $NaNO_2$ with HCl at temperature below 5 °C, producing the first intermediate nitrous acid because of the protonation of nitrite anion. The next intermediate is formed as a result of a second protonation to yield the nitrogen electrophile cation NO^+ after a molecule of water is lost. This NO^+ is then attacked by the alone pair of electrons in the amine group of **60**, to generate the conjugated diazonium salt with the presence of a chloride anion (Scheme 2.10).

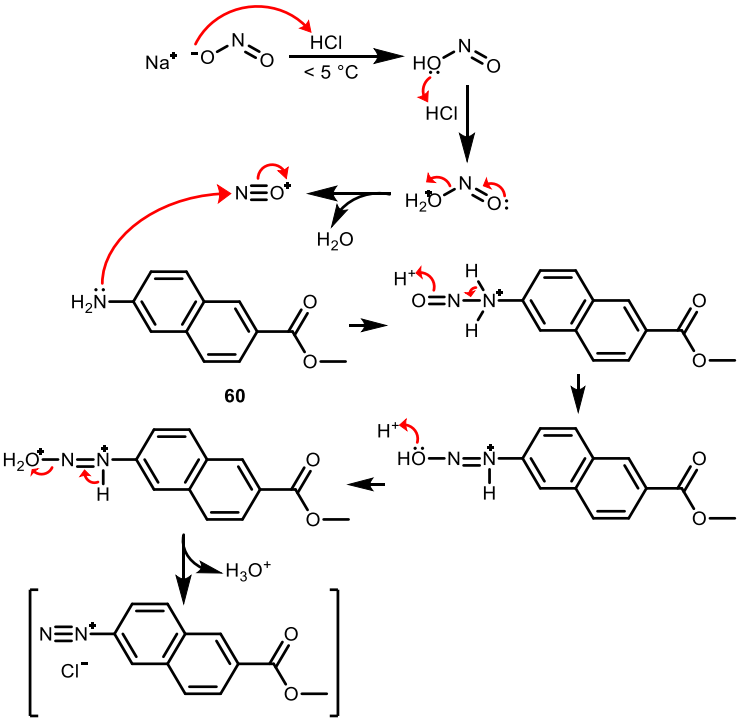

Scheme 2.10. Diazonium salt formation from 6-(methoxycarbonyl)naphthalen-2-aminium chloride **60**.

The diazonium salt decomposes when exposed to temperatures above 5 °C, resulting in the formation of an aryl carbocation and nitrogen gas (N_2). Ferrocene reagent **61** or **62** then can react *in situ* with this unstable aryl carbocation formed to yield the corresponding naphthoate **63** or **64** (Scheme 2.11).

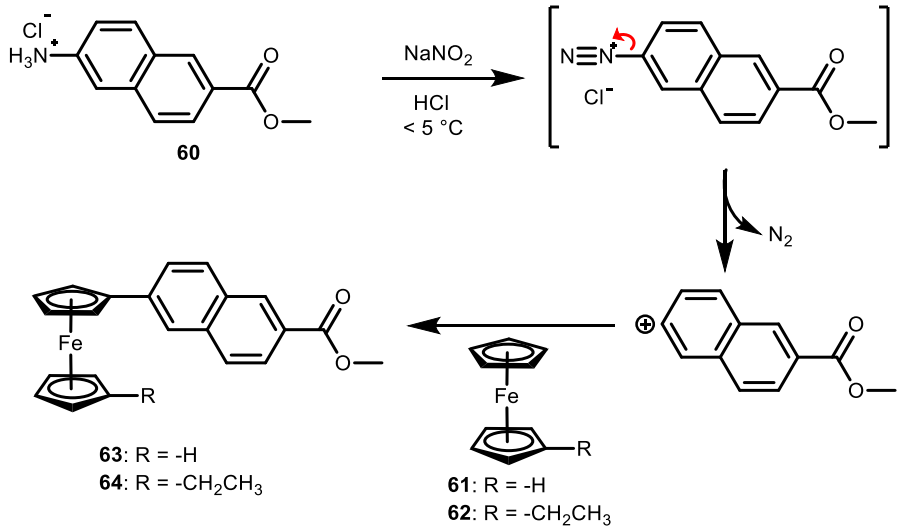

Scheme 2.11. Reaction mechanism of the diazonium coupling between 6-(methoxycarbonyl)naphthalen-2-aminium chloride **60** and ferrocene **61** or ethyl ferrocene **62**.

2.2.5 Base hydrolysis of esters

The ester group of the corresponding ferrocenyl esters can be effectively removed by base hydrolysis to yield the subsequent ferrocenyl carboxylic acid, as shown in Scheme 2.12 for ferrocenyl naphthoates **63** and **64**. The procedure is similar to that used for the synthesis of the previous ferrocenyl dipeptide esters in Dr. Peter Kenny's research group.[183–189,192–195]

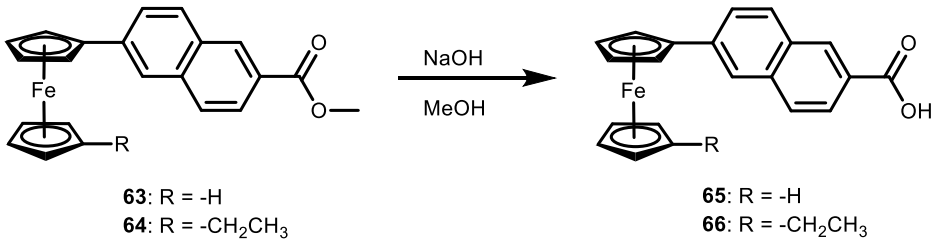

Scheme 2.12. Base hydrolysis of ferrocenyl naphthoates **63** and **64**.

The base hydrolysis of the ferrocenyl esters **69**, **74**-**76** and **81** using the same protocol as above yielded the ferrocenyl carboxylic acids shown in Figure 2.8.

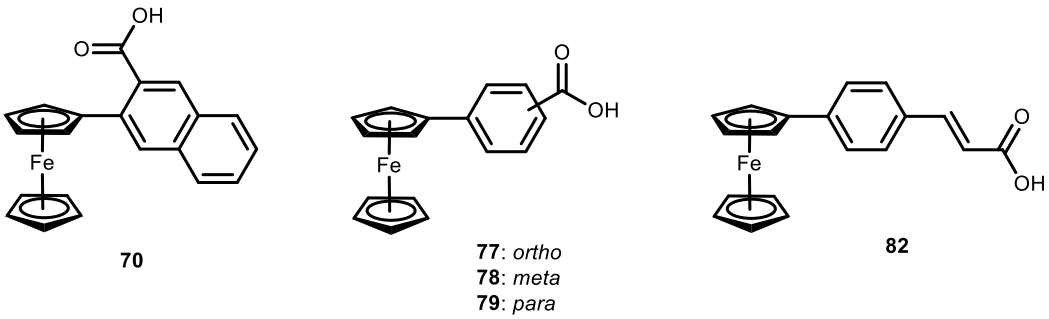

Figure 2.8. Products of base hydrolysis of ferrocenyl esters **69**, **74**-**76** and **81**.

This is the usual method for hydrolysing esters. Unlike the reversible hydrolysis under acidic conditions, hydrolysis under alkali conditions is a one-way reaction and the products are easier to separate.[202] The reaction mechanism for the base hydrolysis of methyl 6-ferrocenyl-2-naphthoate **63** is explained below; and the base hydrolysis reactions of the other ferrocenyl esters follows the same mechanism. Base hydrolysis is a two steps reaction: the first product generated is the sodium salt; then this intermediate can be easily transformed into the carboxylic acid itself by adding an excess of a strong acid such as hydrochloric acid (HCl), as shown in as shown in Scheme 2.13.

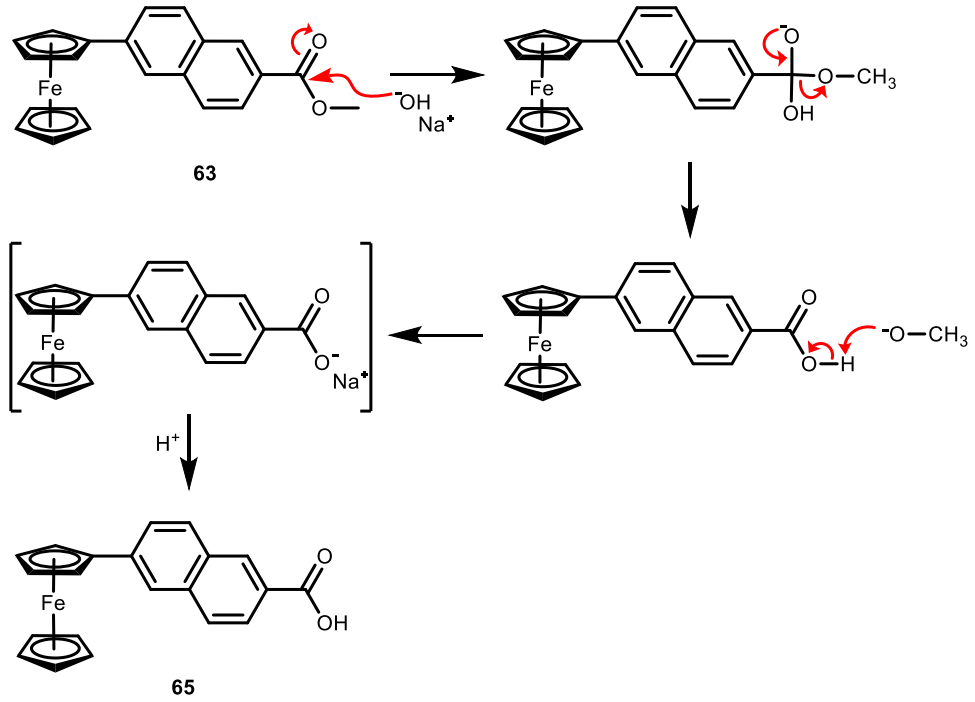

Scheme 2.13. Reaction mechanism of the base hydrolysis of methyl 6-ferrocenyl-2-naphthoate **63**.

2.2.6 Introduction of the amino moieties via EDC/NHS coupling

The last step was the introduction of the desired amino moiety into the corresponding ferrocenyl carboxylic acids, which can be achieved by the condensation of the carboxylic acid with the amino group of the required reagent to generate an amide bond. Standard methods of EDC/NHS coupling were employed for this purpose, as shown in Scheme 2.14 for the ferrocenyl 6,2-naphthoyl series. The procedure is similar to that used for the synthesis of the previous ferrocenyl dipeptide esters in Dr. Peter Kenny's research group.[181,183–195]

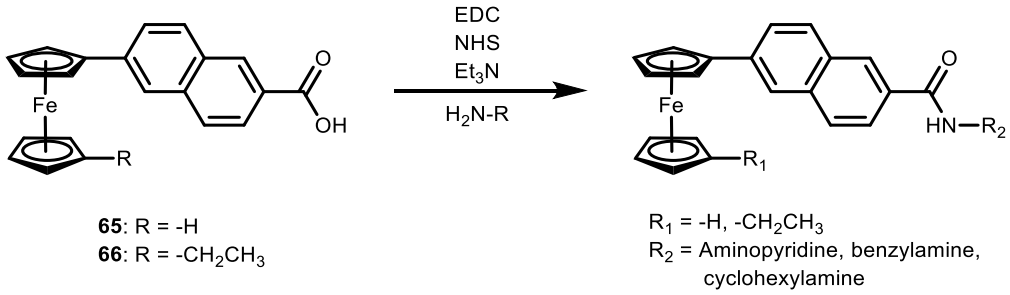

Scheme 2.14. Introduction of amino moieties into ferrocenyl naphthoic acids **65** and **66**.

The EDC/NHS coupling of the ferrocenyl carboxylic acids **70**, **77**-**79** and **82** with the corresponding amines yielded the final products with general structures shown in Figure 2.9.

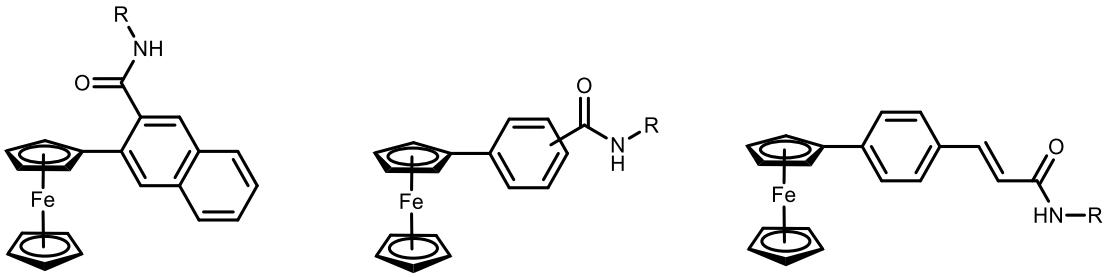

R = Benzylamine, cyclohexylamine

Figure 2.9. General structures of final products after introduction of amino moieties.

Reaction between carboxylic acids and amines at room temperatures produce salts.[203] Hence, the first step is the conversion the -OH end of the carboxylic acid into a good leaving group before the reaction with the amine.[204] The activation of the carboxylic acid could be reached by a reaction with thionyl chloride ($SOCl_2$) to generate a carboxylic acyl chloride, following the mechanism showed before on Scheme 2.7. Nevertheless,

acid chlorides are not an option prior to amide bond formation by virtue of their tendency to undergo side reactions such as hydrolysis, racemisation or cleavage of protecting groups.[205,206] For this reason, the synthetic route proposed to achieve the activation of the carboxylic acid group via EDC/NHS method. The mechanism for this protocol is shown for 6-ferrocenyl-2-naphthoic acid **65**; other ferrocenyl carboxylic acids follows the same mechanism. The use of a carbodiimide like *N*-(3-dimethylaminopropyl)-*N*′-carbodiimide hydrochloride (EDC) **88** has been proved to be an efficient way to activate a carboxylic group. This reaction comprises the formation of an *O*-acylisourea derivative **89** (Scheme 2.15).[202]

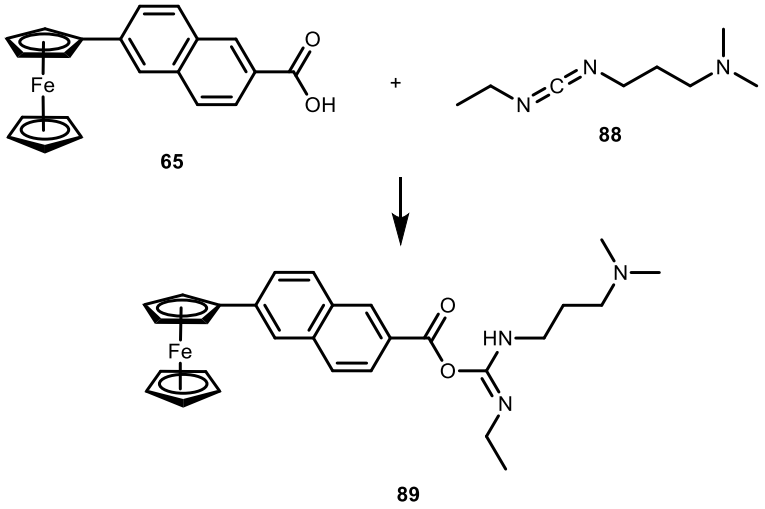

Scheme 2.15. Reaction between 6-ferrocenyl-2-naphthoic acid **65** and EDC **88**.

This *O*-acylisourea intermediate **89** is highly reactive, hence intramolecular rearrangements such as the acyl transfer which lead to the formation of a less reactive *N*-acyl-urea **90** (Scheme 2.16) can represent a disadvantage in terms of poor yields and interference with final product purification.[203,206,207]

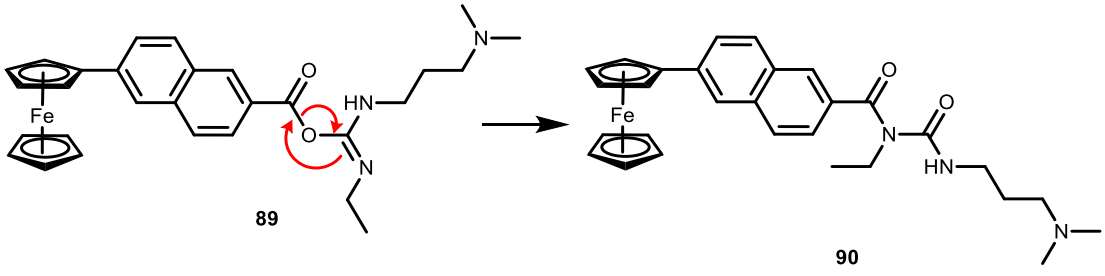

Scheme 2.16. Intramolecular acyl transfer of *O*-acylisourea **89** to *N*-acyl-urea **90**.

Consequently, the use of an auxiliary nucleophile such as *N*-hydroxysuccinimide (NHS) **91** can stabilize the *O*-acylisourea intermediate **89** by transforming it into a more stable NHS-ester **92**, which can still react with the amino group of the required reagent to lead the amide bond formation (Scheme 2.17).[206,207] The subproduct 1-(3-(dimethylamino)propyl)-3-ethylurea **93** can be extracted with water, facilitating the later purification of the desired products.[206]

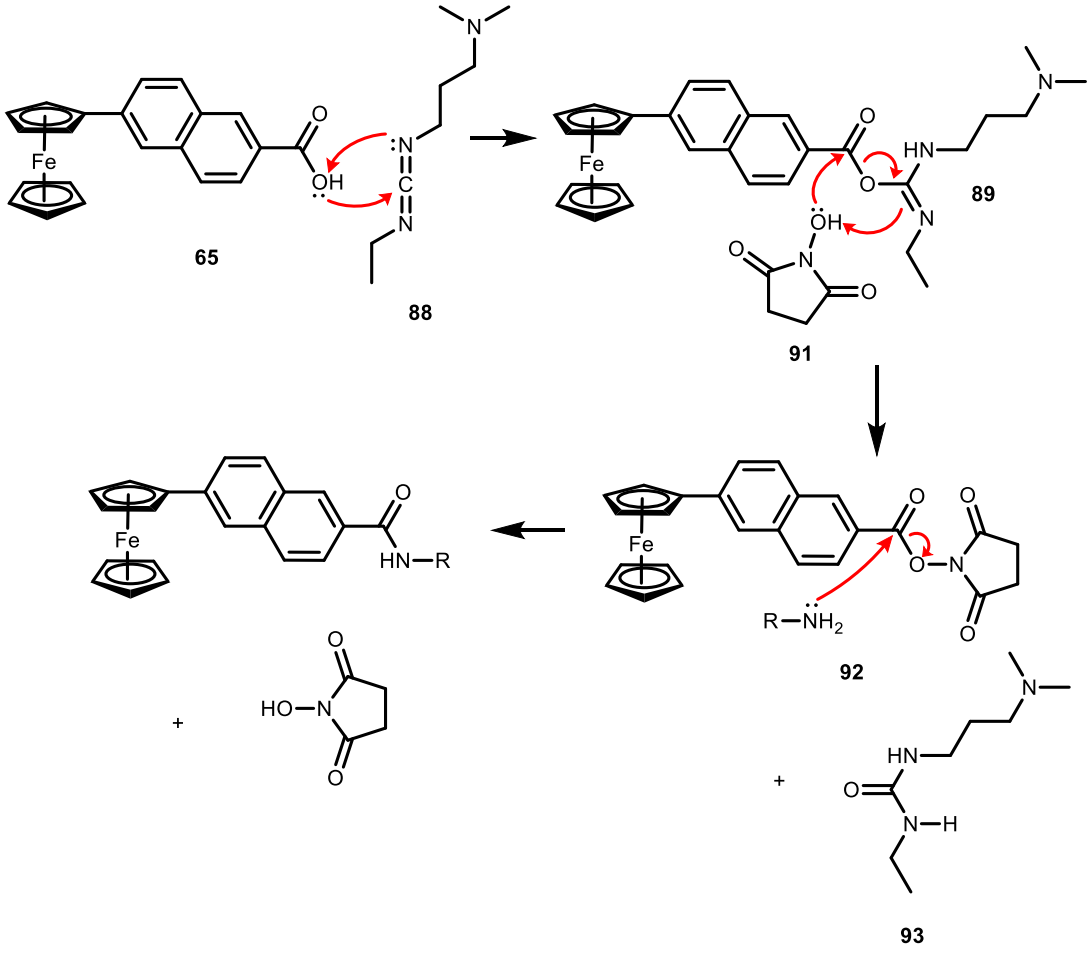

Scheme 2.17. Reaction mechanism for amide bond formation using EDC/NHS coupling.

2.3 Results

2.3.1 6-Ferrocenyl-2-naphthoyl series

The starting material for this series was the commercially available 6-amino-2-naphthoic acid **59**. The esterification of this carboxylic acid furnished the 6-(methoxycarbonyl)naphthalen-2-aminium chloride **60** with 90% yield. Ferrocene **61** was introduced via diazonium coupling, thus methyl 6-ferrocenyl-2-naphthoate **63** (26% yield) was obtained. Subsequent base hydrolysis produced the corresponding 6-ferrocenyl-2-naphthoic acid **65** with 96% yield.

6-Ferrocenyl-2-naphthoic acid **65** was reacted with the three aminopyridines **94**-**96**, benzylamine **97** and cyclohexylamine **98** (Figure 2.10) via EDC/NHS coupling protocol. Reaction of **65** with 2-aminopyridine **94** and 3-aminopyridine **95** yielded the corresponding 6-ferrocenyl-*N*-(pyridin-2-yl)-2-naphthamide **99** and 6-ferrocenyl-*N*-(pyridin-3-yl)-2-naphthamide **100** in high yields (93% and 92%, respectively). However, the EDC/NHS coupling of **65** with 4-aminopyridine **96** did not proceed in the same manner; possible factors that may have influenced on this unusual result are discussed in Section 2.5.9. Spectroscopic and spectrometric analysis shown in Sections 2.5.9, 2.6.9, 2.11.1 and 2.12 suggest that the final compound obtained from this reaction was the NHS-ester intermediate 2,5-dioxopyrrolidin-1-yl 6-ferrocenyl-2-naphthoate **101**, which was obtained with a percentage yield of 53%.

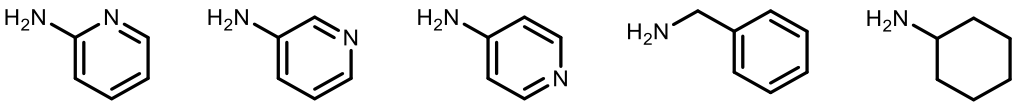

94 **95** **96** **97** **98**

Figure 2.10. Chemical structures of the three aminopyridines **94**-**96**, benzylamine **97** and cyclohexylamine **98**.

The coupling of 6-ferrocenyl-2-naphthoic acid **65** with benzylamine **97** and cyclohexylamine **98** yielded the desired *N*-benzyl-6-ferrocenyl-2-naphthamide **102** and *N*-cyclohexyl-6-ferrocenyl-2-naphthamide **103**, with percentage yields of 17% and 11%, respectively. All the final novel products of this series are shown in Figure 2.11.

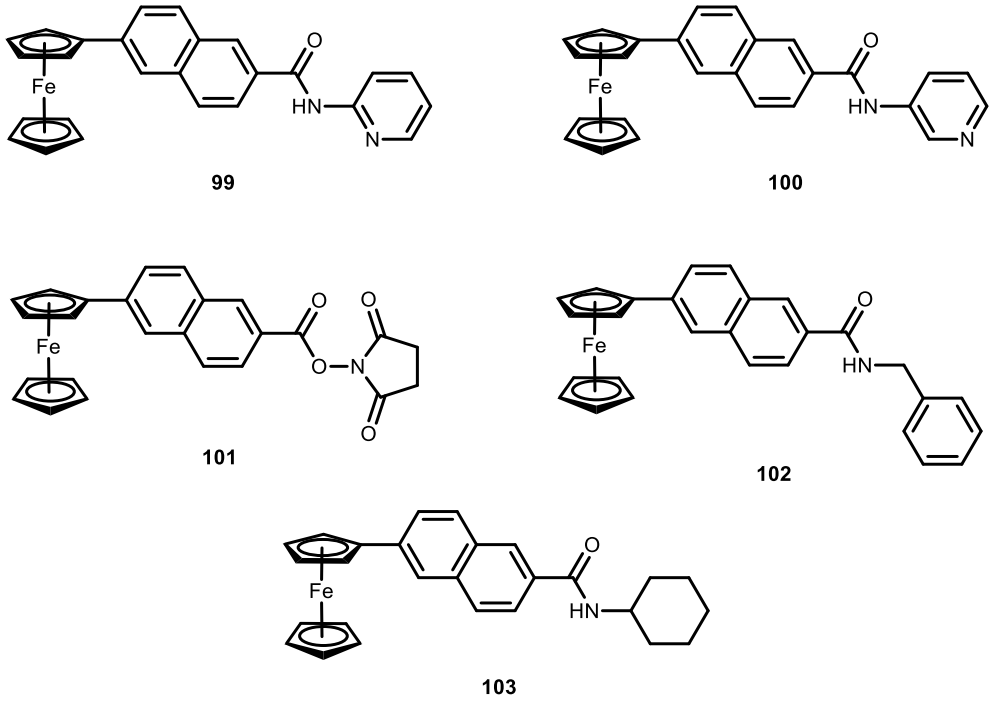

Figure 2.11. Novel ferrocenyl derivatives **99**-**103** from 6-ferrocenyl-2-naphthoyl series.

2.3.2 6-(1′-Ethyl)ferrocenyl-2-naphthoyl series

This series started with the diazonium coupling of ethyl ferrocene **62** to the previously prepared 6-(methoxycarbonyl)naphthalen-2-aminium chloride **60**, to obtain methyl 6-(1′-ethyl)ferrocenyl-2-naphthoate **64** with 17% yield. Subsequent base hydrolysis produced the corresponding 6-(1′-ethyl)ferrocenyl-2-naphthoic acid **66** with 62% yield.

The EDC/NHS coupling reaction of 6-(1′-ethyl)ferrocenyl-2-naphthoic acid **66** with 4-aminopyridine **96** followed the same pattern as observed previously for **65**, and the final product was identified as the corresponding NHS-ester intermediate 2,5-dioxopyrrolidin-1-yl 6-(1′-ethyl)ferrocenyl-2-naphthoate **104**, with a percentage yield of 14%.The coupling of 6-(1′-ethyl)ferrocenyl-2-naphthoic acid **66** with benzylamine **97** and cyclohexylamine **98** yielded the expected *N*-benzyl-6-(1′-ethyl)ferrocenyl-2-naphthamide **105** (27% yield) and *N*-cyclohexyl-6-(1′-ethyl)ferrocenyl-2-naphthamide **106** (25% yield), respectively. All the final novel products of this series are shown in Figure 2.12 below.

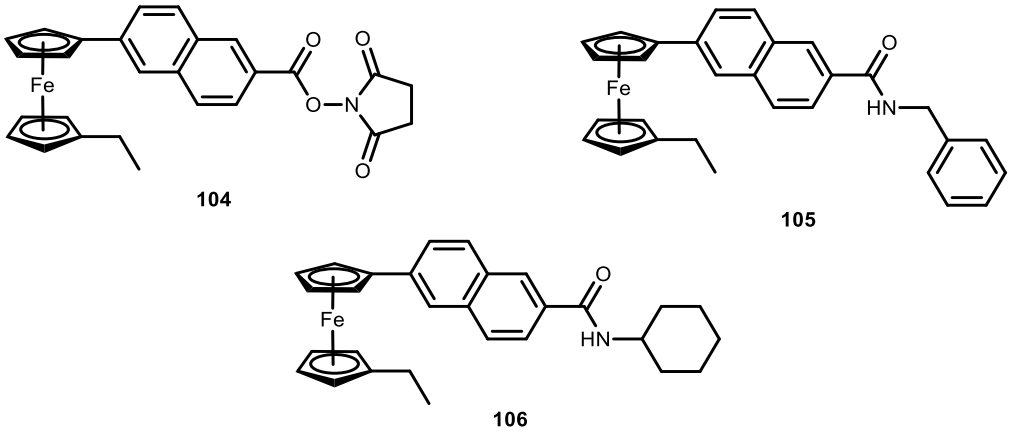

Figure 2.12. Novel ferrocenyl derivatives **104**-**106** from 6-(1′-ethyl)ferrocenyl-2-naphthoyl series.

2.3.3 3-Ferrocenyl-2-naphthoyl series

The starting material for this series was the commercially available 3-amino-2-naphthoic acid **67**. The esterification of this carboxylic acid furnished the 3-(methoxycarbonyl)naphthalen-2-aminium chloride **68** with 92% yield. The ferrocene **61** moiety was introduced to **68** via diazonium coupling, and methyl 3-ferrocenyl-2-naphthoate **69** was obtained (35% yield). Successive base hydrolysis yielded the corresponding 3-ferrocenyl-2-naphthoic acid **70** with 95% yield.

3-ferrocenyl-2-naphthoic acid **70** was reacted with benzylamine **97** and cyclohexylamine **98** via EDC/NHS coupling protocol, furnishing the desired *N*-benzyl-3-ferrocenyl-2-naphthamide **107** with 22% yield and *N*-(cyclohexylmethyl)-3-ferrocenyl-2-naphthamide **108** with 36% yield, respectively (Figure 2.13).

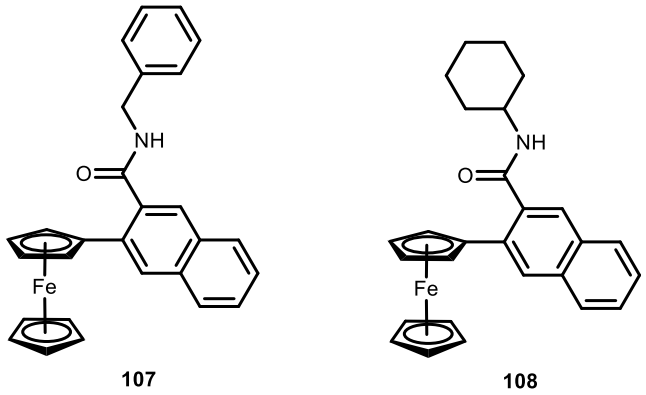

Figure 2.13. Novel ferrocenyl derivatives **107** and **108** from 3-ferrocenyl-2-naphthoyl series.

2.3.4 *Ortho*-, *meta*- and *para*-ferrocenyl-benzoyl series

The starting materials for these series were the commercially available ethyl *ortho*-aminobenzoate **71**, ethyl *meta*-aminobenzoate **72** and ethyl *para*-aminobenzoate **73**. The ferrocene **61** moiety was introduced to each via diazonium coupling, obtaining the corresponding analogues ethyl *ortho*-ferrocenylbenzoate **74** (39% yield), ethyl *meta*-ferrocenylbenzoate **75** (14% yield) and ethyl *para*-ferrocenylbenzoate **76** (34% yield). Consecutive base hydrolysis furnished the required *ortho*-ferrocenylbenzoic acid **77**, *meta*-ferrocenylbenzoic acid **78** and *para*-ferrocenylbenzoic acid **79**, with percentages yield of 96%, 86% and 97%, respectively.

The EDC/NHS coupling reaction of the ferrocenylbenzoic acids **77**-**79** with 4-aminopyridine **96** followed the same pattern as observed previously for **65** and **66**, and the final products were identified as the corresponding NHS-ester intermediates: 2,5-dioxopyrrolidin-1-yl 2-ferrocenylbenzoate **109** (17% yield), 2,5-dioxopyrrolidin-1-yl 3-ferrocenylbenzoate **110** (8% yield) and 2,5-dioxopyrrolidin-1-yl 4-ferrocenylbenzoate **111** (44% yield).

The ferrocenylbenzoic acids **77**-**79** were reacted with benzylamine **97** and cyclohexylamine **98** via EDC/NHS coupling, furnishing the desired derivatives: *N*-benzyl-2-ferrocenylbenzamide **112** (26% yield), *N*-benzyl-3-ferrocenylbenzamide **113** (41% yield) and *N*-benzyl-4-ferrocenylbenzamide **114** (25% yield), respectively; and *N*-cyclohexyl-2-ferrocenylbenzamide **115** (28% yield), *N*-cyclohexyl-3-ferrocenylbenzamide **116** (42% yield) and *N*-cyclohexyl-4-ferrocenylbenzamide **117** (20% yield), respectively. All the final novel products of these series are shown in Figure 2.14 below.

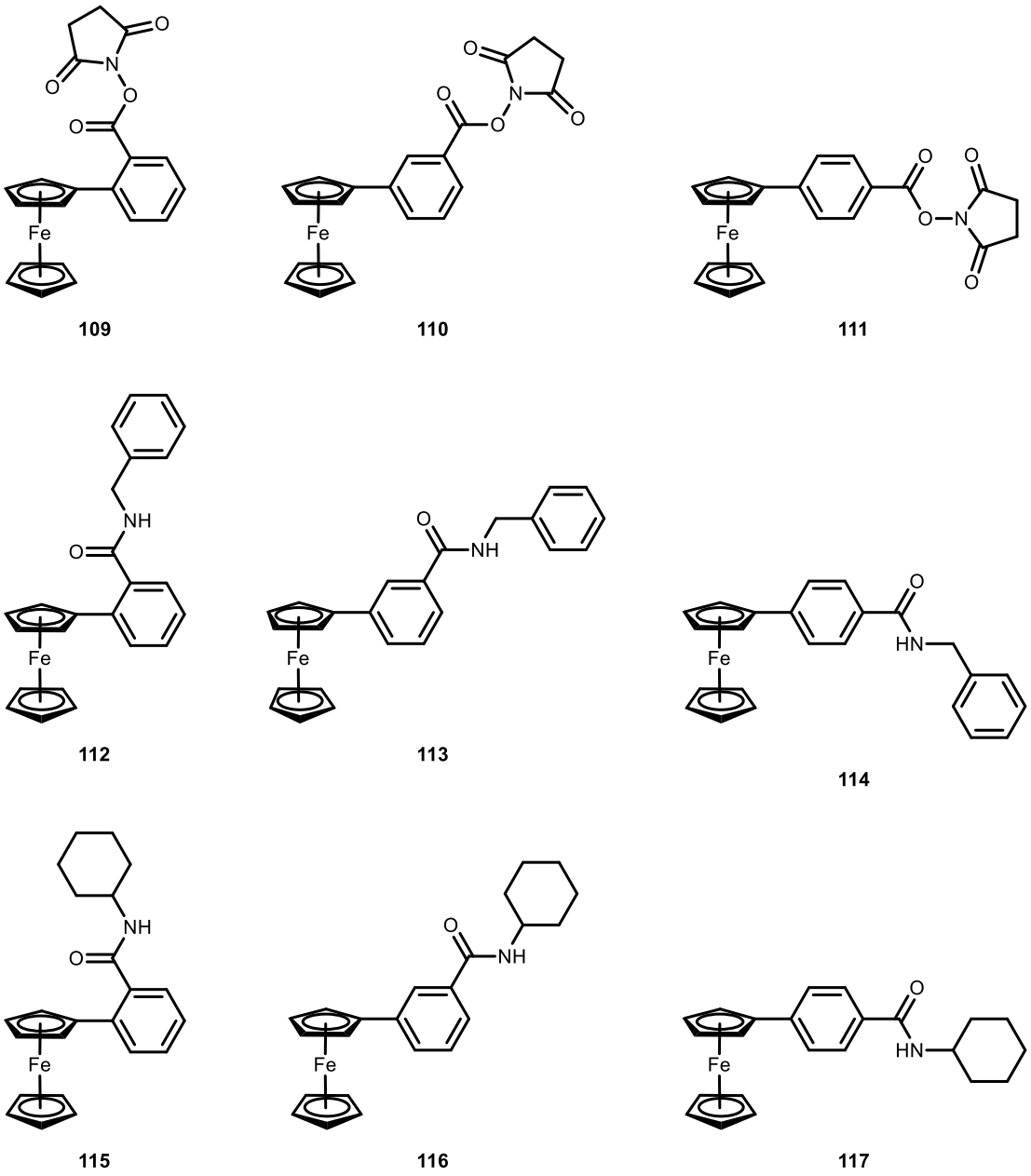

Figure 2.14. Novel ferrocenyl derivatives **109**-**117** from o*rtho*-, *meta*- and *para*-ferrocenyl-benzoyl series.

2.3.5 4-Ferrocenyl-cinammoyl series

The starting material for this series was the commercially available ethyl 4-aminocinnamate **80**. The ferrocene **61** moiety was introduced to **80** via diazonium coupling, and ethyl 4-ferrocenyl cinnamate **81** was obtained (17% yield). Consequent base hydrolysis yielded the corresponding 4-ferrocenyl cinnamic acid **82** with 96% yield.

The EDC/NHS coupling reaction of 4-ferrocenyl cinnamic acid **82** with 4-aminopyridine **96** followed the same pattern as observed previously for **65**, and the final product was identified as the corresponding NHS-ester intermediate 1-(3-(4-ferrocenylphenyl)acryloyl)pyrrolidine-2,5-dione **118** (15% yield).

4-ferrocenyl cinnamic acid **82** was reacted with benzylamine **97** and cyclohexylamine **98** via EDC/NHS coupling protocol, furnishing the desired derivatives *N*-benzyl-3-(4-ferrocenylphenyl)acrylamide **119** and *N*-cyclohexyl-3-(4-ferrocenylphenyl)acrylamide **120** with percentage yields of 13% and 10%, respectively. All the final novel products of this series are shown in Figure 2.15 below.

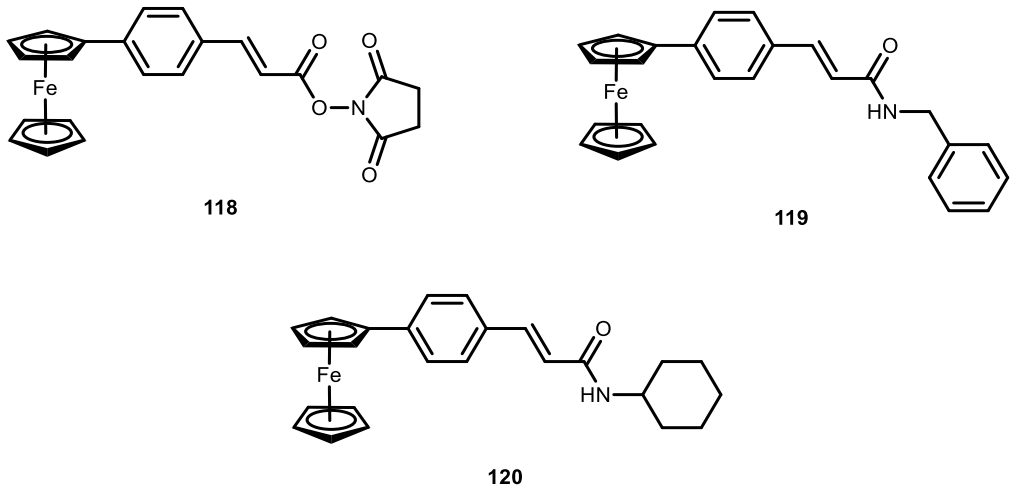

Figure 2.15. Novel ferrocenyl derivatives **118**-**120** from 4-ferrocenyl-cinammoyl series.

2.4 Purification and yields of novel heterocyclic functionalised ferrocenyl derivatives

The novel ferrocenyl naphthoyl, benzoyl and cinnamoyl derivatives were prepared by standard peptide coupling conditions. The corresponding carboxylic acid was coupled with 2-aminopyridine **94**, 3-aminopyridine **95**, benzylamine **97** or cyclohexylamine **98**; all compounds gave spectroscopic and analytical data in accordance with their proposed structures, except for the coupling reaction with 4-aminopyridine **96**, where the corresponding NHS-esters were identified as final products. Most of the crude products were purified by column chromatography using different ratios of ethyl acetate, diethyl ether and hexane as eluents. The purified compounds were obtained as yellow, orange or red solids with yields ranging from 8 to 93%. Table 2.1 summarizes the yields for all the novel ferrocenyl derivatives. The intermediates synthesized are not included in this table.

Table 2.1. Percentage yields for novel heterocyclic functionalised ferrocenyl derivatives **99**-**120**.

Compound name	No.	% Yield
6-ferrocenyl-*N*-(pyridin-2-yl)-2-naphthamide	**99**	93
6-ferrocenyl-*N*-(pyridin-3-yl)-2-naphthamide	**100**	92
2,5-dioxopyrrolidin-1-yl 6-ferrocenyl-2-naphthoate	**101**	53
N-benzyl-6-ferrocenyl-2-naphthamide	**102**	17
N-cyclohexyl-6-ferrocenyl-2-naphthamide	**103**	11
2,5-dioxopyrrolidin-1-yl 6-(1′-ethyl)ferrocenyl-2-naphthoate	**104**	14
N-benzyl-6-(1′-ethyl)ferrocenyl-2-naphthamide	**105**	27
N-cyclohexyl-6-(1′-ethyl)ferrocenyl-2-naphthamide	**106**	25
N-benzyl-3-ferrocenyl-2-naphthamide	**107**	22
N-cyclohexyl-3-ferrocenyl-2-naphthamide	**108**	36
2,5-dioxopyrrolidin-1-yl 2-ferrocenylbenzoate	**109**	17
2,5-dioxopyrrolidin-1-yl 3-ferrocenylbenzoate	**110**	8
2,5-dioxopyrrolidin-1-yl 4-ferrocenylbenzoate	**111**	44
N-benzyl-2-ferrocenylbenzamide	**112**	26
N-benzyl-3-ferrocenylbenzamide	**113**	41
N-benzyl-4-ferrocenylbenzamide	**114**	25
N-cyclohexyl-2-ferrocenylbenzamide	**115**	28
N-cyclohexyl-3-ferrocenylbenzamide	**116**	42
N-cyclohexyl-4-ferrocenylbenzamide	**117**	20
1-(3-(4-ferrocenylphenyl)acryloyl)pyrrolidine-2,5-dione	**118**	15
N-benzyl-3-(4-ferrocenylphenyl)acrylamide	**119**	13
N-cyclohexyl-3-(4-ferrocenylphenyl)acrylamide	**120**	10

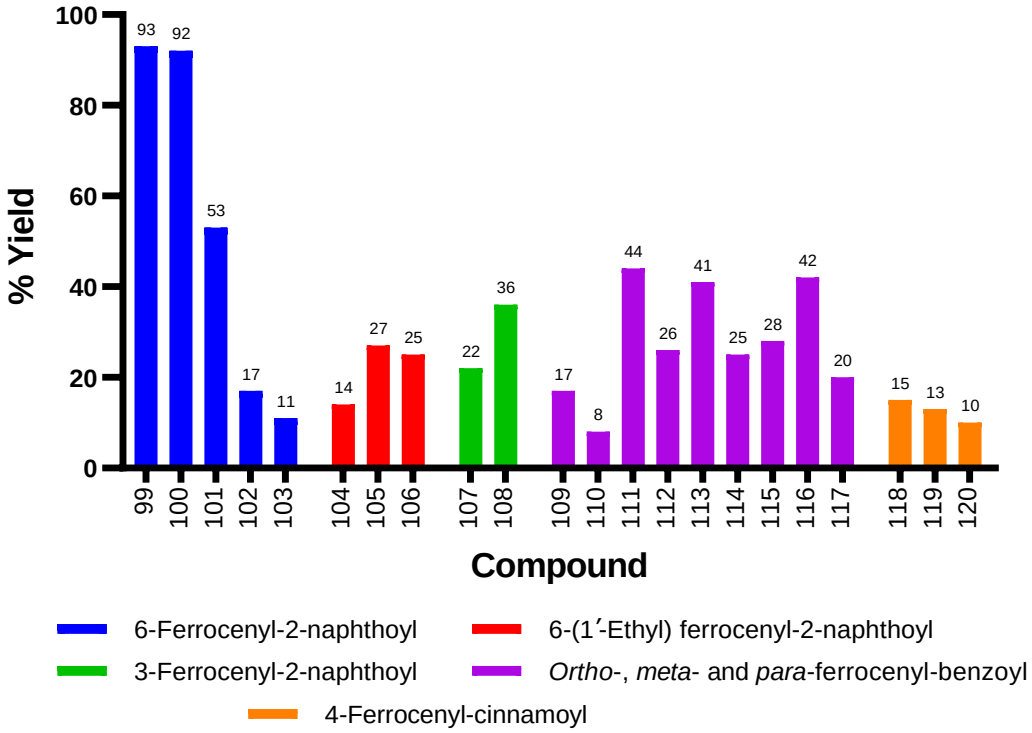

Figure 2.16. Yield percentages of novel heterocyclic functionalised ferrocenyl derivatives **99**-**120**.

As observed from Figure 2.16, yields for the aminopyridine derivatives **99** and **100** were the highest overall, as final products were recovered by extraction. When column purification was needed, yields obtained for the benzoyl series were generally better than those obtained for the naphthoyl and cinnamoyl derivatives. The steric hindrance of the bulky naphthoyl group may influence the low yields obtained for these series compared with their benzoyl analogues. The cinnamoyl series showed the lowest yields in general.

2.5 ^{1}H NMR studies of novel heterocyclic functionalised ferrocenyl derivatives

The ^{1}H NMR experiments of the 6-(1′-ethyl)ferrocenyl-2-naphthoyl series were performed in $CDCl_3$, and the spectra of the rest of the derivatives were recorded in DMSO-d_6 as they showed limited solubility in other deuterated solvents. Each peak reported in this section was assigned using a combination of different NMR analysis, including ^{1}H, ^{13}C, COSY, HSQC and HMBC. As an example, the assignment of compound **107** is given in detail in Section 2.8.1.

2.5.1 Aromatic ^{1}H NMR analysis

The chemical shifts of the aromatic protons from the spacer groups appear between δ 7.12 and δ 8.62. The splitting pattern varied depending on the substitution of the naphthalene or benzene rings, and some signals may overlap due to their proximity in chemical shifts. For the 6-ferrocenyl-2-naphthoyl and 6-(1′-ethyl)ferrocenyl-2-naphthoyl series, a singlet, singlet, multiplet, doublet of doublets pattern is generally observed, integrating for one, one, three and one proton, respectively. In the spectra of the 3-ferrocenyl-2-naphthoyl series, a singlet, doublet, doublet, singlet, triplet of doublets, triplet of doublets pattern is detected, with each peak integrating for one proton. The *ortho*-ferrocenyl-benzoyl series generally give rise to a doublet, triplet, triplet, doublet pattern, with each peak integrating for one proton. The *meta*-ferrocenyl-benzoyl series have a singlet, doublet, doublet, triplet pattern in most of the cases, integrating for one proton each. The *para*-ferrocenyl-benzoyl and 4-ferrocenyl-cinammoyl series give the typical *para*-disubstituted aromatic splitting pattern with two doublets that both integrate for two protons. These signals are summarised in Table 2.2.

Table 2.2. Aromatic linker ^{1}H NMR spectral data for novel heterocyclic functionalised ferrocenyl derivatives **99**-**120**. Values are given in ppm.

Compound	Spacer linker	δ H_{ar} on spacer linker
99	Naphthoyl	8.54, 8.08, 8.04, 7.94, 7.84
100		8.53, 8.07, 8.03, 7.95, 7.93, 7.83
101		8.79, 8.17, 8.08, 8.00, 7.93
102		8.46, 8.06, 7.95, 7.83
103		8.38, 8.05, 7.95, 7.90, 7.82
104		8.62, 7.98, 7.80, 7.65
105		8.19, 7.77, 7.60
106		8.13, 7.76, 7.61
107		8.34, 8.00, 7.94, 7.80, 7.55, 7.51
108		8.32, 7.99, 7.93, 7.71, 7.54, 7.50
109	Benzoyl	8.00, 7.68, 7.67, 7.44
110		8.02, 7.78, 7.76, 7.42
111		7.99, 7.79
112		7.80, 7.40, 7.26
113		8.02, 7.73, 7.72, 7.41
114		7.83, 7.63
115		7.79, 7.38, 7.22, 7.12
116		7.92, 7.71, 7.66, 7.38
117		7.76, 7.60
118		7.54, 7.52
119		7.58, 7.49
120		7.57, 7.47

In the benzylamine derivatives **102**, **105**, **107**, **112**-**114** and **119**, the aromatic protons appear between δ 7.25 and δ 7.36. The splitting pattern varied depending on the complexity of the spacer linker, as signals overlapped due to their proximity in chemical shifts: for compounds from naphthoyl series, the benzylamine protons appear as two multiplets integrating for four and one protons, respectively; for compounds from benzoyl series, the protons in the *ortho*, *meta* and *para* positions of benzylamine were shown in three different signals integrating for two, two and one proton, respectively (Table 2.3).

Table 2.3. Aromatic ^{1}H NMR spectral data for benzylamine derivatives **102**, **105**, **107**, **112**-**114** and **119**. Values are given in ppm.

Compound	Spacer linker	δ H_{ar} on benzylamine
102	Naphthoyl	7.36, 7.26
105		7.33, 7.26
107		7.36, 7.28
112	Benzoyl	7.32, 7.26, 7.20
113		7.36, 7.35, 7.26
114		7.34, 7.33, 7.25
119		7.35, 7.31, 7.26

2.5.2 Amide ^{1}H NMR analysis

In amide derivatives, this proton appears between δ 7.98 and δ 9.20 when DMSO-d_6 was used as the solvent, and between δ 6.02 and δ 6.45 when spectra were performed in $CDCl_3$ (Table 2.4). This difference is due to hydrogen bond interactions between the amide proton and the S=O bond of DMSO-d_6; since $CDCl_3$ does not possess the same ability to form hydrogen bonds, these amide protons are most likely to appear more upfield.[208,209]

Table 2.4. Amide ^{1}H NMR spectral data for novel heterocyclic functionalised ferrocenyl derivatives **102**-**103**, **105**-**108**, **112**-**117** and **119**-**120**. Values are given in ppm.

Compound	δ N-H	Compound	δ N-H
102	9.20	**113**	9.09
103	8.34	**114**	9.02
105	6.45	**115**	8.04
106	6.02	**116**	8.22
107	8.94	**117**	8.15
108	8.27	**119**	8.61
112	8.72	**120**	7.98

2.5.3 Ferrocenyl ^{1}H NMR analysis

In the ferrocenyl region, the splitting pattern varied depending on the substitution of the cyclopentadienyl rings. For the derivatives with monosubstituted ferrocene **99**-**103** and **107**-**120**, three signals are observed: the *ortho* η^5-$C_5\underline{H}_4$ protons appear between δ 4.55 and δ 5.03 and the *meta* η^5-$C_5\underline{H}_4$ protons appear between δ 4.24 and δ 4.52, both signals as triplets or singlets integrating for two protons each; the five protons of the unsubstituted η^5-$C_5\underline{H}_5$ ring appear as a singlet between δ 4.02 and δ 4.10 (Table 2.5).

Table 2.5. Ferrocenyl ^{1}H NMR spectral data for novel heterocyclic functionalised ferrocenyl derivatives **99**-**103** and **107**-**120**. Values are given in ppm.

Compound	δ *ortho* on η^5-$C_5\underline{H}_4$	δ *meta* on η^5-$C_5\underline{H}_4$	δ η^5-$C_5\underline{H}_5$
99	4.98	4.46	4.05
100	4.98	4.46	4.05
101	5.03	4.50	4.07
102	4.97	4.46	4.05
103	4.96	4.45	4.05
107	4.70	4.29	4.08
108	4.74	4.33	4.10
109	4.64	4.34	4.10
110	4.83	4.39	4.03
111	4.99	4.52	4.06
112	4.55	4.24	4.06
113	4.86	4.39	4.04
114	4.89	4.41	4.03
115	4.59	4.29	4.07
116	4.85	4.39	4.03
117	4.88	4.41	4.02
118	4.84	4.39	4.03
119	4.85	4.40	4.03
120	4.84	4.39	4.03

For the disubstituted ferrocene moiety in the 6-(1′-ethyl)ferrocenyl-2-naphthoyl derivatives **104**-**106**, four signals are observed: for the cyclopentadiene ring attached to the naphthoyl spacer group (η^5-$C_5\underline{H}_4$-naphthoyl), the *ortho* protons appear between δ 4.65 and δ 4.68 and the *meta* η^5-$C_5\underline{H}_4$ protons appear between δ 4.29 and δ 4.34, both signals as fine triplets (J = 1.7 – 1.8 Hz) integrating for two protons each; for the cyclopentadiene ring attached to the ethyl group (η^5-$C_5\underline{H}_4$-ethyl), the *ortho* protons appear as singlets integrating for one proton each between δ 3.93 and δ 4.03, and the *meta* protons appear as a doublet of doublets between δ 3.87 and δ 3.89 integrating for two protons (Table 2.6).

Table 2.6. Ferrocenyl ^{1}H NMR spectral data for novel 6-(1′-ethyl)ferrocenyl-2-naphthoyl derivatives **104**-**106**. Values are given in ppm.

Compound	η^5-C_5H_4-naphthoyl		η^5-C_5H_4-ethyl	
	δ *Cortho*	δ *Cmeta*	δ *Cortho*	δ *Cmeta*
104	4.68	4.34	4.03, 3.94	3.89
105	4.66	4.29	4.02, 3.93	3.87
106	4.65	4.29	4.02, 3.93	3.87

2.5.4 Ethyl ^{1}H NMR analysis from ethyl ferrocene derivatives

In the 6-(1′-ethyl)ferrocenyl-2-naphthoyl series, the protons of the ethyl group (-CH_2CH_3) attached to the cyclopentadiene ring show unusual multiplicities from the synthesis of the intermediate methyl 6-(1′-ethyl)ferrocenyl-2-naphthoate **64**, and maintained the same for all derivatives **104**-**106**. The methylene protons (-$C\underline{H}_2CH_3$) appear as three quartets between δ 2.06 and δ 2.62 integrating for two protons in total, as shown in Figure 2.17A; and the methyl protons (-$CH_2C\underline{H}_3$) appear as two triplets between δ 0.96 and δ 1.19 integrating for three protons in total, as shown in Figure 2.17B. These signals are summarized in Table 2.7.

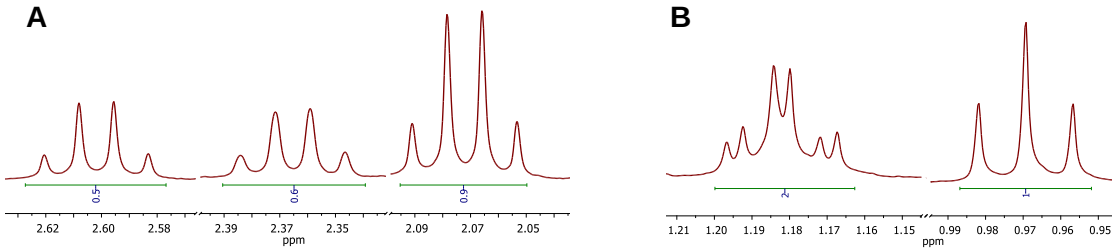

Figure 2.17. Alkyl region of the ^{1}H NMR spectra of *N*-benzyl-6-(1′-ethyl)ferrocenyl-2-naphthamide **105**. **A.** 2.05-2.62 ppm. **B.** 0.95-1.21 ppm.

Table 2.7. Ethyl ^{1}H NMR spectral data for novel 6-(1′-ethyl)ferrocenyl-2-naphthoyl derivatives **104**-**106**. Values are given in ppm.

Compound	δ -$C\underline{H}_2$- on η^5-$C_5\underline{H}_4$-ethyl	δ -$C\underline{H}_3$ on η^5-$C_5\underline{H}_4$-ethyl
104	2.62, 2.38, 2.06	1.19, 0.96
105	2.60, 2.37, 2.07	1.18, 0.96
106	2.61, 2.37, 2.07	1.19, 0.96

These interesting splitting patterns are in accordance with the spectra of the *N*-(1′-alkyl-6-ferrocenyl-2-naphthoyl) amino acid and dipeptide derivatives. For the synthesis of methyl 6-(1′-ethyl)ferrocenyl-2-naphthoate **64**, ethyl ferrocene **62** was reacted with 6-(methoxycarbonyl)naphthalen-2-aminium chloride **60** directly without protection; thus there are two possible ways of bonding that yield isomers in each case:[195]

(i) **60** could bound to the same or different cyclopentadienyl ring of **62** where the ethyl group is located (Figure 2.18), however this is less likely to happen due to steric effects of the ethyl group.

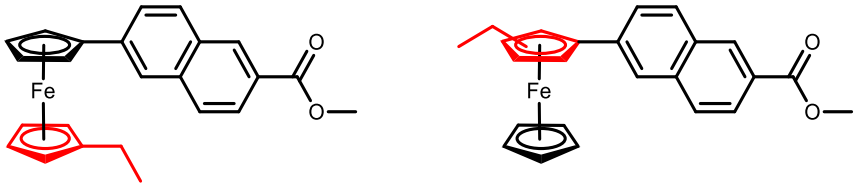

Figure 2.18. The proposed structures of isomers of methyl 6-(1′-ethyl)ferrocenyl-2-naphthoate **64**.

(ii) atropisomers I, II and III of **64** can be formed due to two unsymmetrically substituted ring by binding of **60** either to the same or different ring as the ethyl group in **62** (Figure 2.19); these are thought to be the main products as in the synthesis of *N*-(1′-alkyl-6-ferrocenyl-2-naphthoyl) amino acid and dipeptide derivatives by Lu[195], where the presence of three isomers impossible to separate was confirmed by variable temperature ^{1}H NMR and HPLC-UV.

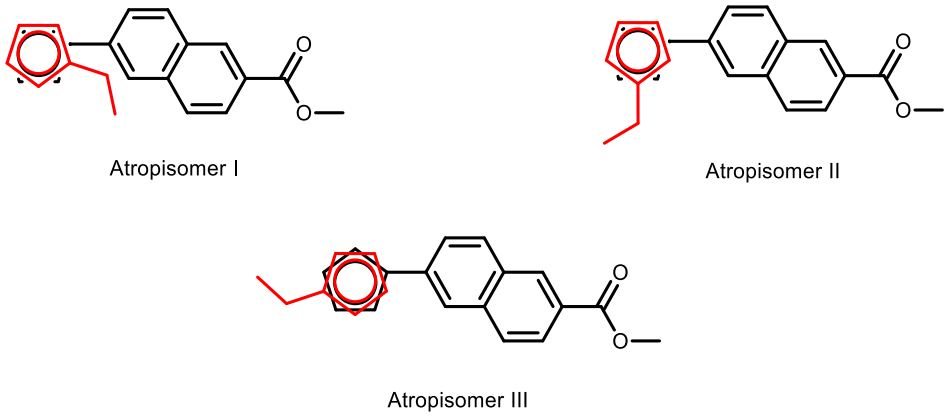

Figure 2.19. The proposed structures of atropisomers I, II and III of methyl 6-(1′-ethyl)ferrocenyl-2-naphthoate **64**.

2.5.5 Methylene ^{1}H NMR analysis from NHS-ester and benzylamine derivatives

The protons of the two methylene groups in the NHS-ester derivatives **101**, **104**, **109**-**111** and **118** appear between δ 2.87 and δ 2.93, always as a broad singlet integrating for four protons. The protons of the methylene group next to the aromatic ring in the benzylamine derivatives **102**, **105**, **107**, **112**-**114** and **119** appear between δ 4.36 and δ 4.65, always as a doublet due to coupling with the adjacent NH group (J = 6.0 Hz) and integrating for two protons. These signals are summarised in Table 2.8.

Table 2.8. Methylene ^{1}H NMR spectral data for NHS-ester and benzylamine derivatives. Values are given in ppm.

Compound	Derivative	δ -CH_2-	Compound	Derivative	δ -CH_2-
101	NHS ester	2.93	**102**	Benzylamine	4.55
104		2.88	**105**		4.65
109		2.90	**107**		4.45
110		2.92	**112**		4.36
111		2.90	**113**		4.52
118		2.87	**114**		4.49
			119		4.41

2.5.6 Aliphatic ^{1}H NMR analysis from cyclohexylamine derivatives

Cyclohexane ring can adopt both chair and boat conformations; however, the chair structure has the lowest total energy, and is therefore the most stable. In substituted cyclohexanes, different studies have confirmed that the equatorial conformation is favoured for the same reason (Figure 2.20).[210–214]

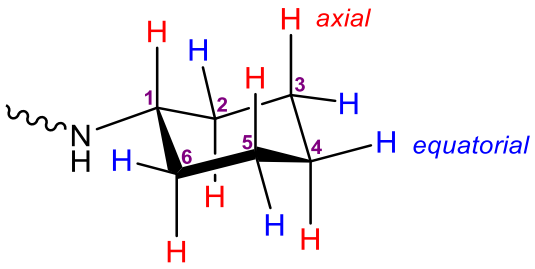

Figure 2.20. Equatorial conformation of cyclohexylamine group.

For this reason, the spectra of the cyclohexylamine derivatives **103**, **106**, **108**, **115**-**117** and **120** were the most complex due to the different axial and equatorial hydrogens in cyclohexyl moiety. These aliphatic protons appear between δ 0.86 and δ

3.97, generally as multiplets in different signals for each equivalent position with respect to the amine group, although in some cases they overlap due to proximity in chemical shifts. The general order observed is: the *ipso* proton on C1, in the lowest field; a set of three signals belonging to a pair of the *ortho* protons on C2 and C6, a pair of the *meta* protons in C3 and C5, and one *para* proton on C4; and a complex multiplet integrating for the remaining four *ortho* and *meta* protons, next to a multiplet due to the lasting *para* proton (Table 2.9).

Table 2.9. Aliphatic ^{1}H NMR spectral data for cyclohexylamine derivatives **103**, **106**, **108**, **115**-**117** and **120**. Values are given in ppm.

Compound	δ *ipso* on C1	δ *ortho* on C2 and C6	δ *meta* on C3 and C5	δ *para* on C4
103	3.82	1.87, 1.35	1.76, 1.35	1.63, 1.17
106	3.97	2.02, 1.40	1.72, 1.40	1.61, 1.17
108	3.71	1.85, 1.27	1.72, 1.27	1.59, 1.12
115	3.63	1.76, 1.15	1.68, 1.26	1.56, 1.07
116	3.78	1.85, 1.33	1.76, 1.33	1.63, 1.15
117	3.77	1.82, 1.32	1.75, 1.32	1.62, 1.14
120	3.66	1.80, 1.23	1.71, 1.23	1.58, 0.86

2.5.7 Olefinic ^{1}H NMR analysis from cinnamoyl derivatives

For the cinnamoyl series **118**-**120**, the olefinic protons appear as two doublets with coupling constants equal to ~16 Hz, integrating for one proton each: the first one between δ 7.37 and δ 7.46, and the second one between δ 6.43 and δ 6.69 (Table 2.10).

Table 2.10. Olefinic ^{1}H NMR spectral data for novel ferrocenyl cinnamoyl derivatives **118**-**120**. Values are given in ppm.

Compound	δ benzoyl-C**H**=CH-	δ benzoyl-CH=C**H**-
118	7.37	6.43
119	7.46	6.69
120	7.38	6.61

2.5.8 ^{1}H NMR studies of 6-ferrocenyl-*N*-(pyridin-2-yl)-2-naphthamide 99

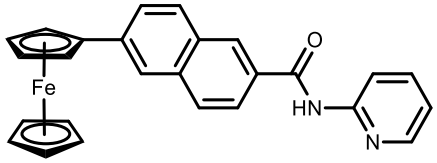

99

In the ^{1}H NMR spectrum of **99**, the six protons of the 6,2-disubstituted naphthoyl group appears as two singlets at δ 8.54 and δ 8.08, a doublet at δ 8.04, a singlet at δ 7.94 and a doublet of doublets at δ 7.84, integrating for one, one, one, two and one protons each. For the 2-aminopyridine moiety, the four protons in the ring appear as three doublet of doublet of doublets at δ 7.88, δ 7.35 and δ 6.46, and a doublet of triplets at δ 6.42; all integrating for one proton each. The amide proton peak appears at δ 5.85 as a broad singlet integrating for one proton. In the ferrocenyl region, the peaks due to the *ortho* and *meta* protons on the η^5-C_5H_4 ring appear as two triplets at δ 4.98 and δ 4.46 respectively, integrating for two protons each; and the singlet due to the unsubstituted η^5-C_5H_5 ring appears at δ 4.05 and integrates for five protons (Figure 2.21 to Figure 2.23).

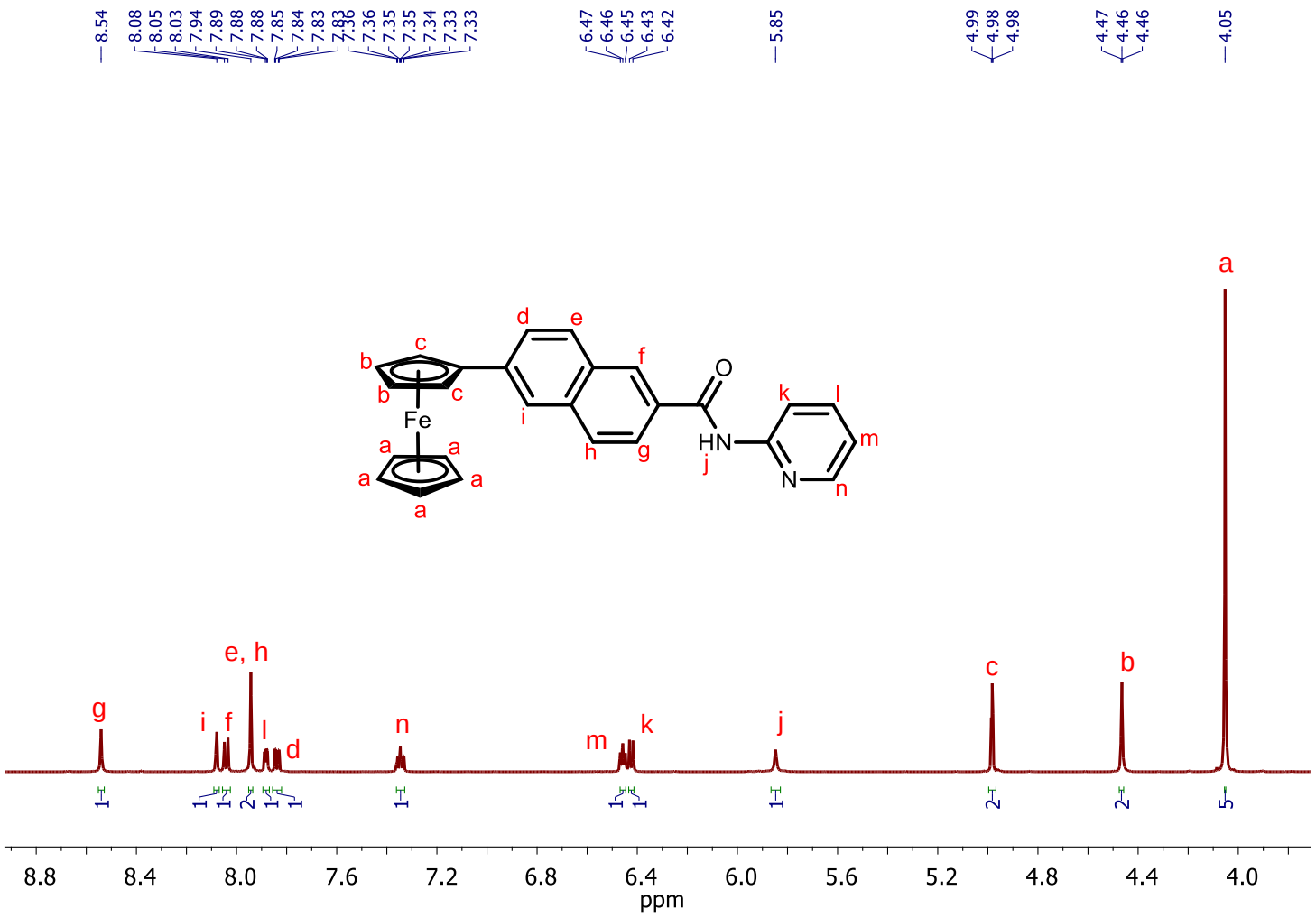

Figure 2.21. ^{1}H NMR spectrum of 6-ferrocenyl-*N*-(pyridin-2-yl)-2-naphthamide **99**.

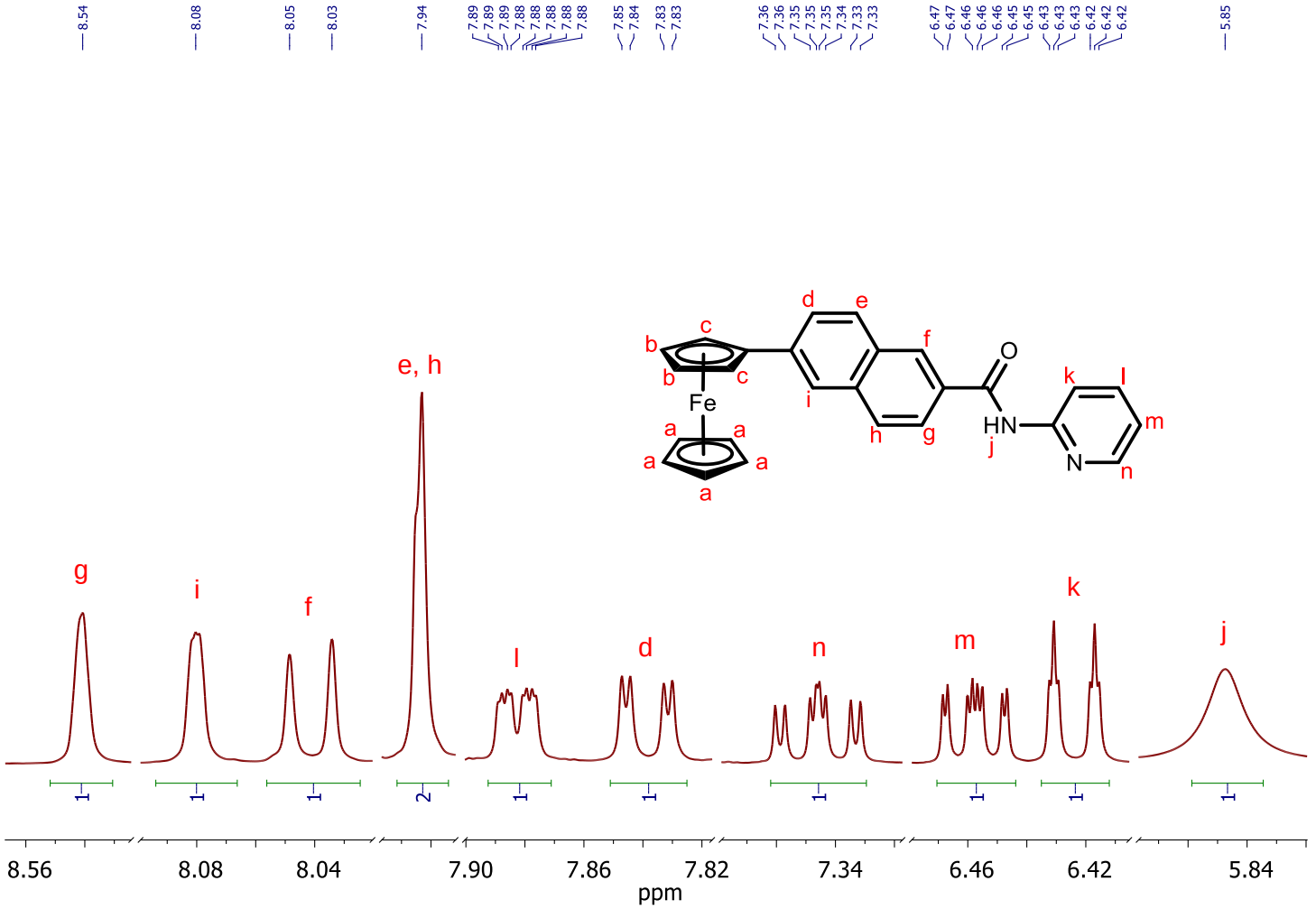

Figure 2.22. Zoom in the ^{1}H NMR spectrum of 6-ferrocenyl-*N*-(pyridin-2-yl)-2-naphthamide **99**: the aromatic and aminopyridine regions (5.84-8.56 ppm).

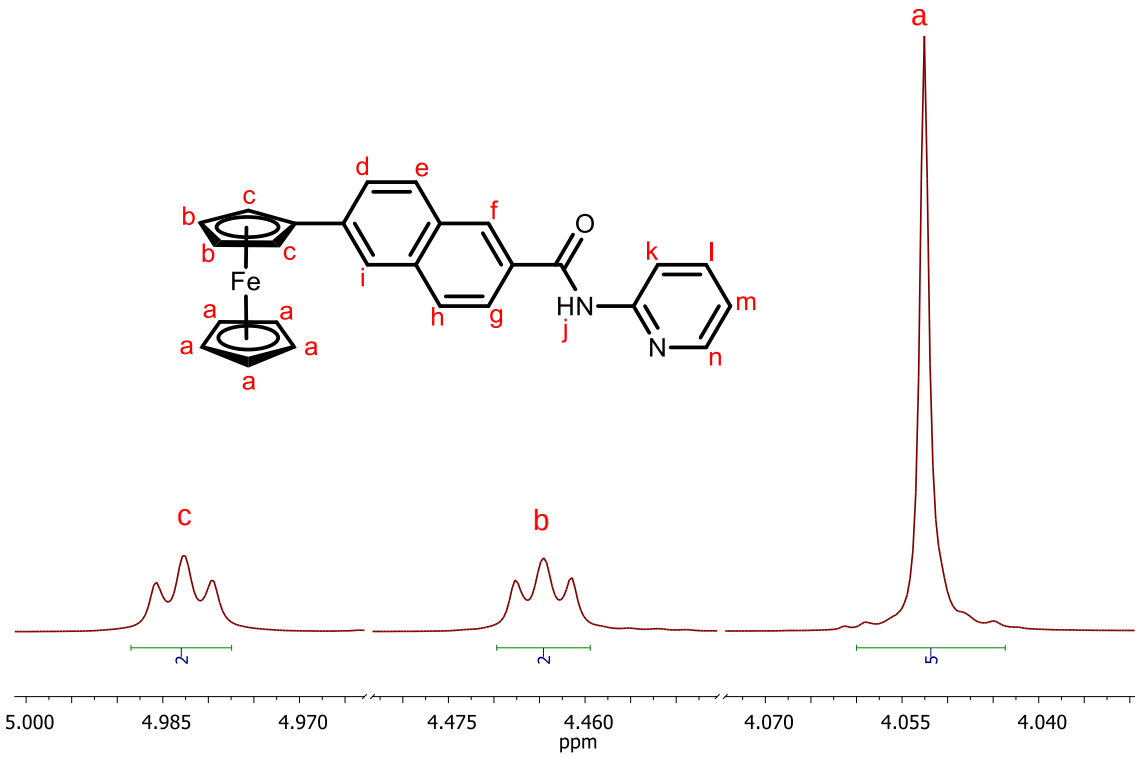

Figure 2.23. Zoom in the ^{1}H NMR spectrum of 6-ferrocenyl-*N*-(pyridin-2-yl)-2-naphthamide **99**: the ferrocenyl region (4.04-5.00 ppm).

2.5.9 ^{1}H NMR studies of 2,5-dioxopyrrolidin-1-yl 6-ferrocenyl-2-naphthoate 101

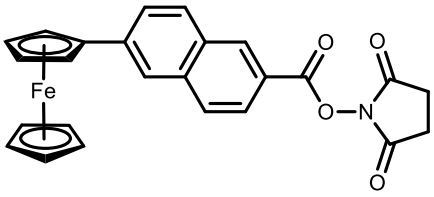

101

The EDC/NHS coupling of 6-ferrocenyl-2-naphthoic acid **65** with 2-aminopyridine **94** and 3-aminopyridine **95** yielded the 6-ferrocenyl-N-(pyridin-2-yl)-2-naphthamide **99** and 6-ferrocenyl-N-(pyridin-3-yl)-2-naphthamide **100**, respectively, in high yields as the products were obtained after filtration and no further column purification was necessary. These products were easily identified by ^{1}H NMR as both showed the corresponding signals for aminopyridine moieties between δ 6.42 and δ 7.92, as shown in Figure 2.21 for compound **99**. However, the equivalent reaction with 4-aminopyridine **96** did not proceed in the same manner.

The filtered product of the reaction of 6-ferrocenyl-2-naphthoic acid **65** with 4-aminopyridine **96** was analysed by ^{1}H NMR at room temperature, and the signals of the aminopyridine moiety were observed along with two sets of ferrocenyl signals. This led to the discussion if two ferrocenyl isomers were being formed.[215] For this reason, the ^{1}H NMR spectra of the filtered product was obtained at various temperatures ranging from 20 to 120 °C, in order to reach the coalescence temperature (T_c).

When NMR spectra is performed at room temperature, the rate of interconversion of the exchanging atoms or groups is slow on the NMR time scale for detection, and therefore different signals are observed separately. However, there is a fast exchange at higher temperatures and hence the separate signals due to isomers coalesce to form one broad signal. The coalescence temperature (T_c) is the temperature at which the two peaks in the slow exchange process merge to give one maximum. As the temperature increases above T_c, the exchange become faster and the signal continues to narrow (Figure 2.24).[216–218]

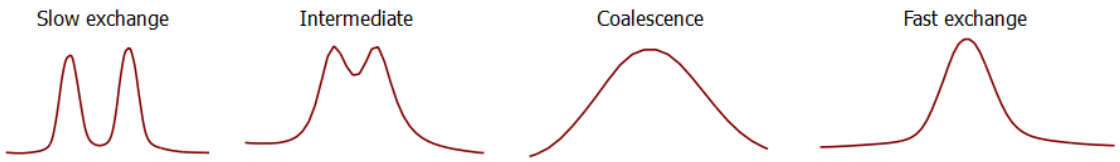

Figure 2.24. Effect of exchange of chemically equivalent nuclei on NMR line shapes.

The variable temperature study of the ^{1}H NMR spectrum of the filtered product was performed at 20, 40, 60, 80, 100 and 120 °C in DMSO-d_6 (Figure 2.25 and Figure 2.26). The aminopyridine signals (Figure 2.26B) become less intense as the temperature increases, and some of them have even disappeared at 100 °C. In contrast, the aromatic region (Figure 2.26A) does not alter significantly upon heating, neither the double set of signals in the ferrocenyl region (Figure 2.26C). This suggest that *a)* there are not two ferrocenyl isomers present in the molecule, or *b)* the coalescence temperature of this mixture of compounds is not within the range between 20 and 120 °C. DMSO-d_6 is the deuterated solvent that has the highest boiling point compared with other deuterated solvents (acetone-d_6, C_6D_6, $CDCl_3$, DMF-d_6), therefore no further investigations were carried out for temperature.

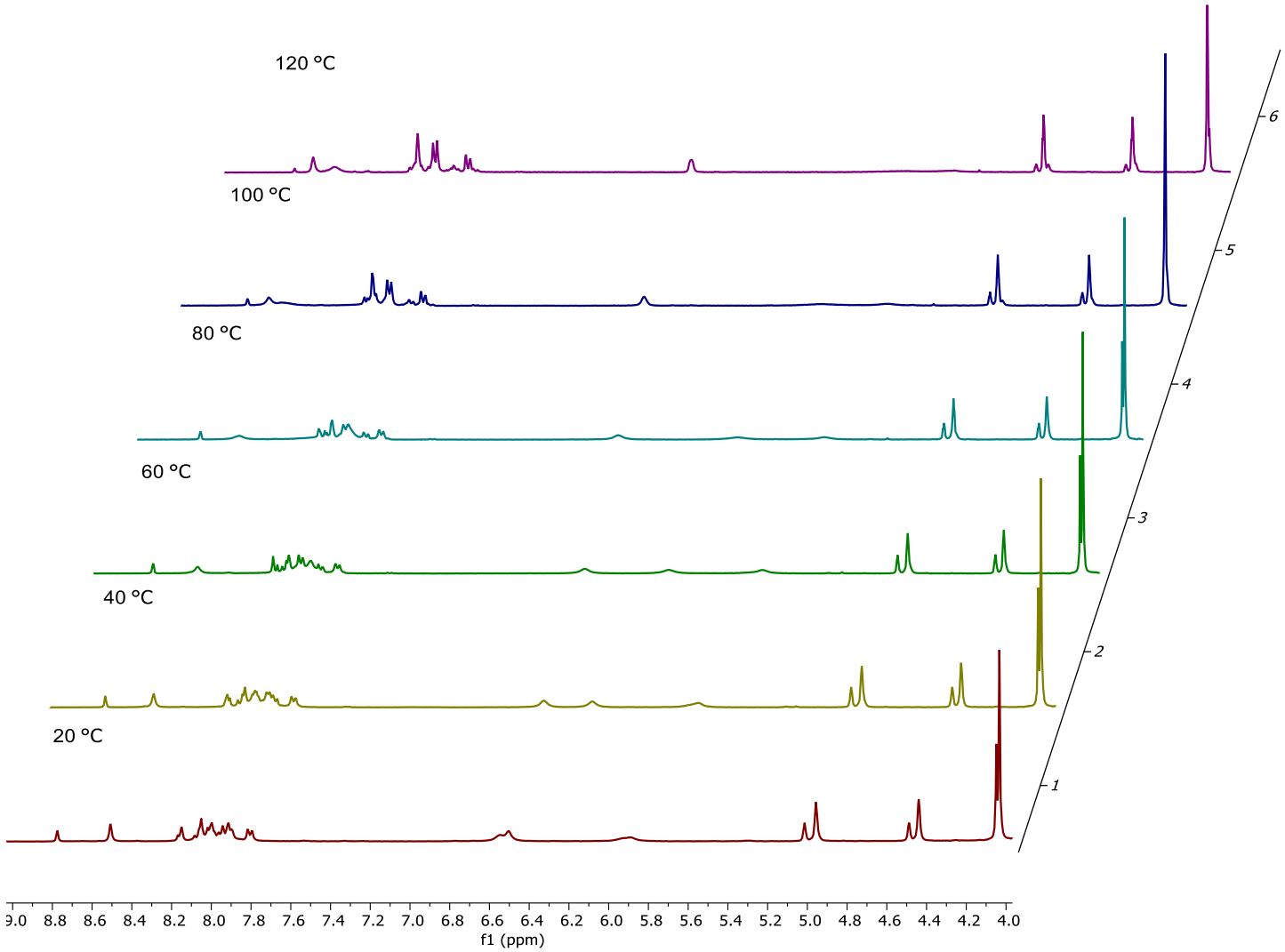

Figure 2.25. Variable temperature NMR study of filtered product of the EDC/NHS coupling of 6-ferrocenyl-2-naphthoic acid **65** with 4-aminopyridine **96**.

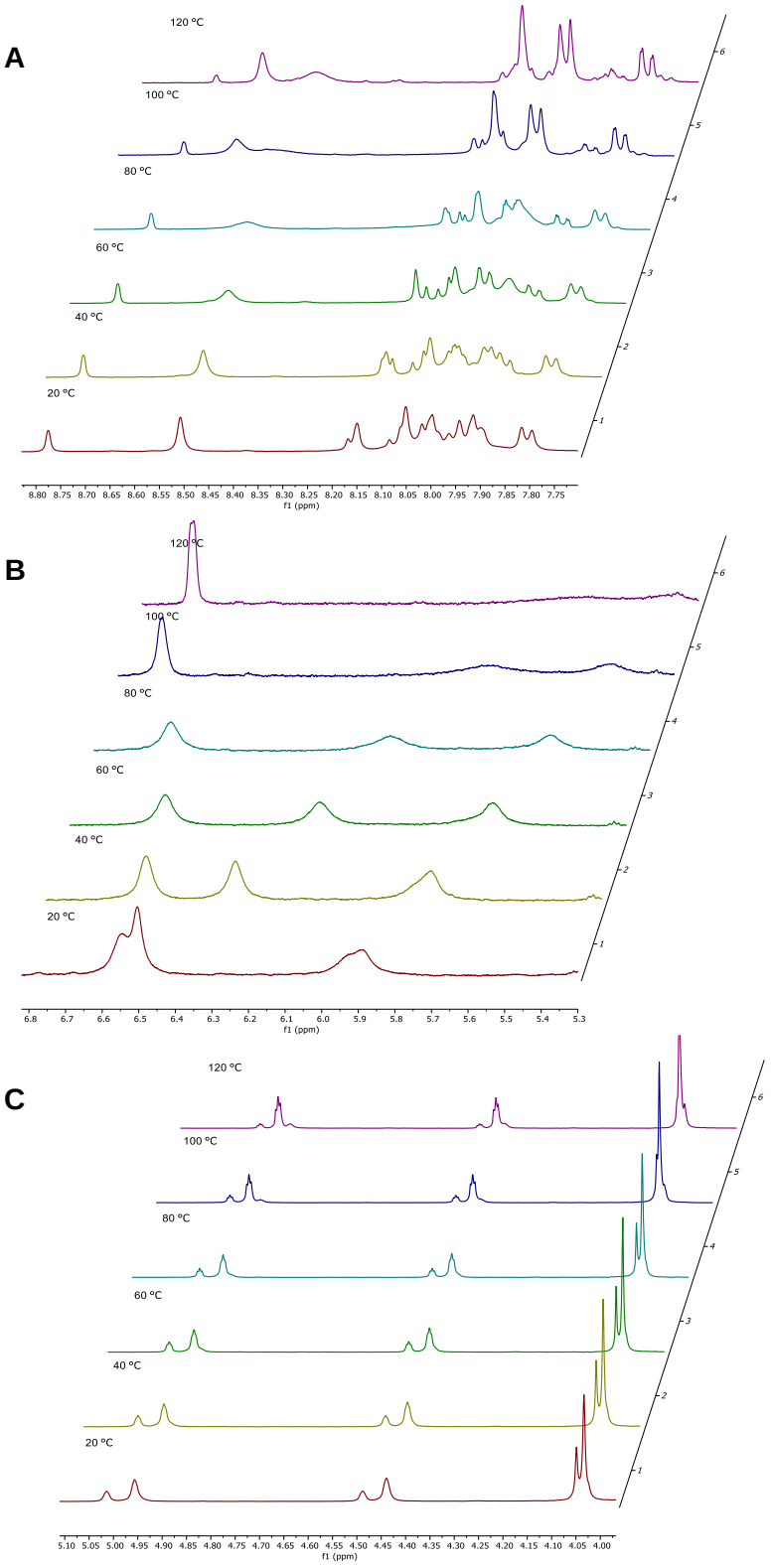

Figure 2.26. Zoom in the variable temperature NMR study of filtered product of the EDC/NHS coupling of 6-ferrocenyl-2-naphthoic acid **65** with 4-aminopyridine **96**. **A.** The aromatic region (7.7-8.8 ppm). **B.** The aminopyridine region (5.3-6.8 ppm). **C.** The ferrocenyl region (4.0-5.1 ppm).

The mixture of the filtered product was purified by column chromatography (eluent 1:1 hexane:ethyl acetate) and the most intense spot isolated. In the ^{1}H NMR analysis of this product (Figure 2.27 to Figure 2.28), the presence of a signal at δ 2.9 integrating for four protons was the key to conclude that the EDC/NHS coupling of 6-ferrocenyl-2-naphthoic acid **65** with 4-aminopyridine **96** did not proceed in the same manner as with the other aminopyridines **94** and **95**, yielding instead the NHS-ester intermediate 2,5-dioxopyrrolidin-1-yl 6-ferrocenyl-2-naphthoate **101**, as this signal is not observed in the other aminopyridine derivatives **99** and **100**. This signal belongs to the two methylene groups present in the NHS ring.

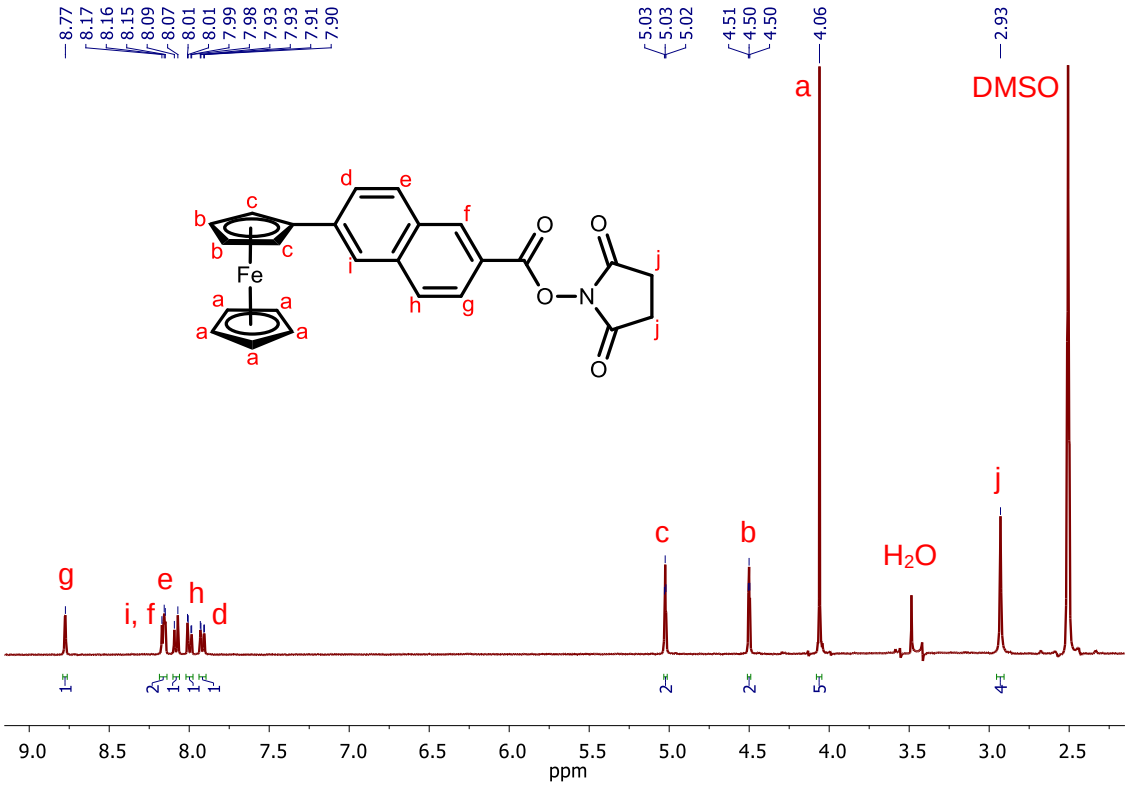

Figure 2.27. ^{1}H NMR spectrum of 2,5-dioxopyrrolidin-1-yl 6-ferrocenyl-2-naphthoate **101**.

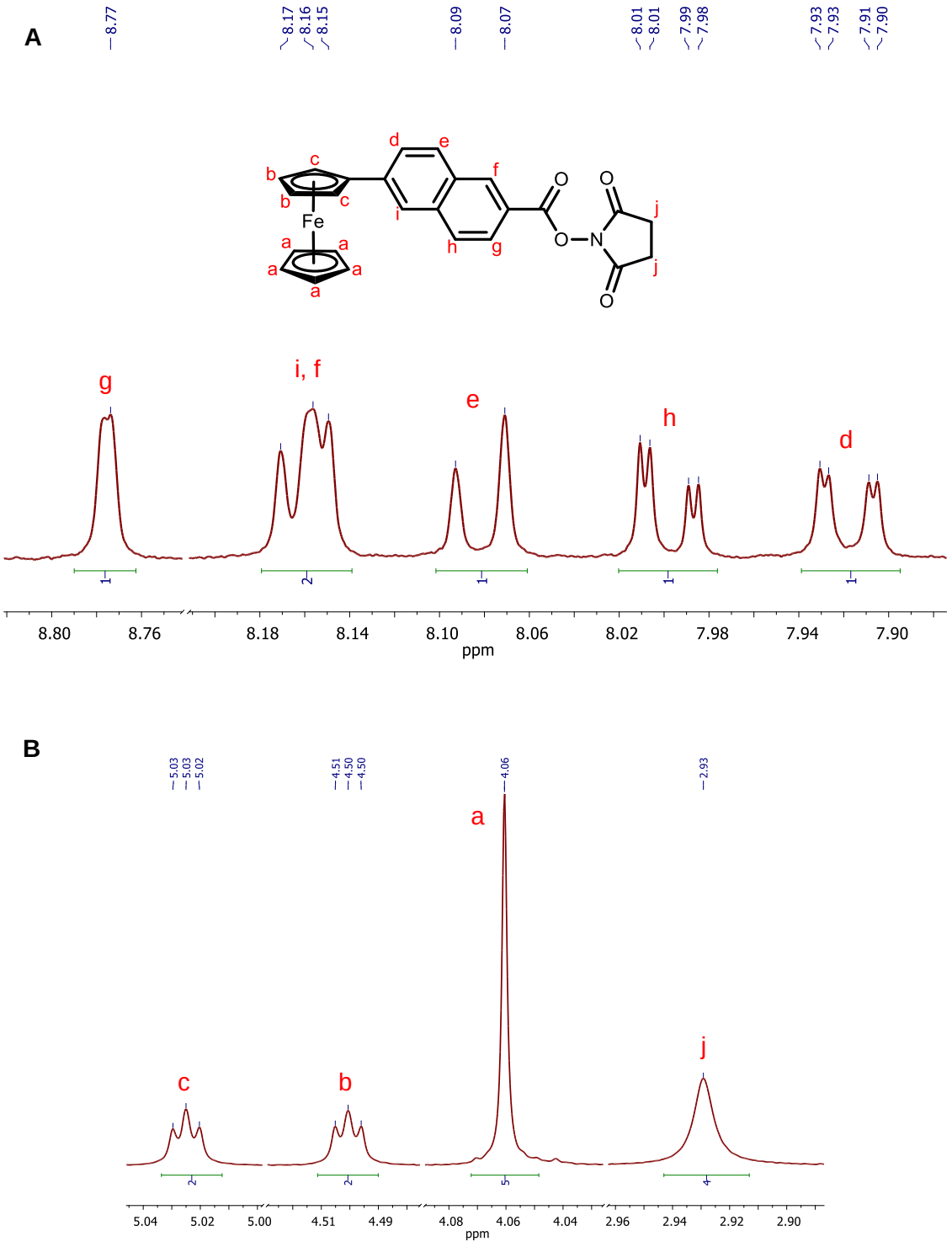

Figure 2.28. Zoom in the ^{1}H NMR spectrum of 2,5-dioxopyrrolidin-1-yl 6-ferrocenyl-2-naphthoate **101**. **A.** The aromatic region (7.90-8.80 ppm). **B.** The ferrocenyl region (2.90-5.04 ppm).

The difference in the EDC/NHS coupling with aminopyridines **94**-**96** may have relationship with the strength of their acidity, as there is evidence that the pK_a value of organic ligands affect the composition of a complex. As observed in Table 2.11, 4-aminopyridine **96** have a high pK_a value, which indicates that **96** exists as both 4-aminopyridine and 4-aminopyridinium in aqueous medium (Figure 2.29). The pK_a values of 2-aminopyridine **94** and 3-aminopyridine **95** are significantly lower than that of **96** due to the absence of resonant structure in protonated form. In addition, EDC reagent is used in its hydrochloride form, so **96** could be protonated by the HCl group hence preventing the reaction of interest from happening. Furthermore, the pK_a value of **96** is relatively closer to that of triethylamine, which is used as base in the mechanism of EDC/NHS coupling; this suggest that **96** may be competing with the role of base during the reaction.[219–222]

Table 2.11. pK_a values of aminopyridines **94**-**96** and triethylamine.

Key	Compound name	pK_a
94	2-aminopyridine	6.86
95	3-aminopyridine	5.98
96	4-aminopyridine	9.17
Et_3N	Triethylamine	10.80

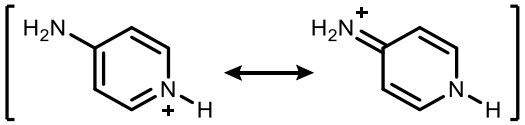

Figure 2.29. Resonant structures of 4-aminopyridine **96**.

Other analysis such as ^{13}C NMR (Section 0), COSY, HSQC, HMBC, IR and mass spectrometry (Section 2.11.1) confirmed the isolation of product **101** as the NHS-ester derivative. This pattern was also observed in the reaction of 4-aminopyridine **96** with other ferrocenyl-carboxylic acids such as 6-(1′-ethyl)ferrocenyl-2-naphthoic acid **66**, *ortho*-ferrocenylbenzoic acid **77**, *meta*-ferrocenylbenzoic acid **78**, *para*-ferrocenylbenzoic acid **79** and 4-ferrocenyl cinnamic acid **82**, yielding in all the cases the corresponding NHS-esters: 2,5-dioxopyrrolidin-1-yl 6-(1′-ethyl)ferrocenyl-2-naphthoate **104**, 2,5-dioxopyrrolidin-1-yl 2-ferrocenylbenzoate **109** (structure confirmed by X-ray study on Section 2.12), 2,5-dioxopyrrolidin-1-yl 3-ferrocenylbenzoate **110**, 2,5-dioxopyrrolidin-1-yl 4-ferrocenylbenzoate **111** and 1-(3-(4-ferrocenylphenyl)acryloyl)pyrrolidine-2,5-dione **118**, respectively. Literature research exposed other studies that have reported the failure of coupling aminopyridines, reflecting their probably low nucleophilicity. For this reason, no further EDC/NHS coupling reactions were performed with the aminopyridines **94**-**96**.[223–234]

2.5.10 ^{1}H NMR studies of *N*-benzyl-3-ferrocenyl-2-naphthamide 107

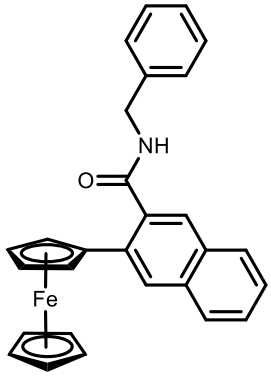

107

In the ^{1}H NMR spectrum of **107**, the amide proton peak appears downfield at δ 8.94; this signal integrates for one proton and appear as a triplet due to coupling with the adjacent methylene protons of the benzylamine moiety. The six protons of the 3,2-disubstituted naphthoyl group appear as a singlet at δ 8.34, two doublets at δ 8.00 and δ 7.94, a singlet at δ 7.80, and two doublet of doublet of doublets at δ 7.55 and δ 7.51; all integrating for one proton each. The remaining five aromatic protons belonging to the benzylamine appears as a doublet at δ 7.36 integrating for four protons, and a quintet at δ 7.28 integrating for one proton. The methylene protons appear as a doublet at δ 4.45 integrating for two protons. In the ferrocenyl region, the peaks due to the *ortho* and *meta* protons on the η^5-C_5H_4 ring appear as two triplets at δ 4.70 and δ 4.29 respectively, integrating for two protons each; and the singlet due to the unsubstituted η^5-C_5H_5 ring appears at δ 4.08 and integrates for five protons (Figure 2.30 to Figure 2.31).

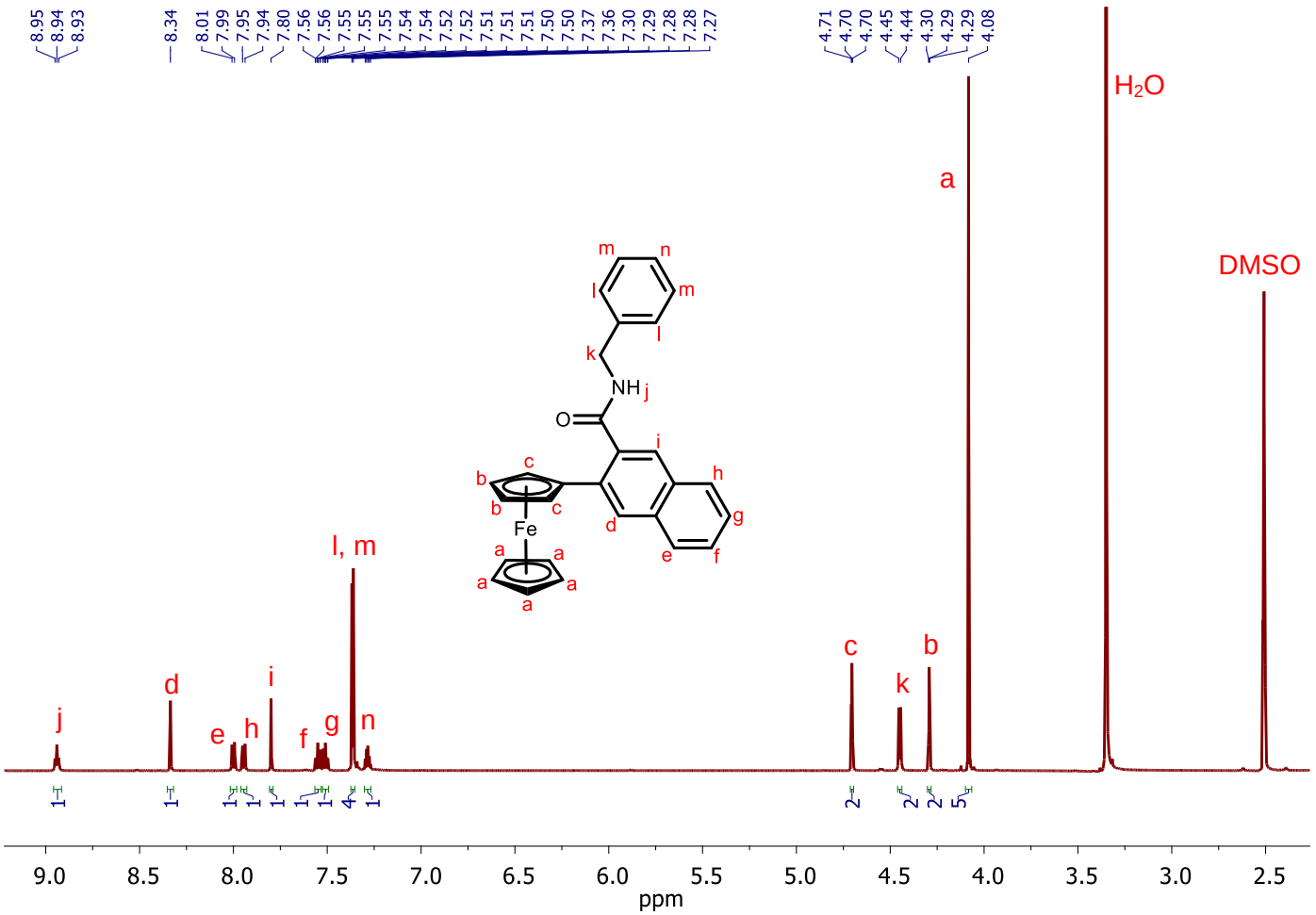

Figure 2.30. ^{1}H NMR spectrum of *N*-benzyl-3-ferrocenyl-2-naphthamide **107**.

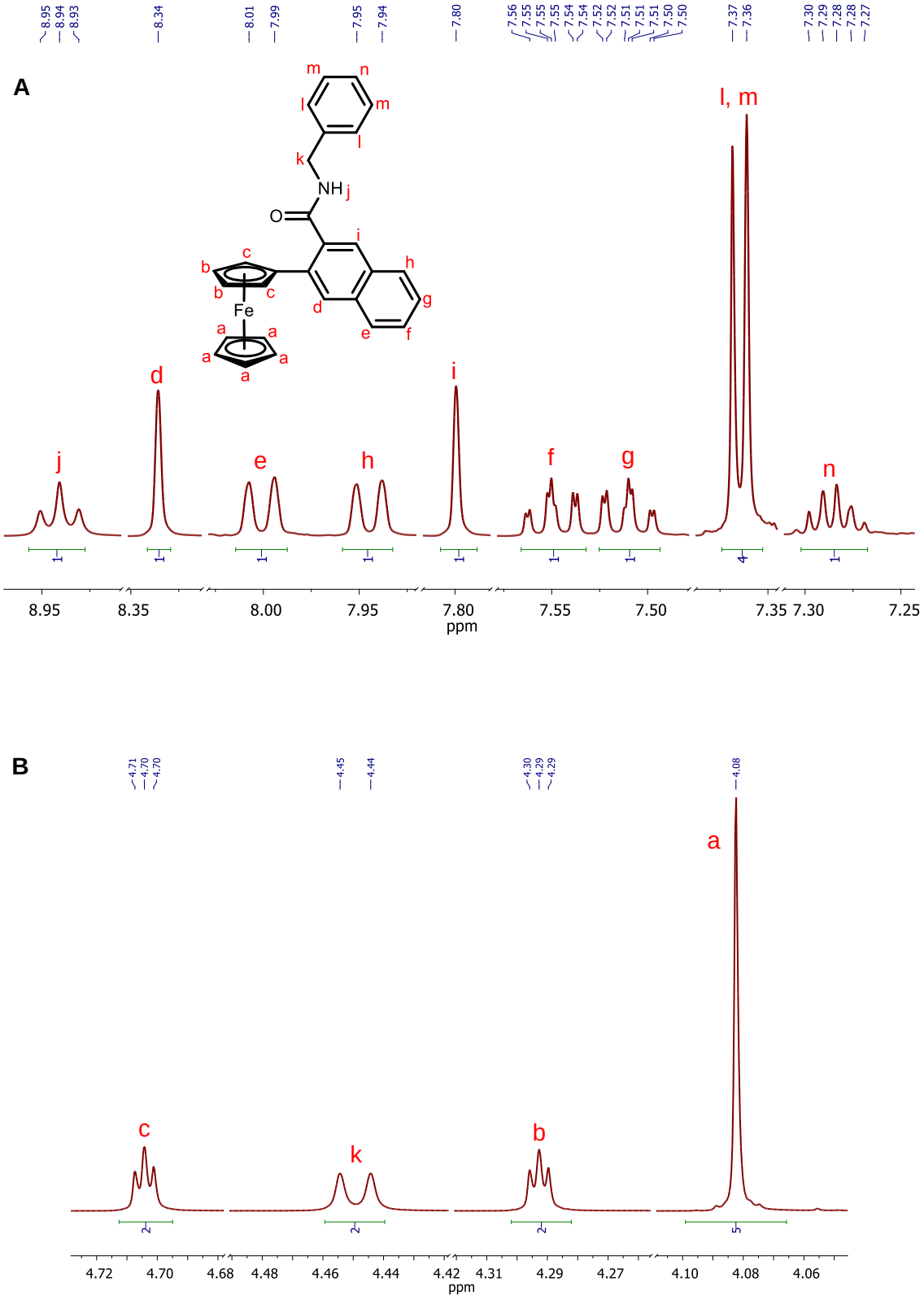

Figure 2.31. Zoom in the ^{1}H NMR spectrum of *N*-benzyl-3-ferrocenyl-2-naphthamide **107**. **A.** The aromatic region (7.25-8.95 ppm). **B.** The ferrocenyl region (4.06-4.72 ppm).

2.6 ^{13}C and DEPT-135 NMR studies of novel heterocyclic functionalised ferrocenyl derivatives

Whereas a ^{13}C spectrum shows positive peaks for every non-equivalent carbon in the molecule, in a DEPT-135 spectrum only methine and methyl carbons are present as positive signals, whilst methylene carbons are shown as negative signals and quaternary carbons are absent. ^{13}C and DEPT-135 spectra were obtained for all the compounds synthesized in this study, both intermediaries and novel ferrocenyl derivatives. The ^{13}C and DEPT-135 NMR experiments of the 6-(1′-ethyl)ferrocenyl-2-naphthoyl series were performed in $CDCl_3$, and the spectra of the rest of the derivatives were performed in DMSO-d_6 as they showed limited solubility in other deuterated solvents. Each peak reported in this section was assigned using a combination of different NMR analysis, including ^{1}H, ^{13}C, COSY, HSQC and HMBC.

2.6.1 Carbonyl ^{13}C NMR analysis

The carbonyl carbons appear at downfield positions. The amide carbon appears between δ 164.6 and δ 170.2. The isolation of NHS-ester derivatives was confirmed with two signals observed between δ 162.1 and δ 178.5; these belong to the ester group and the equivalent carbonyl groups in the NHS ring. All these carbonyl signals were confirmed as absent in DEPT-135 spectra, and are summarised in Table 2.12.

Table 2.12. Carbonyl ^{13}C NMR spectral data for novel heterocyclic functionalised ferrocenyl derivatives **99**-**120**. Values are given in ppm.

Compound	δ C=O	Compound	δ C=O
99	168.0	**110**	171.0, 164.6
100	168.4	**111**	170.9, 162.1
101	170.9, 162.5	**112**	170.2
102	166.8	**113**	166.6
103	165.9	**114**	166.5
104	169.4, 162.2	**115**	169.1
105	167.4	**116**	165.8
106	166.7	**117**	165.7
107	170.1	**118**	178.5, 169.7
108	169.1	**119**	165.6
109	171.0, 164.3	**120**	164.6

2.6.2 Aromatic ^{13}C NMR analysis

The chemical shifts of the aromatic carbons from the spacer groups appear between δ 120.9 and δ 148.6. Ten peaks are observed for derivatives with naphthalene ring, which corresponds to the ten non-equivalent carbon atoms. For derivatives with benzene ring, the number of signals depends on the position of the substituents: *ortho* and *meta* rings give six peaks as all carbons are non-equivalent, but *para* rings show only four peaks as they contain equivalent carbons. The corresponding quaternary carbons of each set were easily identified with DEPT-135 spectra, as four peaks from naphthalene ring and two peaks from benzene ring are absent. These signals are summarised in Table 2.13 for naphthoyl derivatives and in Table 2.14 for benzoyl and cinnamoyl derivatives.

Table 2.13. Aromatic linker ^{13}C NMR spectral data for novel ferrocenyl naphthoyl derivatives **99**-**108**. Values are given in ppm.

Compound	δ C_{ar} on spacer linker
99	140.1*, 135.8*, 131.2*, 130.8, 129.6, 128.1, 127.7*, 126.5, 126.0, 123.2
100	139.7*, 135.6*, 131.2*, 130.5, 129.5, 129.1*, 127.9, 126.3, 126.2, 123.2
101	142.2*, 136.8*, 132.7, 130.9*, 130.1, 129.2, 127.2, 125.3, 123.3, 120.9*
102	139.3*, 135.0*, 131.3*, 131.2*, 129.2, 127.9, 127.8,126.4, 125.0, 123.2
103	139.0*, 134.9*, 131.8*, 131.2*, 129.1, 127.7, 127.6, 126.3, 125.2, 123.2,
104	141.5*, 136.7*, 132.8, 130.8*, 129.4, 128.2, 126.4, 125.6, 123.0, 121.1*
105	139.2*, 135.2*, 131.2*, 130.6*, 128.7, 128.3, 127.3, 126.1, 123.9, 123.0
106	139.0*, 135.0*, 131.4*, 131.2*, 128.7, 127.9, 127.0, 126.0, 124.0, 123.0,
107	136.1*, 134.5*, 133.3*, 131.1*, 128.5, 128.0, 127.9, 127.4, 126.7, 126.5
108	136.6*, 134.5*, 133.3*, 131.1*, 128.5, 128.1, 127.8, 127.3, 126.6, 126.4,

* Quaternary carbon signal, absent in DEPT-135 spectra.

Table 2.14. Aromatic linker ^{13}C NMR spectral data for novel benzoyl and cinnamoyl derivatives **109**-**120**. Values are given in ppm.

Compound	δ C_{ar} on spacer linker
109	140.5*, 133.1, 132.3, 129.5, 126.7, 125.2*
110	141.9*, 130.6, 129.1, 127.3, 126.6, 124.9*
111	148.6*, 130.6, 126.7, 121.4*
112	137.2*, 136.3*, 130.4, 129.0, 127.2, 126.0,
113	139.8*, 129.2, 128.9, 125.4*, 125.3, 124.7,
114	140.3*, 131.9*, 127.9, 125.9
115	137.7*, 136.2*, 130.4, 128.7, 127.6, 125.9,
116	139.6*, 135.4*, 129.0, 128.7, 125.3, 124.7,
117	142.7*, 132.5*, 127.9, 125.7,
118	141.4*, 133.1*, 128.3, 126.6,
119	141.3*, 132.8*, 128.2, 126.6
120	141.1*, 132.9 *, 128.0, 126.6

* Quaternary carbon signal, absent in DEPT-135 spectra.

The aromatic carbons of the benzylamine derivatives **102**, **105**, **107**, **112**-**114** and **119** appear between δ 127.2 and δ 143.2 as four signals, one for each of the non-equivalent carbons in the substituted benzene ring of benzylamine: *ipso*, *ortho*, *meta* and *para*, respectively. The C_{ipso} is straightforwardly identified as it is absent in DEPT-135 spectra, and it is found more downfield compared with the rest of the benzylamine peaks (Table 2.15).

Table 2.15. Aromatic ^{13}C NMR spectral data for benzylamine derivatives **102**, **105**, **107**, **112**-**114** and **119**. Values are given in ppm.

Compound	δ C_{ar} on benzylamine
102	140.2*, 128.8, 127.7, 127.2
105	138.3*, 128.9, 128.0, 127.7
107	139.6*, 128.7, 128.1, 127.3
112	139.6*, 128.6, 128.0, 127.5
113	140.2*, 128.8, 127.7, 127.2
114	143.2*, 128.7, 127.7, 127.2
119	139.9*, 128.8, 127.9, 127.3

2.6.3 Ferrocenyl ^{13}C NMR analysis

The number of peaks for the ferrocenyl carbons varied depending on the substitution of the cyclopentadienyl rings. For the derivatives with monosubstituted ferrocene **99**-**103** and **107**-**120**, four signals are observed. Three peaks correspond to the non-equivalent carbons in the monosubstituted cyclopentadienyl ring η-C_5H_4: *ipso* (between δ 82.2 and δ 85.2), *ortho* (between δ 66.8 and δ 69.6) and *meta* (between δ 68.5 and δ 70.4); the equivalent five carbons of the unsubstituted η-C_5H_5 ring appear as a single intense peak between δ 69.8 and δ 70.3. These signals are summarized in Table 2.16. For the disubstituted ferrocene moiety in the 6-(1′-ethyl)ferrocenyl-2-naphthoyl derivatives **104**-**106**, one peak is observed for each of the ten inequivalent carbons between δ 65.6 and δ 92.1. These signals are summarized in Table 2.17. The C_{ipso} of each set is directly identified as it is absent in DEPT-135 spectra and found more downfield compared with the rest of the ferrocene peaks.

Table 2.16. Ferrocenyl ^{13}C NMR spectral data for novel heterocyclic functionalised ferrocenyl derivatives **99**-**103** and **107**-**120**. Values are given in ppm.

Compound	δ *ipso* on η^5-$\underline{C}_5H_4$	δ *ortho* on η^5-$\underline{C}_5H_4$	δ *meta* on η^5-$\underline{C}_5H_4$	δ η^5-$\underline{C}_5H_5$
99	84.4	67.2	70.1	70.0
100	84.5	67.2	70.0	69.9
101	83.8	67.4	70.4	70.1
102	84.6	67.1	70.0	69.9
103	84.6	67.1	69.9	69.8
107	84.9	69.4	68.7	70.0
108	85.1	69.4	68.6	70.0
109	83.5	69.6	69.4	70.3
110	84.3	66.8	69.7	69.9
111	82.2	67.6	70.9	70.3
112	84.9	69.2	68.7	69.9
113	84.6	66.9	69.6	69.9
114	83.7	67.1	69.9	70.0
115	85.2	69.2	68.5	69.9
116	84.7	67.0	69.5	69.9
117	83.8	67.0	69.9	70.0
118	84.4	66.8	69.7	69.9
119	84.2	66.9	69.8	69.9
120	84.3	66.9	69.8	69.9

Table 2.17. Ferrocenyl ^{13}C NMR spectral data for novel 6-(1′-ethyl)ferrocenyl-2-naphthoyl derivatives **104**-**106**. Values are given in ppm.

Compound	η^5-$\underline{C}_5H_4$-naphthoyl			η^5-$\underline{C}_5H_4$-ethyl		
	δ C*ipso*	δ C*ortho*	δ C*meta*	δ C*ipso*	δ C*ortho*	δ C*meta*
104	83.8	67.1, 65.9	70.3, 69.2	92.1	70.2, 70.0	69.0, 68.9
105	83.3	69.3, 65.7	70.1, 67.1	89.4	70.0, 68.9	70.2, 69.1
106	84.4	67.1, 65.6	70.0, 68.9	92.0	70.2, 70.1	69.3, 69.1

2.6.4 Ethyl ^{13}C NMR analysis from ethyl ferrocene derivatives

The ethyl group (-CH_2CH_3) attached to the cyclopentadiene ring in the 6-(1′-ethyl)ferrocenyl-2-naphthoyl series **104**-**106** give two peaks for each carbon: the methyl carbon (-$\underline{C}H_3$) appear at δ 14.7 and is maintained in DEPT-135 spectra, whilst the methylene carbon (-$\underline{C}H_2CH_3$) appear between δ 21.5 and δ 21.6 and become negative in DEPT-135 spectra. These signals are summarized in Table 2.18.

Table 2.18. Ethyl ^{13}C NMR spectral data for novel 6-(1′-ethyl)ferrocenyl-2-naphthoyl derivatives **104**-**106**. Values are given in ppm.

Compound	δ -$\underline{C}H_2$- on η^5-C_5H_4-ethyl	δ -$\underline{C}H_3$ on η^5-C_5H_4-ethyl
104	21.5	14.7
105	21.6	14.7
106	21.6	14.7

2.6.5 Methylene ^{13}C NMR analysis from NHS-ester and benzylamine derivatives

Compounds **101**, **104**, **109**-**111** and **118** show a peak between δ 25.6 and δ 26.0 which appears as negative in DEPT-135 spectra, hence belonging to a methylene group; this signal was key to identify those compounds as the respective NHS-ester derivatives. In the benzylamine derivatives **102**, **105**, **107**, **112**-**114** and **119**, the carbons of the methylene group next to the aromatic ring appear between δ 42.8 and δ 44.3, and are also displayed as negative in DEPT-135 spectra (Table 2.19).

Table 2.19. Methylene ^{13}C NMR spectral data for NHS-ester and benzylamine derivatives. Values are given in ppm.

Compound	Derivative	δ -$\underline{C}H_2$
101	NHS-ester	26.0
104		25.7
109		26.0
110		26.0
111		26.0
118		25.6
102	Benzylamine	43.2
105		44.3
107		43.1
112		42.9
113		43.1
114		43.0
119		42.8

2.6.6 Aliphatic ^{13}C NMR analysis from cyclohexylamine derivatives

The carbons of the cyclohexylamine moiety on **103**, **106**, **108**, **115**-**117** and **120** appear as four signals, one for each non-equivalent position on the ring. The general order observed, according with positions previously established in Figure 2.20, is: the *ipso* carbon C1 in the lowest field (between δ 48.0 and δ 48.9), the *ortho* carbons C2 and C6 (between δ 32.6 and δ 33.4), the *para* carbon C4 (between δ 25.6 and δ 25.8) and the *meta* carbons C3 and C5 (between δ 25.0 and δ 25.5). These signals are summarized in Table 2.20. Except for the *ipso* carbon, all the rest of the signals are displayed as negative peaks on DEPT-135 spectra as they belong to methylene carbons.

Table 2.20. Aliphatic ^{13}C NMR spectral data for cyclohexylamine derivatives **103**, **106**, **108**, **115**-**117** and **120**. Values are given in ppm.

Compound	δ *ipso* C1	δ *ortho* C2 and C6	δ *meta* C3 and C5	δ *para* C4
103	48.9	33.0	25.5	25.8
106	48.8	33.4	25.0	25.6
108	48.5	32.7	25.2	25.7
115	48.3	32.6	25.2	25.7
116	48.9	33.0	25.5	25.8
117	48.7	32.9	25.5	25.8
120	48.0	33.0	25.0	25.7

2.6.7 Olefinic ^{13}C NMR analysis from cinnamoyl derivatives

For the cinnamoyl series **118**-**120**, the olefinic carbons appear as two signals. The first signal appears more downfield between δ 138.7 and δ 141.3, due to this carbon being closer to the benzoyl group; the second signal is observed between δ 121.3 and δ 122.5 (Table 2.21).

Table 2.21. Olefinic ^{13}C NMR spectral data for novel ferrocenyl cinnamoyl derivatives **118**-**120**. Values are given in ppm.

Compound	δ benzoyl-CH=CH-	δ benzoyl-CH=CH-
118	141.3	122.5
119	139.4	121.3
120	138.7	121.9

2.6.8 ^{13}C and DEPT-135 NMR studies of 6-ferrocenyl-*N*-(pyridin-2-yl)-2-naphthamide 99

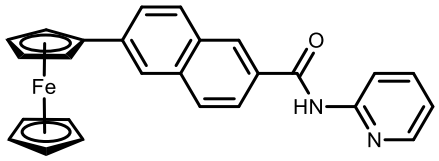

99

In the ^{13}C NMR spectrum of **99**, the carbonyl from the amide group appears downfield at δ 168.0 and it is absent from the DEPT-135 spectrum due to its quaternary nature. The aromatic non-equivalent carbons of the 6,2-disubstituted naphthoyl group are observed as ten individual peaks: the signals at δ 140.1, δ 135.8, δ 131.2 and δ 127.7 are not present in the DEPT-135 spectrum, thus identifying themselves as quaternary carbons; the six remaining carbons appear at δ 130.8, δ 129.6, δ 128.1, δ 126.5, δ 126.0 and δ 123.2, respectively. In the ferrocenyl region, the signal at δ 84.4 is not present in the DEPT-135 spectrum and thus it is assigned as the *ipso* carbon on the η^5-C_5H_4 ring; the five equivalent carbons on the unsubstituted η^5-C_5H_5 ring appear as an intense peak at δ 70.0; and the *meta* and *ortho* carbons on the η^5-C_5H_4 ring are shown at δ 70.1 and δ 67.2, respectively. For the 2-aminopyridine moiety, the *ipso* carbon is directly identified downfield at δ 160.2 as it is absent from the DEPT-135 spectrum; the remaining four non-equivalent carbons in the pyridine ring are observed at δ148.1, δ 137.4, δ 112.2 and δ 108.4, respectively (Figure 2.32 and Figure 2.33).

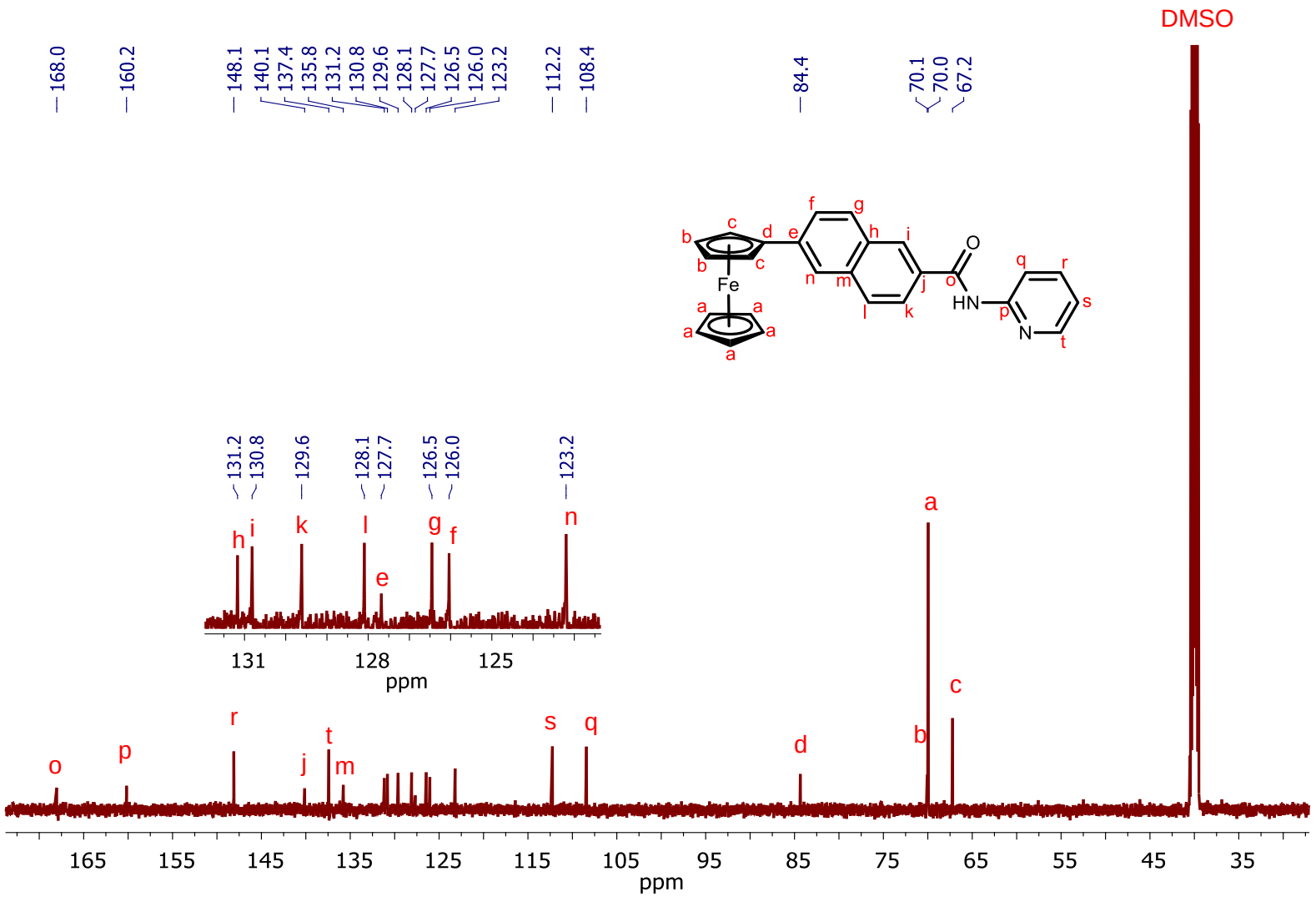

Figure 2.32. ^{13}C NMR spectrum of 6-ferrocenyl-*N*-(pyridin-2-yl)-2-naphthamide **99**.

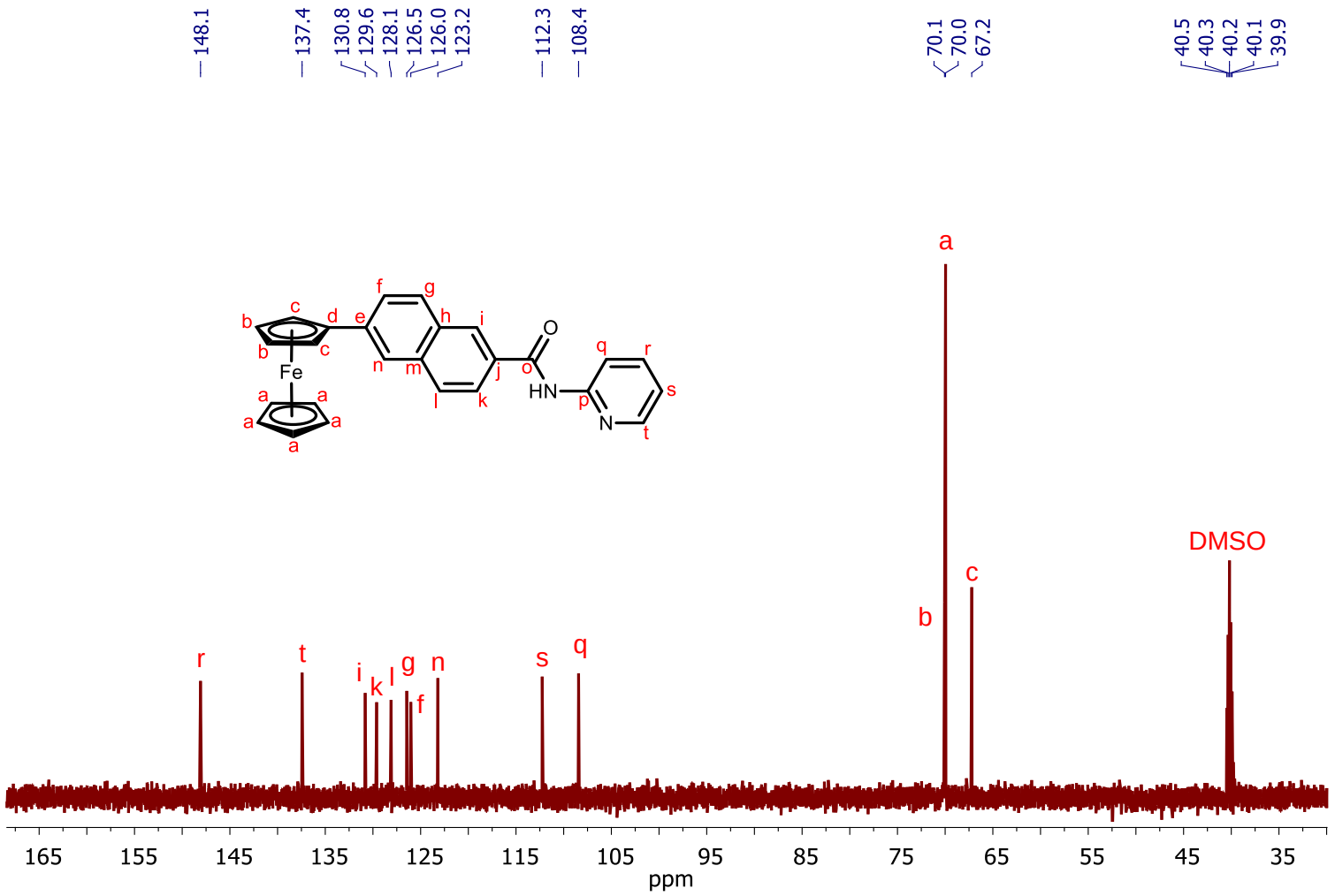

Figure 2.33. DEPT-135 NMR spectrum of 6-ferrocenyl-*N*-(pyridin-2-yl)-2-naphthamide **99**.

2.6.9 ^{13}C and DEPT-135 NMR studies of 2,5-dioxopyrrolidin-1-yl 6-ferrocenyl-2-naphthoate 101

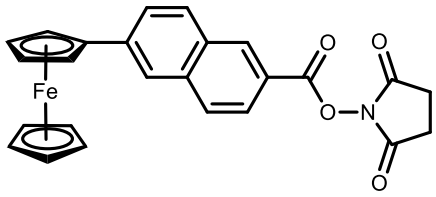

101

The ^{13}C spectrum of **101** displays two signals downfield at δ 170.9 and δ 162.5, which are absent from DEPT-135 hence revealing their quaternary nature; these can be assigned to the equivalent carbonyl groups in the NHS ring and the carbonyl carbon from the ester group, respectively. The aromatic region shows ten individual peaks, representing the ten non-equivalent carbons of the 6,2-disubstituted naphthoyl group: the signals at δ 142.2, δ 136.8, δ 130.9 and δ 120.9 are absent in the DEPT-135 spectrum, henceforth identifying them as quaternary carbons; the six remaining carbons appear at δ 132.7, δ 130.1, δ 129.2, δ 127.2, δ 125.3 and δ 123.3, respectively. In the ferrocenyl region, the signal at δ 83.8 is not present in the DEPT-135 spectrum and thus it is assigned as the *ipso* carbon on the η^5-C_5H_4 ring; the five equivalent carbons on the unsubstituted η^5-C_5H_5 ring appear as an intense peak at δ 70.1; and the *meta* and *ortho* carbons on the η^5-C_5H_4 ring are shown at δ 70.4 and δ 67.4, respectively. Finally, there is a signal upfield at δ 26.02, which was key to identify the product as the NHS-derivative because it appears as negative in the DEPT-135, hence belonging to a methylene group, which is indeed present in the NHS ring (Figure 2.34 and Figure 2.35).

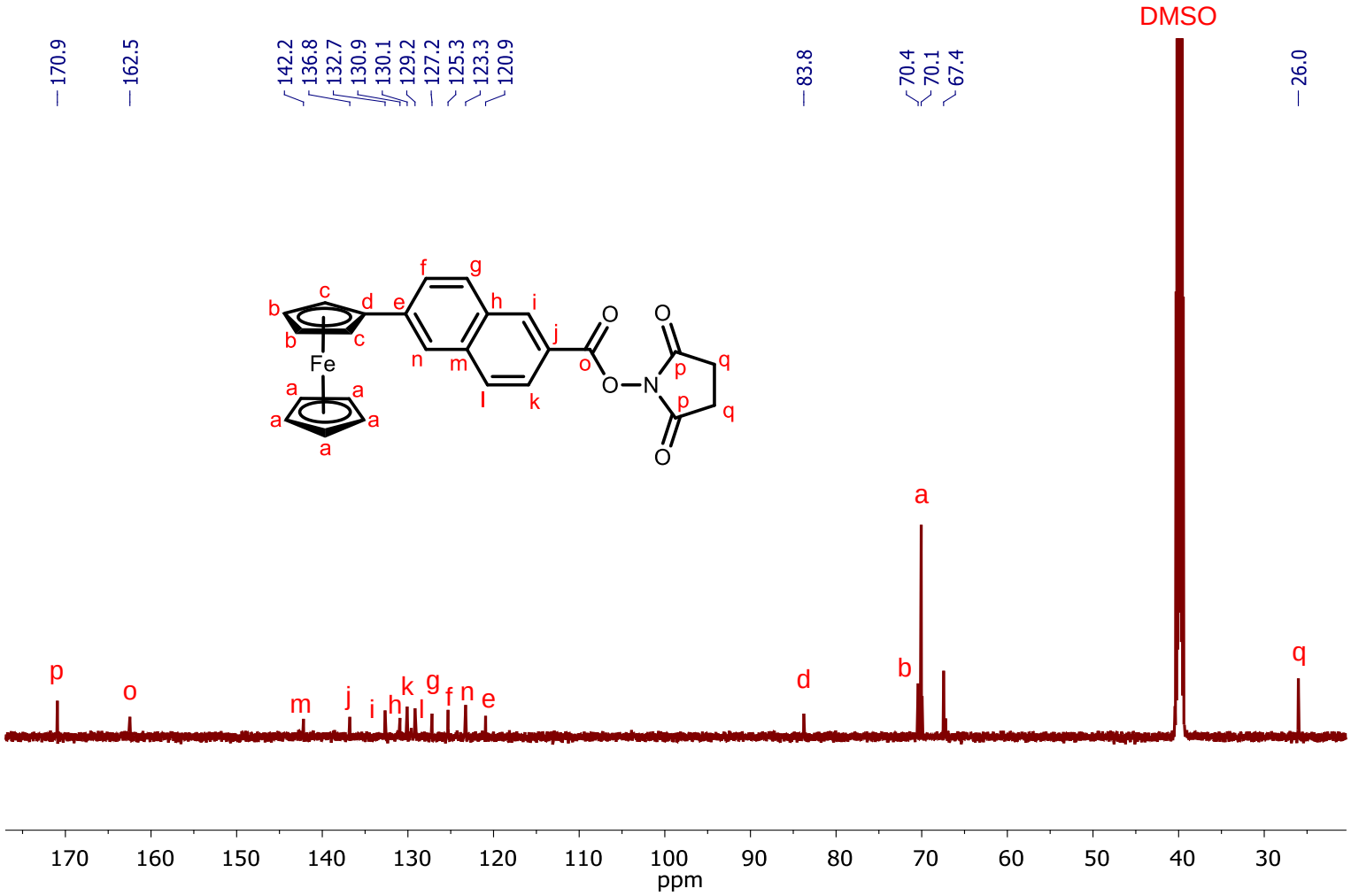

Figure 2.34. ^{13}C NMR spectrum of 2,5-dioxopyrrolidin-1-yl 6-ferrocenyl-2-naphthoate **101**.

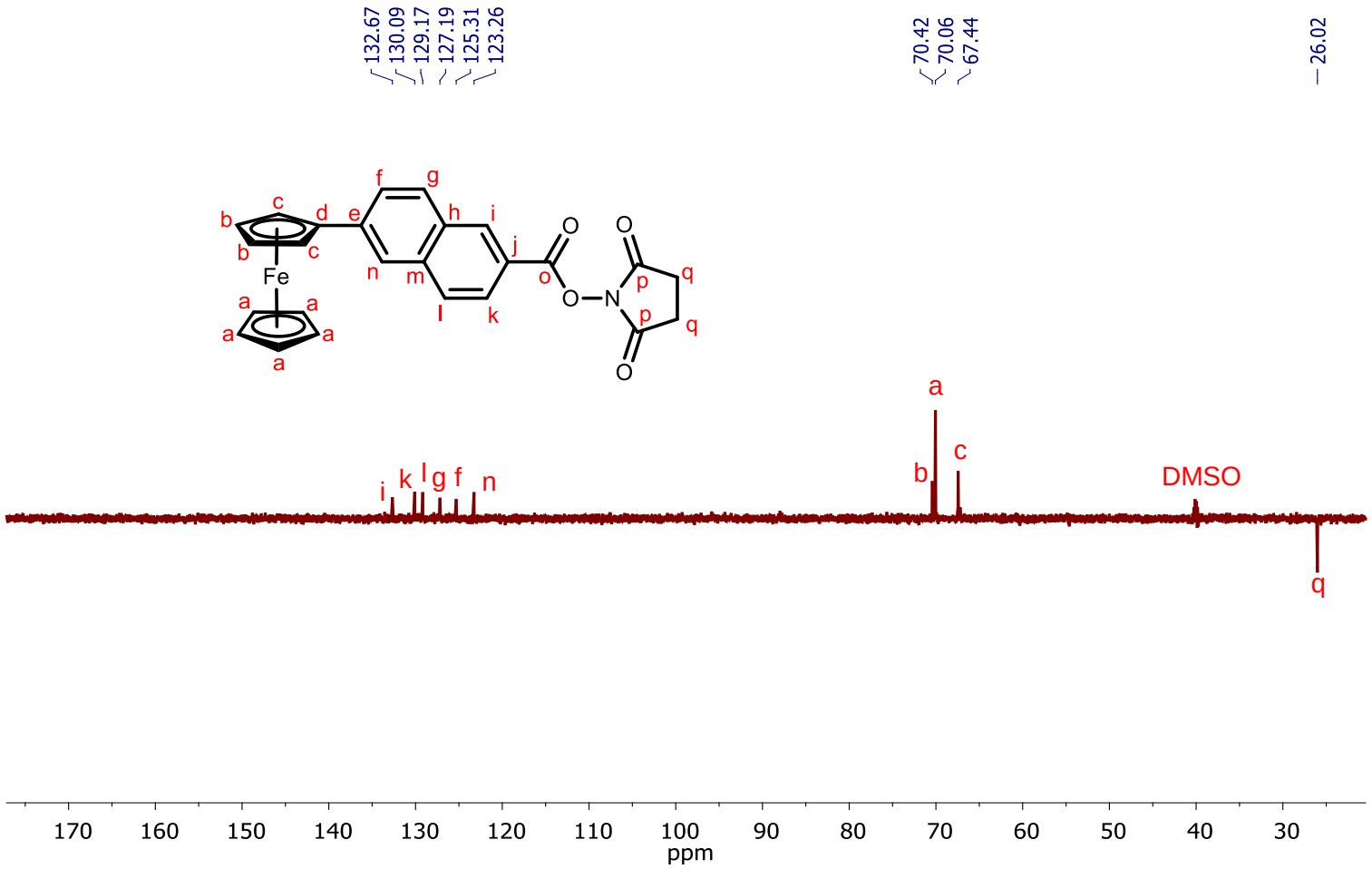

Figure 2.35. DEPT-135 NMR spectrum of 2,5-dioxopyrrolidin-1-yl 6-ferrocenyl-2-naphthoate **101**.

2.6.10 ^{13}C and DEPT-135 NMR studies of *N*-cyclohexyl-4-ferrocenylbenzamide 117

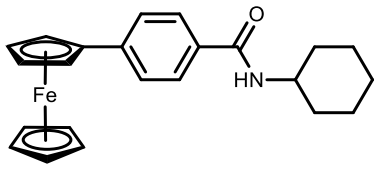

117

In the ^{13}C NMR spectrum of **117**, the carbonyl carbon peak appears downfield at δ 165.7, and it is absent from the DEPT-135 spectrum. The aromatic region shows four signals at δ 142.7, δ 132.5, δ 127.9 and δ 125.7, representing the four non-equivalent carbon atoms of the benzoyl spacer group; the first two peaks are not present in the DEPT-135 spectrum, indicating their quaternary nature. In the ferrocenyl region, the signal at δ 83.8 is absent in the DEPT-135 spectrum and therefore it is assigned as the *ipso* carbon on the η^5-C_5H_4 ring; the five equivalent carbons on the unsubstituted η^5-C_5H_5 ring appear as an intense peak at δ 70.0; and the *meta* and *ortho* carbons on the η^5-C_5H_4 ring are shown at δ 69.9 and δ 67.0, respectively. For the cyclohexylamine moiety, the *ipso* carbon is displayed more downfield compared to the rest, at δ 48.7; then the non-equivalent *ortho*, *para* and *meta* carbons are observed at δ 32.9, δ 25.8 and δ 25.5, respectively, and they appear as negative signals in the DEPT-135 spectrum (Figure 2.36 and Figure 2.37).

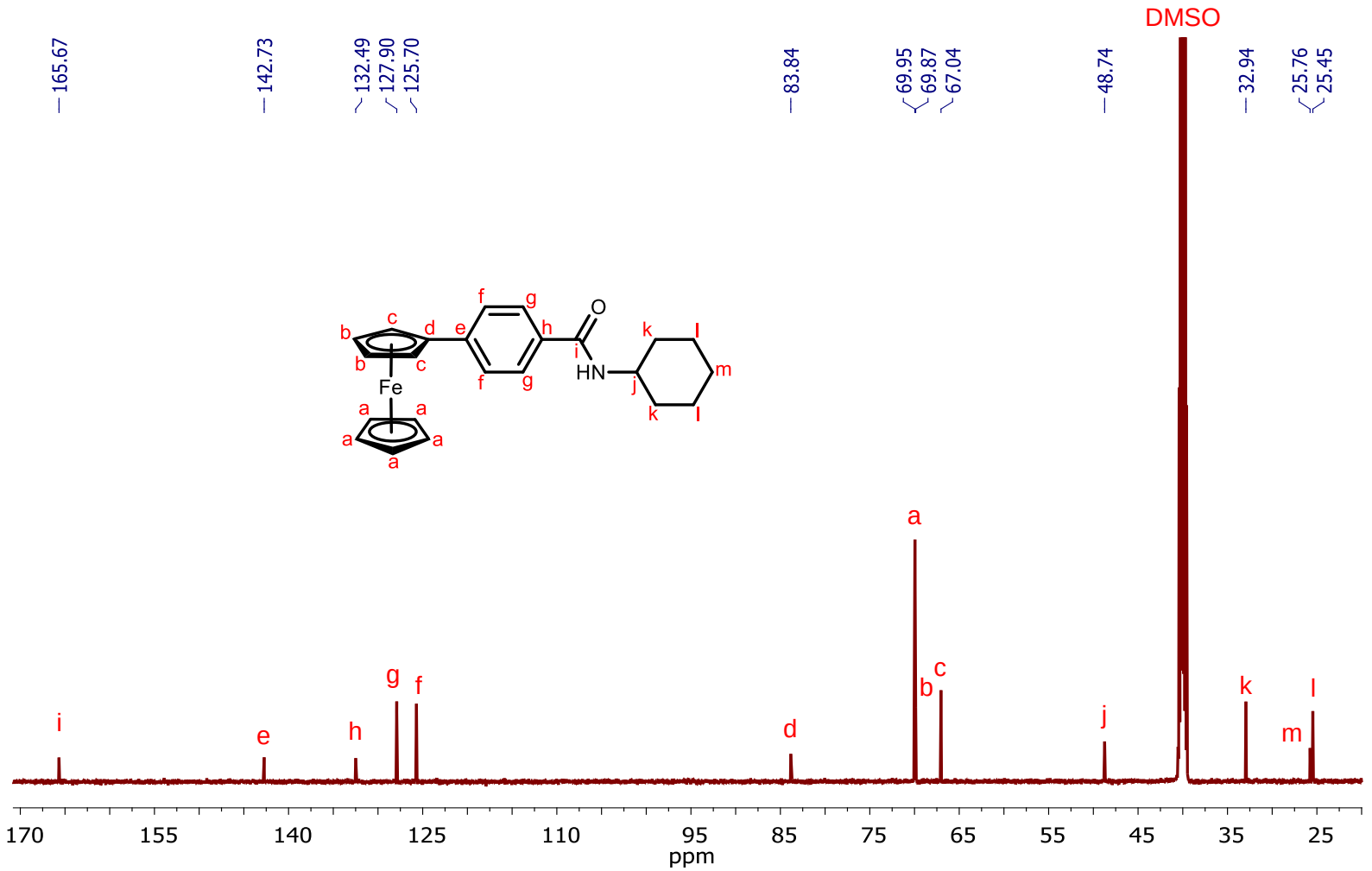

Figure 2.36. ^{13}C NMR spectrum of *N*-cyclohexyl-4-ferrocenylbenzamide **117**.

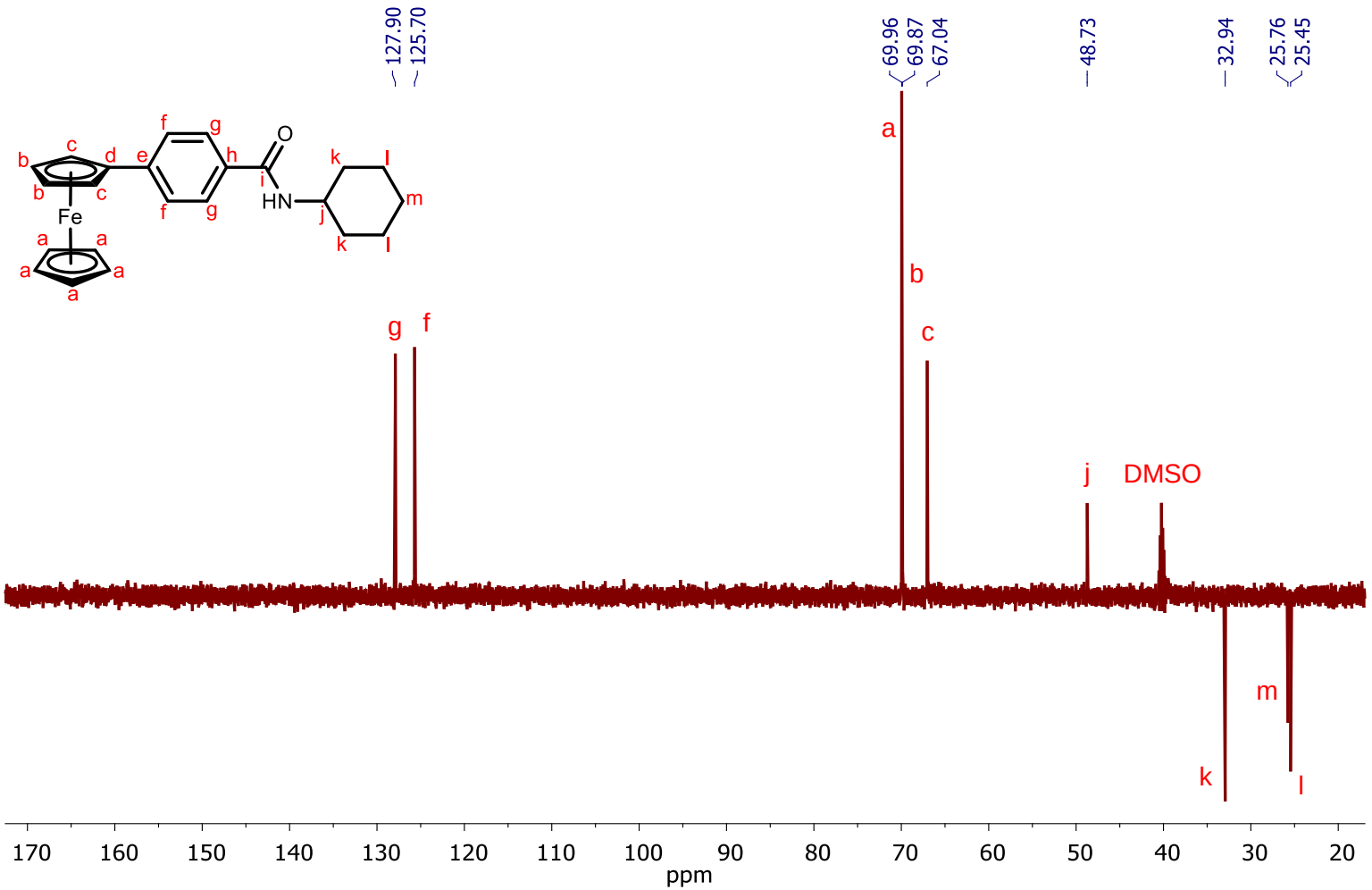

Figure 2.37. DEPT-135 NMR spectrum of *N*-cyclohexyl-4-ferrocenylbenzamide **117**.

2.7 COSY studies of novel heterocyclic functionalised ferrocenyl derivatives

The peaks in all ^{1}H NMR spectra were assigned with the help of the corresponding COSY analysis. The COSY (Correlation Spectroscopy) experiment is a simple and useful 2D experiment to reveal coupling between vicinal protons as it provides a map of the ^{1}H-^{1}H coupling network in a molecule. In a COSY spectrum, the ^{1}H NMR is found on both axes; lines can be drawn from the signals in the two-dimensional field to the peaks on each axis to determine which COSY signals go with a given proton NMR signal.[217,235]

COSY spectra were obtained for all the compounds synthesized in this study, both intermediaries and novel ferrocenyl derivatives. The COSY NMR experiments of the 6-(1′-ethyl)ferrocenyl-2-naphthoyl series were performed in $CDCl_3$, and the spectra of the rest of the derivatives were performed in DMSO-d_6 as they showed limited solubility in other deuterated solvents.

2.7.1 COSY study of *N*-benzyl-3-ferrocenyl-2-naphthamide 107

The ^{1}H NMR spectrum of **107** was previously presented in Section 2.5.10 as Figure 2.30 for reference. The COSY spectrum of **107** shows distinct spots on the diagonal with each spot corresponding to the same peak on each coordinate axis. It is clear that the amide proton (δ 8.94) correlates with the adjacent methylene protons of the benzylamine moiety (δ 4.45); this relationship was useful to identify the methylene peak as it appeared inside the ferrocenyl region. In the spots belonging to the 3,2-disubstituted naphthoyl group, it is observed that only four protons show coupling with each other, as the two remaining protons do not have neighbouring protons and thus their spots remain alone. Besides the total integration for five, the aromatic protons belonging to the benzylamine were confirmed as the spot at δ 7.36 correlates only with the spot at δ 7.28. In the ferrocenyl region, coupling is also present between the *ortho* (δ 4.70) and *meta* (δ 4.29) protons on the η^5-C_5H_4 ring (Figure 2.38).

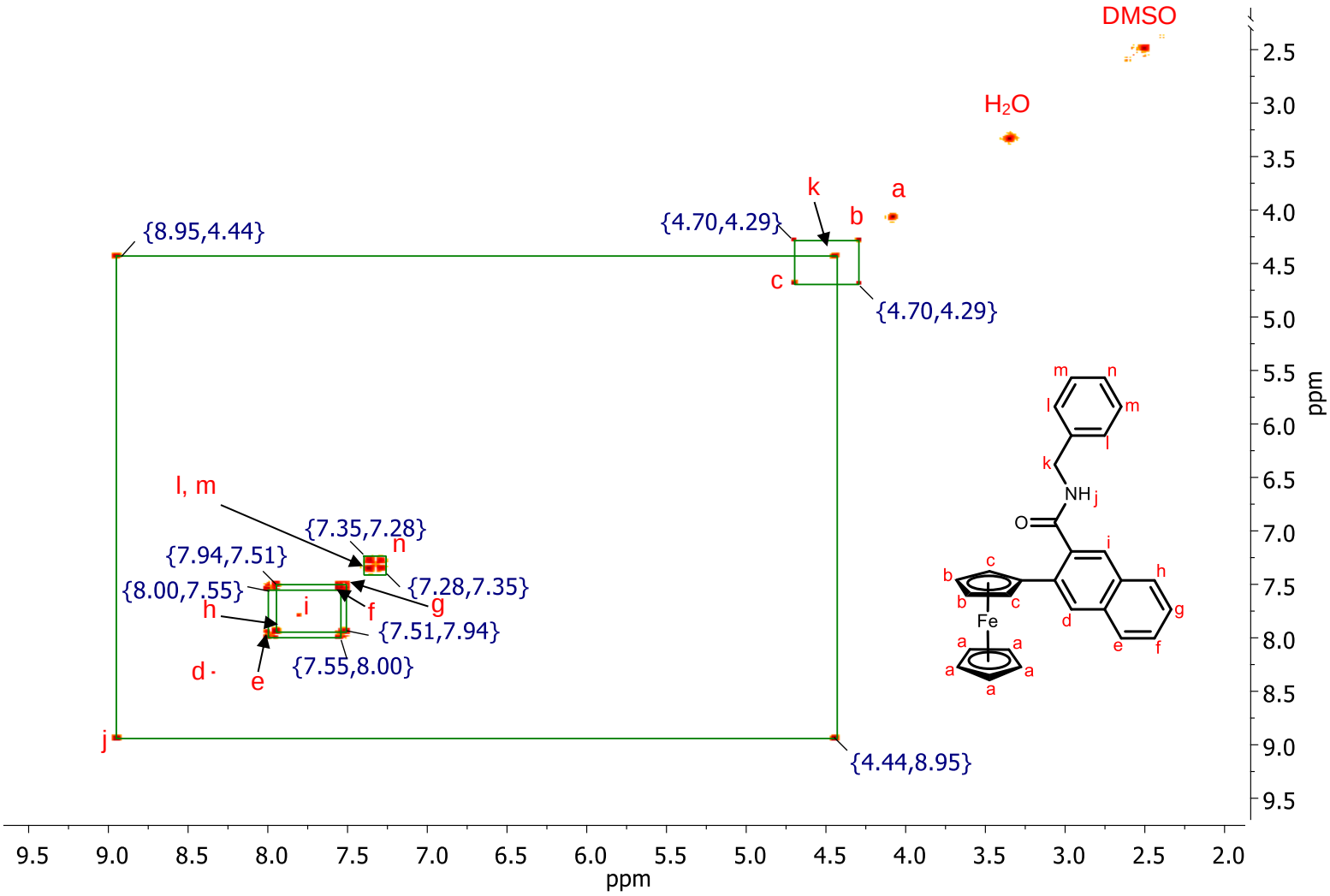

Figure 2.38. COSY spectrum of *N*-benzyl-3-ferrocenyl-2-naphthamide **107**.

2.8 HSQC and HMBC studies of novel heterocyclic functionalised ferrocenyl derivatives

HSQC (Heteronuclear Single Quantum Correlation) is a technique where two different types of nuclei (usually ^{1}H and ^{13}C) are correlated in a 2D experiment; therefore, the cross peaks of HSQC spectra associate the chemical shift of a proton with the chemical shift of the directly bonded carbon. In the other hand, HMBC (Heteronuclear Multiple Bond Correlation) utilizes multiple-bond coupling; consequently, the cross peaks shown in a HMBC spectra are between protons and carbons that are two or three bonds away, and direct one-bond cross peaks are suppressed. The combination of HSQC and HMBC represents a powerful way for tracing out the carbon skeleton of an organic compound.[235–237] The HSQC and HMBC experiments of the 6-(1′-ethyl)ferrocenyl-2-naphthoyl series were performed in $CDCl_3$, and the spectra of the rest of the derivatives were performed in DMSO-d_6 as they showed limited solubility in other deuterated solvents.

2.8.1 HSQC and HMBC studies of *N*-benzyl-3-ferrocenyl-2-naphthamide 107

The HSQC and HMBC spectra for compound **107** are shown in Figure 2.39 and Figure 2.40, respectively. The correlation sites and cross peaks can be contrasted with the ^{1}H and COSY NMR spectra of the same compound previously presented in Figure 2.30 and Figure 2.38, as follows:

In the ferrocenyl region, three peaks are observed in the proton spectrum: two triplets at δ 4.70 and δ 4.29, and a singlet at δ 4.08. As the singlet peak integrates for five protons, it can be assigned to the five protons **a** in the unsubstituted η^5-C_5H_5 ring. The two triplets integrates for two protons each, hence they can be assigned to the protons **b** and **c** on the η^5-C_5H_4 ring. A carbon signal is shown at δ 85.0, and it is assigned to the *ipso* carbon **o** on the η^5-C_5H_4 ring because it is the only ferrocenyl signal absent in the DEPT-135 spectrum. A cross peak between the triplet at δ 4.29 and this carbon signal **o** at δ 85.0 is observed in HMBC spectrum; therefore, this triplet at δ 4.29 is assigned to the *meta* protons **b** on the η^5-C_5H_4 ring, as they are two bonds away and one-bond cross peaks are suppressed from HMBC spectra. Consequently, the triplet at δ 4.70 can be assigned to the *ortho* protons **c** on the η^5-C_5H_4 ring. A second cross peak is shown for carbon **o** and the proton signal at δ 8.34; which integrates for one proton; therefore, this can be assigned to the aromatic proton **d** as it is the only proton two bonds away from **o**.

The carbonyl **t** from the amide group can be straightforwardly identified as it appears more downfield in the carbon spectra (δ 170.1). There are cross peaks between this carbon **t** and the proton signals at δ 7.80 and δ 4.45 in the HMBC spectrum; therefore, the signal at δ 7.80, which integrates for one proton, can be assigned to the aromatic proton **i** as it is the only proton two bonds away from **t**. The signal at δ 4.45 appears as a doublet integrating for two protons, and it shows HSQC correlation with the carbon at δ 43.1, which appears as negative in DEPT-135 spectra, hence indicating that belongs to $-CH_2-$ group; therefore, this signals belongs to the methylene protons **k**, which are also two bonds away from **t** and thus agreeing with the cross peak shown in the HMBC spectrum.

The methylene protons **k** (δ 4.45) also show cross peak with the carbon signal at δ 128.1 in the HMBC spectrum; therefore, this signal can be assigned to the *ortho* carbons **l** in the benzylamine moiety, as they are two bonds away from **k**. This carbon signal **l** shows HSQC correlation with the proton site at δ 7.36, which in turn also shows HSQC correlation with the carbon site at δ 128.7; hence, the proton signal at δ 7.36 can be assigned to the *ortho* and *meta* protons (**l** and **m**) from benzylamine moiety, and this signal integrates for four protons which are also related by COSY. Consequently, the carbon signal at δ 128.7 can be assigned to the *meta* carbons **m** in the benzylamine moiety. These protons also show cross peak with the carbon signal at δ 127.3, which then can be assigned to the remaining site **n** from benzylamine moiety; this agrees with the HSQC spectrum, as this carbon has a correlation site with the proton signal at δ 7.28, which integrates for one proton (**n**) and appears as a quintet due to the neighbouring protons (**l** and **m**). The signal appearing more downfield at δ 8.94 can be assigned to the amide proton **j**, as it integrates for one proton and appear as a triplet due to coupling with the adjacent two methylene protons of the benzylamine moiety.

In the aromatic region, the six protons of the 3,2-disubstituted naphthoyl group appear as a singlet at δ 8.34, two doublets at δ 8.00 and δ 7.94, a singlet at δ 7.80, and two doublet of doublet of doublets at δ 7.55 and δ 7.51; all integrating for one proton each. Their corresponding sites can be assigned due to the multiplicity of each signal: the singlets belongs to either **d** or **i**, the doublets are **e** or **h**, and the doublet of doublets are **f** or **g**. The signals at δ 8.34 and δ 7.80 were already assigned to **d** and **i**, respectively, due to HMBC cross peaks with **o** and **t**, respectively. The proton signal **i** shows HMBC cross peak with the carbon signal at δ 128.0, which has a correlation with the doublet at δ 7.94 according to HSQC spectrum; thus, this signal can be assigned to the site **h**,

because it is the only proton two bonds away from **i**. And therefore, the remaining doublet at δ 8.00 can be assigned to the proton **e**, which has a HSQC correlation with carbon at δ 127.9; this carbon signal **e** shows a HMBC cross peak with the proton at δ 7.51, which is a doublet of doublet and therefore belongs to either **f** or **g**; thus, this signal can be assigned to **g** because it is two bonds away from **e**. Consequently, the remaining signal at δ 7.55 can be assigned to the proton **f**. The quaternary carbons **p**-**s** can be identified at δ 136.1, δ 134.5, δ 133.3 and δ 131.1, as these signals are absent from DEPT-135 spectrum. The previously identified proton **g** (δ 7.51) shows HMBC cross peak with the carbon at δ 131.1, thus identifying it as **r** because it is the only quaternary carbon two bonds away from **g**. The previously identified proton **d** (δ 8.34) shows HMBC cross peak with the carbon at δ 136.1; there are two quaternary carbons which are two bonds away from **d**: **r** and **s**; as **r** had been already assigned, then this carbon signal at δ 136.1 belongs to the site **s**. The previously identified proton **h** (δ 7.94) shows HMBC cross peak with the carbon at δ 133.3, thus identifying it as **q** because it is the only quaternary carbon two bonds away from **h**. Consequently, the carbon signal at δ 134.5 can be assigned to the remaining quaternary site **p**.

A full assignment of chemical shifts for compound **107** is outlined in Table 2.22.

Table 2.22. C-H correlation data from HSQC spectrum for *N*-benzyl-3-ferrocenyl-2-naphthamide **107**. Values are given in ppm.

Site	^{1}H NMR	^{13}C NMR	HSQC	Site	^{1}H NMR	^{13}C NMR	HSQC
a	4.08	-	70.0	**o**	-	84.9	-
b	4.29	-	68.7	**p**	-	134.5	-
c	4.70	-	69.4	**q**	-	133.3	-
d	8.34	-	128.5	**r**	-	131.1	-
e	8.00	-	127.9	**s**	-	136.1	-
f	7.55	-	127.4	**t**	-	170.1	-
g	7.51	-	126.5	**u**	-	139.6	-
h	7.94	-	128.0	Carbons **o**-**u** are quaternary, thus no H attached to them.			
i	7.80	-	126.7				
j	8.94	-	-				
k	4.45	-	43.1				
l	7.36	-	128.1				
m	7.36	-	128.7				
n	7.28	-	127.3				

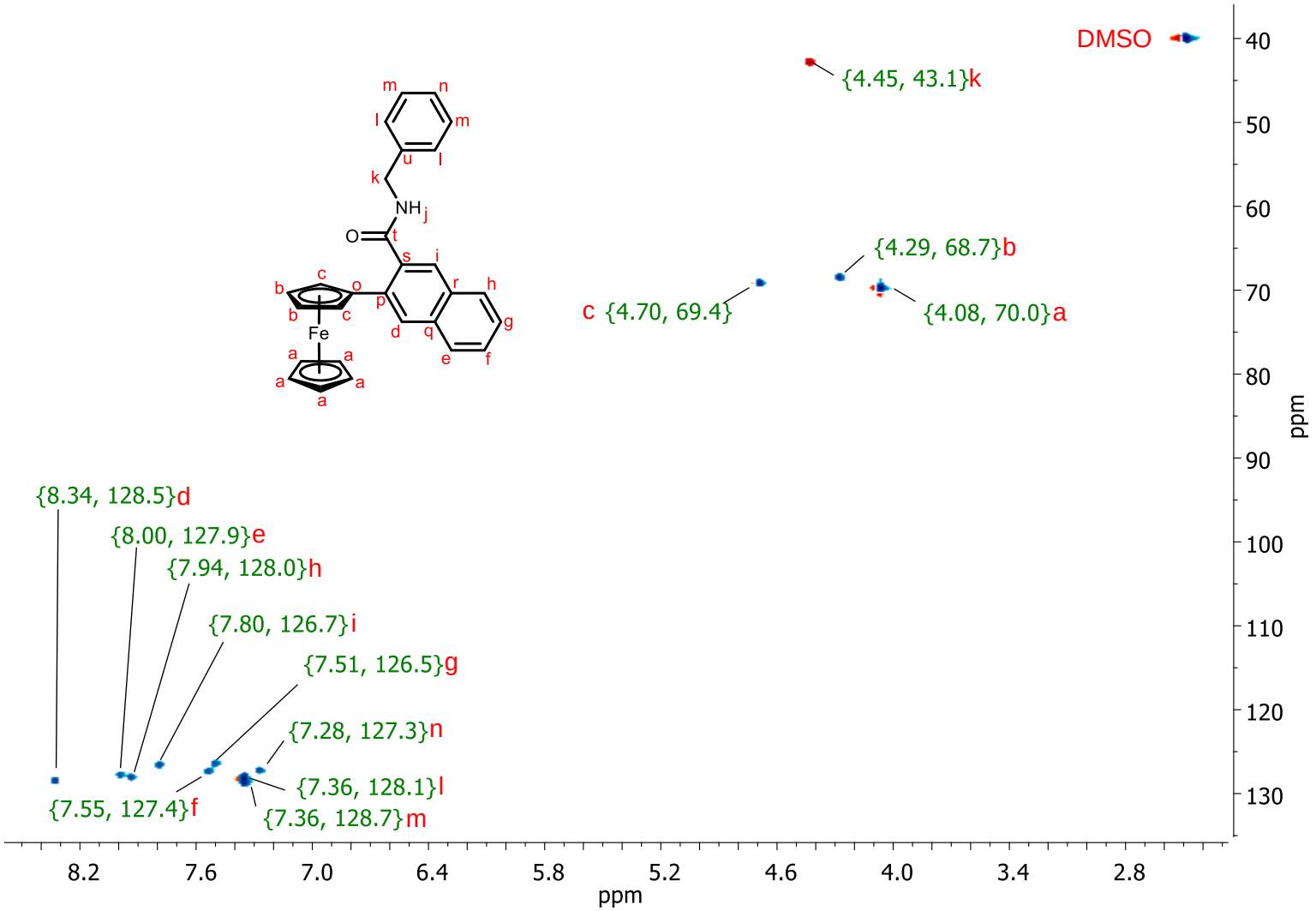

Figure 2.39. HSQC spectrum of *N*-benzyl-3-ferrocenyl-2-naphthamide **107**.

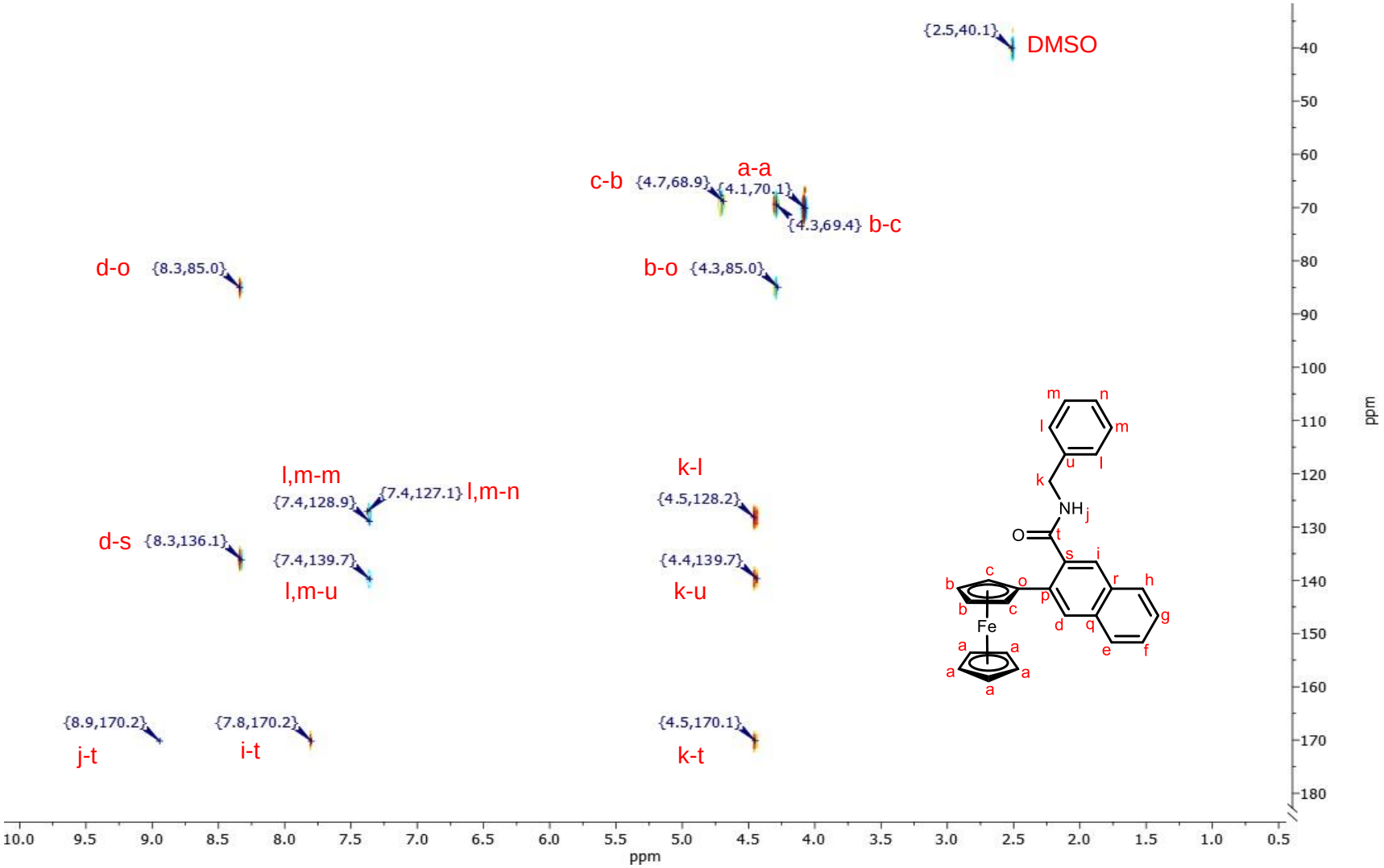

Figure 2.40. HMBC spectrum of *N*-benzyl-3-ferrocenyl-2-naphthamide **107**.

2.9 Infrared studies of novel heterocyclic functionalised ferrocenyl derivatives

Infrared (IR) spectroscopy is a technique based in the fact that compounds can absorb IR radiation and therefore a variety of molecular vibrations are induced, for example stretching, bending, rocking, etc. Substitution patterns of aromatic moieties appears in the lower region (also called fingerprint region). However, the higher region above 1500 cm^{-1} is the most informative as many functional groups can be identified here through their specific vibrations.[238,239]

The IR spectra of the novel heterocyclic functionalised ferrocenyl derivatives **99**-**120** were obtained as pure solids. For compounds containing amide bond, the spectra showed a weak sharp band above 3000 cm^{-1} that refer to the N-H stretching. For derivatives containing saturated moieties, absorption arising from the C-H stretching occurred in the region of ~3000–2840 cm^{-1}: methyl group showed two distinct bands appearing in ~2962 cm^{-1} and ~2872 cm^{-1}, resulting from asymmetrical and symmetrical stretching modes, respectively; whilst the methylene group stretches were found near ~2926 cm^{-1} (asymmetrical) and ~2853 cm^{-1} (symmetrical). In the carbonyl (C=O) region: a) for cyclic imides (NHS derivatives), two carbonyl stretches were observed from ~1770–1732 cm^{-1} and from ~1736–1680 cm^{-1}, corresponding to the two C=O groups; these overlapped to the band associated to the ester carbonyl, which usually appears around 1750 to 1735 cm^{-1}; and b) the carbonyl from the amide bond occurred at lower frequencies, between ~1650–1620 cm^{-1}. The bands in the region of ~1600–1500 cm^{-1} are characteristic of most six-membered aromatic rings.[238–241] Table 2.23 summarizes the most characteristic bands shown for the novel heterocyclic functionalised ferrocenyl derivatives **99**-**120**.

Table 2.23. Selected IR data for novel heterocyclic functionalised ferrocenyl derivatives **99**-**120**. Values are given in cm^{-1}.

Compound	N-H	C-H	C=O	Aromatic
99	3,254	3,078, 2,922	1,623	1,562 – 1,491
100	3,334	3,077, 2,984	1,624	1,584 – 1,483
101	*	3,090, 2,954	1,766, 1,732	1,625 – 1,508
102	3,286	3,101, 2,936	1,632	1,601 – 1,490
103	3,333	3,059, 2,931	1,624	1,550 – 1,492
104	*	3,093, 2,963	1,764, 1,737	1,623 – 1,506
105	3,237	2,962, 2,872	1,629	1,580 – 1,458
106	3,292	3,087, 2,925	1,624	1,602 – 1,533
107	3,224	3,055, 2,928	1,621	1,588 – 1,494
108	3,306	3,054, 2,922	1,622	1,584 – 1,493
109	*	3,103, 2,920	1,758, 1,728	1,600 – 1,501
110	*	3,095, 2,924	1,738, 1,681	1,604 – 1,503
111	*	3,081, 2,925	1,761, 1,728	1,604 – 1,526
112	3,334	3,033, 2,933	1,639	1,596 – 1,494
113	3,284	3,078, 2,921	1,629	1,602 – 1,498
114	3,293	3,090, 2,932	1,636	1,606 – 1,520
115	3,236	3,080, 2,929	1,628	1,603 – 1,502
116	3,287	3,083, 2,926	1,626	1,598 – 1,497
117	3,233	3,081, 2,924	1,626	1,610 – 1,519
118	*	3,090, 2,922	1,759, 1,732	1,599 – 1,523
119	3,237	3,035, 2,921	1,649	1,602 – 1,497
120	3,231	3,049, 2,925	1,647	1,600 – 1,525

* NHS-ester derivatives do not have N-H group.

2.9.1 Infrared studies of ferrocenyl-benzoyl derivatives 109 and 115

Figure 2.41 shows a comparison between IR spectra of two *ortho*-ferrocenyl derivatives: 2,5-dioxopyrrolidin-1-yl 2-ferrocenylbenzoate **109** and *N*-cyclohexyl-2-ferrocenylbenzamide **115**. The N-H stretching of the amide **115** appears in 3236 cm^{-1}; this band is not shown for **109**, verifying that no amide bond was formed hence the NHS intermediate was isolated. The saturated C-H stretching and bending bands in the general region of ~3100 cm^{-1}–2850 cm^{-1} are weak in **109** as only two methylene groups are found in the imide ring; these bands are more intense for **115** as a result of the cyclohexyl group. The presence of two carbonyl stretches in 1758 cm^{-1} and 1728 cm^{-1} is a diagnostic marker for cyclic imide **109**; the latter band is more intense because the carbonyl from the ester moiety is overlapped underneath. The carbonyl of **115** is part of the amide group, therefore appears at lower frequency; it is shown as a sharp band in 1628 cm^{-1}.

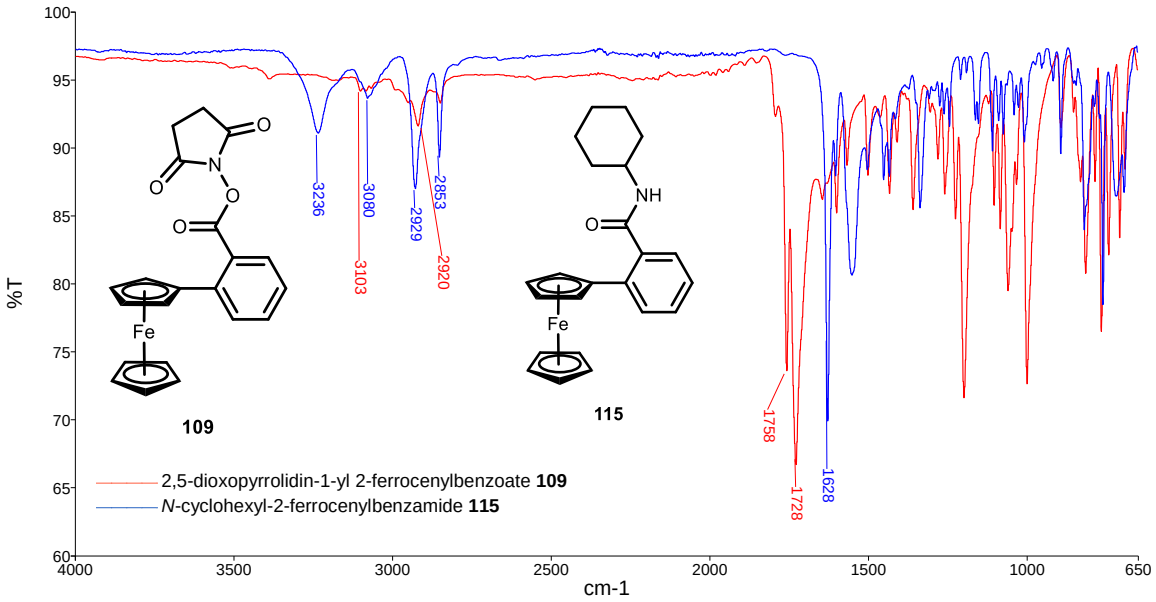

Figure 2.41. IR spectra comparison of 2,5-dioxopyrrolidin-1-yl 2-ferrocenylbenzoate **109** and *N*-cyclohexyl-2-ferrocenylbenzamide **115**.

2.10 UV-Vis spectroscopic studies of novel heterocyclic functionalised ferrocenyl derivatives

Electronic transitions between energy levels of most organic compounds can be associated to specific spectral signals in the ultraviolet and visible range (190 to 800 nm). These transitions are usually from a filled molecular orbital to a higher energy, vacant molecular orbital. Therefore, the wavelength of absorption refers to the separation of the energy levels of the orbitals involved in the transition. The absorptions located above 200 nm show the excitations of electrons from *p* and *d* orbitals, π orbitals and specifically π conjugated systems; thus, this is the most informative region of the UV-Vis spectra.[238,239]

The UV-Vis spectra of the novel derivatives **99**-**120** were obtained at a concentration of 1 mM. Extinction coefficients ε (L·mol^{-1}·cm^{-1}) were calculated from the Beer-Lambert Law: $A = \varepsilon \cdot C \cdot l$, where A is absorbance, C is concentration (mol/L) and l is the path length of the cell (cm).

The 6-ferrocenyl-2-naphthoyl derivatives give the strongest absorptions, with local maxima at ~378 nm and ~456 nm. The absorbance at ~378 nm is attributed to a π to π* transition of the aromatic spacer group, and the absorbance at ~456 nm can be assigned to a metal to ligand charge transfer band (MLCT). The absorbance due to the π to π* transition of the aromatic spacer group is much weaker for the 3-ferrocenyl-2-naphthoyl

derivatives, showing only one absorbance with a local maxima of 451. In the case of the benzoyl and cinnamoyl derivatives, the absorbances are much weaker with local maxima at ~365 nm and ~454 nm; from these series, *para* derivatives show the highest absorptions. Table 2.24 summarizes the selected maximum absorbances shown for the novel ferrocenyl naphthoyl, benzoyl and cinnamoyl derivatives **99**-**120**, and their corresponding extinction coefficients ε ($L \cdot mol^{-1} \cdot cm^{-1}$).

Table 2.24. Selected UV-Vis data for novel heterocyclic functionalised ferrocenyl derivatives **99**-**120**.

Compound	$\lambda_{max\ 1}$ (nm)	ε_1 ($L \cdot mol^{-1} \cdot cm^{-1}$)	$\lambda_{max\ 2}$ (nm)	ε_2 ($L \cdot mol^{-1} \cdot cm^{-1}$)
99	379	2,638	455	1,306
100	378	2,259	456	1,133
101	391	2,494	473	1,727
102	377	2,896	452	1,289
103	370	2,370	452	941
104	-	-	469	3,409
105	376	2,025	451	940
106	374	1,929	452	863
107	-	-	451	465
108	-	-	451	406
109	364	1,128	447	494
110	-	-	445	450
111	377	2,218	472	1,223
112	-	-	447	129
113	-	-	446	179
114	351	2,289	451	674
115	-	-	447	206
116	-	-	452	233
117	352	2,484	451	790
118	-	-	480	2,653
119	374	1,276	456	493
120	373	2,945	455	1,099

2.10.1 UV-Vis comparison of benzylamine derivatives 102, 105, 107, 112-114 and 119

The effect of conjugation of the aromatic spacer group can be compared in the UV-Vis spectra of the benzylamine derivatives of all series, shown in Figure 2.42. Compounds **102** and **105** from the 6-ferrocenyl-2-naphthoyl series have the strongest absorptions. Compound **107** belongs to the 3-ferrocenyl-2-naphthoyl series, and exhibits weaker absorption even when the spacer group is also naphthoyl. Compounds **112**, **113** and **114** corresponds to the benzoyl series (*ortho*, *meta* and *para*, respectively), and compound **119** is the cinnamoyl derivative; it can be noticed that the *ortho* derivative shows the weakest absorption overall.

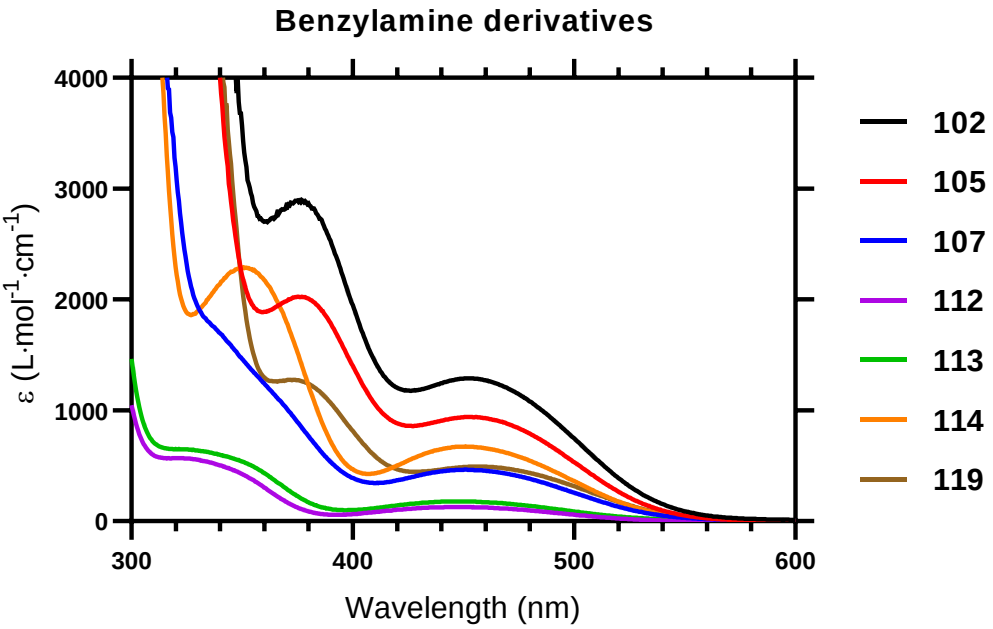

Figure 2.42. UV-Vis spectra of benzylamine derivatives **102**, **105**, **107**, **112**-**114** and **119**.

Extinction coefficients ε are a function of how efficiently a chromophore absorbs UV or visible radiation. For this reason, conjugation plays a key role in the absorption of UV-Vis radiation: when the π to π* transition of the aromatic spacer group occurs, the energy separation between the ground and excited states is reduced, hence the system absorbs at longer wavelengths and with a greatly increased intensity.[242]

These results suggest that the naphthoyl group and the (η-C_5H_4) group of the 6-ferrocenyl-2-naphthoyl derivatives **102** and **105** may be lying roughly in the same plane, hence creating a large chromophore which led to strong absorbances due to the high degree of conjugation. The weakness of the absorbance because of the π to π* transition of the aromatic spacer group of the 3-ferrocenyl-2-naphthoyl derivative **107** suggest that the (η-C_5H_4) group and the naphthoyl group may not be lying in the same plane, therefore presenting a barrier to efficient conjugation. The benzoyl series have a shorter chromophore hence their absorbances are considerably less intense than the naphthoyl series. Nevertheless, it is clear that the intensity of absorption is also consequence of their degree of conjugation, as *para* **114** and cinnamoyl **119** derivatives show much higher absorptions compared to *ortho* **112** and *meta* **113** derivatives.

2.10.2 UV-Vis comparison of benzoyl NHS-ester derivatives 109-111

The effect of conjugation in the absorption of UV-Vis radiation can be also confirmed in the spectra of the benzoyl NHS-ester derivatives **109**-**111**. The *para* derivative **111** exhibits the highest absorption from the benzoyl series because of the extent of their conjugation, followed by the *ortho* derivative **109**; the *meta* derivative **110** shows the weakest absorption (Figure 2.43).

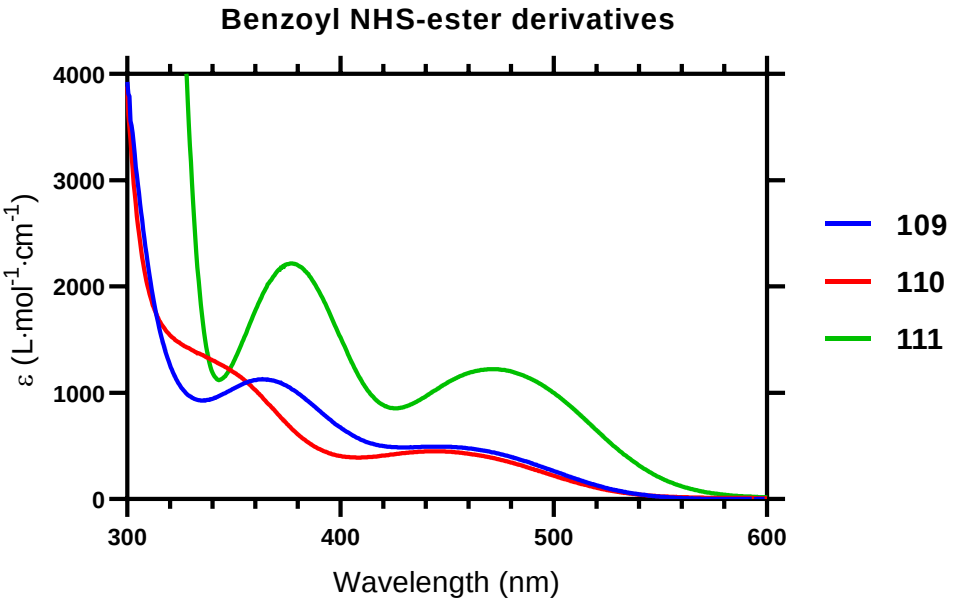

Figure 2.43. UV-Vis spectra of benzoyl NHS-ester derivatives **109**-**111**.

2.11 Mass spectrometric studies of novel heterocyclic functionalised ferrocenyl derivatives

Mass spectrometry enables the identification of the molecular mass of a compound. The sample is induced to ionize in the vapour phase, the ions produced are sorted according to their mass (*m*) to charge (*z*) ratios (*m*/*z*), and then recorded in a mass spectrum showing their relative abundances. An electron is ejected from the molecule M to give a cation radical called the molecular ion $M^{+\bullet}$ or parent ion, with the same mass but one less electron than the neutral molecule.[235,239,241,242]

2.11.1 Mass spectrometric study of 2,5-dioxopyrrolidin-1-yl 6-ferrocenyl-2-naphthoate 101

Electrospray ionization (ESI) mass spectrometry is a soft technique ideal for non-volatile compounds, hence it was employed in the analysis of 2,5-dioxopyrrolidin-1-yl 6-ferrocenyl-2-naphthoate **101**, and confirmed the correct relative molecular mass for this compound. The sequence specific fragment ions are shown in Figure 2.44A. The mass spectra revealed the presence of the molecular ion $M^{+\bullet}$ at *m*/*z* 453. A product ion at *m*/*z* 356 confirms the presence of a ferrocenyl naphthoyl ester subunit. The signal at *m*/*z* 339 is due to the cleavage at the ferrocenyl naphthoyl carbonyl group. The NHS subunit is observed in the signal at *m*/*z* 114 (Figure 2.44B).

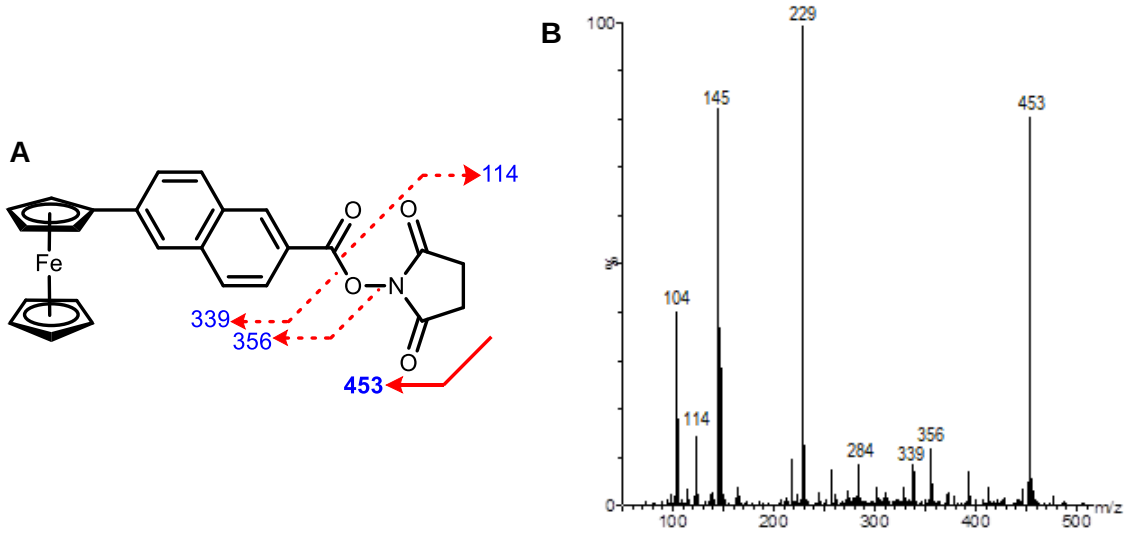

Figure 2.44. Mass spectrometric study of 2,5-dioxopyrrolidin-1-yl 6-ferrocenyl-2-naphthoate **101**. **A.** Product ions observed. **B.** ESI mass spectrum.

2.12 X-ray crystallography study of 2,5-dioxopyrrolidin-1-yl 2-ferrocenylbenzoate 109

Crystals suitable for X-ray crystallographic determination of compound **109** were grown from dichloromethane, yielding orange block shaped crystals. Figure 2.45 shows the molecular structure of 2,5-dioxopyrrolidin-1-yl 2-ferrocenylbenzoate **109** showing 50% probability ellipsoids for non-hydrogen atoms.

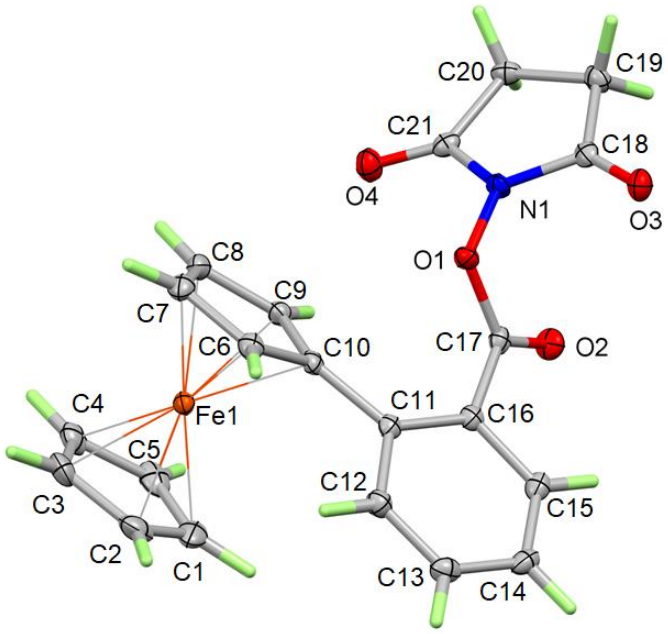

Figure 2.45. Structure of 2,5-dioxopyrrolidin-1-yl 2-ferrocenylbenzoate **109** showing 50% probability ellipsoids for non-hydrogen atoms.

Compound **109** crystallises in the monoclinic space group $P2_1/c$. All the bond lengths and angles are in the expected ranges. There are no very obvious intermolecular interactions. The principal dimensions are: carboxylate ester C=O 1.1955 (18) Å, C-O 1.3958 (17) Å and O-N 1.3880 (15) Å, and O=C-O 121.68 (13)°. The cyclopentadienyl rings of the ferrocene unit are in the eclipsed conformation. The interplanar angle between the Cp ring containing C6-C10 and the attached phenyl ring (C11-C16) is 34.86 (6)°; this data demonstrates the existence of a distortion in the molecule, which is evident from Figure 2.45. The steric hindrance due to the *ortho* position has forced the atoms of **109** to adopt this strained conformation in the solid state, resulting in a loss of co-planarity of the conjugating groups. This is supported by the torsion angles for the C12-C11-C10, C16-C11-C10 and O1-C17-C16 bonds, which were calculated to be 117.51 (12)°, 125.14 (13)° and 112.16 (11)°, respectively. A similar observation has been reported in the X-ray crystallography study of the intermediate methyl 3-ferrocenyl-2-naphthoate **69**.[188]

Table 2.25. Crystal data and structure refinement for 2,5-dioxopyrrolidin-1-yl 2-ferrocenylbenzoate **109**.

Details	Compound 109
Empirical formula	$C_{21}H_{17}NO_4Fe$
Formula weight	403.21
Temperature/K	100.01(10)
Crystal system	Monoclinic
Space group	$P2_1/c$
a/Å	20.1605(3)
b/Å	7.47160(10)
c/Å	11.4251(2)
α/°	90
β/°	100.4280(10)
γ/°	90
Volume/Å^3	1692.55(5)
Z	4
ρ_{calc} g/cm^3	1.582
μ/mm^{-1}	7.394
F(000)	832.0
Crystal size/mm^3	0.248 × 0.095 × 0.085
Radiation	CuKα (λ = 1.54184)
2θ range for data collection/°	8.92 to 149.404
Index ranges	-24 ≤ h ≤ 22, -9 ≤ k ≤ 7, -12 ≤ l ≤ 14
Reflections collected	10221
Independent reflections	3326 [R_{int} = 0.0193, R_{sigma} = 0.0194]
Data/restraints/parameters	3326/0/244
Goodness-of-fit on F^2	1.035
Final R indexes [I>=2σ (I)]	R_1 = 0.0241, wR_2 = 0.0595
Final R indexes [all data]	R_1 = 0.0258, wR_2 = 0.0604
Largest diff. peak/hole / e Å^{-3}	0.26/-0.30

Table 2.26. Selected bond lengths (Å) for 2,5-dioxopyrrolidin-1-yl 2-ferrocenylbenzoate **109**.

Bond	Length (Å)	Bond	Length (Å)
Fe1—C1	2.0404 (16)	O4—C21	1.2015 (18)
Fe1—C6	2.0506 (14)	N1—C18	1.3860 (18)
O1—N1	1.3880 (15)	N1—C21	1.3966 (18)
O1—C17	1.3958 (17)	C10—C11	1.4792 (18)
O2—C17	1.1955 (18)	C11—C16	1.405 (2)
O3—C18	1.2078 (17)	C16—C17	1.484 (2)

Table 2.27. Selected bond angles (°) for 2,5-dioxopyrrolidin-1-yl 2-ferrocenylbenzoate **109**.

Bond	Angle (°)	Bond	Angle (°)
C11—C10—Fe1	122.68 (10)	O2—C17—O1	121.68 (13)
C12—C11—C10	117.51 (12)	O3—C18—C19	130.06 (13)
C12—C11—C16	117.30 (13)	O3—C18—N1	124.01 (13)
C16—C11—C10	125.14 (13)	O4—C21—C20	129.75 (13)
C18—N1—O1	120.80 (11)	O4—C21—N1	125.17 (14)
O1—C17—C16	112.16 (11)	N1—C18—C19	105.93 (11)
O1—N1—C21	122.37 (11)	N1—C21—C20	105.08 (12)
O2—C17—C16	125.98 (13)	N1—O1—C17	111.14 (10)

2.13 Proposed synthesis for *N*-(5-ferrocenyl-1-naphthoyl) derivatives

2.13.1 Introduction

The general synthetic route proposed for the *N*-(5-ferrocenyl-1-naphthoyl) derivatives is outlined in Scheme 2.18. This route is slightly different than the synthesis mentioned before because no 5-amino-1-naphthoic acid was commercially available, but 1,5-diaminonaphthalene **83** was chosen as a suitable substitute. The starting material **83** was treated with acetic anhydride [$(CH_3CO)_2O$] and pyridine, resulting in the protection of one of the amino groups and the formation of the *N*-acetyl derivative **84**; previous studies showed the BOC protected species could not be prepared.[194] The *N*-(5-aminonaphthalen-1-yl)acetamide **84** then would undergo a diazonium coupling reaction to generate the *N*-(5-ferrocenylnaphthalen-1-yl)acetamide **85**, which would be then deprotected to yield 1-ferrocenyl-5-aminonaphthalene **86**. Compound **86** was expected to be coupled with the three aminopyridines **94**-**96**, benzylamine **97** and cyclohexylamine **98** via EDC/NHS coupling protocol. The procedure is similar to that used for the synthesis of the previous ferrocenyl dipeptide esters in Dr. Peter Kenny's research group.[181,183–195]

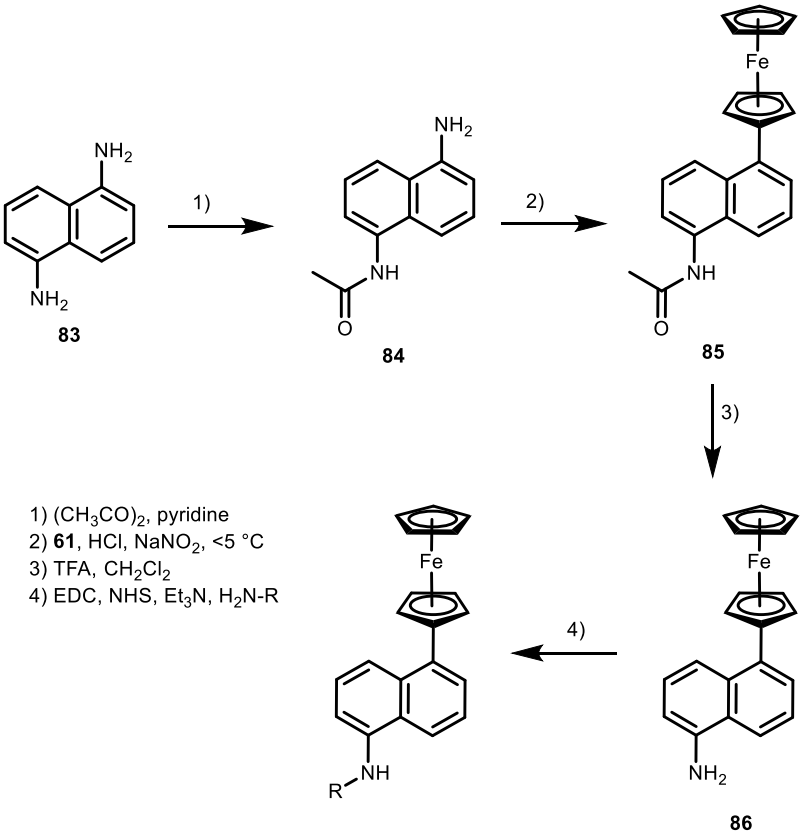

Scheme 2.18. The general reaction scheme proposed for the synthesis of *N*-(5-ferrocenyl-1-naphthoyl) derivatives.

2.13.2 Protection of the amine group via acetylation

The acetyl group was proposed in order to protect one of the amine groups present in the starting material 1,5-diaminonaphthalene **83**. This group can be introduced via acetic anhydride [$(CH_3CO)_2O$] and pyridine, resulting in the formation of the *N*-acetyl derivative **84** (Scheme 2.19). The procedure is similar to that used for the synthesis of the previous ferrocenyl dipeptide esters in Dr. Peter Kenny's research group.[181,183–195] The mechanism of this reaction is detailed in Scheme 2.20.[243]

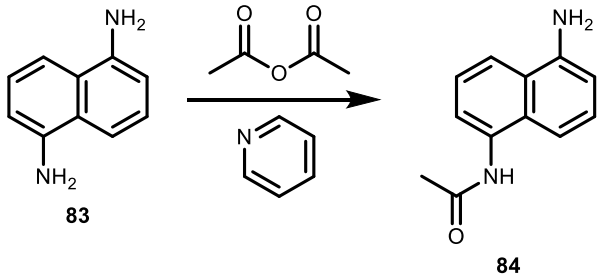

Scheme 2.19. Acetylation of the amino group in 1,5-diaminonaphthalene **83** using acetic anhydride and pyridine.

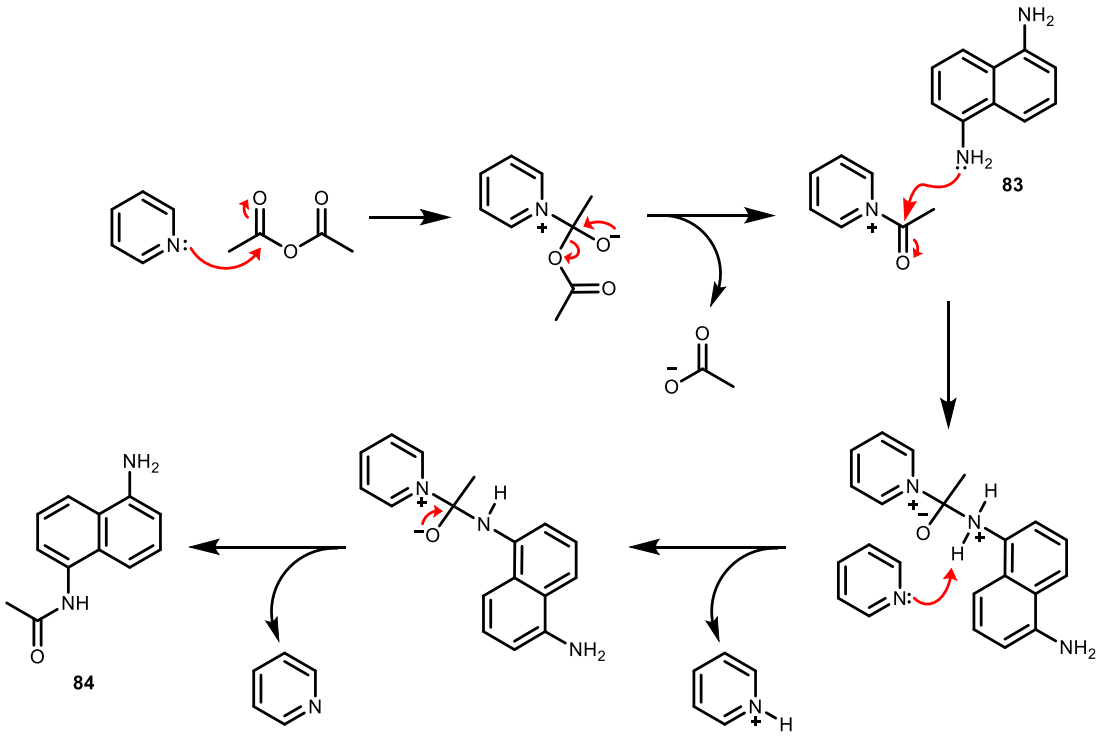

Scheme 2.20. Reaction mechanism of the acetylation of 1,5-diaminonaphthalene **83** using acetic anhydride and pyridine.

2.13.2.1 Purification and yield of *N*-(5-aminonaphthalen-1-yl)acetamide 84

The acetylation step was proposed as an uncomplicated way to protect one amino group of the starting material 1,5-diaminonaphthalene **83**; however, when the reaction was carried out, it was observed that the main product was the di-acetylated derivative **121**. Therefore, a low yield was obtained for the desired product *N*-(5-aminonaphthalen-1-yl)acetamide **84**.

Acetic anhydride was added to a solution of 1,5-diaminonaphthalene **83** and pyridine. After reacting for 24 h with stirring at rt, the resulting mixture was poured onto HCl on ice to precipitate a lilac solid, which was identified by ^{1}H NMR as the di-acetylated product *N*,*N*′-(naphthalene-1,5-diyl)diacetamide **121**. This product was disregarded via vacuum filtration, and the desired product *N*-(5-aminonaphthalen-1-yl)acetamide **84** was present in the filtered solution. The crude product was purified by column chromatography, using a mixture of ethyl acetate and hexane as the mobile phase. The purified compound was furnished as a brown/purple solid with a yield of 14%.

2.13.2.2 ^{1}H NMR studies of compounds 84 and 121

The ^{1}H NMR spectrum of the di-acetylated product *N*,*N*′-(naphthalene-1,5-diyl)diacetamide **121** is shown in Figure 2.46. In this spectrum, there is a singlet at δ 9.97 with integration for two protons, which are the two new amide groups formed. The 1,5-disubstituted naphthoyl region confirms the presence of six protons, which appear as two apparent doublets at δ 7.91 and δ 7.67, and a triplet at δ 7.52, integrating for two protons each. The success of the reaction can be seen in the singlet at δ 2.18 integrating for six protons, which belong to the new CH_3- groups formed during the acetylation of the starting material **83**. These integrals concluded this is the di-acetylated product **121**.

The ^{1}H NMR spectrum of the *N*-(5-aminonaphthalen-1-yl)acetamide **84** is shown in Figure 2.47. In this spectrum, there is a singlet at δ 9.72 with integration for one proton, belonging to the new amide group formed. The 1,5-disubstituted naphthoyl region confirms the presence of six protons, which appear as two apparent doublets at δ 7.89 and δ 7.58 with integration for one proton each, a triplet at δ 7.32 with integration for one proton, an apparent doublet at δ 7.23 with integration for two protons, and a doublet of doublets at δ 6.69 with integration for one proton. There is a singlet at δ 5.73 integrating for two protons, which correspond to the remaining amino group. The success of the reaction can be observed with the singlet at δ 2.15 integrating for three protons, which belong to the new CH_3- group formed during the acetylation of the starting material **83**.

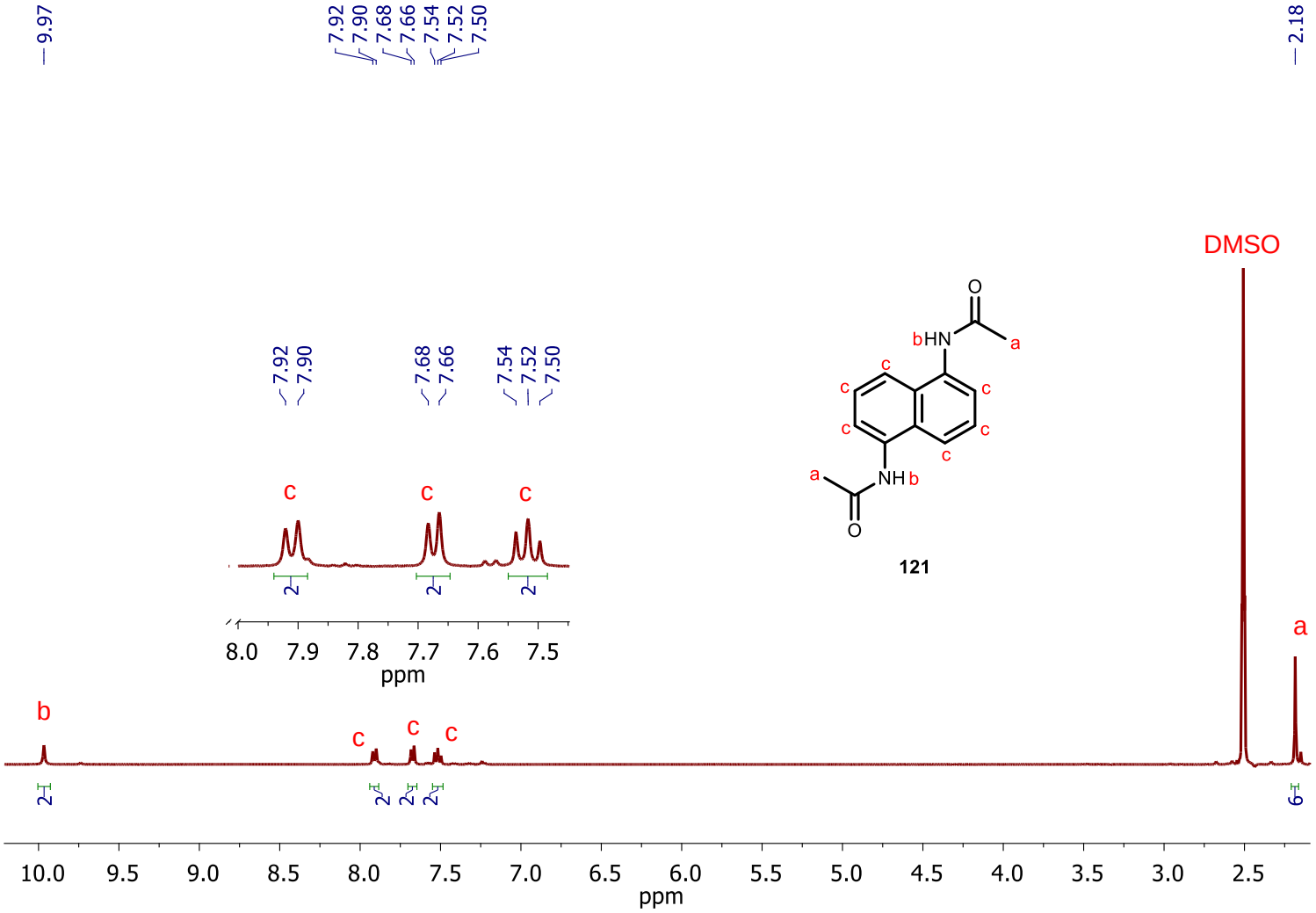

Figure 2.46. ^{1}H NMR spectrum of *N*,*N*′-(naphthalene-1,5-diyl)diacetamide **121**.

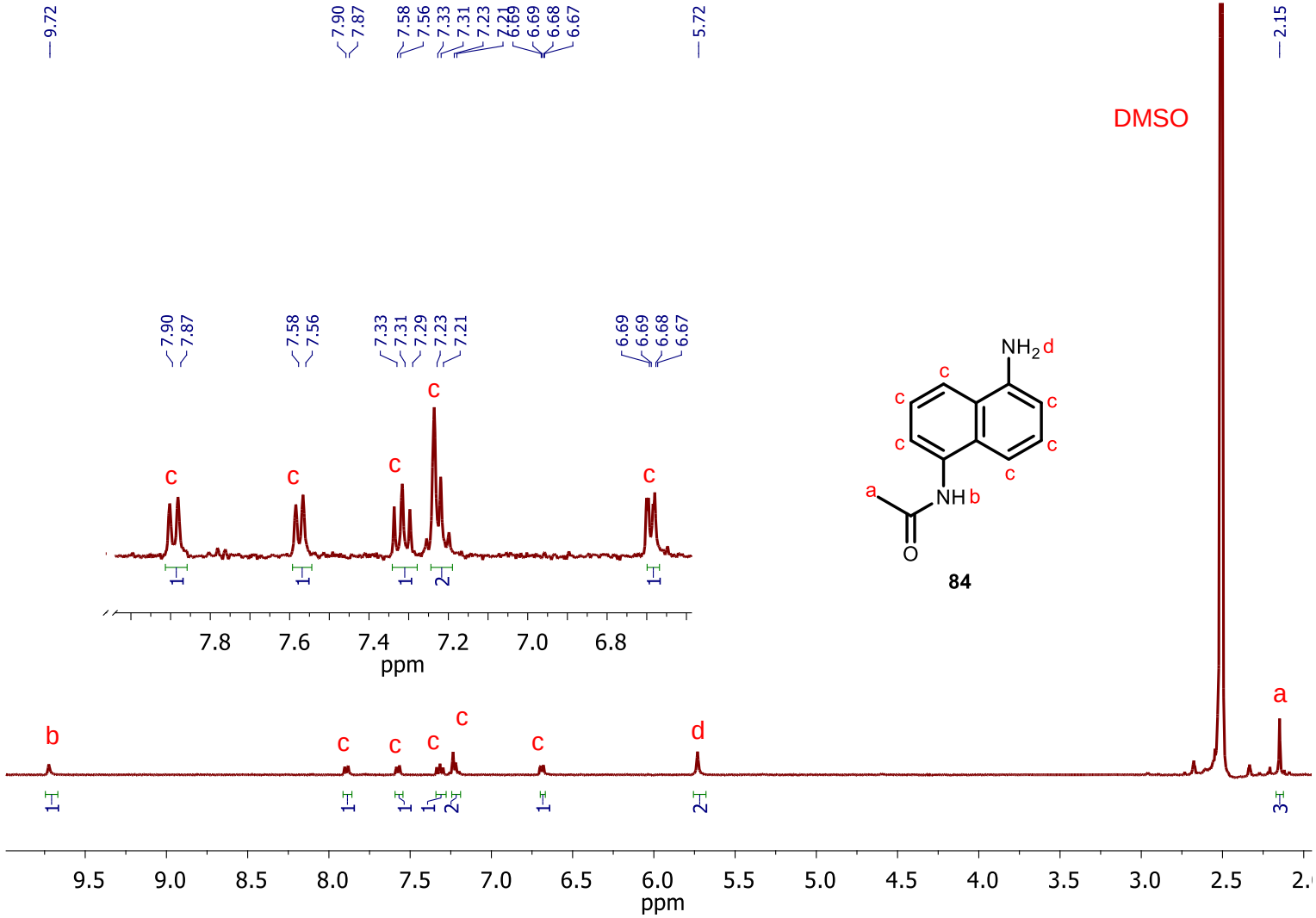

Figure 2.47. ^{1}H NMR spectrum of *N*-(5-aminonaphthalen-1-yl)acetamide **84**.

The information obtained from these ^{1}H NMR studies can be contrasted in Table 2.28 and Table 2.29.

Table 2.28. ^{1}H NMR spectral data of *N*,*N*′-(naphthalene-1,5-diyl)diacetamide **121**.

δ (ppm)	Multiplicity	Integration	Location	*J* (Hz)
9.97	s	2H	-CONH-	-
7.91	d	2H	H_{ar}	8.36
7.67	d	2H		7.32
7.52	t	2H		7.94
2.18	s	6H	CH_3-	-

Table 2.29. ^{1}H NMR spectral data of *N*-(5-aminonaphthalen-1-yl)acetamide **84**.

δ (ppm)	Multiplicity	Integration	Location	*J* (Hz)
9.72	s	1H	-CONH-	-
7.89	d	1H	H_{ar}	8.40
7.58	d	1H		7.48
7.32	t	1H		8.14
7.23	d	2H		6.48
6.69	dd	1H		6.52, 2.28
5.73	s	2H	NH_2-	-
2.15	s	3H	CH_3-	-

2.13.3 Introduction of the ferrocenyl moiety via diazonium coupling

Ferrocene **61** was tried to be introduced into the *N*-(5-aminonaphthalen-1-yl)acetamide **84** via standard diazonium coupling protocol to yield the *N*-(5-ferrocenylnaphthalen-1-yl)acetamide **85** (Scheme 2.21). The procedure is similar to that used for the synthesis of the previous ferrocenyl dipeptide esters in Dr. Peter Kenny's research group.[181,183–195]

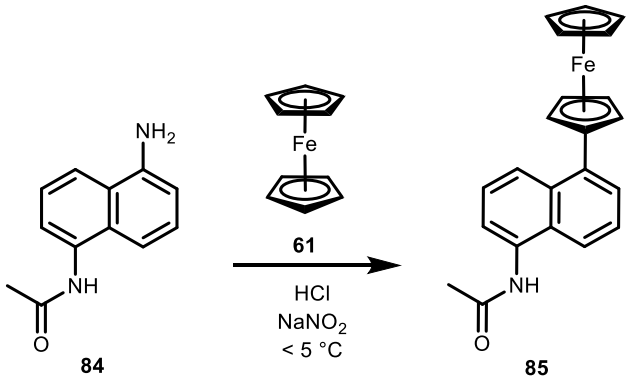

Scheme 2.21. Expected diazonium coupling reaction of *N*-(5-aminonaphthalen-1-yl)acetamide **84** with ferrocene **61**.

However, this reaction did not succeed with the procedure effectively described in Section 2.2.4 for the rest of the novel heterocyclic functionalised ferrocenyl derivatives. Experimental conditions were varied in diverse ways in order to approach the desired product **85**, as shown in Table 2.30. Nevertheless, this reaction was not fruitful. A possible explanation for this failure is further discussed in Section 2.13.4.

Table 2.30. Experimental conditions varied for diazonium coupling reaction of *N*-(5-aminonaphthalen-1-yl)acetamide **84** with ferrocene **61**.

Trial	*N*-(5-aminonaphthalen-1-yl)acetamide 84 (eq)	HCl (eq)	$NaNO_2$ (eq)	Ferrocene 61 (eq)	T (°C)	*t* (h)
1	0.85	12.5	1.0	1.0	5	24
2	0.85	12.5	1.0	1.0	5	48
3	0.85	12.5	1.0	1.0	5	72
4	0.85	12.5	1.0	1.0	0	24
5	0.85	12.5	1.0	1.0	0	48
6	0.85	12.5	1.0	1.0	0	72
7	1.0	15.0	1.0	1.0	5	24
8	1.0	15.0	1.0	1.0	5	48
9	1.0	15.0	1.0	1.0	5	72
10	0.85	12.5	1.0	1.0	< 0	48

The direct diazonium coupling reaction between ferrocene **61** and the starting material 1,5-diaminonaphthalene **83** without protection of any of the amino groups was also tried, but no evidence of the new product was observed again. As product **85** could not be obtained, this synthetic route was abandoned.

2.13.4 Discussion

The acetylation of the starting material 1,5-diaminonaphthalene **83** did not proceed as expected because the diacetylated derivative *N*,*N*′-(naphthalene-1,5-diyl)diacetamide **121** was the main product of the reaction, in spite of the fact that *N*-(5-aminonaphthalen-1-yl)acetamide **84** was obtained in a low yield.

The coupling reaction of **84** with ferrocene **61**, however, was not successful. A steric hindrance is not a plausible explanation for 1,5-orientation, because this substitution reaction has been proven effective in compounds with 3,2-orientation (more hindered). Therefore, it can be possible that the substituent groups by themselves are impeding the course of the reaction. A comparison between **84** and its 6,2-analogue **60**, which has been successfully coupled to ferrocene **61**, shows that the main difference lies in the electron-donating behaviour of the -NHCO- group in **84**, contrasting with the electron-withdrawing group -COO- of **60** (Figure 2.48).

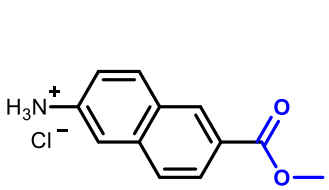

60

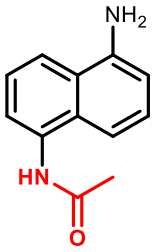

84

Figure 2.48. Structural comparison between compounds **60** and **84**.

There are some related precedents in the literature, as the comparison of the electrostatic potential surfaces between benzenediazonium cation **122** and *p*-nitrobenzenediazonium cation **123** which are shown in Figure 2.49 (red means a more negative potential and blue means a more positive potential). These diagrams illustrate the stronger diazonium group's positive polarization by the electron-withdrawing nitro group.[244]

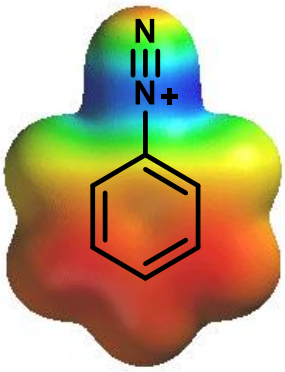

122

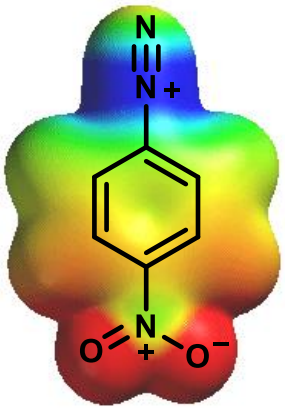

123

Figure 2.49. Electrostatic potential surfaces of benzenediazonium cation **122** and the *p*-nitrobenzenediazonium cation **123**.

These results suggest that if an electron-withdrawing group is orientated *para* to the azo group, the electrophilicity of the diazonium cation will be increased. As the electron-withdrawing group -COO- of **60** was replaced by the electron-donating group -NHCO- in **84** in the tried synthesis of *N*-(5-ferrocenylnaphthalen-1-yl)acetamide **85**, it can be possible that the electrophilicity of the diazonium ion was reduced, triggering a less/none favoured electrophilic aromatic substitution.

2.14 Conclusions

Previous *in vitro* studies have shown the antineoplastic activity against H1299 and SK-MEL-28 cancer cell lines exhibited by both *N*-{(ferrocenyl)benzoyl} and *N*-{(ferrocenyl)naphthoyl} bioconjugates, which consist of three key moieties: a ferrocenyl redox-active centre, an aromatic conjugated linker and an amino acid or dipeptide ester chain.[188,189] The present research sought to further explore the structure-activity relationship (SAR) of these compounds by modification of each moiety, in order to enhance their anti-proliferative effect.

The primary focus of this SAR study was centred on replacing the amino acid or dipeptide ester chain by short amino cyclic molecules such as aminopyridine, benzylamine or cyclohexylamine. Thus, a series of novel heterocyclic functionalised ferrocenyl derivatives **99**-**120** were prepared using EDC/NHS coupling protocol, a procedure similar to that used for the synthesis of the previous ferrocenyl dipeptide esters in Dr. Peter Kenny's research group.[181,183–195]. The corresponding ferrocenyl carboxylic acid was coupled with 2-aminopyridine **94**, 3-aminopyridine **95**, 4-aminopyridine **96**, benzylamine **97** or cyclohexylamine **98**; and purification by column chromatography furnished the novel compounds as yellow, orange or red solids with yields ranging from 8 to 93%. These derivatives were characterised by a range of spectroscopic techniques including ^{1}H NMR, ^{13}C NMR, DEPT-135, COSY, HSQC, HMBC, IR, UV-Vis and MS. All compounds gave spectroscopic and analytical data in accordance with their expected structures, except for the coupling reaction with 4-aminopyridine **96** where the corresponding NHS-esters were obtained.

An X-ray crystallography study confirmed the isolation of the NHS-ester **109**, and illustrates the out-of-plane position adopted by the ferrocene group. The formation of the NHS-ester intermediates may have relationship with the high pK_a value of 4-aminopyridine **96** compared with 2-aminopyridine **94** and 3-aminopyridine **95**, as there is evidence that the pK_a of organic ligands affect the composition of a complex. Furthermore, the pK_a of **96** is relatively closer to that of Et_3N, which is used as base in the mechanism of EDC/NHS coupling; this suggest that **96** may be competing with the role of base during the reaction. In addition, **96** could be protonated by the HCl group in EDC hydrochloride, hence preventing the reaction of interest from happening.[219–222]

A series of *N*-(5-ferrocenyl-1-naphthoyl) derivatives were proposed as an attractive scenario for the preparation of analogues of the previously analysed compounds, using a different conjugated linker such as 1,5-diaminonaphthalene **83** for the study of the SAR. The first step consisted on the monoacetylation of one amine group

in the symmetric starting material **83**; however, the main product obtained was the diacetylated compound *N*,*N*′-(naphthalene-1,5-diyl)diacetamide **121**, thus the expected *N*-(5-aminonaphthalen-1-yl)acetamide **84** was obtained with poor yield. Furthermore, diazonium coupling of this compound **84** with ferrocene **61** did not furnish the *N*-(5-ferrocenylnaphthalen-1-yl)acetamide **85** as anticipated. This failure was associated to the effect of the substituent -NHCO- in **84** (electron-donating group). Consequently, this synthetic route was abandoned.

2.15 Experimental procedures

2.15.1 General information

All starting materials and reactants used were acquired from Sigma Aldrich, Fluorochem Limited, Tokyo Chemical Industry UK Limited or Lennox Chemicals. Commercial grade reagents were used without further purification; where necessary, solvents were dried over $MgSO_4$ prior to use. The course of the reactions was followed by TLC, using silica gel as stationary phase, different mixtures of solvents (ethyl acetate, hexane, diethyl ether) as mobile phases, and UV light as expositor.

Purification of obtained products was carried out by column chromatography using Riedel-Haën silica gel as stationary phase, and different mixtures of solvents as mobile phases. Melting points were recorded on a Griffin melting point apparatus and are uncorrected. Elemental analysis were carried out by Dr. Mayra A. Hernández-López at Instituto Tecnológico y de Estudios Superiores de Monterrey (Mexico), using a Thermo Scientific FLASH 2000 elemental analyser. IR spectra were determined using a PerkinElmer Spectrum 100 FT-IR with ATR spectrometer. UV-Vis spectra were recorded on a Shimadzu UV-2600 UV-Vis spectrophotometer. Mass spectrometry studies were carried out by Dr. Dilip Rai at Teagasc Food Research Centre Ashtown (Ireland), using a Q-Tof Premier mass spectrometer (Waters Corp., Milford, USA).

NMR spectra were obtained in deuterated solvents (DMSO-d_6 or $CDCl_3$) on a Bruker AC 400 NMR spectrometer operating at either 600 MHz or 400 MHz for ^{1}H and 100 MHz for ^{13}C; chemical shifts (δ) are reported in parts per million (ppm); coupling constants (J) are given in Hertz (Hz), and signals multiplicities are denoted by: s (singlet), d (doublet), dd (doublet of doublets), dt (doublet of triplets), dq (doublet of quartets), ddd (doublet of doublet of doublets), t (triplet), td (triplet of doublets), tt (triplet of triplets), q (quartet), qt (quartet of triplets), quint (quintet), m (multiplet), and br. (broad).

X-ray crystallography studies were conducted by Prof. Vickie McKee at University of Southern Denmark (Denmark). Data was collected at 100(1)K on a Synergy, Dualflex, AtlasS2 diffractometer using Cu$K\alpha$ radiation (λ = 1.54184 Å) and the *CrysAlis PRO* 1.171.40.29a suite. Using SHELXLE and Olex2, the structure was solved by dual space methods (SHELXT) and refined on F using all the reflections (SHELXL-2018/3); all the non-hydrogen atoms were refined using anisotropic atomic displacement parameters and hydrogen atoms were inserted at calculated positions using a riding model.[245–248]

2.15.2 General procedure for the preparation of starting materials

The procedures are similar to those used for the synthesis of the previous ferrocenyl dipeptide esters in Dr. Peter Kenny's research group.[181,183–195]

2.15.2.1 6-(Methoxycarbonyl)naphthalen-2-aminium chloride **60**

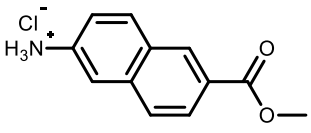

60

6-Amino-2-naphthoic acid **6** (5.03 g, 26.86 mmol) was dissolved in MeOH (50 mL); the solution was cooled on ice until temperature was below 5 °C. Thionyl chloride $SOCl_2$ (10 mL) was added dropwise. The mixture was allowed to react for 48 h with stirring at rt. The precipitate produced was collected under vacuum, washed with hexane and allowed to dry overnight yielding compound **60** as a grey/lilac solid (5.73 g, 90%);

m. p. = 219 – 221 °C (literature: 221 – 223 °C[195]);

^{1}H NMR (400 MHz, DMSO-d_6) δ: 8.43 (1H, s, H_{ar}), 7.92 (1H, d, *J* = 8.7 Hz, H_{ar}), 7.83 (1H, dd, *J* = 8.6 and 1.7 Hz, H_{ar}), 7.70 (1H, d, *J* = 8.6 Hz, H_{ar}), 7.15 (1H, s, H_{ar}), 7.14 (1H, d, *J* = 8.7 Hz, H_{ar}), 3.87 (3H, s, -C$\underline{H}_3$);

^{13}C NMR (100 MHz, DMSO-d_6) δ: 166.6 ($\underline{C}$=O), 136.3 (C_q), 135.4 (C_q), 131.5, 130.5, 129.4 (C_q), 127.6, 126.2 (C_q), 125.4, 121.7, 117.5, 52.4 (-O$\underline{C}$H$_3$).

2.15.2.2 Ethyl ferrocene **62**

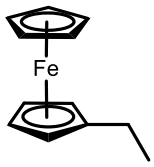

62

Lithium aluminium hydride (1.33 g, 35.10 mmol) was dissolved in dry diethyl ether (60 mL) under nitrogen atmosphere at 0 °C. Acetylferrocene **87** (4.00 g, 17.55 mmol) was slowly added and the reaction mixture was allowed to stir for 30 minutes. Anhydrous aluminium chloride (4.68 g, 35.10 mmol) was slowly added to the reaction mixture and allowed to stir for further 30 minutes. The reaction mixture was refluxed at room temperature for 18 h and quenched on ice after. The diethyl ether layer was washed with water (3 x 30 mL) and dried over $MgSO_4$; the solvent was removed *in vacuo* to yield the crude product. The crude product was purified by column chromatography (eluent 3:2 hexane:ethyl acetate) yielding compound **62** as a dark brown oil (2.77 g, 74%);

^{1}H NMR (400 MHz, $CDCl_3$) δ: 4.04 (5H, s, η^5-C$_5\underline{H}_5$), 4.00 (2H, t, *J* = 1.6 Hz, *meta* on η^5-C$_5\underline{H}_4$-ethyl), 3.97 (2H, t, *J* = 1.6 Hz, *ortho* on η^5-C$_5\underline{H}_4$-ethyl), 2.27 (2H, q, *J* = 7.6 Hz, -C$\underline{H}_2$CH$_3$), 1.10 (3H, t, *J* = 7.6 Hz, -CH$_2$C$\underline{H}_3$);

^{13}C NMR (100 MHz, $CDCl_3$) δ: 91.1 (C_{ipso} η^5-$\underline{C}_5$H$_4$-ethyl), 69.0 (C_{meta} η^5-$\underline{C}_5$H$_4$- ethyl), 67.3 (C_{ortho} η^5-$\underline{C}_5$H$_4$-ethyl), 66.8 (η^5-$\underline{C}_5$H$_5$), 21.9 (-$\underline{C}$H$_2$CH$_3$, -ve DEPT), 14.8 (-CH$_2\underline{C}$H$_3$).

2.15.2.3 Methyl 6-ferrocenyl-2-naphthoate **63**

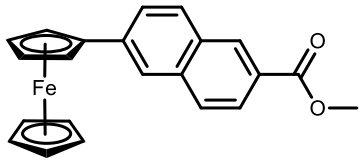

63

Concentrated hydrochloric acid (10.5 mL) was added intermittently and to a cool solution of 6-(methoxycarbonyl)naphthalen-2-aminium chloride **60** (5.36 g, 22.56 mmol) in deionised H_2O (50 mL). A solution of $NaNO_2$ (1.83 g, 26.55 mmol) in deionised H_2O (20 mL) was slowly added to the mixture with stirring, keeping the temperature below 5 °C and furnishing a pale brown/yellow solution. This resulting diazo salt was added to a solution of ferrocene **61** (4.94 g, 26.55 mmol) in diethyl ether (50 mL), and allowed to react for 48 h with stirring at rt. The reaction mixture was filtered under vacuum, and solids were washed with both deionised H_2O and diethyl ether until no more orange colour solution was obtained. Filtered two-layered solution was extracted with diethyl ether (3 x 50 mL); organic phase was dried over $MgSO_4$ and the solvent was removed *in vacuo*. The crude product was purified by column chromatography (eluent 9:1 hexane:diethyl ether) yielding compound **63** as an orange solid (2.18 g, 26%);

m. p. = 158 – 160 °C (literature: 158-159 °C[197]);

^{1}H NMR (400 MHz, DMSO-d_6) δ: 8.59 (1H, s, H_{ar}), 8.10 (1H, s, H_{ar}), 8.07 (1H, d, *J* = 8.7 Hz, H_{ar}), 7.96 (2H, m, H_{ar}), 7.86 (1H, dd, *J* = 8.6 and 1.7 Hz, H_{ar}), 4.99 (2H, t, *J* = 1.9 Hz, *ortho* on η^5-$C_5\underline{H}_4$), 4.47 (2H, t, *J* = 1.9 Hz, *meta* on η^5-$C_5\underline{H}_4$), 4.06 (5H, s, η^5-$C_5\underline{H}_5$), 3.92 (3H, s, -$C\underline{H}_3$);

^{13}C NMR (100 MHz, DMSO-d_6) δ: 166.8 ($\underline{C}$=O), 140.4 (C_q), 135.4 (C_q), 130.9 (C_q), 130.4, 129.0, 127.8, 126.2, 125.3 (C_q), 125.0, 122.6, 84.0 (C_{ipso} η^5-$\underline{C}_5H_4$), 69.9 (C_{meta} η^5-$\underline{C}_5H_4$), 69.8 (η^5-$\underline{C}_5H_5$), 67.1 (C_{ortho} η^5-$\underline{C}_5H_4$), 52.4 (-O$\underline{C}H_3$).

2.15.2.4 Methyl 6-(1′-ethyl)ferrocenyl-2-naphthoate **64**

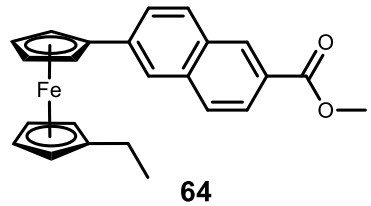

64

Concentrated hydrochloric acid (5 mL) was added intermittently and to a cool solution of 6-(methoxycarbonyl)naphthalen-2-aminium chloride **60** (1.84 g, 7.72 mmol) in deionised H_2O (20 mL). A solution of $NaNO_2$ (0.53 g, 7.72 mmol) in deionised H_2O (10 mL) was slowly added to the mixture with stirring, keeping the temperature below 5 °C and furnishing a pale brown/yellow solution. This resulting diazo salt was added to a solution of ethyl ferrocene **62** (2.07 g, 9.65 mmol) in diethyl ether (50 mL), and allowed to react for 48 h with stirring at rt. The reaction mixture was washed with deionised H_2O, brine and diethyl ether (3 x 30 mL); organic phase was dried over $MgSO_4$ and the solvent was removed *in vacuo*. The crude product was purified by column chromatography (eluent 9:1 hexane:diethyl ether) yielding compound **64** as a brown/orange solid (0.53 g, 17%);

m. p. = 165 – 167 °C (literature: 163-164 °C[195]);

^{1}H NMR (600 MHz, $CDCl_3$) δ: 8.51 (1H, t, *J* = 8.8 Hz, H_{ar}), 7.99 (1H, dd, *J* = 8.7 and 1.7 Hz, H_{ar}), 7.79 (3H, m, H_{ar}), 7.61 (1H, dd, *J* = 8.6 and 1.6 Hz, H_{ar}), 4.66 (2H, t, *J* = 1.8 Hz, *ortho* on η^5-C_5H_4-naphthoyl), 4.30 (2H, t, *J* = 1.8 Hz, *meta* on η^5-C_5H_4-naphthoyl), 4.04 (3H, s, -OCH_3), 4.02 (1H, s, *ortho* on η^5-C_5H_4-ethyl), 3.93 (1H, s, *ortho* on η^5-C_5H_4-ethyl), 3.91 (2H, t, *J* = 1.8 Hz, *meta* on η^5-C_5H_4-ethyl), 2.61 (0.3H, q, *J* = 7.5 Hz, -CH_2CH$_3$), 2.37 (0.4H, q, *J* = 7.5 Hz, -CH_2CH$_3$), 2.08 (1.3H, q, *J* = 7.5 Hz, -CH_2CH$_3$), 1.18 (1.6H, t, *J* = 7.5 Hz, -CH$_2$CH_3), 0.97 (1.3H, t, *J* = 7.5 Hz, -CH$_2$CH_3);

^{13}C NMR (100 MHz, $CDCl_3$) δ: 167.4 (C=O), 140.4 (C_q), 135.9 (C_q), 131.0 (C_q), 130.9, 128.8 (C_q), 127.7, 125.9, 125.7, 123.0, 122.9, 90.6 (C_{ipso} η^5-C_5H_4-ethyl), 84.2 (C_{ipso} η^5-C_5H_4-naphthoyl), 70.1 (C_{meta} η^5-C_5H_4-naphthoyl), 69.1 (C_{meta} η^5-C_5H_4-ethyl), 69.0 (C_{ortho} η^5-C_5H_4-ethyl), 67.2 (C_{ortho} η^5-C_5H_4-naphthoyl), 52.2 (-OCH$_3$), 21.2 (-CH$_2$CH$_3$, -ve DEPT), 14.7 (-CH$_2$CH$_3$).

2.15.2.5 6-Ferrocenyl-2-naphthoic acid **65**

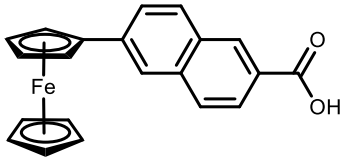

65

A solution of 10% NaOH (10 mL) was added to methyl 6-ferrocenyl-2-naphthoate **63** (0.48 g, 1.30 mmol) dissolved in MeOH (10 mL). The mixture was refluxed at 100 °C for 18 h with stirring. The solution was cooled on ice to promote precipitation, and then acidified with concentrated HCl until pH = 2 was reached. The precipitate formed was filtered via vacuum and washed with cold deionised water yielding compound **65** as a bright orange solid (0.45 g, 96%);

m. p. = 203 °C decomp. (literature: 205 °C decomp.[197]);

^{1}H NMR (400 MHz, DMSO-d_6) δ: 13.02 (1H, br. s, -COOH), 8.54 (1H, s, H_{ar}), 8.08 (1H, s, H_{ar}), 8.04 (1H, d, *J* = 8.6 Hz, H_{ar}), 7.94 (2H, s, H_{ar}), 7.84 (1H, d, *J* = 8.4 Hz, H_{ar}), 4.98 (2H, t, *J* = 1.8 Hz, *ortho* on η^5-C_5H_4), 4.46 (2H, t, *J* = 1.8 Hz, *meta* on η^5-C_5H_4), 4.05 (5H, s, η^5-C_5H_5);

^{13}C NMR (100 MHz, DMSO-d_6) δ: 168.0 (C=O), 140.2 (C_q), 135.8 (C_q), 131.2 (C_q), 130.8, 129.6, 128.1, 127.6 (C_q), 126.5, 126.0, 123.2, 84.4 (C_{ipso} η^5-C_5H_4), 70.1 (C_{meta} η^5-C_5H_4), 70.0 (η^5-C_5H_5), 67.2 (C_{ortho} η^5-C_5H_4).

2.15.2.6 6-(1′-Ethyl)ferrocenyl-2-naphthoic acid **66**

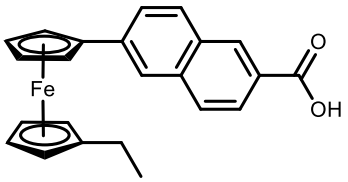

66

A solution of 10% NaOH (20 mL) was added to methyl 6-(1′-ethyl)ferrocenyl-2-naphthoate **64** (0.53 g, 1.34 mmol) dissolved in MeOH (40 mL). The mixture was refluxed at 100 °C for 18 h with stirring. The solution was cooled on ice to promote precipitation, and then acidified with concentrated HCl until pH = 2 was reached. The precipitate formed was filtered via vacuum and washed with cold deionised water yielding compound **66** as an orange solid (0.45 g, 96%);

m. p. = 153 – 155 °C;

^{1}H NMR (400 MHz, $CDCl_3$) δ: 13.11 (1H, br. s, -COO<u>H</u>), 8.57 (1H, s, H_{ar}), 8.02 (1H, d, *J* = 8.6 Hz, H_{ar}), 7.82 (3H, quint, *J* = 8.6 Hz, H_{ar}), 7.64 (1H, d, *J* = 8.4 H_{ar}), 4.68 (2H, t, *J* = 1.8 Hz, *ortho* on η^5-C_5<u>H_4</u>-naphthoyl), 4.32 (2H, t, *J* = 1.8 Hz, *meta* on η^5-C_5<u>H_4</u>-naphthoyl), 4.03 (1H, s, *ortho* on η^5-C_5<u>H_4</u>-ethyl), 3.94 (1H, s, *ortho* on η^5-C_5<u>H_4</u>-ethyl), 3.88 (2H, t, *J* = 2.0 Hz, *meta* on η^5-C_5<u>H_4</u>-ethyl), 2.62 (0.4H, q, *J* = 7.5 Hz, -C<u>H_2</u>CH_3), 2.38 (0.5H, q, *J* = 7.4 Hz, -C<u>H_2</u>CH_3), 2.09 (1.1H, q, *J* = 7.5 Hz, -C<u>H_2</u>CH_3), 1.19 (1.4H, t, *J* = 7.5 Hz, -CH_2C<u>H_3</u>), 0.98 (1.6H, t, *J* = 7.5 Hz, -CH_2C<u>H_3</u>);

^{13}C NMR (100 MHz, $CDCl_3$) δ: 168.4 (<u>C</u>=O), 134.7 (C_q), 132.9 (C_q), 131.7 (C_q), 129.6, 129.3 (C_q), 128.7, 127.6, 126.7, 124.0, 123.1, 90.4 (C_{ipso} η^5-<u>C_5</u>H_4-ethyl), 84.0 (C_{ipso} η^5-<u>C_5</u>H_4-naphthoyl), 71.3 (C_{meta} η^5-<u>C_5</u>H_4-naphthoyl), 69.4 (C_{meta} η^5-<u>C_5</u>H_4-ethyl), 67.0 (C_{ortho} η^5-<u>C_5</u>H_4-ethyl), 66.2 (C_{ortho} η^5-<u>C_5</u>H_4-naphthoyl), 21.2 (-<u>C</u>H_2CH_3, -ve DEPT), 14.9 (-CH_2<u>C</u>H_3).

2.15.2.7 3-(Methoxycarbonyl)naphthalen-2-aminium chloride **68**

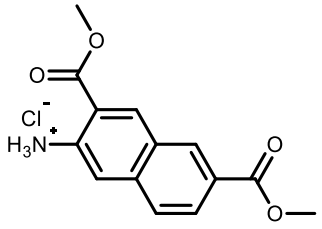

68

3-Amino-2-naphthoic acid **67** (1.00 g, 5.36 mmol) was dissolved in MeOH (50 mL); the solution was cooled on ice until temperature was below 5 °C. Thionyl chloride $SOCl_2$ (5 mL) was added dropwise. The mixture was allowed to react for 48 h with stirring at rt. The precipitate produced was collected under vacuum, washed with hexane and allowed to dry overnight yielding compound **68** as a pale brown solid (0.93 g, 73%);

m. p. = 188 – 190 °C (literature: 185-187 °C[197]);

^{1}H NMR (400 MHz, DMSO-d_6) δ: 8.59 (1H, s, H_{ar}), 7.98 (1H, d, *J* = 8.2 Hz, H_{ar}), 7.78 (1H, d, *J* = 8.3 Hz, H_{ar}), 7.58 (1H, s, H_{ar}), 7.57 (1H, t, *J* = 8.1 Hz, H_{ar}), 7.40 (1H, t, *J* = 8.1 Hz, H_{ar}), 3.91 (3H, s, -C<u>H_3</u>);

^{13}C NMR (100 MHz, DMSO-d_6) δ: 166.6 (<u>C</u>=O), 136.1 (C_q), 135.3 (C_q), 131.4, 129.5, 129.0 (C_q), 128.4, 126.5 (C_q), 125.1, 118.7, 117.5, 52.6 (-O<u>C</u>H_3).

2.15.2.8 Methyl 3-ferrocenyl-2-naphthoate **69**

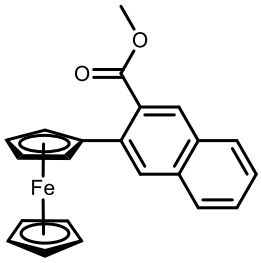

69

Concentrated hydrochloric acid (3 mL) was added intermittently and to a cool solution of 3-(methoxycarbonyl)naphthalen-2-aminium chloride **68** (0.91 g, 3.84 mmol) in deionised H_2O (15 mL). A solution of $NaNO_2$ (0.31 g, 4.52 mmol) in deionised H_2O (5 mL) was slowly added to the mixture with stirring, keeping the temperature below 5 °C and furnishing a pale brown/yellow solution. This resulting diazo salt was added to a solution of ferrocene **61** (0.84 g, 4.52 mmol) in diethyl ether (15 mL), and allowed to react for 48 h with stirring at rt. The reaction mixture was washed with deionised H_2O and extracted with diethyl ether (3 x 10 mL); organic phase was dried over $MgSO_4$ and the solvent was removed *in vacuo*. The crude product was purified by column chromatography (eluent 3:2 hexane:diethyl ether) yielding compound **69** as bright red crystals (0.50 g, 35%);

m. p. = 114 – 116 °C (literature: 119-120 °C[197]);

^{1}H NMR (400 MHz, DMSO-d_6) δ: 8.40 (1H, s, H_{ar}), 8.07 (1H, s, H_{ar}), 8.05 (1H, d, *J* = 8.4 Hz, H_{ar}), 7.98 (1H, d, *J* = 8.1 Hz, H_{ar}), 7.61 (1H, td, *J* = 7.5 and 1.1 Hz, H_{ar}), 7.55 (1H, d, *J* = 8.1 Hz, H_{ar}), 4.59 (2H, t, *J* = 1.8 Hz, *ortho* on η^5-$C_5\underline{H}_4$), 4.36 (2H, t, *J* = 1.8 Hz, *meta* on η^5-$C_5\underline{H}_4$), 4.11 (5H, s, η^5-$C_5\underline{H}_5$), 3.77 (3H, s, -C$\underline{H}_3$);

^{13}C NMR (100 MHz, DMSO-d_6) δ: 169.8 (C=O), 134.6 (C_q), 133.5 (C_q), 130.7 (C_q), 130.3 (C_q), 129.0, 128.1, 128.0, 127.4, 127.0, 126.3, 85.3 (C_{ipso} η^5-C_5H_4), 69.9 (η^5-C_5H_5), 69.2 (C_{ortho} η^5-C_5H_4), 68.6 (C_{meta} η^5-C_5H_4), 52.4 (-O$\underline{C}H_3$).

2.15.2.9 3-Ferrocenyl-2-naphthoic acid **70**

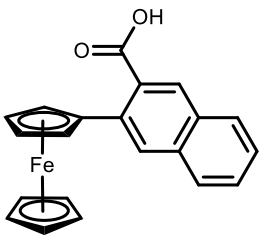

70

A solution of 10% NaOH (5 mL) was added to methyl 3-ferrocenyl-2-naphthoate **69** (0.20 g, 0.54 mmol) dissolved in MeOH (5 mL). The mixture was refluxed at 100 °C for 18 h with stirring. The solution was cooled on ice to promote precipitation, and then acidified with concentrated HCl until pH = 2 was reached. The precipitate formed was filtered via vacuum and washed with cold deionised water yielding compound **70** as an orange/brown solid (0.19 g, 96%);

m. p. = 139 °C decomp. (literature: 145 °C decomp.[197]);

^{1}H NMR (400 MHz, DMSO-d_6) δ: 13.04 (1H, br. s, -COO$\underline{H}$), 8.54 (1H, s, H_{ar}), 8.08 (1H, s, H_{ar}), 8.04 (1H, d, *J* = 8.6 Hz, H_{ar}), 7.94 (2H, s, H_{ar}), 7.84 (1H, d, *J* = 8.4 Hz, H_{ar}), 4.98 (2H, t, *J* = 1.8 Hz, *ortho* on η^5-$C_5\underline{H}_4$), 4.46 (2H, t, *J* = 1.8 Hz, *meta* on η^5-$C_5\underline{H}_4$), 4.05 (5H, s, η^5-$C_5\underline{H}_5$);

^{13}C NMR (100 MHz, DMSO-d_6) δ: 168.0 (C=O), 140.2 (C_q), 135.8 (C_q), 131.2 (C_q), 130.8, 129.6, 128.1, 127.6 (C_q), 126.5, 126.0, 123.2, 84.4 (C_{ipso} η^5-C_5H_4), 70.1 (C_{meta} η^5-C_5H_4), 70.0 (η^5-C_5H_5), 67.2 (C_{ortho} η^5-C_5H_4).

2.15.2.10 Ethyl *ortho*-ferrocenylbenzoate **74**

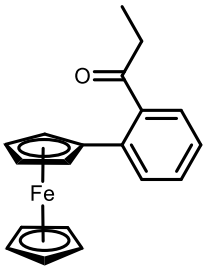

74

Concentrated hydrochloric acid (8 mL) was added intermittently and to a cool solution of ethyl *ortho*-aminobenzoate **71** (3.77 g, 22.84 mmol) in deionised H_2O (40 mL). A solution of $NaNO_2$ (1.85 g, 26.88 mmol) in deionised H_2O (15 mL) was slowly added to the mixture with stirring, keeping the temperature below 5 °C and furnishing a pale-yellow solution. This resulting diazo salt was added to a solution of ferrocene **61** (5.00 g, 26.88 mmol) in diethyl ether (80 mL), and allowed to react for 48 h with stirring at rt. The reaction mixture was washed with deionised H_2O and extracted with diethyl ether (3 x 100 mL); organic phase was dried over $MgSO_4$ and the solvent was removed *in vacuo*. The crude product was purified by column chromatography (eluent 3:2 hexane:diethyl ether) yielding compound **74** as a dark brown oil (3.00 g, 39%);

^{1}H NMR (400 MHz, DMSO-d_6) δ: 7.87 (1H, d, *J* = 7.4 Hz, H_{ar}), 7.50 (1H, t, *J* = 7.4 Hz, H_{ar}), 7.41 (1H, d, *J* = 7.4 Hz, H_{ar}), 7.30 (1H, t, *J* = 7.4 Hz, H_{ar}), 4.47 (2H, t, *J* = 1.8 Hz, *ortho* on η^5-C_5H_4), 4.32 (2H, t, *J* = 1.8 Hz, *meta* on η^5-C_5H_4), 4.14 (2H, q, *J* = 7.2 Hz, -CH_2CH_3), 4.09 (5H, s, η^5-C_5H_5), 1.13 (3H, t, *J* = 7.1 Hz, -CH_2CH_3);

^{13}C NMR (100 MHz, DMSO-d_6) δ: 169.6 (C=O), 137.9 {C_q-(η^5-C_5H_4)}, 132.3 {C_q- (C=O)}, 131.5, 130.6, 128.3, 126.4, 85.7 (C_{ipso} η^5-C_5H_4), 70.0 (η^5-C_5H_5), 69.3 (C_{ortho} η^5-C_5H_4), 68.7 (C_{meta} η^5-C_5H_4), 61.2 (-CH_2CH_3, -ve DEPT), 14.3 (-CH_2CH_3).

2.15.2.11 Ethyl *meta*-ferrocenylbenzoate **75**

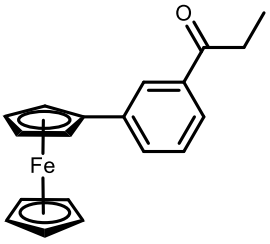

75

Concentrated hydrochloric acid (8 mL) was added intermittently and to a cool solution of ethyl *meta*-aminobenzoate **72** (3.77 g, 22.84 mmol) in deionised H_2O (40 mL). A solution of $NaNO_2$ (1.85 g, 26.88 mmol) in deionised H_2O (15 mL) was slowly added to the mixture with stirring, keeping the temperature below 5 °C and furnishing an orange solution. This resulting diazo salt was added to a solution of ferrocene **61** (5.00 g, 26.88 mmol) in diethyl ether (80 mL), and allowed to react for 48 h with stirring at rt. The reaction mixture was washed with deionised H_2O and extracted with diethyl ether (3 x 100 mL); organic phase was dried over $MgSO_4$ and the solvent was removed *in vacuo*. The crude product was purified by column chromatography (eluent 3:2 hexane:diethyl ether) yielding compound **75** as an orange solid (1.06 g, 14%);

m. p. = 70 – 72 °C (literature: 74 °C – 76 °C[249]);

^{1}H NMR (400 MHz, DMSO-d_6) δ: 8.03 (1H, t, *J* = 1.7 Hz, H_{ar}), 7.84 (1H, dq, *J* = 7.8 Hz and 1.00 Hz, H_{ar}), 7.78 (1H, dt, *J* = 7.7 Hz and 1.3 Hz, H_{ar}), 7.46 (1H, t, *J* = 7.8 Hz, H_{ar}), 4.85 (2H, t, *J* = 1.9 Hz, *ortho* on η^5-C_5H_4), 4.40 (2H, t, *J* = 1.9 Hz, *meta* on η^5-C_5H_4), 4.34 (2H, q, *J* = 7.1 Hz, -CH_2CH_3), 4.03 (5H, s, η^5-C_5H_5), 1.35 (3H, t, *J* = 7.1 Hz, -CH_2CH_3);

^{13}C NMR (100 MHz, DMSO-d_6) δ: 166.3 (C=O), 140.3 {C_q-(η^5-C_5H_4)}, 131.1, 130.6 {C_q-(C=O)}, 129.3, 126.9, 126.4, 84.0 (C_{ipso} η^5-C_5H_4), 69.9 (η^5-C_5H_5), 69.8 (C_{meta} η^5-C_5H_4), 67.0 (C_{ortho} η^5-C_5H_4), 61.3 (-CH_2CH_3, -ve DEPT), 14.7 (-CH_2CH_3).

2.15.2.12 Ethyl *para*-ferrocenylbenzoate **76**

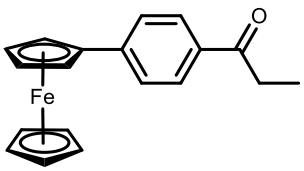

76

Concentrated hydrochloric acid (8 mL) was added intermittently and to a cool solution of ethyl *para*-aminobenzoate **73** (3.77 g, 22.84 mmol) in deionised H_2O (40 mL). A solution of $NaNO_2$ (1.85 g, 26.88 mmol) in deionised H_2O (15 mL) was slowly added to the mixture with stirring, keeping the temperature below 5 °C and furnishing a pale-yellow solution. This resulting diazo salt was added to a solution of ferrocene **61** (5.00 g, 26.88 mmol) in diethyl ether (80 mL), and allowed to react for 48 h with stirring at rt. The reaction mixture was washed with deionised H_2O and extracted with diethyl ether (3 x 100 mL); organic phase was dried over $MgSO_4$ and the solvent was removed *in vacuo*. The crude product was purified by column chromatography (eluent 4:1 hexane:diethyl ether) yielding compound **76** as a dark orange solid (2.60 g, 34%);

m. p. = 88 – 89 °C (literature: 92 °C – 94 °C[249]);

^{1}H NMR (600 MHz, DMSO-d_6) δ: 7.87 (2H, d, *J* = 8.3 Hz, H_{ar} *ortho* to C=O), 7.66 (2H, d, *J* = 8.4 Hz, H_{ar} *meta* to C=O), 4.90 (2H, t, *J* = 1.9 Hz, *ortho* on η^5-C_5H_4), 4.44 (2H, t, *J* = 1.9 Hz, *meta* on η^5-C_5H_4), 4.31 (2H, q, *J* = 7.1 Hz, -CH_2CH_3), 4.02 (5H, s, η^5-C_5H_5), 1.33 (3H, t, *J* = 7.1 Hz, -CH_2CH_3);

^{13}C NMR (100 MHz, DMSO-d_6) δ: 166.2 (C=O), 145.6 {C_q-(η^5-C_5H_4)}, 129.7 (C_{ortho} to C=O), 127.3 {C_q-(C=O)}, 126.1 (C_{meta} to C=O), 83.1 (C_{ipso} η^5-C_5H_4), 70.3 (C_{meta} η^5-C_5H_4), 70.1 (η^5-C_5H_5), 67.3 (C_{ortho} η^5-C_5H_4), 61.0 (-CH_2CH_3, -ve DEPT), 14.7 (-CH_2CH_3).

2.15.2.13 *Ortho*-ferrocenylbenzoic acid **77**

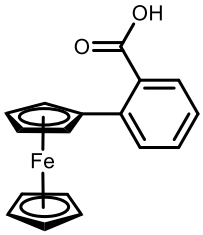

77

A solution of 10% NaOH (30 mL) was added to ethyl *ortho*-ferrocenylbenzoate **74** (2.28 g, 6.81 mmol) dissolved in MeOH (30 mL). The mixture was refluxed at 100 °C for 18 h with stirring. The solution was cooled on ice to promote precipitation, and then acidified with concentrated HCl until pH = 2 was reached. The precipitate formed was filtered via vacuum and washed with cold deionised water yielding compound **77** as a dark orange oil (2.00 g, 96%);

^{1}H NMR (600 MHz, DMSO-d_6) δ: 12.60 (1H, br. s, -COO<u>H</u>), 7.82 (1H, d, J = 7.4 Hz, H_{ar}), 7.44 (1H, td, J = 7.6 Hz and 1.3 Hz, H_{ar}), 7.37 (1H, dd, J = 7.7 Hz and 1.2 Hz, H_{ar}), 7.27 (1H, td, J = 7.5 Hz and 1.0 Hz, H_{ar}), 4.55 (2H, t, J = 1.8 Hz, *ortho* on η^5-C$_5$<u>H</u>$_4$), 4.32 (2H, t, J = 1.8 Hz, *meta* on η^5-C$_5$<u>H</u>$_4$), 4.08 (5H, s, η^5-C$_5$<u>H</u>$_5$);

^{13}C NMR (100 MHz, DMSO-d_6) δ: 171.3 (<u>C</u>=O), 137.1 {<u>C</u>$_q$-(η^5-C$_5$H$_4$)}, 133.7 {<u>C</u>$_q$- (C=O)}, 131.2, 130.0, 127.9, 126.2, 85.5 (C_{ipso} η^5-<u>C</u>$_5$H$_4$), 70.0 (η^5-<u>C</u>$_5$H$_5$), 69.3 (C_{ortho} η^5-<u>C</u>$_5$H$_4$), 68.7 (C_{meta} η^5-<u>C</u>$_5$H$_4$).

2.15.2.14 *Meta*-ferrocenylbenzoic acid **78**

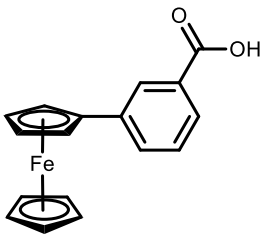

78

A solution of 10% NaOH (20 mL) was added to ethyl *meta*-ferrocenylbenzoate **75** (0.99 g, 2.96 mmol) dissolved in MeOH (40 mL). The mixture was refluxed at 100 °C for 18 h with stirring. The solution was cooled on ice to promote precipitation, and then acidified with concentrated HCl until pH = 2 was reached. The precipitate formed was filtered via vacuum and washed with cold deionised water yielding compound **78** as a yellow solid (0.78 g, 86%);

m. p. = 164 – 166 °C (literature: 160 °C – 162 °C[249]);

^{1}H NMR (600 MHz, DMSO-d_6) δ: 13.02 (1H, br. s, -COO<u>H</u>), 8.03 (1H, t, J = 1.7 Hz, H_{ar}), 7.80 (1H, dt, J = 7.8 Hz and 1.4 Hz, H_{ar}), 7.77 (1H, dt, J = 7.6 Hz and 1.3 Hz, H_{ar}), 7.43 (1H, t, J = 7.7 Hz, H_{ar}), 4.84 (2H, t, J = 1.9 Hz, *ortho* on η^5-C$_5$<u>H</u>$_4$), 4.40 (2H, t, J = 1.8 Hz, *meta* on η^5-C$_5$<u>H</u>$_4$), 4.03 (5H, s, η^5-C$_5$<u>H</u>$_5$);

^{13}C NMR (100 MHz, DMSO-d_6) δ: 167.9 (<u>C</u>=O), 140.1 {<u>C</u>$_q$-(η^5-C$_5$H$_4$)}, 130.7, 129.2, 127.9 {<u>C</u>$_q$- (C=O)}, 127.2, 126.6, 84.2 (C_{ipso} η^5-<u>C</u>$_5$H$_4$), 69.9 (η^5-<u>C</u>$_5$H$_5$), 69.7 (C_{meta} η^5-<u>C</u>$_5$H$_4$), 66.9 (C_{ortho} η^5-<u>C</u>$_5$H$_4$).

2.15.2.15 *Para*-ferrocenylbenzoic acid **79**

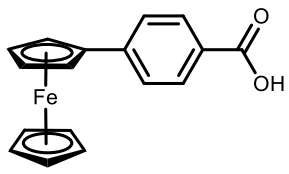

79

A solution of 10% NaOH (30 mL) was added to ethyl *para*-ferrocenylbenzoate **76** (2.60 g, 7.78 mmol) dissolved in MeOH (50 mL). The mixture was refluxed at 100 °C for 18 h with stirring. The solution was cooled on ice to promote precipitation, and then acidified with concentrated HCl until pH = 2 was reached. The precipitate formed was filtered via vacuum and washed with cold deionised water yielding compound **77** as a bright red solid (2.30 g, 97%);

m. p. = 210 °C decomp. (literature: 203 °C decomp.[249]);

^{1}H NMR (400 MHz, DMSO-d_6) δ: 13.01 (1H, br. s, -COO<u>H</u>), 7.85 (2H, d, *J* = 8.5 Hz, H_{ar} *ortho* to C=O), 7.64 (2H, d, *J* = 8.5 Hz, H_{ar} *meta* to C=O), 4.88 (2H, t, *J* = 1.9 Hz, *ortho* on η^5-C_5<u>H_4</u>), 4.43 (2H, t, *J* = 1.8 Hz, *meta* on η^5-C_5<u>H_4</u>), 4.03 (5H, s, η^5-C_5<u>H_5</u>);

^{13}C NMR (100 MHz, DMSO-d_6) δ: 167.9 (<u>C</u>=O), 145.0 {<u>C_q</u>-(η^5-C_5H_4)}, 129.9 (<u>C_{ortho}</u> to C=O), 128.3 {<u>C_q</u>- (C=O)}, 126.1 (<u>C_{meta}</u> to C=O), 83.4 (C_{ipso} η^5-<u>C_5</u>H_4), 70.2 (C_{meta} η^5-<u>C_5</u>H_4), 70.0 (η^5-<u>C_5</u>H_5), 67.2 (C_{ortho} η^5-<u>C_5</u>H_4).

2.15.2.16 Ethyl 4-ferrocenyl cinnamate **81**

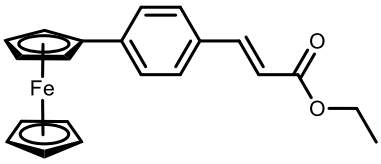

81

Concentrated hydrochloric acid (5 mL) was added intermittently and to a cool solution of ethyl 4-aminocinnamate **80** (1.00 g, 5.23 mmol) in deionised H_2O (10 mL). A solution of $NaNO_2$ (0.42 g, 6.15 mmol) in deionised H_2O (5 mL) was slowly added to the mixture with stirring, keeping the temperature below 5 °C and furnishing a pale-yellow solution. This resulting diazo salt was added to a solution of ferrocene **61** (1.14 g, 6.15 mmol) in diethyl ether (25 mL), and allowed to react for 48 h with stirring at rt. The reaction mixture was washed with deionised H_2O and extracted with diethyl ether (3 x 20 mL); organic phase was dried over $MgSO_4$ and the solvent was removed *in vacuo*. The crude product was purified by column chromatography (eluent 9:1 hexane:diethyl ether) yielding compound **81** as an orange solid (0.40 g, 21%);

m. p. = 92 – 94 °C (literature: 94 °C[194]);

^{1}H NMR (600 MHz, DMSO-d_6) δ: 7.61 (2H, d, *J* = 8.4 Hz, H_{ar}), 7.59 (2H, d, *J* = 8.4 Hz, H_{ar}), 7.57 (1H, d, *J* = 15.0 Hz, -C<u>H</u>=), 6.52 (1H, d, *J* = 15.9 Hz, =C<u>H</u>-), 4.79 (2H, t, *J* = 1.6 Hz, *ortho* on η^5-C_5<u>H_4</u>), 4.33 (2H, t, *J* = 1.6 Hz, *meta* on η^5-C_5<u>H_4</u>), 4.26 (2H, q, *J* = 7.1 Hz, -C<u>H_2</u>CH_3), 3.94 (5H, s, η^5-C_5<u>H_5</u>), 1.34 (3H, t, *J* = 7.1 Hz, -CH_2C<u>H_3</u>);

^{13}C NMR (100 MHz, DMSO-d_6) δ: 166.9 (<u>C</u>=O), 144.8 (-<u>C</u>H=), 142.6 {<u>C_q</u>-(η^5-C_5H_4)}, 131.9 {<u>C_q</u>-(CH=CH)}, 129.0 {<u>C_{meta}</u> to (CH=CH)}, 126.5 {<u>C_{ortho}</u> to (CH=CH)}, 117.2 (=<u>C</u>H-), 83.9

(C_{ipso} η^5-$\underline{C}_5H_4$), 69.9 (η^5-$\underline{C}_5H_5$), 69.8 (C_{meta} η^5-$\underline{C}_5H_4$), 67.0 (C_{ortho} η^5-$\underline{C}_5H_4$), 61.1 (-$\underline{C}H_2CH_3$, -ve DEPT), 14.7 (-$CH_2\underline{C}H_3$).

2.15.2.17 4-Ferrocenyl cinnamic acid **82**

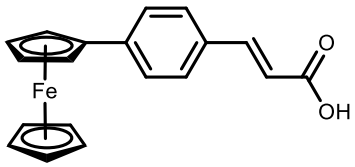

82

A solution of 10% NaOH (5 mL) was added to ethyl 4-ferrocenyl cinnamate **81** (0.40 g, 1.11 mmol) dissolved in MeOH (8 mL). The mixture was refluxed at 100 °C for 18 h with stirring. The solution was cooled on ice to promote precipitation, and then acidified with concentrated HCl until pH = 2 was reached. The precipitate formed was filtered via vacuum and washed with cold deionised water yielding compound **82** as an orange solid (0.35 g, 95%);

m. p. = 240 °C (literature: 253 – 254 °C[194]);

^{1}H NMR (600 MHz, DMSO-d_6) δ: 12.25 (1H, br. s, -COO$\underline{H}$), 7.52 (2H, d, J = 8.4 Hz, H_{ar}), 7.50 (2H, d, J = 8.4 Hz, H_{ar}), 7.48 (1H, d, J = 15.7 Hz, -C$\underline{H}$=), 6.43 (1H, d, J = 16.0 Hz, =C$\underline{H}$-), 4.78 (2H, t, J = 1.6 Hz, *ortho* on η^5-$C_5\underline{H}_4$), 4.32 (2H, t, J = 1.6 Hz, *meta* on η^5-$C_5\underline{H}_4$), 3.94 (5H, s, η^5-$C_5\underline{H}_5$);

^{13}C NMR (100 MHz, DMSO-d_6) δ: 168.3 ($\underline{C}$=O), 144.4 (-$\underline{C}$H=), 142.3 {$\underline{C}_q$-(η^5-C_5H_4)}, 132.1 {$\underline{C}_q$-(CH=CH)}, 128.9 {$\underline{C}_{meta}$ to (CH=CH)}, 126.5 {$\underline{C}_{ortho}$ to (CH=CH)}, 118.3 (=$\underline{C}$H-), 84.0 (C_{ipso} η^5-$\underline{C}_5H_4$), 70.0 (η^5-$\underline{C}_5H_5$), 69.9 (C_{meta} η^5-$\underline{C}_5H_4$), 67.0 (C_{ortho} η^5-$\underline{C}_5H_4$).

2.15.2.18 *N*-(5-aminonaphthalen-1-yl)acetamide **84**

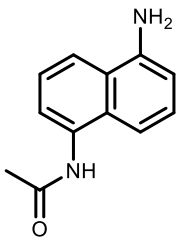

84

Acetic anhydride (3.35 mL, 35.45 mmol) was added to 1,5-diaminonaphthalene **83** (7.01 g, 44.31 mmol) and pyridine (14 mL). The mixture was allowed to react for 24 h with stirring at rt. The resulting solution was poured onto 10% HCl on ice to precipitate the di-acetylated product, which was disregarded via vacuum filtration and washed with deionised H_2O. Filtered solution was adjusted to pH~10 using 1 M NaOH, and extracted with CH_2Cl_2 (3 x 50 mL); organic phase was dried over $MgSO_4$, and the solvent was removed *in vacuo*. The crude product was purified by column chromatography (eluent 2:1 ethyl acetate:hexane) yielding compound **84** as a brown/purple solid (1.01 g, 14%);

m. p. = 165 °C (literature: 166 °C[250]);

^{1}H NMR (400 MHz, DMSO-d_6) δ: 9.72 (1H, s, -CON$\underline{H}$-), 7.89 (1H, d, J = 8.4 Hz, H_{ar}), 7.58 (1H, d, J = 7.5 Hz, H_{ar}), 7.32 (1H, t, J = 8.1 Hz, H_{ar}), 7.23 (2H, d, J = 6.5 Hz, H_{ar}), 6.69 (1H, dd, J = 6.5 and 2.3 Hz, H_{ar}), 5.73 (2H, s, -N$\underline{H}_2$), 2.15 (3H, s, -C$\underline{H}_3$).

2.15.3 General procedure for the preparation of novel heterocyclic functionalised ferrocenyl derivatives

The procedures are similar to those used for the synthesis of the previous ferrocenyl dipeptide esters in Dr. Peter Kenny's research group.[181,183–195]

2.15.3.1 6-Ferrocenyl-*N*-(pyridin-2-yl)-2-naphthamide **99**

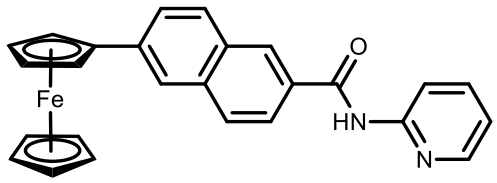

99

6-Ferrocenyl-2-naphthoic acid **65** (0.30 g, 0.84 mmol) was dissolved in dichloromethane (6 mL) at 0 °C. *N*-(3-dimethylaminopropyl)-*N'*-carbodiimide hydrochloride (EDC) **88** (0.16 g, 0.84 mmol), *N*-hydroxysuccinimide (NHS) **91** (0.10 g, 0.84 mmol) and triethylamine (1 mL) were added and the reaction mixture was stirred at 0 °C for 10 min to yield the desired NHS-ester intermediate. 2-aminopyridine **94** (0.36 g, 0.84 mmol) was added and the solution was stirred at 0 °C for 45 min; then raised to room temperature and stirred for further 48 h. The reaction mixture was washed with water and extracted with CH_2Cl_2 (3 x 10 mL); organic phase was dried over $MgSO_4$, and the solvent was removed *in vacuo* yielding compound **99** as a dark red solid (0.34 g, 93%);

m. p. = 162 °C decomp.;

Anal. Calc. for $C_{26}H_{20}N_2OFe$: C, 72.24; H, 4.66; N, 6.48%. Found: C, 71.81; H, 4.19; N, 6.20%;

IR ν_{max}: 3254, 3078, 2922, 1623, 1562 – 1491 cm^{-1};

UV-Vis (DMSO) λ_{max}: 379, 455 nm ε: 2638, 1306 $dm^3\ mol^{-1}\ cm^{-1}$;

^{1}H NMR (600 MHz, DMSO-d_6) δ: 8.54 (1H, s, H_{ar}), 8.08 (1H, s, H_{ar}), 8.04 (1H, d, *J* = 8.6 Hz, H_{ar}), 7.94 (2H, s, H_{ar}), 7.88 (1H, ddd, *J* = 5.1, 1.9 and 0.7 Hz, C=N-CH=CH-C<u>H</u>), 7.84 (1H, dd, *J* = 8.6 and 1.6 Hz, H_{ar}), 7.35 (1H, ddd, *J* = 8.4, 7,1 and 2.0 Hz, C=N-C<u>H</u>), 6.46 (1H, ddd, *J* = 7.0, 5.0 and 1.0 Hz, C=N-CH=C<u>H</u>), 6.42 (1H, dt, *J* = 8.3 and 0.8 Hz, HN-C-C<u>H</u>), 5.85 (1H, br. s, N<u>H</u>), 4.98 (2H, t, *J* = 1.8 Hz, *ortho* on η^5-C_5<u>H_4</u>), 4.46 (2H, t, *J* = 1.8 Hz, *meta* on η^5-C_5<u>H_4</u>), 4.05 (5H, s, η^5-C_5<u>H_5</u>);

^{13}C NMR (100 MHz, DMSO-d_6) δ: 168.0 (<u>C</u>=O), 160.2 (<u>C</u>=N), 148.1 (C=N-CH=CH-<u>C</u>H), 140.1 (C_q), 137.4 (C=N-<u>C</u>H), 135.8 (C_q), 131.2 (C_q), 130.8, 129.6, 128.1, 127.7 (C_q), 126.5, 126.0, 123.2, 112.2 (C=N-CH=<u>C</u>H), 108.4 (HN-C-<u>C</u>H), 84.4 (C_{ipso} η^5-<u>C_5</u>H_4), 70.1 (C_{meta} η^5-<u>C_5</u>H_4), 70.0 (η^5-<u>C_5</u>H_5), 67.2 (C_{ortho} η^5-<u>C_5</u>H_4).

2.15.3.2 6-Ferrocenyl-*N*-(pyridin-3-yl)-2-naphthamide **100**

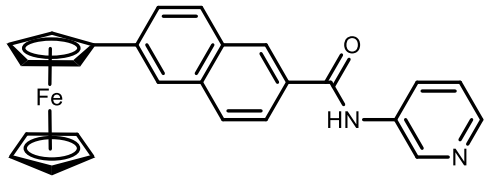

100

The synthesis followed that of **99** using the following reagents: 6-ferrocenyl-2-naphthoic acid **65** (0.30 g, 0.84 mmol), dichloromethane (6 mL), *N*-(3-dimethylaminopropyl)-*N′*-carbodiimide hydrochloride (EDC) **88** (0.16 g, 0.84 mmol), *N*-hydroxysuccinimide (NHS) **91** (0.10 g, 0.84 mmol), triethylamine (1 mL) and 3-aminopyridine **95** (0.36 g, 0.84 mmol). The reaction mixture was washed with water and extracted with CH_2Cl_2 (3 x 10 mL); organic phase was dried over $MgSO_4$, and the solvent was removed *in vacuo* yielding compound **100** as a crimson red solid (0.34 g, 92%);

m. p. = 176 °C decomp.;

Anal. Calc. for $C_{26}H_{20}N_2OFe$: C, 72.24; H, 4.66; N, 6.48%. Found: C, 72.13; H, 5.31; N, 6.72%;

IR ν_{max}: 3334, 3077, 2984, 1624, 1584 – 1483 cm^{-1};

UV-Vis (DMSO) λ_{max}: 378, 456 nm ε: 2259, 1133 $dm^3\ mol^{-1}\ cm^{-1}$;

^{1}H NMR (600 MHz, DMSO-d_6) δ: 8.53 (1H, s, H_{ar}), 8.07 (1H, s, H_{ar}), 8.03 (1H, d, J = 8.6 Hz, H_{ar}), 7.95 (1H, d, J = 1.3 Hz, H_{ar}), 7.93 (1H, s, H_{ar}), 7.92 (1H, d, J = 2.8 Hz, HN-C=C<u>H</u>), 7.83 (1H, dd, J = 8.5 and 1.5 Hz, H_{ar}), 7.72 (1H, dd, J = 4.7 and 1.1 Hz, N=C<u>H</u>), 7.00 (1H, dd, J = 8.1 and 4.6 Hz, HN-C-CH=C<u>H</u>), 6.89 (1H, dq, J = 8.1 and 1.3 Hz, HN-C-C<u>H</u>), 5.27 (1H, br. s, N<u>H</u>), 4.98 (2H, t, J = 1.7 Hz, *ortho* on η^5-C_5<u>H_4</u>), 4.46 (2H, t, J = 1.7 Hz, *meta* on η^5-C_5<u>H_4</u>), 4.05 (5H, s, η^5-C_5<u>H_5</u>);

^{13}C NMR (100 MHz, DMSO-d_6) δ: 168.4 (<u>C</u>=O), 145.3 (HN-<u>C</u>=CH), 139.7 {<u>C_q</u>-(η^5-C_5H_4)}, 137.4 (N=<u>C</u>H), 136.9 (HN-C=<u>C</u>H), 135.6 (C_q), 131.2 (C_q), 130.5, 129.5, 129.1 {<u>C_q</u>-(C=O}, 127.9, 126.3, 126.2, 124.0 (HN-C-CH=<u>C</u>H), 123.2, 120.1 (HN-C-<u>C</u>H), 84.5 (C_{ipso} η^5-<u>C_5</u>H_4), 70.0 (C_{meta} η^5-<u>C_5</u>H_4), 69.9 (η^5-<u>C_5</u>H_5), 67.2 (C_{ortho} η^5-<u>C_5</u>H_4).

2.15.3.3 2,5-Dioxopyrrolidin-1-yl 6-ferrocenyl-2-naphthoate **101**

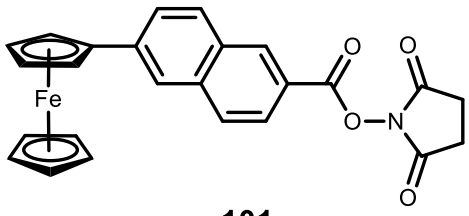

101

The synthesis followed that of **99** using the following reagents: 6-ferrocenyl-2-naphthoic acid **65** (0.30 g, 0.84 mmol), dichloromethane (6 mL), *N*-(3-dimethylaminopropyl)-*N′*-carbodiimide hydrochloride (EDC) **88** (0.16 g, 0.84 mmol), *N*-hydroxysuccinimide (NHS) **91** (0.10 g, 0.84 mmol), triethylamine (1 mL) and 4-aminopyridine **96** (0.36 g, 0.84 mmol). The crude product was purified by column chromatography (eluent 1:1 hexane:ethyl acetate) yielding compound **101** as an orange solid (0.20 g, 53%);

m. p. = 147 °C decomp.;

Anal. Calc. for $C_{25}H_{19}NO_4Fe$: C, 66.25; H, 4.23; N, 3.09%. Found: C, 66.82; H, 4.53; N, 3.00%;

m/*z* (ESI): 453.07 $[M]^{+\bullet}$. $C_{25}H_{19}NO_4Fe$ requires 453.07;

IR ν_{max}: 3090, 2954, 1766, 1732, 1625 – 1508 cm^{-1};

UV-Vis (DMSO) λ_{max}: 391, 473 nm ε: 2494, 1727 $dm^3\ mol^{-1}\ cm^{-1}$;

^{1}H NMR (600 MHz, DMSO-d_6) δ: 8.79 (1H, s, H_{ar}), 8.17 (2H, d, J = 7.8 Hz, H_{ar}), 8.08 (1H, d, J = 8.6 Hz, H_{ar}), 8.00 (1H, dd, J = 8.6 and 1.6 Hz, H_{ar}), 7.93 (1H, dd, J = 8.7 and 1.3 Hz, H_{ar}), 5.03 (2H, t, J = 1.7 Hz, *ortho* on η^5-$C_5\underline{H}_4$), 4.50 (2H, t, J = 1.6 Hz, *meta* on η^5-$C_5\underline{H}_4$), 4.07 (5H, s, η^5-$C_5\underline{H}_5$), 2.93 (4H, br. s, -$C\underline{H}_2$-);

^{13}C NMR (100 MHz, DMSO-d_6) δ: 170.9 (N-$\underline{C}$=O), 162.5 (-$\underline{C}$OO-), 142.2 (C_q), 136.8 (C_q), 132.7, 130.9 (C_q), 130.1, 129.2, 127.2, 125.3, 123.3, 120.9 (C_q), 83.8 (C_{ipso} η^5-$\underline{C}_5H_4$), 70.4 (C_{meta} η^5-$\underline{C}_5H_4$), 70.1 (η^5-$\underline{C}_5H_5$), 67.4 (C_{ortho} η^5-$\underline{C}_5H_4$), 26.0 (-$\underline{C}H_2$-, -ve DEPT).

2.15.3.4 *N*-benzyl-6-ferrocenyl-2-naphthamide **102**

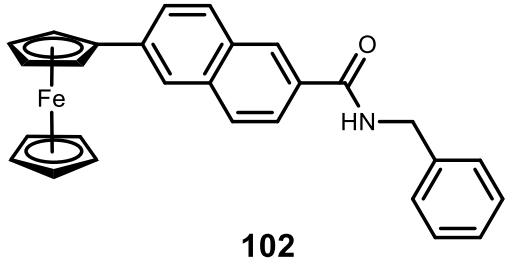

102

The synthesis followed that of **99** using the following reagents: 6-ferrocenyl-2-naphthoic acid **65** (0.21 g, 0.58 mmol), dichloromethane (6 mL), *N*-(3-dimethylaminopropyl)-*N′*-carbodiimide hydrochloride (EDC) **88** (0.11 g, 0.58 mmol), *N*-hydroxysuccinimide (NHS) **91** (0.07 g, 0.58 mmol), triethylamine (1 mL) and benzylamine **97** (0.06 mL, 0.58 mmol). The crude product was purified by column chromatography (eluent 1:1 hexane:ethyl acetate) yielding compound **102** as an orange solid (0.04 g, 17%);

m. p. = 198 – 200 °C;

IR ν_{max}: 3286, 3101, 2936, 1632, 1601 – 1490 cm^{-1};

Anal. Calc. for $C_{28}H_{23}NOFe$: C, 75.52; H, 5.21; N, 3.15%. Found: C, 75.43; H, 5.75; N, 3.25%;

UV-Vis (DMSO) λ_{max}: 377, 452 nm ε: 2896, 1289 $dm^3\ mol^{-1}\ cm^{-1}$;

^{1}H NMR (600 MHz, DMSO-d_6) δ: 9.20 (1H, t, *J* = 6.0, NH), 8.46 (1H, s, H_{ar} naphthoyl), 8.06 (1H, s, H_{ar} naphthoyl), 7.95 (3H, m, H_{ar} naphthoyl), 7.83 (1H, dd, *J* = 8.6 and 1.7 Hz, H_{ar} naphthoyl), 7.36 (4H, m, H_{ar} benzyl), 7.26 (1H, m, H_{ar} benzyl), 4.97 (2H, t, *J* = 1.8 Hz, *ortho* on η^5-C_5H_4), 4.55 (2H, d, *J* = 6.0 Hz, -CH_2-), 4.46 (2H, t, *J* = 1.8 Hz, *meta* on η^5-C_5H_4), 4.05 (5H, s, η^5-C_5H_5);

^{13}C NMR (100 MHz, DMSO-d_6) δ: 166.8 (C=O), 140.2 (C_{ipso} -C_6H_5), 139.3 (C_q), 135.0 {C_q-(C=O)}, 131.3 (C_q), 131.2 {C_q-(η^5-C_5H_4)}, 129.2 (C_{ar} naphthoyl), 128.8 (C_{ar} benzyl), 127.9 (C_{ar} naphthoyl), 127.8 (C_{ar} naphthoyl), 127.7 (C_{ar} benzyl), 127.2 (C_{ar} benzyl), 126.4 (C_{ar} naphthoyl), 125.0 (C_{ar} naphthoyl), 123.2 (C_{ar} naphthoyl), 84.6 (C_{ipso} η^5-C_5H_4), 70.0 (C_{meta} η^5-C_5H_4), 69.9 (η^5-C_5H_5), 67.1 (C_{ortho} η^5-C_5H_4), 43.2 (-CH_2-, -ve DEPT).

2.15.3.5 *N*-cyclohexyl-6-ferrocenyl-2-naphthamide **103**

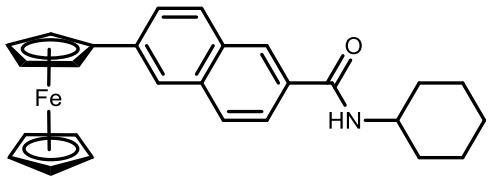

103

The synthesis followed that of **99** using the following reagents: 6-ferrocenyl-2-naphthoic acid **65** (0.21 g, 0.58 mmol), dichloromethane (6 mL), *N*-(3-dimethylaminopropyl)-*N′*-carbodiimide hydrochloride (EDC) **88** (0.11 g, 0.58 mmol), *N*-hydroxysuccinimide (NHS) **91** (0.07 g, 0.58 mmol), triethylamine (1 mL) and cyclohexylamine **98** (0.07 mL, 0.58 mmol). The crude product was purified by column chromatography (eluent 1:1 hexane:ethyl acetate) yielding compound **103** as a pale orange/yellow solid (0.03 g, 11%);

m. p. = 142 °C decomp.;

Anal. Calc. for $C_{27}H_{27}NOFe$: C, 74.15; H, 6.22; N, 3.20%. Found: C, 74.10; H, 6.15; N, 3.48%;

IR ν_{max}: 3333, 3059, 2931, 1624, 1550 – 1492 cm^{-1};

UV-Vis (CH_3CN) λ_{max}: 370, 452 nm ε: 2370, 941 $dm^3\ mol^{-1}\ cm^{-1}$;

^{1}H NMR (600 MHz, DMSO-d_6) δ: 8.38 (1H, s, H_{ar}), 8.34 (1H, d, *J* = 8.0, N<u>H</u>), 8.05 (1H, s, H_{ar}), 7.95 (1H, d, *J* = 8.6 Hz, H_{ar}), 7.90 (2H, s, H_{ar}), 7.82 (1H, dd, *J* = 8.6 and 1.7 Hz, H_{ar}), 4.96 (2H, t, *J* = 3.5 Hz, *ortho* on η^5-C_5<u>H_4</u>), 4.45 (2H, t, *J* = 3.5 Hz, *meta* on η^5-C_5<u>H_4</u>), 4.05 (5H, s, η^5-C_5<u>H_5</u>), 3.82 (1H, m, *ipso* on -C_6<u>H_{11}</u>), 1.87 (2H, d, *J* = 9.3 Hz, *ortho* on -C_6<u>H_{11}</u>), 1.76 (2H, d, *J* = 9.8 Hz, *meta* on -C_6<u>H_{11}</u>), 1.63 (1H, d, *J* = 13.2 Hz, *para* on -C_6<u>H_{11}</u>), 1.35 (4H, quint, *J* = 8.3 Hz, *ortho* and *meta* on -C_6<u>H_{11}</u>), 1.17 (1H, quint, *J* = 6.7 Hz, *para* on -C_6<u>H_{11}</u>);

^{13}C NMR (100 MHz, DMSO-d_6) δ: 165.9 (<u>C</u>=O), 139.0 (C_q), 134.9 {<u>C_q</u>- (C=O)}, 131.8 {<u>C_q</u>-(η^5-C_5H_4)}, 131.2 (C_q), 129.1, 127.7, 127.6, 126.3, 125.2, 123.2, 84.6 (C_{ipso} η^5-<u>C_5</u>H_4), 69.9 (C_{meta} η^5-<u>C_5</u>H_4), 69.8 (η^5-<u>C_5</u>H_5), 67.1 (C_{ortho} η^5-<u>C_5</u>H_4), 48.9 (C_{ipso} -<u>C_6</u>H_{11}), 33.0 (C_{ortho} -<u>C_6</u>H_{11}, -ve DEPT), 25.8 (C_{para} -<u>C_6</u>H_{11}, -ve DEPT), 25.5 (C_{meta} -<u>C_6</u>H_{11}, -ve DEPT).

2.15.3.6 2,5-Dioxopyrrolidin-1-yl 6-(1′-ethyl)ferrocenyl-2-naphthoate **104**

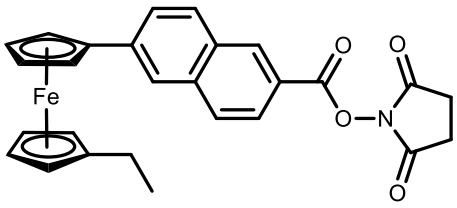

104

The synthesis followed that of **99** using the following reagents: 6-(1′-ethyl)ferrocenyl-2-naphthoic acid **66** (0.10 g, 0.26 mmol), dichloromethane (5 mL), *N*-(3-dimethylaminopropyl)-*N*′-carbodiimide hydrochloride (EDC) **88** (0.05 g, 0.26 mmol), *N*-hydroxysuccinimide (NHS) **91** (0.03 g, 0.26 mmol), triethylamine (1 mL) and 4-aminopyridine **96** (0.02 g, 0.26 mmol). The crude product was purified by column chromatography (eluent 1:1 hexane:ethyl acetate) yielding compound **104** as a bright red solid (0.02 g, 14%);

m. p. = 75 °C decomp.;

Anal. Calc. for $C_{27}H_{23}NO_4Fe$: C, 67.38; H, 4.82; N, 2.91%. Found: C, 67.80; H, 4.70; N, 2.15%;

IR ν_{max}: 3093, 2963, 1764, 1737, 1623 – 1506 cm^{-1};

UV-Vis (CH_3CN) λ_{max}: 469 nm ε: 3409 $dm^3\ mol^{-1}\ cm^{-1}$;

^{1}H NMR (600 MHz, $CDCl_3$) δ: 8.62 (1H, s, H_{ar}), 7.98 (1H, dd, *J* = 8.6 and 1.7 Hz, H_{ar}), 7.80 (3H, quint, *J* = 7.5 Hz, H_{ar}), 7.65 (1H, dd, *J* = 8.5 and 1.7 Hz, H_{ar}), 4.68 (2H, t, *J* = 1.8 Hz, *ortho* on η^5-$C_5\underline{H}_4$-naphthoyl), 4.34 (2H, t, *J* = 1.7 Hz, *meta* on η^5-$C_5\underline{H}_4$-naphthoyl), 4.03 (1H, s, *ortho* on η^5-$C_5\underline{H}_4$-ethyl), 3.94 (1H, s, *ortho* on η^5-$C_5\underline{H}_4$-ethyl), 3.89 (2H, dd, *J* = 4.8 and 1.5 Hz, *meta* on η^5-$C_5\underline{H}_4$-ethyl), 2.88 (4H, br. s, -$C\underline{H}_2$-C=O), 2.62 (0.4H, q, *J* = 7.5 Hz, -$C\underline{H}_2CH_3$), 2.38 (0.6H, q, *J* = 7.4 Hz, -$C\underline{H}_2CH_3$), 2.06 (1.0H, q, *J* = 7.6 Hz, -$C\underline{H}_2CH_3$), 1.19 (1.4H, t, *J* = 7.6 Hz, -$CH_2C\underline{H}_3$), 0.96 (1.6H, t, *J* = 7.5 Hz, -$CH_2C\underline{H}_3$);

^{13}C NMR (100 MHz, $CDCl_3$) δ: 169.4 (N-$\underline{C}$=O), 162.2 (-$\underline{C}$OO-), 141.5 (C_q), 136.7 (C_q), 132.8, 130.8 (C_q), 129.4, 128.2, 126.4, 125.6, 123.0, 121.1 (C_q), 92.1 (C_{ipso} η^5-$\underline{C}_5H_4$-ethyl), 83.8 (C_{ipso} η^5-$\underline{C}_5H_4$-naphthoyl), 70.3 (C_{meta} η^5-$\underline{C}_5H_4$-naphthoyl), 70.2 (C_{ortho} η^5-$\underline{C}_5H_4$-ethyl), 70.0 (C_{ortho} η^5-$\underline{C}_5H_4$-ethyl), 69.2 (C_{meta} η^5-$\underline{C}_5H_4$-naphthoyl), 69.0 (C_{meta} η^5-$\underline{C}_5H_4$-ethyl), 68.9 (C_{meta} η^5-$\underline{C}_5H_4$-ethyl), 67.1 (C_{ortho} η^5-$\underline{C}_5H_4$-naphthoyl), 65.9 (C_{ortho} η^5-$\underline{C}_5H_4$-naphthoyl), 25.7 (-$\underline{C}H_2$-C=O, -ve DEPT), 21.5 (-$\underline{C}H_2CH_3$, -ve DEPT), 14.7 (-$CH_2\underline{C}H_3$).

2.15.3.7 *N*-benzyl-6-(1′-ethyl)ferrocenyl-2-naphthamide **105**

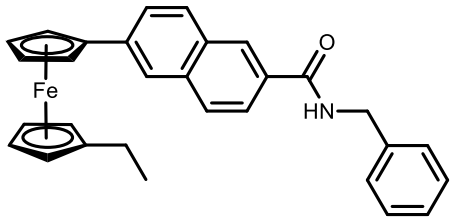

105

The synthesis followed that of **99** using the following reagents: 6-(1′-ethyl)ferrocenyl-2-naphthoic acid **66** (0.08 g, 0.21 mmol), dichloromethane (3 mL), *N*-(3-dimethylaminopropyl)-*N*′-carbodiimide hydrochloride (EDC) **88** (0.04 g, 0.21 mmol), *N*-hydroxysuccinimide (NHS) **91** (0.02 g, 0.21 mmol), triethylamine (1 mL) and benzylamine **97** (0.02 mL, 0.21 mmol). The crude product was purified by column chromatography (eluent 1:1 hexane:ethyl acetate) yielding compound **105** as a bright red solid (0.03 g, 27%);

m. p. = 64 – 66 °C;

Anal. Calc. for $C_{30}H_{27}NOFe$: C, 76.12; H, 5.75; N, 2.96%. Found: C, 75.34; H, 5.92; N, 3.09%;

IR ν_{max}: 3237, 2962, 2872, 1629, 1580 – 1458 cm^{-1};

UV-Vis (CH_3CN) λ_{max}: 376, 451 nm ε: 2025, 940 $dm^3\ mol^{-1}\ cm^{-1}$;

^{1}H NMR (600 MHz, $CDCl_3$) δ: 8.19 (1H, s, H_{ar} naphthoyl), 7.77 (4H, m, H_{ar} naphthoyl), 7.60 (1H, ddd, *J* = 8.5, 4.5 and 1.7 Hz, H_{ar} naphthoyl), 7.33 (4H, m, H_{ar} benzyl), 7.26 (1H, m, H_{ar} benzyl), 6.45 (1H, t, *J* = 5.0 Hz, -NH-), 4.66 (2H, t, *J* = 1.7 Hz, *ortho* on η^5-C_5H_4-naphthoyl), 4.65 (2H, d, *J* = 5.0 Hz, -CH_2- benzyl), 4.29 (2H, t, *J* = 1.7 Hz, *meta* on η^5-C_5H_4-naphthoyl), 4.02 (1H, s, *ortho* on η^5-C_5H_4-ethyl), 3.93 (1H, s, *ortho* on η^5-C_5H_4-ethyl), 3.87 (2H, dd, *J* = 4.9 and 1.6 Hz, *meta* on η^5-C_5H_4-ethyl), 2.60 (0.5H, q, *J* = 7.5 Hz, -CH_2CH_3), 2.37 (0.6H, q, *J* = 7.5 Hz, -CH_2CH_3), 2.07 (0.9H, q, *J* = 7.5 Hz, -CH_2CH_3), 1.18 (2H, td, *J* = 7.5 and 2.3 Hz, -CH_2CH_3), 0.96 (1H, t, *J* = 7.5 Hz, -CH_2CH_3);

^{13}C NMR (100 MHz, $CDCl_3$) δ: 167.4 (C=O), 139.2 {C_q-(η^5-C_5H_4)}, 138.3 (C_{ipso} -C_6H_5), 135.2 {C_q-(C=O)}, 131.2 (C_q), 130.6 (C_q), 128.9 (C_{ar} benzyl), 128.7 (C_{ar} naphthoyl), 128.3 (C_{ar} naphthoyl), 128.0 (C_{ar} benzyl), 127.7 (C_{ar} benzyl), 127.3 (C_{ar} naphthoyl), 126.1 (C_{ar} naphthoyl), 123.9 (C_{ar} naphthoyl), 123.0 (C_{ar} naphthoyl), 89.4 (C_{ipso} η^5-C_5H_4-ethyl), 83.3 (C_{ipso} η^5-C_5H_4-naphthoyl), 70.2 (C_{meta} η^5-C_5H_4-ethyl), 70.1 (C_{meta} η^5-C_5H_4-naphthoyl), 70.0 (C_{ortho} η^5-C_5H_4-ethyl), 69.3 (C_{ortho} η^5-C_5H_4-naphthoyl), 69.1 (C_{meta} η^5-C_5H_4-ethyl), 68.9 (C_{ortho} η^5-C_5H_4-ethyl), 67.1 (C_{meta} η^5-C_5H_4-naphthoyl), 65.7 (C_{ortho} η^5-C_5H_4-naphthoyl), 44.3 (-CH_2- benzyl, -ve DEPT), 21.6 (-CH_2CH_3, -ve DEPT), 14.7 (-CH_2CH_3).

2.15.3.8 *N*-cyclohexyl-6-(1′-ethyl)ferrocenyl-2-naphthamide **106**

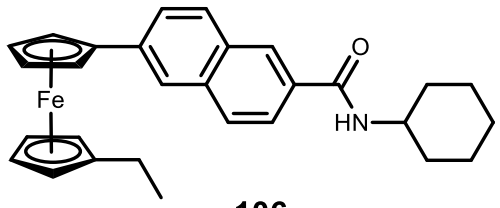

106

The synthesis followed that of **99** using the following reagents: 6-(1′-ethyl)ferrocenyl-2-naphthoic acid **66** (0. 10 g, 0.24 mmol), dichloromethane (3 mL), *N*-(3-dimethylaminopropyl)-*N*′-carbodiimide hydrochloride (EDC) **88** (0.05 g, 0.24 mmol), *N*-hydroxysuccinimide (NHS) **91** (0.03 g, 0.24 mmol), triethylamine (1 mL) and cyclohexylamine **98** (0.03 mL, 0.24 mmol). The crude product was purified by column chromatography (eluent 2:1 hexane:ethyl acetate) yielding compound **106** as a red/orange solid (0.03 g, 25%);

m. p. = 75 – 77 °C;

Anal. Calc. for $C_{29}H_{31}NOFe$: C, 74.84; H, 6.71; N, 3.01%. Found: C, 75.48; H, 6.23; N, 2.99%;

IR ν_{max}: 3292, 3087, 2925, 1624, 1602 – 1533 cm^{-1};

UV-Vis (CH_3CN) λ_{max}: 374, 452 nm ε: 1929, 863 $dm^3\ mol^{-1}\ cm^{-1}$;

^1H NMR (600 MHz, $CDCl_3$) δ: 8.13 (1H, s, H_{ar}), 7.76 (4H, m, H_{ar}), 7.61 (1H, ddd, *J* = 8.5, 4.3 and 1.7 Hz, H_{ar}), 6.02 (1H, d, *J* = 7.3 Hz, -NH-), 4.65 (2H, t, *J* = 1.7 Hz, *ortho* on η^5-C_5H_4-naphthoyl), 4.29 (2H, t, *J* = 1.8 Hz, *meta* on η^5-C_5H_4-naphthoyl), 4.02 (1H, s, *ortho* on η^5-C_5H_4-ethyl), 3.97 (1H, m, *ipso* on -C_6H_{11}), 3.93 (1H, s, *ortho* on η^5-C_5H_4-ethyl), 3.87 (2H, dd, *J* = 5.4 and 1.6 Hz, *meta* on η^5-C_5H_4-ethyl), 2.61 (0.4H, q, *J* = 7.5 Hz, -CH_2CH_3), 2.37 (0.6H, q, *J* = 7.2 Hz, -CH_2CH_3), 2.07 (1H, q, *J* = 7.5 Hz, -CH_2CH_3), 2.02 (2H, dd, *J* = 12.4 and 3.5 Hz, *ortho* on -C_6H_{11}), 1.72 (2H, dt, *J* = 13.3 and 3.5 Hz, *meta* on -C_6H_{11}), 1.61 (1H, dt, *J* = 13.1 and 3.5 Hz, *para* on -C_6H_{11}), 1.40 (4H, dd, *J* = 12.6 and 3.2 Hz, *ortho* and *meta* on -C_6H_{11}), 1.19 (1.5H, t, *J* = 7.5 Hz, -CH_2CH_3), 1.17 (1H, m, *para* on -C_6H_{11}), 0.96 (1.5H, t, *J* = 7.5 Hz, -CH_2CH_3);

^{13}C NMR (100 MHz, $CDCl_3$) δ: 166.7 (C=O), 139.0 (C_q), 135.0 (C_q), 131.4 (C_q), 131.2 (C_q), 128.7, 127.9, 127.0, 126.0, 124.0, 123.0, 92.0 (C_{ipso} η^5-C_5H_4-ethyl), 84.4 (C_{ipso} η^5-C_5H_4-naphthoyl), 70.2 (C_{ortho} η^5-C_5H_4-ethyl), 70.1 (C_{ortho} η^5-C_5H_4-ethyl), 70.0 (C_{meta} η^5-C_5H_4-naphthoyl), 69.3 (C_{meta} η^5-C_5H_4-ethyl), 69.1 (C_{meta} η^5-C_5H_4-ethyl), 68.9 (C_{meta} η^5-C_5H_4-naphthoyl), 67.1 (C_{ortho} η^5-C_5H_4-naphthoyl), 65.6 (C_{ortho} η^5-C_5H_4-naphthoyl), 48.8 (C_{ipso} -C_6H_{11}), 33.4 (C_{ortho} -C_6H_{11}, -ve DEPT), 25.6 (C_{para} -C_6H_{11}, -ve DEPT), 25.0 (C_{meta} -C_6H_{11}, -ve DEPT), 21.6 (-CH_2CH_3, -ve DEPT), 14.7 (-CH_2CH_3).

2.15.3.9 *N*-benzyl-3-ferrocenyl-2-naphthamide **107**

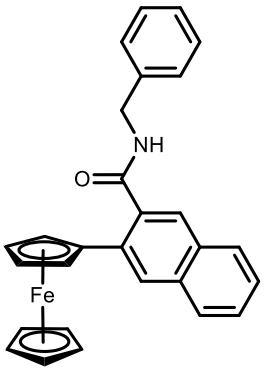

107

The synthesis followed that of **99** using the following reagents: 3-ferrocenyl-2-naphthoic acid **70** (0.20 g, 0.55 mmol), dichloromethane (6 mL), *N*-(3-dimethylaminopropyl)-*N*′-carbodiimide hydrochloride (EDC) **88** (0.10 g, 0.55 mmol), *N*-hydroxysuccinimide (NHS) **91** (0.06 g, 0.55 mmol), triethylamine (1 mL) and benzylamine **97** (0.06 mL, 0.55 mmol). The crude product was purified by column chromatography (eluent 1:1 hexane:diethyl ether) yielding compound **107** as a yellow solid (0.05 g, 22%);

m. p. = 160 °C;

Anal. Calc. for $C_{28}H_{23}NOFe$: C, 75.52; H, 5.21; N, 3.15%. Found: C, 75.90; H, 5.26; N, 3.28%;

IR ν_{max}: 3224, 3055, 2928, 1621, 1588 – 1494 cm^{-1};

UV-Vis (CH_3CN) λ_{max}: 451 nm ε: 465 $dm^3\ mol^{-1}\ cm^{-1}$;

^{1}H NMR (600 MHz, DMSO-d_6) δ: 8.94 (1H, t, *J* = 6.0, N<u>H</u>), 8.34 (1H, s, H_{ar} naphthoyl), 8.00 (1H, d, *J* = 8.1 Hz, H_{ar} naphthoyl), 7.94 (1H, d, *J* = 8.0 Hz, H_{ar} naphthoyl), 7.80 (1H, s, H_{ar} naphthoyl), 7.55 (1H, ddd, *J* = 8.1, 6.9 and 1.3 Hz, H_{ar} naphthoyl), 7.51 (1H, ddd, *J* = 8.0, 6.9 and 1.3 Hz, H_{ar} naphthoyl), 7.36 (4H, d, *J* = 4.4 Hz, H_{ar} benzyl), 7.28 (1H, quint, *J* = 4.3 Hz, H_{ar} benzyl), 4.70 (2H, t, *J* = 1.8 Hz, *ortho* on η^5-C_5<u>H_4</u>), 4.45 (2H, d, *J* = 6.1 Hz, -C<u>H_2</u>-), 4.29 (2H, t, *J* = 1.8 Hz, *meta* on η^5-C_5<u>H_4</u>), 4.08 (5H, s, η^5-C_5<u>H_5</u>);

^{13}C NMR (100 MHz, DMSO-d_6) δ: 170.1 (<u>C</u>=O), 139.6 (C_{ipso} -<u>C_6H_5</u>), 136.1 {<u>C_q</u>-(C=O)}, 134.5 {<u>C_q</u>-(η^5-C_5H_4)}, 133.3 (C_q), 131.1 (C_q), 128.7 (<u>C_{ar}</u> benzyl), 128.5 (<u>C_{ar}</u> naphthoyl), 128.1 (<u>C_{ar}</u> benzyl), 128.0 (<u>C_{ar}</u> naphthoyl), 127.9 (<u>C_{ar}</u> naphthoyl), 127.4 (<u>C_{ar}</u> naphthoyl), 127.3 (<u>C_{ar}</u> benzyl), 126.7 (<u>C_{ar}</u> naphthoyl), 126.5 (<u>C_{ar}</u> naphthoyl), 84.9 (C_{ipso} η^5-<u>C_5H_4</u>), 70.0 (η^5-<u>C_5H_5</u>), 69.4 (C_{ortho} η^5-<u>C_5H_4</u>), 68.7 (C_{meta} η^5-<u>C_5H_4</u>), 43.1 (-<u>C</u>H_2-, -ve DEPT).

2.15.3.10 *N*-cyclohexyl-3-ferrocenyl-2-naphthamide **108**

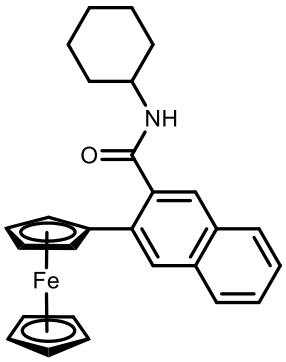

108

The synthesis followed that of **99** using the following reagents: 3-ferrocenyl-2-naphthoic acid **70** (0.13 g, 0.37 mmol), dichloromethane (3 mL), *N*-(3-dimethylaminopropyl)-*N*′-carbodiimide hydrochloride (EDC) **88** (0.07 g, 0.37 mmol), *N*-hydroxysuccinimide (NHS) **91** (0.04 g, 0.37 mmol), triethylamine (1 mL) and cyclohexylamine **98** (0.04 mL, 0.37 mmol). The crude product was purified by column chromatography (eluent 3:2 diethyl ether:hexane) yielding compound **108** as a pale orange solid (0.06 g, 36%);

m. p. = 166 – 167 °C;

Anal. Calc. for $C_{27}H_{27}NOFe$: C, 74.15; H, 6.22; N, 3.20%. Found: C, 74.06; H, 6.07; N, 3.76%;

IR ν_{max}: 3306, 3054, 2922, 1622, 1584 – 1493 cm^{-1};

UV-Vis (CH_3CN) λ_{max}: 451 nm ε: 406 $dm^3\ mol^{-1}\ cm^{-1}$;

^{1}H NMR (600 MHz, DMSO-d_6) δ: 8.32 (1H, s, H_{ar}), 8.27 (1H, d, *J* = 7.9, NH), 7.99 (1H, d, *J* = 8.2 Hz, H_{ar}), 7.93 (1H, d, *J* = 8.0 Hz, H_{ar}), 7.71 (1H, s, H_{ar}), 7.54 (1H, td, *J* = 7.4 and 1.3 Hz, H_{ar}), 7.50 (1H, td, *J* = 7.4 and 1.2 Hz, H_{ar}), 4.74 (2H, t, *J* = 1.9 Hz, *ortho* on η^5-C_5H_4), 4.33 (2H, t, *J* = 1.8 Hz, *meta* on η^5-C_5H_4), 4.10 (5H, s, η^5-C_5H_5), 3.71 (1H, m, *ipso* on -C_6H_{11}), 1.85 (2H, dd, *J* = 12.1 and 2.7 Hz, *ortho* on -C_6H_{11}), 1.72 (2H, dt, *J* = 13.2 and 3.5 Hz, *meta* on -C_6H_{11}), 1.59 (1H, dt, *J* = 12.5 and 3.5 Hz, *para* on -C_6H_{11}), 1.27 (4H, m, *ortho* and *meta* on -C_6H_{11}), 1.12 (1H, m, *para* on -C_6H_{11});

^{13}C NMR (100 MHz, DMSO-d_6) δ: 169.1 (C=O), 136.6 {C_q-(C=O)}, 134.5 {C_q-(η^5-C_5H_4)}, 133.3 (C_q), 131.1 (C_q), 128.5, 128.1, 127.8, 127.3, 126.6, 126.4, 85.1 (C_{ipso} η^5-C_5H_4), 70.0 (η^5-C_5H_5), 69.4 (C_{ortho} η^5-C_5H_4), 68.6 (C_{meta} η^5-C_5H_4), 48.5 (C_{ipso} -C_6H_{11}), 32.7 (C_{ortho} -C_6H_{11}, -ve DEPT), 25.7 (C_{para} -C_6H_{11}, -ve DEPT), 25.2 (C_{meta} -C_6H_{11}, -ve DEPT).

2.15.3.11 2,5-Dioxopyrrolidin-1-yl 2-ferrocenylbenzoate **109**

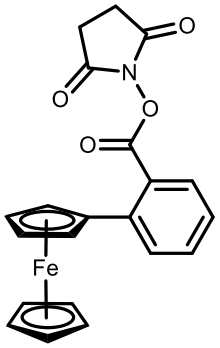

109

The synthesis followed that of **99** using the following reagents: *ortho*-ferrocenylbenzoic acid **77** (0.49 g, 1.61 mmol), dichloromethane (40 mL), *N*-(3-dimethylaminopropyl)-*N*′-carbodiimide hydrochloride (EDC) **88** (0.31 g, 1.61 mmol), *N*-hydroxysuccinimide (NHS) **91** (0.19 g,1.61 mmol), triethylamine (2 mL) and 4-aminopyridine **96** (0.15 g, 1.61 mmol). The crude product was purified by column chromatography (eluent 1:1 hexane:ethyl acetate) yielding compound **109** as dark orange/red crystals (0.11 g, 17%);

m. p. = 171 – 173 °C;

Anal. Calc. for $C_{21}H_{17}NO_4Fe$: C, 62.55; H, 4.25; N, 3.47%. Found: C, 62.66; H, 4.53; N, 3.53%;

IR ν_{max}: 3103, 2920, 1758, 1728, 1600 – 1501 cm^{-1};

UV-Vis (CH_3CN) λ_{max}: 364, 447 nm ε: 1128, 494 $dm^3\ mol^{-1}\ cm^{-1}$;

^{1}H NMR (600 MHz, DMSO-d_6) δ: 8.00 (1H, d, J = 7.7 Hz, H_{ar}), 7.68 (1H, td, J = 7.6 and 1.4 Hz, H_{ar}), 7.67 (1H, dd, J = 7.9 and 1.0 Hz, H_{ar}), 7.44 (1H, td, J = 7.6 and 0.9 Hz, H_{ar}), 4.67 (2H, t, J = 1.8 Hz, *ortho* on η^5-$C_5\underline{H}_4$), 4.36 (2H, t, J = 1.8 Hz, *meta* on η^5-$C_5\underline{H}_4$), 4.11 (5H, s, η^5-$C_5\underline{H}_5$), 2.88 (4H, br. d, J = 3.6 Hz, -$C\underline{H}_2$-);

^{13}C NMR (100 MHz, DMSO-d_6) δ: 171.0 (N-$\underline{C}$=O), 164.3 (-$\underline{C}$OO-), 140.5 {$\underline{C}_q$-(η^5-C_5H_4)}, 133.1, 132.3, 129.5, 126.7, 125.2 {$\underline{C}_q$-(C=O)}, 83.5 (C_{ipso} η^5-$\underline{C}_5H_4$), 70.3 (η^5-$\underline{C}_5H_5$), 69.6 (C_{ortho} η^5-$\underline{C}_5H_4$), 69.4 (C_{meta} η^5-$\underline{C}_5H_4$), 26.0 (-$\underline{C}H_2$-, -ve DEPT).

2.15.3.12 2,5-Dioxopyrrolidin-1-yl 3-ferrocenylbenzoate **110**

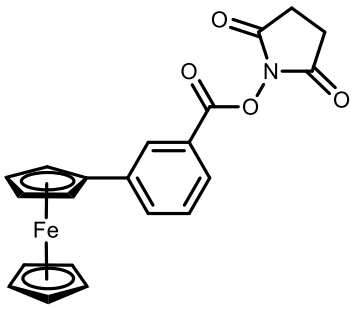

110

The synthesis followed that of **99** using the following reagents: *meta*-ferrocenylbenzoic acid **78** (0.20 g, 0.66 mmol), dichloromethane (7 mL), *N*-(3-dimethylaminopropyl)-*N′*-carbodiimide hydrochloride (EDC) **88** (0.13 g, 0.66 mmol), *N*-hydroxysuccinimide (NHS) **91** (0.08 g,0.66 mmol), triethylamine (1 mL) and 4-aminopyridine **96** (0.06 g, 0.66 mmol). The crude product was purified by column chromatography (eluent 1:1 hexane:ethyl acetate) yielding compound **110** as a dark orange solid (0.02 g, 8%);

m. p. = 126 – 128 °C;

Anal. Calc. for $C_{21}H_{17}NO_4Fe$: C, 62.55; H, 4.25; N, 3.47%. Found: C, 62.10; H, 4.49; N, 3.50%;

IR ν_{max}: 3095, 2924, 1738, 1681, 1604 – 1503 cm^{-1};

UV-Vis (CH_3CN) λ_{max}: 445 nm ε: 450 $dm^3\ mol^{-1}\ cm^{-1}$;

^{1}H NMR (600 MHz, DMSO-d_6) δ: 8.02 (1H, s, H_{ar}), 7.78 (1H, d, J = 7.5 Hz, H_{ar}), 7.76 (1H, d, J = 7.7 Hz, H_{ar}), 7.42 (1H, t, J = 7.7 Hz, H_{ar}), 4.83 (2H, t, J = 1.8 Hz, *ortho* on η^5-$C_5\underline{H}_4$), 4.39 (2H, t, J = 1.8 Hz, *meta* on η^5-$C_5\underline{H}_4$), 4.03 (5H, s, η^5-$C_5\underline{H}_5$), 2.92 (4H, br. s, -$C\underline{H}_2$-);

^{13}C NMR (100 MHz, DMSO-d_6) δ: 171.0 (N-$\underline{C}$=O), 164.6 (-$\underline{C}$OO-), 141.9 {$\underline{C}_q$-(η^5-C_5H_4)}, 130.6, 129.1, 127.3, 126.6, 124.9 {$\underline{C}_q$-(C=O)}, 84.3 (C_{ipso} η^5-$\underline{C}_5H_4$), 69.9 (η^5-$\underline{C}_5H_5$), 69.7 (C_{meta} η^5-$\underline{C}_5H_4$), 66.8 (C_{ortho} η^5-$\underline{C}_5H_4$), 26.0 (-$\underline{C}H_2$-, -ve DEPT).

2.15.3.13 2,5-Dioxopyrrolidin-1-yl 4-ferrocenylbenzoate **111**

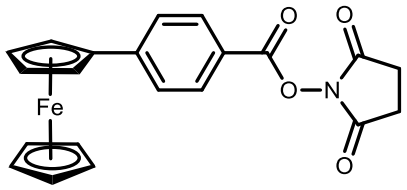

111

The synthesis followed that of **99** using the following reagents: *para*-ferrocenylbenzoic acid **79** (0.25 g, 0.83 mmol), dichloromethane (7 mL), *N*-(3-dimethylaminopropyl)-*N′*-carbodiimide hydrochloride (EDC) **88** (0.16 g, 0.83 mmol), *N*-hydroxysuccinimide (NHS) **91** (0.09 g,0.83 mmol), triethylamine (1 mL) and 4-aminopyridine **96** (0.08 g, 0.83 mmol). The crude product was purified by column chromatography (eluent 1:1 hexane:ethyl acetate) yielding compound **111** as a dark red solid (0.15 g, 44%);

m. p. = 231 – 233 °C;

Anal. Calc. for $C_{21}H_{17}NO_4Fe$: C, 62.55; H, 4.25; N, 3.47%. Found: C, 62.73; H, 4.54; N, 3.53%;

IR ν_{max}: 3081, 2925, 1761, 1728, 1604 – 1526 cm^{-1};

UV-Vis (CH_3CN) λ_{max}: 377, 472 nm ε: 2218, 1223 $dm^3\ mol^{-1}\ cm^{-1}$;

^{1}H NMR (600 MHz, DMSO-d_6) δ: 7.99 (2H, d, J = 8.5 Hz, H_{ar}), 7.79 (2H, d, J = 8.5 Hz, H_{ar}), 4.99 (2H, t, J = 3.8 Hz, *ortho* on η^5-$C_5\underline{H}_4$), 4.52 (2H, t, J = 3.7 Hz, *meta* on η^5-$C_5\underline{H}_4$), 4.06 (5H, s, η^5-$C_5\underline{H}_5$), 2.90 (4H, br. s, -$C\underline{H}_2$-);

^{13}C NMR (100 MHz, DMSO-d_6) δ: 170.9 (N-$\underline{C}$=O), 162.1 (-$\underline{C}$OO-), 148.6 {$\underline{C}_q$-(η^5-C_5H_4)}, 130.6, 126.7, 121.4 {$\underline{C}_q$-(C=O)}, 82.2 (C_{ipso} η^5-$\underline{C}_5H_4$), 70.9 (C_{meta} η^5-$\underline{C}_5H_4$), 70.3 (η^5-$\underline{C}_5H_5$), 67.6 (C_{ortho} η^5-$\underline{C}_5H_4$), 26.0 (-$\underline{C}H_2$-, -ve DEPT).

2.15.3.14 *N*-benzyl-2-ferrocenylbenzamide **112**

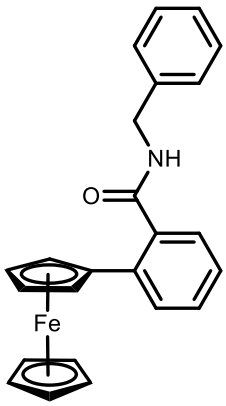

112

The synthesis followed that of **99** using the following reagents: *ortho*-ferrocenylbenzoic acid **77** (0.38 g, 1.23 mmol), dichloromethane (15 mL), *N*-(3-dimethylaminopropyl)-*N*′-carbodiimide hydrochloride (EDC) **88** (0.24 g, 1.23 mmol), *N*-hydroxysuccinimide (NHS) **91** (0.14 g, 1.23 mmol), triethylamine (2.5 mL) and benzylamine **97** (0.13 mL, 1.23 mmol). The crude product was purified by column chromatography (eluent 7:3 hexane:ethyl acetate) yielding compound **112** as an orange solid (0.12 g, 24%);

m. p. = 117 – 119 °C;

Anal. Calc. for $C_{24}H_{21}NOFe$: C, 72.93; H, 5.36; N, 3.54%. Found: C, 73.61; H, 5.71; N, 4.45%;

IR ν_{max}: 3334, 3033, 2933, 1639, 1596 – 1494 cm^{-1};

UV-Vis (CH_3CN) λ_{max}: 447 nm ε: 129 $dm^3\ mol^{-1}\ cm^{-1}$;

^{1}H NMR (600 MHz, DMSO-d_6) δ: 8.72 (1H, t, *J* = 5.9 Hz, NH), 7.80 (1H, d, *J* = 7.7 Hz, H_{ar} benzoyl), 7.40 (1H, t, *J* = 7.1 Hz, H_{ar} benzoyl), 7.32 (2H, t, *J* = 7.4 Hz, *ortho* on -C_6H_5), 7.26 (4H, m, 2 H_{ar} benzoyl and 2 *meta* on -C_6H_5), 7.20 (1H, d, *J* = 7.1 Hz, *para* on -C_6H_5), 4.55 (2H, s, *ortho* on η^5-C_5H_4), 4.36 (2H, d, *J* = 6.0 Hz, -CH_2-), 4.24 (2H, s, *meta* on η^5-C_5H_4), 4.06 (5H, s, η^5-C_5H_5);

^{13}C NMR (100 MHz, DMSO-d_6) δ: 170.2 (C=O), 139.6 (C_{ipso} -C_6H_5), 137.2 {C_q-(C=O)}, 136.3 {C_q-(η^5-C_5H_4)}, 130.4, 129.0, 128.6 (C_{ortho} -C_6H_5), 128.0 (C_{meta} -C_6H_5), 127.5 (C_{para} -C_6H_5), 127.2, 126.0, 84.9 (C_{ipso} η^5-C_5H_4), 69.9 (η^5-C_5H_5), 69.2 (C_{ortho} η^5-C_5H_4), 68.7 (C_{meta} η^5-C_5H_4), 42.9 (-CH_2-, -ve DEPT).

2.15.3.15 *N*-benzyl-3-ferrocenylbenzamide **113**

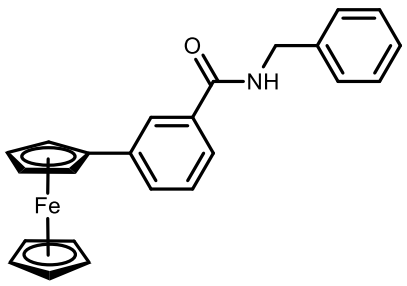

113

The synthesis followed that of **99** using the following reagents: *meta*-ferrocenylbenzoic acid **78** (0.20 g, 0.67 mmol), dichloromethane (6 mL), *N*-(3-dimethylaminopropyl)-*N*′-carbodiimide hydrochloride (EDC) **88** (0.13 g, 0.67 mmol), *N*-hydroxysuccinimide (NHS) **91** (0.08 g, 0.67 mmol), triethylamine (1 mL) and benzylamine **97** (0.07 mL, 0.67 mmol). The crude product was purified by column chromatography (eluent 3:2 hexane:ethyl acetate) yielding compound **113** as pale orange needles (0.11 g, 41%);

m. p. = 209 – 211 °C;

Anal. Calc. for $C_{24}H_{21}NOFe$: C, 72.93; H, 5.36; N, 3.54%. Found: C, 72.28; H, 4.90; N, 3.90%;

IR ν_{max}: 3284, 3078, 2921, 1629, 1602 – 1498 cm^{-1};

UV-Vis (CH_3CN) λ_{max}: 446 nm ε: 179 $dm^3\ mol^{-1}\ cm^{-1}$;

^1H NMR (600 MHz, DMSO-d_6) δ: 9.09 (1H, t, J = 5.9 Hz, NH), 8.02 (1H, t, J = 1.5 Hz, H_{ar} benzoyl), 7.73 (1H, d, J = 1.7 Hz, H_{ar} benzoyl), 7.72 (1H, d, J = 1.6 Hz, H_{ar} benzoyl), 7.41 (1H, t, J = 7.7 Hz, H_{ar} benzoyl), 7.36 (2H, s, *ortho* on -C_6H_5), 7.35 (2H, d, J = 1.5 Hz, *meta* on -C_6H_5), 7.26 (1H, m, *para* on -C_6H_5), 4.86 (2H, t, J = 1.8 Hz, *ortho* on η^5-C_5H_4), 4.52 (2H, d, J = 6.0 Hz, -CH_2-), 4.39 (2H, t, J = 1.8 Hz, *meta* on η^5-C_5H_4), 4.04 (5H, s, η^5-C_5H_5);

^{13}C NMR (100 MHz, DMSO-d_6) δ: 166.6 (C=O), 140.2 (C_{ipso} -C_6H_5), 139.8 {C_q-(η^5-C_5H_4)}, 129.2, 128.9, 128.8 (C_{meta} -C_6H_5), 127.7 (C_{ortho} -C_6H_5), 127.2 (C_{para} -C_6H_5), 125.4 {C_q-(C=O)}, 125.3, 124.7, 84.6 (C_{ipso} η^5-C_5H_4), 69.9 (η^5-C_5H_5), 69.6 (C_{meta} η^5-C_5H_4), 66.9 (C_{ortho} η^5-C_5H_4), 43.1 (-CH_2-, -ve DEPT).

2.15.3.16 *N*-benzyl-4-ferrocenylbenzamide **114**

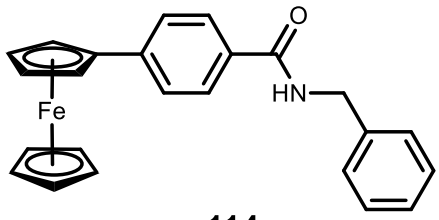

114

The synthesis followed that of **99** using the following reagents: *para*-ferrocenylbenzoic acid **79** (0.16 g, 0.53 mmol), dichloromethane (6 mL), *N*-(3-dimethylaminopropyl)-*N′*-carbodiimide hydrochloride (EDC) **88** (0.10 g, 0.53 mmol), *N*-hydroxysuccinimide (NHS) **91** (0.06 g, 0.53 mmol), triethylamine (1.5 mL) and benzylamine **97** (0.06 mL, 0.53 mmol). The crude product was purified by column chromatography (eluent 1:1 hexane:ethyl acetate) yielding compound **114** as a golden solid (0.05 g, 25%);

m. p. = 176 – 177 °C;

Anal. Calc. for $C_{24}H_{21}NOFe$: C, 72.93; H, 5.36; N, 3.54%. Found: C, 72.36; H, 5.49; N, 4.24%;

IR ν_{max}: 3293, 3090, 2932, 1636, 1606 – 1520 cm^{-1};

UV-Vis (CH_3CN) λ_{max}: 351, 451 nm ε: 2289, 674 $dm^3\ mol^{-1}\ cm^{-1}$;

^{1}H NMR (600 MHz, DMSO-d_6) δ: 9.02 (1H, t, *J* = 6.0 Hz, N<u>H</u>), 7.83 (2H, d, *J* = 8.3 Hz, H_{ar} benzoyl), 7.63 (2H, d, *J* = 8.4 Hz, H_{ar} benzoyl), 7.34 (2H, d, *J* = 0.8 Hz, *ortho* on -C_6<u>H_5</u>), 7.33 (2H, s, *meta* on -C_6<u>H_5</u>), 7.25 (1H, m, *para* on -C_6<u>H_5</u>), 4.89 (2H, t, *J* = 1.7 Hz, *ortho* on η^5-C_5<u>H_4</u>), 4.49 (2H, d, *J* = 6.0 Hz, -C<u>H_2</u>-), 4.41 (2H, t, *J* = 1.7 Hz, *meta* on η^5-C_5<u>H_4</u>), 4.03 (5H, s, η^5-C_5<u>H_5</u>);

^{13}C NMR (100 MHz, DMSO-d_6) δ: 166.5 (<u>C</u>=O), 143.2 (C_{ipso} -<u>C_6H_5</u>), 140.3 {<u>C_q</u>-(η^5-C_5H_4)}, 131.9 {<u>C_q</u>-(C=O)}, 128.7 (C_{ortho} -<u>C_6H_5</u>), 127.9, 127.7 (C_{meta} -<u>C_6H_5</u>), 127.2 (C_{para} -<u>C_6H_5</u>), 125.9, 83.7 (C_{ipso} η^5-<u>C_5</u>H_4), 70.0 (η^5-<u>C_5H_5</u>), 69.9 (C_{meta} η^5-<u>C_5</u>H_4), 67.1 (C_{ortho} η^5-<u>C_5</u>H_4), 43.0 (-<u>C</u>H_2-, -ve DEPT).

2.15.3.17 *N*-cyclohexyl-2-ferrocenylbenzamide **115**

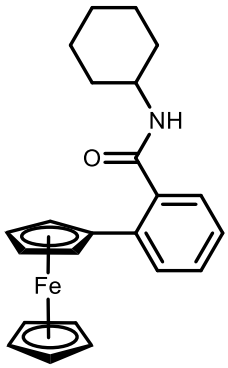

115

The synthesis followed that of **99** using the following reagents: *ortho*-ferrocenylbenzoic acid **77** (0.53 g, 1.74 mmol), dichloromethane (15 mL), *N*-(3-dimethylaminopropyl)-*N*′-carbodiimide hydrochloride (EDC) **88** (0.33 g, 1.74 mmol), *N*-hydroxysuccinimide (NHS) **91** (0.20 g, 1.74 mmol), triethylamine (3 mL) and cyclohexylamine **98** (0.20 mL, 1.74 mmol). The crude product was purified by column chromatography (eluent 7:3 hexane:ethyl acetate) yielding compound **115** as a yellow solid (0.19 g, 28%);

m. p. = 149 – 151 °C;

Anal. Calc. for $C_{23}H_{25}NOFe$: C, 71.33; H, 6.51; N, 3.62%. Found: C, 70.77; H, 6.01; N, 4.29%;

IR ν_{max}: 3236, 3080, 2929, 1628, 1603 – 1502 cm^{-1};

UV-Vis (CH_3CN) λ_{max}: 447 nm ε: 206 $dm^3\ mol^{-1}\ cm^{-1}$;

^{1}H NMR (600 MHz, DMSO-d_6) δ: 8.04 (1H, d, J = 7.9 Hz, NH), 7.79 (1H, d, J = 7.9 Hz, H_{ar}), 7.38 (1H, td, J = 7.6 and 1.3 Hz, H_{ar}), 7.22 (1H, td, J = 7.4 and 0.9 Hz, H_{ar}), 7.12 (1H, dd, J = 7.6 and 1.2 Hz, H_{ar}), 4.59 (2H, t, J = 1.8 Hz, *ortho* on η^5-C_5H_4), 4.29 (2H, t, J = 1.8 Hz, *meta* on η^5-C_5H_4), 4.07 (5H, s, η^5-C_5H_5), 3.63 (1H, m, *ipso* on -C_6H_{11}), 1.76 (2H, dd, J = 12.5 and 3.0 Hz, *ortho* on -C_6H_{11}), 1.68 (2H, dt, J = 13.3 and 3.4 Hz, *meta* on -C_6H_{11}), 1.56 (1H, dd, J = 9.2 and 3.7 Hz, *para* on -C_6H_{11}), 1.26 (2H, qt, J = 12.6 and 3.1 Hz, *meta* on -C_6H_{11}), 1.15 (2H, qd, J = 12.3 and 2.9 Hz, *ortho* on -C_6H_{11}), 1.07 (1H, dt, J = 12.4 and 3.4 Hz, *para* on -C_6H_{11});

^{13}C NMR (100 MHz, DMSO-d_6) δ: 169.1 (C=O), 137.7 {C_q-(C=O)}, 136.2 {C_q-(η^5-C_5H_4)}, 130.4, 128.7, 127.6, 125.9, 85.2 (C_{ipso} η^5-C_5H_4), 69.9 (η^5-C_5H_5), 69.2 (C_{ortho} η^5-C_5H_4), 68.5 (C_{meta} η^5-C_5H_4), 48.3 (C_{ipso} -C_6H_{11}), 32.6 (C_{ortho} -C_6H_{11}, -ve DEPT), 25.7 (C_{para} -C_6H_{11}, -ve DEPT), 25.2 (C_{meta} -C_6H_{11}, -ve DEPT).

2.15.3.18 *N*-cyclohexyl-3-ferrocenylbenzamide **116**

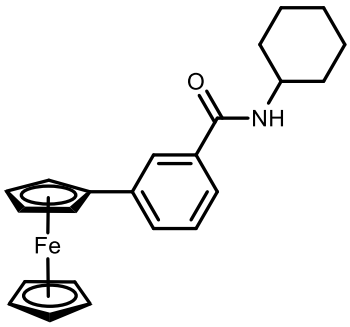

116

The synthesis followed that of **99** using the following reagents: *meta*-ferrocenylbenzoic acid **78** (0.21 g, 0.68 mmol), dichloromethane (6 mL), *N*-(3-dimethylaminopropyl)-*N*′-carbodiimide hydrochloride (EDC) **88** (0.13 g, 0.68 mmol), *N*-hydroxysuccinimide (NHS) **91** (0.08 g, 0.68 mmol), triethylamine (1 mL) and cyclohexylamine **98** (0.08 mL, 0.68 mmol). The crude product was purified by column chromatography (eluent 3:2 hexane:ethyl acetate) yielding compound **116** as an orange solid (0.11 g, 42%);

m. p. = 185 – 187 °C;

Anal. Calc. for $C_{23}H_{25}NOFe$: C, 71.33; H, 6.51; N, 3.62%. Found: C, 70.92; H, 6.64; N, 4.41%;

IR ν_{max}: 3287, 3083, 2926, 1626, 1598 – 1497 cm^{-1};

UV-Vis (CH_3CN) λ_{max}: 452 nm ε: 233 $dm^3\ mol^{-1}\ cm^{-1}$;

^{1}H NMR (600 MHz, DMSO-d_6) δ: 8.22 (1H, d, J = 8.0 Hz, NH), 7.92 (1H, s, H_{ar}), 7.71 (1H, d, J = 7.7 Hz, H_{ar}), 7.66 (1H, d, J = 7.7 Hz, H_{ar}), 7.38 (1H, t, J = 7.7 Hz, H_{ar}), 4.85 (2H, t, J = 1.7 Hz, *ortho* on η^5-C_5H_4), 4.39 (2H, t, J = 1.7 Hz, *meta* on η^5-C_5H_4), 4.03 (5H, s, η^5-C_5H_5), 3.78 (1H, m, *ipso* on -C_6H_{11}), 1.85 (2H, d, J = 8.9 Hz, *ortho* on -C_6H_{11}), 1.76 (2H, d, J = 9.7 Hz, *meta* on -C_6H_{11}), 1.63 (1H, d, J = 12.8 Hz, *para* on -C_6H_{11}), 1.33 (4H, m, *ortho* and *meta* on -C_6H_{11}), 1.15 (1H, m, *para* on -C_6H_{11});

^{13}C NMR (100 MHz, DMSO-d_6) δ: 165.8 (C=O), 139.6 {C_q-(η^5-C_5H_4)}, 135.4 {C_q-(C=O)}, 129.0, 128.7, 125.3, 124.7, 84.7 (C_{ipso} η^5-C_5H_4), 69.9 (η^5-C_5H_5), 69.5 (C_{meta} η^5-C_5H_4), 67.0 (C_{ortho} η^5-C_5H_4), 48.9 (C_{ipso} -C_6H_{11}), 33.0 (C_{ortho} -C_6H_{11}, -ve DEPT), 25.8 (C_{para} -C_6H_{11}, -ve DEPT), 25.5 (C_{meta} -C_6H_{11}, -ve DEPT).

2.15.3.19 *N*-cyclohexyl-4-ferrocenylbenzamide **117**

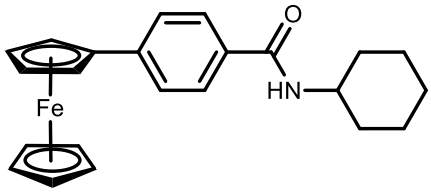

117

The synthesis followed that of **99** using the following reagents: *para*-ferrocenylbenzoic acid **79** (0.26 g, 0.86 mmol), dichloromethane (6 mL), *N*-(3-dimethylaminopropyl)-*N′*-carbodiimide hydrochloride (EDC) **88** (0.17 g, 0.86 mmol), *N*-hydroxysuccinimide (NHS) **91** (0.10 g, 0.86 mmol), triethylamine (1.5 mL) and cyclohexylamine **98** (0.10 mL, 0.86 mmol). The crude product was purified by column chromatography (eluent 1:1 hexane:ethyl acetate) yielding compound **117** as a pale orange solid (0.07 g, 20%);

m. p. = 258 °C decomp.;

Anal. Calc. for $C_{23}H_{25}NOFe$: C, 71.33; H, 6.51; N, 3.62%. Found: C, 70.84; H, 6.33; N, 4.35%;

IR ν_{max}: 3233, 3081, 2924, 1626, 1610 – 1519 cm^{-1};

UV-Vis (DMSO) λ_{max}: 352, 451 nm ε: 2484, 790 $dm^3\ mol^{-1}\ cm^{-1}$;

^{1}H NMR (600 MHz, DMSO-d_6) δ: 8.15 (1H, d, J = 7.7 Hz, NH), 7.76 (2H, d, J = 8.0 Hz, H_{ar}), 7.60 (2H, d, J = 8.0 Hz, H_{ar}), 4.88 (2H, s, *ortho* on η^5-C_5H_4), 4.41 (2H, s, *meta* on η^5-C_5H_4), 4.02 (5H, s, η^5-C_5H_5), 3.77 (1H, m, *ipso* on -C_6H_{11}), 1.82 (2H, br. s, *ortho* on -C_6H_{11}), 1.75 (2H, br s, *meta* on -C_6H_{11}), 1.62 (1H, d, J = 11.7 Hz, *para* on -C_6H_{11}), 1.32 (4H, m, *ortho* and *meta* on -C_6H_{11}), 1.14 (1H, m, *para* on -C_6H_{11});

^{13}C NMR (100 MHz, DMSO-d_6) δ: 165.7 (C=O), 142.7 {C_q-(η^5-C_5H_4)}, 132.5 {C_q-(C=O)}, 127.9, 125.7, 83.8 (C_{ipso} η^5-C_5H_4), 70.0 (η^5-C_5H_5), 69.9 (C_{meta} η^5-C_5H_4), 67.0 (C_{ortho} η^5-C_5H_4), 48.7 (C_{ipso} -C_6H_{11}), 32.9 (C_{ortho} -C_6H_{11}, -ve DEPT), 25.8 (C_{para} -C_6H_{11}, -ve DEPT), 25.5 (C_{meta} -C_6H_{11}, -ve DEPT).

2.15.3.20 1-(3-(4-Ferrocenylphenyl)acryloyl)pyrrolidine-2,5-dione **118**

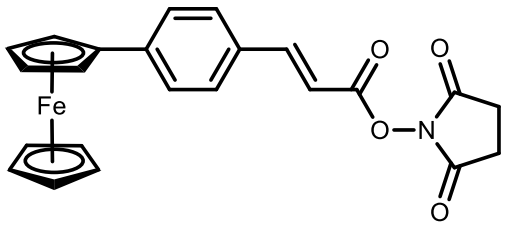

118

The synthesis followed that of **99** using the following reagents: 4-ferrocenyl cinnamic acid **82** (0.15 g, 0.45 mmol), dichloromethane (10 mL), *N*-(3-dimethylaminopropyl)-*N′*-carbodiimide hydrochloride (EDC) **88** (0.09 g, 0.45 mmol), *N*-hydroxysuccinimide (NHS) **91** (0.05 g,0.45 mmol), triethylamine (1 mL) and 4-aminopyridine **96** (0.04 g, 0.45 mmol). The crude product was purified by column chromatography (eluent 1:1 hexane:ethyl acetate) yielding compound **118** as dark orange/red needles (0.03 g, 15%);

m. p. = 214 °C decomp.;

Anal. Calc. for $C_{23}H_{19}NO_4Fe$: C, 64.36; H, 4.46; N, 3.26%. Found: C, 63.50; H, 4.52; N, 3.52%;

IR ν_{max}: 3090, 2922, 1759, 1732, 1599 – 1523 cm^{-1};

UV-Vis (CH_3CN) λ_{max}: 480 nm ε: 2653 $dm^3\ mol^{-1}\ cm^{-1}$;

^{1}H NMR (600 MHz, DMSO-d_6) δ: 7.54 (2H, d, J = 8.3 Hz, H_{ar}), 7.52 (2H, d, J = 8.2 Hz, H_{ar}), 7.37 (1H, d, J = 15.8 Hz, -C<u>H</u>=), 6.43 (1H, d, J = 15.9 Hz, =C<u>H</u>-), 4.84 (2H, t, J = 1.7 Hz, *ortho* on η^5-C_5<u>H_4</u>), 4.39 (2H, t, J = 1.7 Hz, *meta* on η^5-C_5<u>H_4</u>), 4.03 (5H, s, η^5-C_5<u>H_5</u>), 2.87 (4H, br. s, -C<u>H_2</u>-);

^{13}C NMR (100 MHz, DMSO-d_6) δ: 178.5 (N-<u>C</u>=O), 169.7 (-<u>C</u>OO-), 141.4 {<u>C_q</u>-(η^5-C_5H_4)}, 141.3 (-<u>C</u>H=), 133.1 {<u>C_q</u>-(CH=CH)}, 128.3, 126.6, 122.5 (=<u>C</u>H-), 84.4 (C_{ipso} η^5-<u>C_5H_4</u>), 69.9 (η^5-<u>C_5H_5</u>), 69.7 (C_{meta} η^5-<u>C_5H_4</u>), 66.8 (C_{ortho} η^5-<u>C_5H_4</u>), 25.6 (-<u>C</u>H_2-, -ve DEPT).

2.15.3.21 *N*-benzyl-3-(4-ferrocenylphenyl)acrylamide **119**

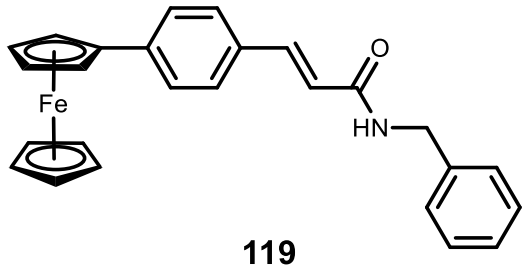

119

The synthesis followed that of **99** using the following reagents: 4-ferrocenyl cinnamic acid **82** (0.12 g, 0.35 mmol), dichloromethane (4 mL), *N*-(3-dimethylaminopropyl)-*N*′-carbodiimide hydrochloride (EDC) **88** (0.07 g, 0.35 mmol), *N*-hydroxysuccinimide (NHS) **91** (0.04 g, 0.35 mmol), triethylamine (1 mL) and benzylamine **97** (0.04 mL, 0.35 mmol). The crude product was purified by column chromatography (eluent 3:2 hexane:ethyl acetate) yielding compound **119** as an orange solid (0.02 g, 13%);

m. p. = 199 – 200 °C;

Anal. Calc. for $C_{26}H_{23}NOFe$: C, 74.12; H, 5.50; N, 3.32%. Found: C, 73.75; H, 5.37; N, 4.20%;

IR ν_{max}: 3237, 3035, 2921, 1649, 1602 – 1497 cm^{-1};

UV-Vis (DMSO) λ_{max}: 374, 456 nm ε: 1276, 493 $dm^3\ mol^{-1}\ cm^{-1}$;

^{1}H NMR (600 MHz, DMSO-d_6) δ: 8.61 (1H, t, *J* = 5.9 Hz, NH), 7.58 (2H, d, *J* = 8.3 Hz, H_{ar} cinnamoyl), 7.49 (2H, d, *J* = 8.3 Hz, H_{ar} cinnamoyl), 7.46 (1H, d, *J* = 15.7 Hz, -CH=), 7.35 (2H, t, *J* = 7.4 Hz, *meta* on -C_6H_5), 7.31 (2H, d, *J* = 7.0 Hz, *ortho* on -C_6H_5), 7.26 (1H, tt, *J* = 7.2 and 1.0 Hz, *para* on -C_6H_5), 6.69 (1H, d, *J* = 15.8 Hz, =CH-), 4.85 (2H, t, *J* = 3.7 Hz, *ortho* on η^5-C_5H_4), 4.41 (2H, d, *J* = 6.0 Hz, -CH_2-), 4.40 (2H, t, *J* = 3.7 Hz, *meta* on η^5-C_5H_4), 4.03 (5H, s, η^5-C_5H_5);

^{13}C NMR (100 MHz, DMSO-d_6) δ: 165.6 (C=O), 141.3 {C_q-(η^5-C_5H_4)}, 139.9 (C_{ipso} -C_6H_5), 139.4 (-CH=), 132.8 {C_q-(CH=CH)}, 128.8 (C_{meta} -C_6H_5), 128.2 {C_{ortho} to (CH=CH)}, 127.9 (C_{ortho} -C_6H_5), 127.3 (C_{para} -C_6H_5), 126.6 {C_{meta} to (CH=CH)}, 121.3 (=CH-), 84.2 (C_{ipso} η^5-C_5H_4), 69.9 (η^5-C_5H_5), 69.8 (C_{meta} η^5-C_5H_4), 66.9 (C_{ortho} η^5-C_5H_4), 42.8 (-CH_2-, -ve DEPT).

2.15.3.22 *N*-cyclohexyl-3-(4-ferrocenylphenyl)acrylamide **120**

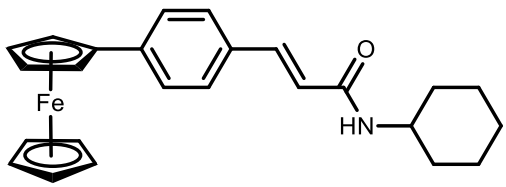

120

The synthesis followed that of **99** using the following reagents: 4-ferrocenyl cinnamic acid **82** (0.11 g, 0.32 mmol), dichloromethane (4 mL), *N*-(3-dimethylaminopropyl)-*N′*-carbodiimide hydrochloride (EDC) **88** (0.06 g, 0.32 mmol), *N*-hydroxysuccinimide (NHS) **91** (0.04 g, 0.32 mmol), triethylamine (1 mL) and cyclohexylamine **98** (0.04 mL, 0.32 mmol). The crude product was purified by column chromatography (eluent 1:1 hexane:ethyl acetate) yielding compound **120** as an orange solid (0.01 g, 10%);

m. p. = 234 °C decomp.;

Anal. Calc. for $C_{25}H_{27}NOFe$: C, 72.65; H, 6.58; N, 3.39%. Found: C, 72.80; H, 6.33; N, 4.14%;

IR ν_{max}: 3231, 3049, 2925, 1647, 1600 – 1525 cm^{-1};

UV-Vis (DMSO) λ_{max}: 373, 455 nm ε: 2945, 1099 $dm^3\ mol^{-1}\ cm^{-1}$;

^{1}H NMR (600 MHz, DMSO-d_6) δ: 7.98 (1H, d, J = 7.9 Hz, NH), 7.57 (2H, d, J = 8.3 Hz, H_{ar} cinnamoyl), 7.47 (2H, d, J = 8.3 Hz, H_{ar} cinnamoyl), 7.38 (1H, d, J = 15.7 Hz, -CH=), 6.61 (1H, d, J = 15.7 Hz, =CH-), 4.84 (2H, t, J = 1.8 Hz, *ortho* on η^5-C_5H_4), 4.39 (2H, t, J = 1.8 Hz, *meta* on η^5-C_5H_4), 4.03 (5H, s, η^5-C_5H_5), 3.66 (1H, m, *ipso* on -C_6H_{11}), 1.80 (2H, dd, J = 12.4 and 3.2 Hz, *ortho* on -C_6H_{11}), 1.71 (2H, dt, J = 13.1 and 3.7 Hz, *meta* on -C_6H_{11}), 1.58 (1H, dt, J = 12.8 and 3.7 Hz, *para* on -C_6H_{11}), 1.23 (4H, m, *ortho* and *meta* on -C_6H_{11}), 0.86 (1H, m, *para* on -C_6H_{11});

^{13}C NMR (100 MHz, DMSO-d_6) δ: 164.6 (C=O), 141.1 {C_q-(η^5-C_5H_4)}, 138.7 (-CH=), 132.9 {C_q-(CH=CH)}, 128.0 {C_{ortho} to (CH=CH)}, 126.6 {C_{meta} to (CH=CH)}, 121.9 (=CH-), 84.3 (C_{ipso} η^5-C_5H_4), 69.9 (η^5-C_5H_5), 69.8 (C_{meta} η^5-C_5H_4), 66.9 (C_{ortho} η^5-C_5H_4), 48.0 (C_{ipso} -C_6H_{11}), 33.0 (C_{ortho} -C_6H_{11}, -ve DEPT), 25.7 (C_{para} -C_6H_{11}, -ve DEPT), 25.0 (C_{meta} -C_6H_{11}, -ve DEPT).

C H A P T E R 3

3 *In vitro* biological evaluation of novel ferrocenyl derivatives

My contribution to Chapter 3 was the investigation of the *in vitro* anti-proliferative activity of a series of ferrocenyl derivatives, including: (a) novel heterocyclic functionalised ferrocenyl derivatives **99**-**120** and their starting materials, (b) *N*-(1′-alkyl-6-ferrocenyl-2-naphthoyl) amino acid and dipeptide esters **130**-**143**, and (c) *N*-(ferrocenylmethylamino acid)-fluorinated benzene carboxamides **144**-**154**. These experiments involved the analysis of the cell viability in two cell lines after exposure to the ferrocenyl derivatives, and determination of the IC_{50} of suitable candidates after the preliminary screening. These studies were carried out at Laboratory of Genomics and Genetic Engineering – School of Graduates in Sciences – Faculty of Chemical Sciences at Universidad Autónoma de Nuevo León (Monterrey, Mexico) under the supervision of Dr. Mónica A. Ramírez-Cabrera and Dr. Eder Arredondo-Espinoza.
Compounds **130**-**154** were previously synthesised and characterised by Lingli Lu within Dr. Peter Kenny's research group at DCU.

3.1 Introduction

3.1.1 Cell culture

Tissue culture is defined as the removal of cells, tissues, or organs from a plant or animal and their posterior location into an artificial habitat for further growth. This habitat normally consists of a medium (liquid or semi-solid) that supplies all the nutrients essential for survival and growth, inside a suitable culture flask (glass or plastic). *Organ culture* refers to the culture of organs (whole or pieces) for the analysis of their continued function or development. *Cell culture* is the term for the removal of cells from the organ pieces before or during cultivation, hence disturbing their normal interconnections with neighbouring cells.[251,252]

Animal cell culture was first launched by Harrison in 1907. However, several improvements developed in the late 1940's to early 1950's made cell culture universally available as one of the main tools used in the life sciences. The first and most important developments were antibiotics; their usage avoided many of the contamination troubles that impacted earlier experiments. Second, the addition of techniques to cultivate continuously growing cell lines, like the use of trypsin to pull cells out of the culture flasks. The management of these cell lines led to standardized, chemically defined culture media that enabled the process of growing cells.[251,253,254]

3.1.2 Miniaturised *in vitro* colorimetric assays

In vitro assays with cultured cells are commonly used for cell viability and cytotoxicity tests in drug screening. They are also used in oncological research to evaluate both compound toxicity and tumour cell growth inhibition during drug development because they are quick, inexpensive and do not require the use of animals.[255,256] The use of miniature *in vitro* colorimetric endpoint assays provides data about the capability of a substance to either enhance cell growth or generate cell death. These assays include the determination of cell number after the cells have been exposed to the test substance for a specific period of time.[257]

Tetrazolium dye assays such as MTT and other closely related tetrazolium dyes including XTT, MTS and the WSTs can be used to measure cytotoxicity (loss of viable cells) or cytostatic activity (alteration from proliferation to inertness) of potential medicinal agents. In these analysis, it can be concluded that the test substance has an anti-proliferative effect on exposed cells if there is a reduction in cell number compared to

unexposed controls.[258,259] Different parameters must be considered for the selection of the most suitable cell viability assay, such as the availability in the laboratory where the study is to be performed, test compounds, detection mechanism, specificity and sensitivity.[255]

3.1.2.1 MTT assay

The MTT assay is a colorimetric technique commonly used in studies to estimate cell viability due to its low cost and ease of use. The MTT reagent 3-(4,5-dimethylthiazol-2-yl)-2,5-diphenyltetrazolium bromide **124** is a yellow water-soluble salt that is converted into insoluble formazan crystals **125** in the presence of succinate dehydrogenase within the mitochondria of metabolically active cells via cleavage of the tetrazolium ring (Scheme 3.1). The insoluble purple MTT formazan crystals **125** can be solubilized by DMSO or detergent for further spectrophotometric determination.[259,260] Besides the solubilization step, the quite poor sensitivity of this assay is another considerable limitation. Furthermore, some compounds can influence the mitochondrial enzymes that are responsible for converting the MTT dye **124** to formazan **125**, but not eventually kill the cells.[257,259]

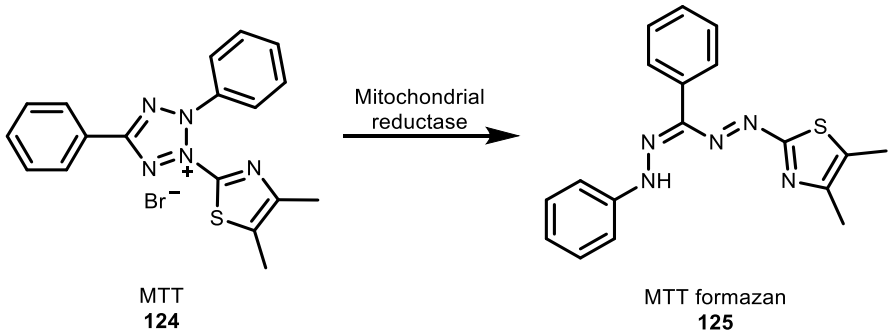

Scheme 3.1. Reduction of MTT **124** to MTT formazan **125**.

3.1.2.2 Neutral red uptake assay

In the neutral red uptake cytotoxicity assay, live cells accumulate neutral red dye 3-amino-7-dimethylamino-2-methylphenazine hydrochloride **126** (Figure 3.1) into their lysosomes. Therefore, the loss of neutral red uptake is proportional to loss of cell viability.[258,261] A major disadvantage of the assay is the induction of precipitation of the neutral red dye **126** into visible, fine, needle-like crystals, which affects the accuracy of the absorbance readings used to detect the presence of the dye.[262,263]

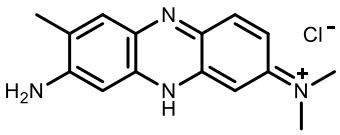

Neutral red
126

Figure 3.1. Structure of neutral red **126**.

3.1.2.3 WST-1 assay

The WST-1 assay is a colorimetric technique used to assess the cell viability in any *in vitro* model. This assay is based on the reduction of WST-1 reactant 2-(4-iodophenyl)-3-(4-nitrophenyl)-5-(2,4-disulfophenyl)-2H-tetrazolium, monosodium salt **127** (pale yellow), leading to the production of formazan **128** (dark yellow) as shown in Scheme 3.2.[264]

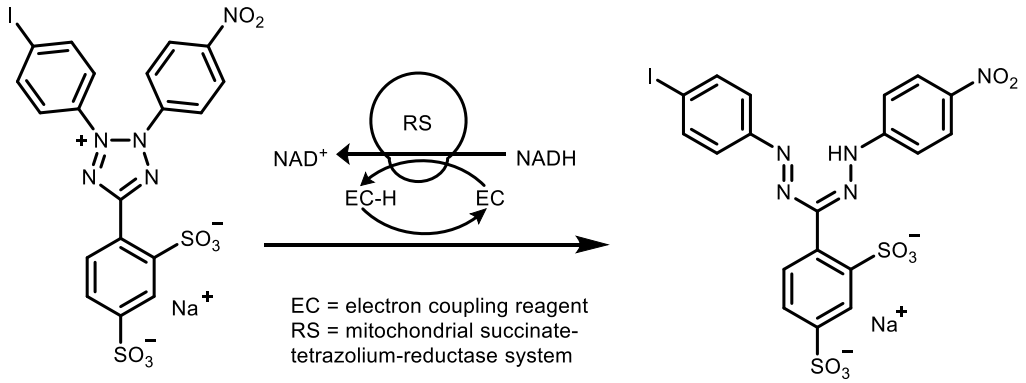

WST-1
127

WST-1 formazan
128

Scheme 3.2. Reduction of the tetrazolium salt WST-1 **127** to WST-1 formazan **128**.

Some authors point out that this reaction is carried out by cellular dehydrogenases, i.e. outside the cell; whilst others indicate that it is due to the mitochondrial dehydrogenases.[265,266] In any case, the complex RS is only active in living cells, since mitochondria of dead cells no longer performs functions; therefore, the formazan produced is directly proportional to the number of viable cells. The amount of formazan **128** is measured in an absorbance reader at 450 nm wavelength.[267,268] WST-1 assay is a non-radioactive, fast method which no requires washing, harvesting or solubilization steps like MTT, XTT or MTS assays, being more sensitive and convenient because the entire assay can be performed directly in the well plate.[269–271] For these reasons, the WST-1 assay was the chosen colorimetric end-point assay for the *in vitro* biological analysis of compounds in this research work.

3.2 Anti-proliferative evaluation of novel ferrocenyl derivatives

3.2.1 Cell lines

Chemotherapy involves the use of agents which are cytotoxic, i.e. they kill or damage cells. Although the main target is cancer cells, chemotherapeutic compounds travel throughout the body in the bloodstream and can find and affect normal cells too. Therefore, toxicity is a common side effect in chemotherapy treatments. Other side effects include nausea, fatigue, sickness, constipation, diarrhoea, vomiting, sleep disturbance, and appetite changes.[83–87] For this reason, the novel heterocyclic functionalised ferrocenyl derivatives **99**-**120** were tested against both a cancerous and a non-cancerous cell line in order to compare their selectivity towards each type of cells. SiHa cell line belongs to human cervical carcinoma, and Chang cell line is derived from human liver and widely used as a human normal hepatocyte model.[272,273] The comparison of the inhibition of cell growth between SiHa and Chang cell lines can suggest if the novel ferrocenyl derivatives present a certain degree of selectivity towards cancerous and non-cancerous cells, thus leading to a lower toxicity side effect. A series of *N*-(1′-alkyl-6-ferrocenyl-2-naphthoyl) amino acid and dipeptide esters **130**-**143** and *N*-(ferrocenylmethylamino acid)-fluorinated benzene carboxamides **144**-**154** were also tested against SiHa and Chang cell lines. These compounds were synthesised and characterised by Lu.[195] Due to the large number of derivatives, only compounds showing stronger anti-proliferative effects on SiHa cell line with less toxicity against Chang cells were then selected for further determination of IC_{50} value, which corresponds to the concentration of the drug required for 50% inhibition of cell growth.

3.2.2 Screening and IC_{50} determination

The *in vitro* cytotoxicity of different series of ferrocenyl derivatives was evaluated by performing a screening of every compound at a single dose in both SiHa human cervical carcinoma and Chang human liver cell lines. A stock solution of each derivative was prepared in a suitable solvent (DMSO, H_2O or EtOH). Diluted solutions of the test samples were prepared at a 2x final concentration by adding the cell culture medium with a calculated amount of the stock solution. The screenings were performed in triplicate by treating individual wells of a 96-well plate containing the cells with 100 μL of each diluted solution. Positive (vincristine **129** for SiHa cell line or Triton X-100 for Chang cell line), negative (cell with medium) and blank (empty wells) controls were also included in the

assays. The plate was then incubated for 24 h. At this point, cell survival was established via the WST-1 assay. The averages of the screenings were normalised using the blank value and are expressed as the percentage cell viability ± standard deviation (relative to the negative control). Standard deviations were calculated using data obtained from three independent experiments. For IC_{50} determination, the same procedure was followed but a serial dilution of a range of concentrations was used instead of a single dose. The IC_{50} value was calculated using GraphPad Prism 8 software, and standard deviations were calculated using data obtained from three independent experiments.

3.3 *In vitro* study of novel heterocyclic functionalised ferrocenyl derivatives 99-120

The *in vitro* anticancer activity of the novel ferrocenyl naphthoyl, benzoyl and cinnamoyl derivatives **99**-**120** synthesized and characterized in this thesis project was studied along with the corresponding ferrocenyl carboxylic acids from which they were derived: 6-ferrocenyl-2-naphthoic acid **65**, 6-(1′-ethyl)ferrocenyl-2-naphthoic acid **66**, 3-ferrocenyl-2-naphthoic acid **70**, *ortho*-ferrocenylbenzoic acid **77**, *meta*-ferrocenylbenzoic acid **78**, *para*-ferrocenylbenzoic acid **79** and 4-ferrocenyl cinnamic acid **82**, in order to identify the effect of the substituents coupled to the structures. Screenings of each compound at a single dose of 10 μM in SiHa human cervical carcinoma and Chang human liver cell lines were performed.

3.3.1 *In vitro* evaluation in SiHa cell line

The percentages of viability of SiHa human cervical carcinoma cell line after exposure to the novel heterocyclic functionalised ferrocenyl derivatives **99**-**120**, the corresponding ferrocenyl carboxylic acids **65**, **66**, **70**, **77**-**79** and **82**, and the reference compound vincristine **129** are shown in Table 3.1 and plotted in Figure 3.2.

Table 3.1. Cell viability percentage at 10 μM in SiHa human cervical carcinoma cells for novel heterocyclic functionalised ferrocenyl derivatives **99**-**120**, their starting materials **65**, **66**, **70**, **77**-**79** and **82**, and reference compound vincristine **129**.

Compound name	No.	% cell viability
6-Ferrocenyl-2-naphthoic acid	**65**	84 ± 2
6-Ferrocenyl-*N*-(pyridin-2-yl)-2-naphthamide	**99**	88 ± 4
6-Ferrocenyl-*N*-(pyridin-3-yl)-2-naphthamide	**100**	82 ± 1
2,5-Dioxopyrrolidin-1-yl 6-ferrocenyl-2-naphthoate	**101**	82 ± 5
N-benzyl-6-ferrocenyl-2-naphthamide	**102**	93 ± 3
N-cyclohexyl-6-ferrocenyl-2-naphthamide	**103**	80 ± 1
6-(1′-Ethyl)ferrocenyl-2-naphthoic acid	**66**	77 ± 1
2,5-Dioxopyrrolidin-1-yl 6-(1′-ethyl)ferrocenyl-2-naphthoate	**104**	73 ± 2
N-benzyl-6-(1′-ethyl)ferrocenyl-2-naphthamide	**105**	82 ± 3
N-cyclohexyl-6-(1′-ethyl)ferrocenyl-2-naphthamide	**106**	98 ± 1
3-Ferrocenyl-2-naphthoic acid	**70**	92 ± 1
N-benzyl-3-ferrocenyl-2-naphthamide	**107**	95 ± 1
N-cyclohexyl-3-ferrocenyl-2-naphthamide	**108**	78 ± 1
Vincristine	**129**	33 ± 1
Ortho-ferrocenylbenzoic acid	**77**	90 ± 5
Meta-ferrocenylbenzoic acid	**78**	96 ± 1
Para-ferrocenylbenzoic acid	**79**	97 ± 1
2,5-Dioxopyrrolidin-1-yl 2-ferrocenylbenzoate	**109**	93 ± 4
2,5-Dioxopyrrolidin-1-yl 3-ferrocenylbenzoate	**110**	65 ± 1
2,5-Dioxopyrrolidin-1-yl 4-ferrocenylbenzoate	**111**	63 ± 1
N-benzyl-2-ferrocenylbenzamide	**112**	90 ± 2
N-benzyl-3-ferrocenylbenzamide	**113**	86 ± 2
N-benzyl-4-ferrocenylbenzamide	**114**	93 ± 3
N-cyclohexyl-2-ferrocenylbenzamide	**115**	86 ± 4
N-cyclohexyl-3-ferrocenylbenzamide	**116**	83 ± 7
N-cyclohexyl-4-ferrocenylbenzamide	**117**	95 ± 1
4-Ferrocenyl cinnamic acid	**82**	95 ± 5
1-(3-(4-Ferrocenylphenyl)acryloyl)pyrrolidine-2,5-dione	**118**	84 ± 4
N-benzyl-3-(4-ferrocenylphenyl)acrylamide	**119**	90 ± 7
N-cyclohexyl-3-(4-ferrocenylphenyl)acrylamide	**120**	93 ± 7
Vincristine	**129**	33 ± 1

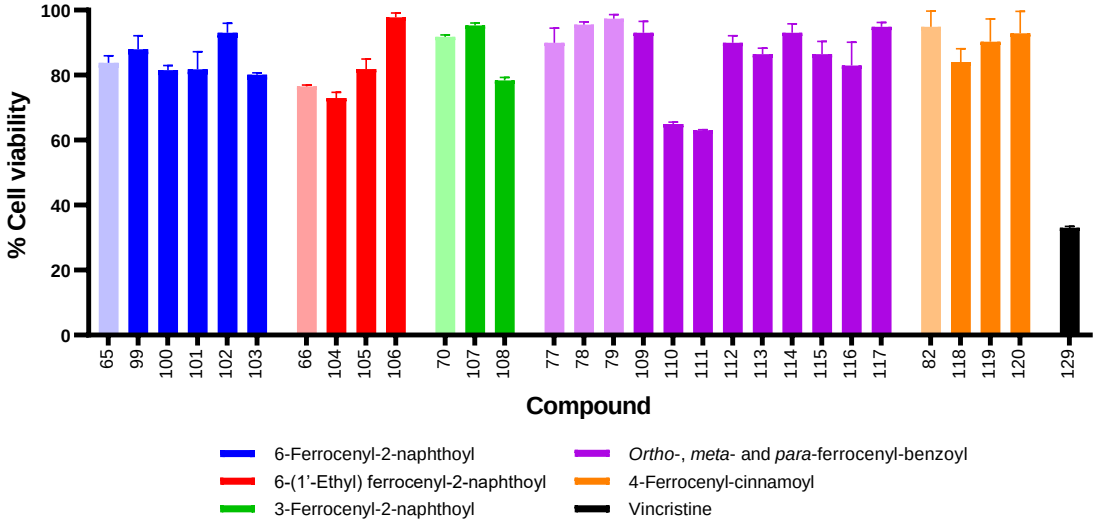

Figure 3.2. Cell viability percentage at 10 μM in SiHa human cervical carcinoma cells for novel heterocyclic functionalised ferrocenyl derivatives **99**-**120**, their starting materials **65**, **66**, **70**, **77**-**79** and **82**, and reference compound vincristine **129**. Data presented as an average of triplicate measurements ± S.D.

As observed, the novel heterocyclic functionalised ferrocenyl derivatives **99**-**120** and their starting materials **65**, **66**, **70**, **77**-**79** and **82** did not show great antiproliferative effect in SiHa cells, as most derivatives showed high cell viability values. Only a few compounds showed regular growth inhibition, with general cell viability values below 80%. However, these values are still not comparable to the chemotherapeutic medication vincristine **129** (33 ± 1%). The strongest growth inhibition found in the naphthoyl series belong to compounds **104** (73 ± 2%) and **108** (78 ± 1%); it is worthy to note that starting material **66** also exhibited an antiproliferative effect below 80% (77 ± 1%). In the benzoyl series, the higher anti-proliferative effect was displayed by compounds **110** (65 ± 1%) and **111** (63 ± 1%), being the highest inhibitors of cell growth of all the compounds tested. As a general trend, compounds from the 6-(1′-ethyl)ferrocenyl-2-naphthoyl series exhibited the strongest growth inhibition, with an average of 84% cell viability; also, NHS derivatives were the most active, with an average of 76% cell viability.

3.3.2 *In vitro* evaluation in Chang cell line

The percentages of viability of Chang human liver cell line after exposure to the novel heterocyclic functionalised ferrocenyl derivatives **99**-**120**, the corresponding ferrocenyl carboxylic acids **65**, **66**, **70**, **77**-**79** and **82**, and the reference compound vincristine **129** are shown in Table 3.2 and plotted in Figure 3.3.

Table 3.2. Cell viability percentage at 10 μM in Chang human liver cells for novel heterocyclic functionalised ferrocenyl derivatives **99**-**120** and their starting materials **65**, **66**, **70**, **77**-**79** and **82**.

Compound name	No.	% cell viability
6-ferrocenyl-2-naphthoic acid	**65**	78 ± 12
6-ferrocenyl-*N*-(pyridin-2-yl)-2-naphthamide	**99**	85 ± 4
6-ferrocenyl-*N*-(pyridin-3-yl)-2-naphthamide	**100**	83 ± 2
2,5-dioxopyrrolidin-1-yl 6-ferrocenyl-2-naphthoate	**101**	97 ± 1
N-benzyl-6-ferrocenyl-2-naphthamide	**102**	94 ± 1
N-cyclohexyl-6-ferrocenyl-2-naphthamide	**103**	82 ± 5
6-(1′-ethyl)ferrocenyl-2-naphthoic acid	**66**	95 ± 1
2,5-dioxopyrrolidin-1-yl 6-(1′-ethyl)ferrocenyl-2-naphthoate	**104**	79 ± 5
N-benzyl-6-(1′-ethyl)ferrocenyl-2-naphthamide	**105**	87 ± 1
N-cyclohexyl-6-(1′-ethyl)ferrocenyl-2-naphthamide	**106**	94 ± 3
3-ferrocenyl-2-naphthoic acid	**70**	73 ± 2
N-benzyl-3-ferrocenyl-2-naphthamide	**107**	81 ± 1
N-cyclohexyl-3-ferrocenyl-2-naphthamide	**108**	82 ± 7
ortho-ferrocenylbenzoic acid	**77**	96 ± 2
meta-ferrocenylbenzoic acid	**78**	84 ± 6
para-ferrocenylbenzoic acid	**79**	87 ± 2
2,5-dioxopyrrolidin-1-yl 2-ferrocenylbenzoate	**109**	84 ± 5
2,5-dioxopyrrolidin-1-yl 3-ferrocenylbenzoate	**110**	81 ± 2
2,5-dioxopyrrolidin-1-yl 4-ferrocenylbenzoate	**111**	70 ± 2
N-benzyl-2-ferrocenylbenzamide	**112**	93 ± 5
N-benzyl-3-ferrocenylbenzamide	**113**	95 ± 1
N-benzyl-4-ferrocenylbenzamide	**114**	88 ± 2
N-cyclohexyl-2-ferrocenylbenzamide	**115**	74 ± 4
N-cyclohexyl-3-ferrocenylbenzamide	**116**	92 ± 7
N-cyclohexyl-4-ferrocenylbenzamide	**117**	89 ± 1
4-ferrocenyl cinnamic acid	**82**	87 ± 5
1-(3-(4-ferrocenylphenyl)acryloyl)pyrrolidine-2,5-dione	**118**	95 ± 3
N-benzyl-3-(4-ferrocenylphenyl)acrylamide	**119**	86 ± 3
N-cyclohexyl-3-(4-ferrocenylphenyl)acrylamide	**120**	92 ± 1

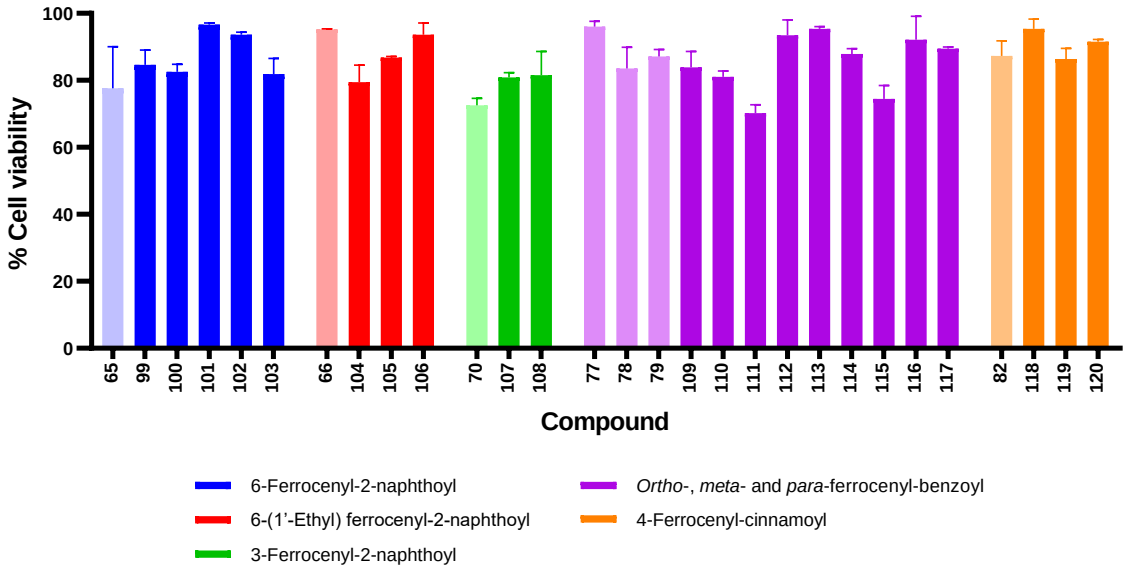

Figure 3.3. Cell viability percentage at 10 μM in Chang human liver cells for novel heterocyclic functionalised ferrocenyl derivatives **99**-**120** and their starting materials **65**, **66**, **70**, **77**-**79** and **82**. Data presented as an average of triplicate measurements ± S.D.

As observed, no compound showed a significant inhibition in the growth of Chang cells, as most derivatives tested showed cell viability values greater than 70%. These are good results as it suggests that the novel heterocyclic functionalised ferrocenyl derivatives show very little toxicity towards the non-cancerous cell line Chang. In the naphthoyl series, derivatives showing less than 10% growth inhibition were compounds **101** (97 ± 1%), **102** (94 ± 1%) and **106** (94 ± 3%); it is important to note that starting material **66** also show excellent non-cytotoxic activity, with cell viability value of 95 ± 1%. The weakest growth inhibition (less than 10%) found in the benzoyl series belong to compounds **112** (93 ± 5%), **113** (95 ± 1%), **116** (92 ± 7%), **188** (95 ± 3%) and **120** (92 ± 1%); also, the starting material **77** showed little growth inhibition (96 ± 2%). As a general trend, compounds from 4-ferrocenyl-cinammoyl series exhibited the weakest growth inhibition over all, with an average of 91% cell viability; also, derivatives with benzylamine moiety were the less cytotoxic, with an average of 89% cell viability.

3.3.3 *In vitro* comparison study in both SiHa and Chang cell lines

A comparison of the percentages of viability in both SiHa human cervical carcinoma and Chang human liver cell lines after exposure to the novel heterocyclic functionalised ferrocenyl derivatives **99**-**120** and their corresponding ferrocenyl carboxylic acids **65**, **66**, **70**, **77**-**79** and **82** is shown in Table 3.3 and Figure 3.4. For naphthoyl series, compounds **66**, **104** and **108** are more toxic than others in SiHa cell line, with cell viability values between 72-78%. For benzoyl derivatives, compounds **110** and **111** showed strongest anti-proliferative effect in SiHa cells, with cell viability values between 63-64%. These derivatives show limited toxicity against Chang cells, with cell viability values between 70-95%. These results suggest that these compounds have some selectivity between cancerous and non-cancerous cells, thus they could be considered for cancer treatment.

Table 3.3. Comparison of cell viability percentage at 10 μM in SiHa and Chang cell lines for novel heterocyclic functionalised ferrocenyl derivatives **99**-**120** and their carboxylic acids **65**, **66**, **70**, **77**-**79** and **82**.

Compound name	No.	% cell viability in SiHa	% cell viability in Chang
6-ferrocenyl-2-naphthoic acid	**65**	84 ± 2	78 ± 12
6-ferrocenyl-*N*-(pyridin-2-yl)-2-naphthamide	**99**	88 ± 4	85 ± 4
6-ferrocenyl-*N*-(pyridin-3-yl)-2-naphthamide	**100**	82 ± 1	83 ± 2
2,5-dioxopyrrolidin-1-yl 6-ferrocenyl-2-naphthoate	**101**	82 ± 5	97 ± 1
N-benzyl-6-ferrocenyl-2-naphthamide	**102**	93 ± 3	94 ± 1
N-cyclohexyl-6-ferrocenyl-2-naphthamide	**103**	80 ± 1	82 ± 5
6-(1′-ethyl)ferrocenyl-2-naphthoic acid	**66**	77 ± 1	95 ± 1
2,5-dioxopyrrolidin-1-yl 6-(1′-ethyl)ferrocenyl-2-naphthoate	**104**	73 ± 2	79 ± 5
N-benzyl-6-(1′-ethyl)ferrocenyl-2-naphthamide	**105**	82 ± 3	87 ± 1
N-cyclohexyl-6-(1′-ethyl)ferrocenyl-2-naphthamide	**106**	98 ± 1	94 ± 3
3-ferrocenyl-2-naphthoic acid	**70**	92 ± 1	73 ± 2
N-benzyl-3-ferrocenyl-2-naphthamide	**107**	95 ± 1	81 ± 1
N-cyclohexyl-3-ferrocenyl-2-naphthamide	**108**	78 ± 1	82 ± 7
ortho-ferrocenylbenzoic acid	**77**	33 ± 1	96 ± 2
meta-ferrocenylbenzoic acid	**78**	90 ± 5	84 ± 6
para-ferrocenylbenzoic acid	**79**	96 ± 1	87 ± 2
2,5-dioxopyrrolidin-1-yl 2-ferrocenylbenzoate	**109**	97 ± 1	84 ± 5
2,5-dioxopyrrolidin-1-yl 3-ferrocenylbenzoate	**110**	93 ± 4	81 ± 2
2,5-dioxopyrrolidin-1-yl 4-ferrocenylbenzoate	**111**	65 ± 1	70 ± 2
N-benzyl-2-ferrocenylbenzamide	**112**	63 ± 1	93 ± 5
N-benzyl-3-ferrocenylbenzamide	**113**	90 ± 2	95 ± 1
N-benzyl-4-ferrocenylbenzamide	**114**	86 ± 2	88 ± 2
N-cyclohexyl-2-ferrocenylbenzamide	**115**	93 ± 3	74 ± 4
N-cyclohexyl-3-ferrocenylbenzamide	**116**	86 ± 4	92 ± 7
N-cyclohexyl-4-ferrocenylbenzamide	**117**	83 ± 7	89 ± 1
4-ferrocenyl cinnamic acid	**82**	95 ± 1	87 ± 5
1-(3-(4-ferrocenylphenyl)acryloyl)pyrrolidine-2,5-dione	**118**	95 ± 5	95 ± 3
N-benzyl-3-(4-ferrocenylphenyl)acrylamide	**119**	84 ± 4	86 ± 3
N-cyclohexyl-3-(4-ferrocenylphenyl)acrylamide	**120**	90 ± 7	92 ± 1

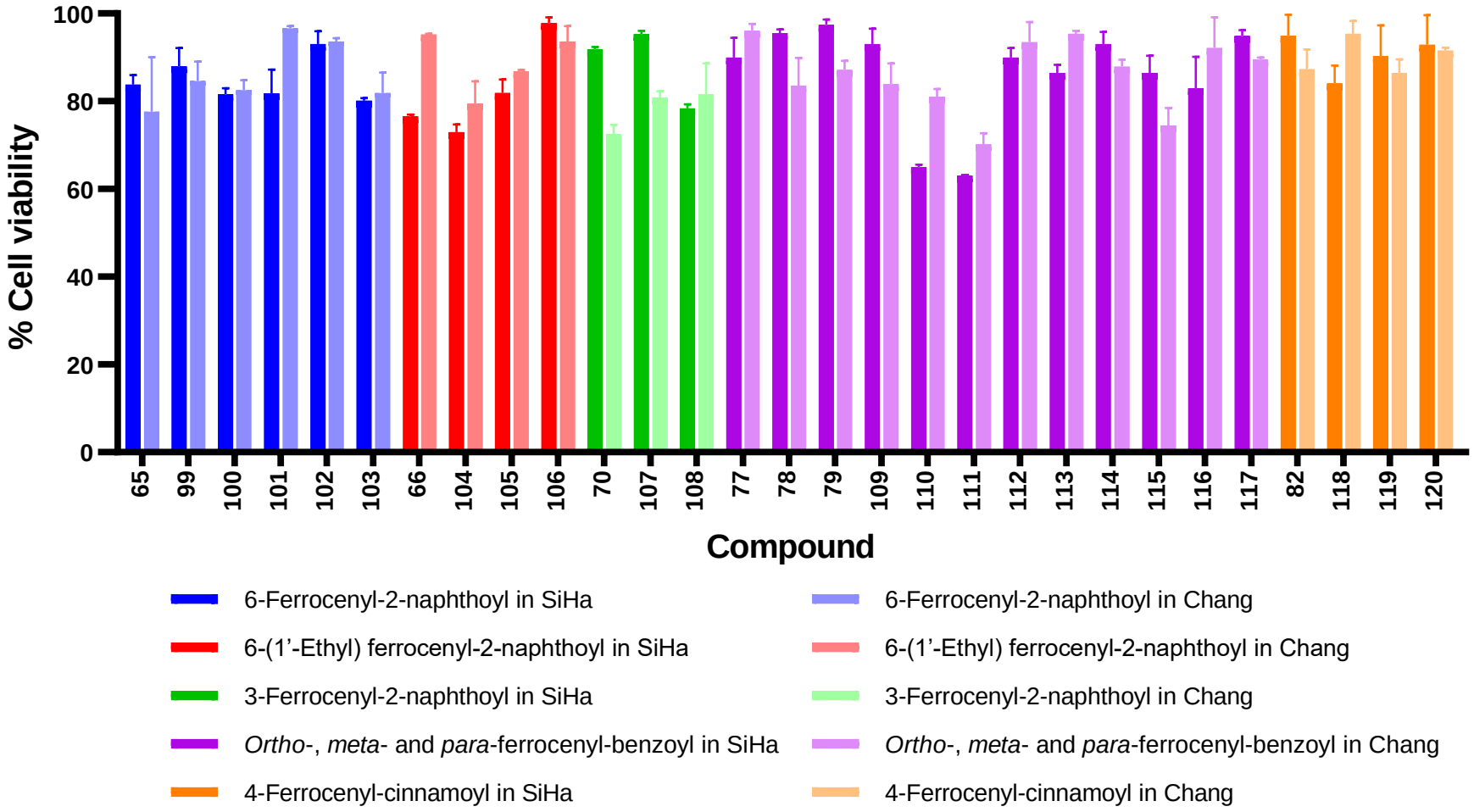

Figure 3.4. Comparison of cell viability percentage at 10 μM in SiHa and Chang cell lines for novel heterocyclic functionalised ferrocenyl derivatives **99**-**120** and their carboxylic acids **65**, **66**, **70**, **77**-**79** and **82**. Data presented as an average of triplicate measurements ± S.D.

3.4 *In vitro* study of *N*-(1′-alkyl-6-ferrocenyl-2-naphthoyl) amino acid and dipeptide esters 130-143

The *in vitro* anticancer activity of a series of *N*-(1′-alkyl-6-ferrocenyl-2-naphthoyl) amino acid and dipeptide esters **130**-**143** previously synthesized and characterized by Lu[195] was studied. These compounds follow the general structure of ferrocenyl amino acid and dipeptide derivatives previously presented earlier, with the innovation that the ferrocene core has been alkylated (Figure 3.5). The alkyl group is thought to be important in further decreasing the redox potential of these compounds.[195]

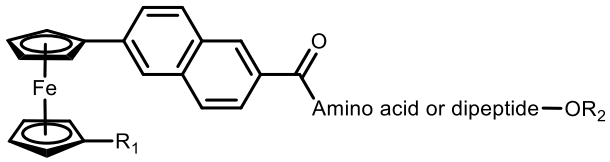

R_1 and R_2 = -CH_3, -CH_2CH_3

Figure 3.5. General structure of the *N*-(1′-alkyl-6-ferrocenyl-2-naphthoyl) amino acid and dipeptide esters **130**-**143**.

The structures of the *N*-(1′-methyl) derivatives **130**-**136** are presented in Figure 3.6, and the *N*-(1′-ethyl) derivatives **137**-**143** are shown in Figure 3.7. Screenings of each compound at a single dose of 200 μM in both SiHa human cervical carcinoma and Chang human liver cell lines were performed.

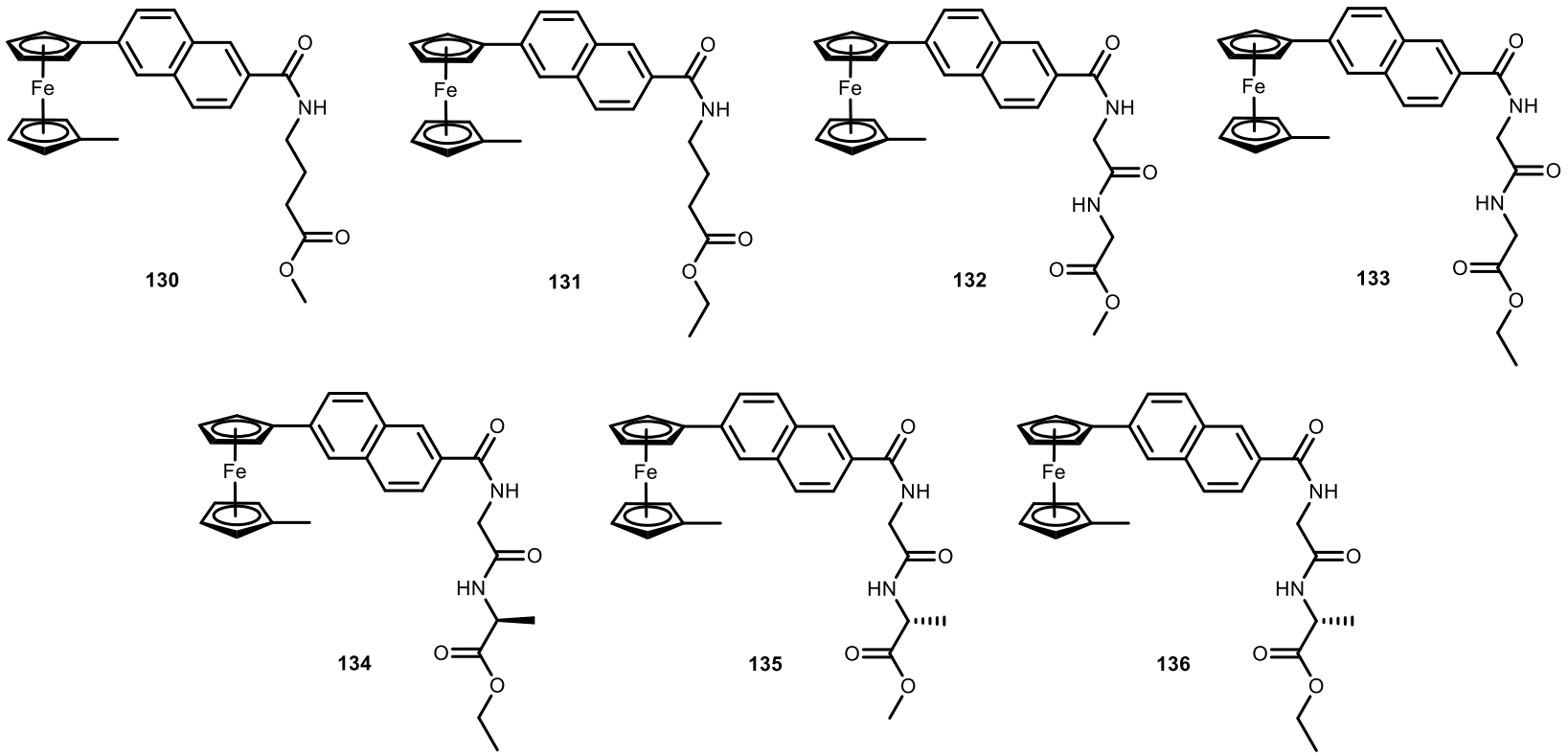

Figure 3.6. Structures of *N*-(1′-methyl-6-ferrocenyl-2-naphthoyl) amino acid and dipeptide esters **130**-**136**.

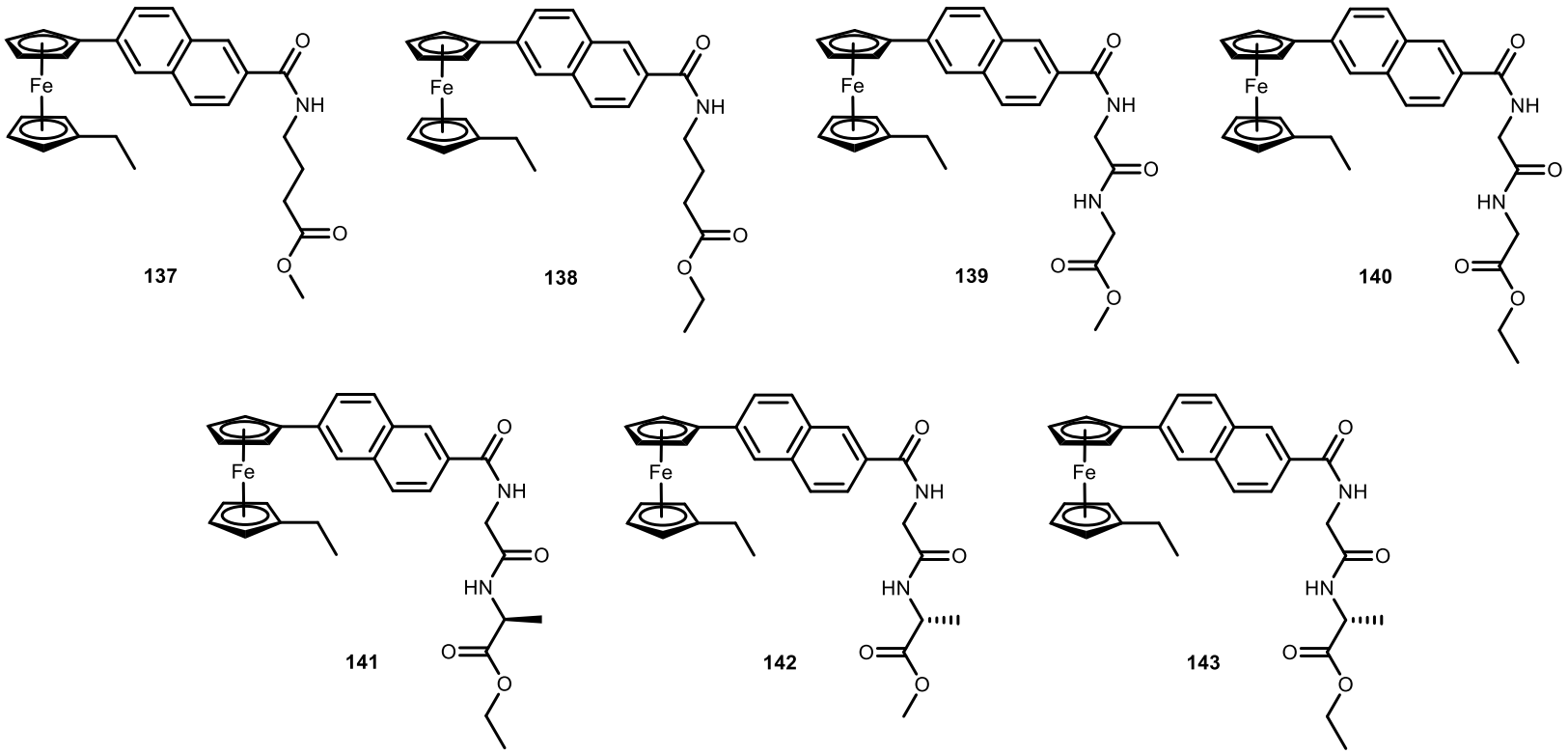

Figure 3.7. Structures of *N*-(1′-ethyl-6-ferrocenyl-2-naphthoyl) amino acid and dipeptide esters **137**-**143**.

3.4.1 *In vitro* evaluation in SiHa cell line

The percentages of viability of SiHa human cervical carcinoma cell line after exposure to derivatives **130**-**143** and the reference compound vincristine **129** are shown in Table 3.4 and Figure 3.8 for *N*-(1′-methyl-6-ferrocenyl-2-naphthoyl) amino acid and dipeptide esters **130**-**136**, and in Table 3.5 and Figure 3.9 for *N*-(1′-ethyl-6-ferrocenyl-2-naphthoyl) amino acid and dipeptide esters **137**-**143**. For the *N*-(1′-methyl-6-ferrocenyl-2-naphthoyl) amino acid and dipeptide esters **130**-**136**, it can be observed that all compounds are more active than reference compound vincristine **129**. Compound **134** exhibits the strongest inhibition growth, with only 2 ± 1% cell viability; followed by compound **132** with 4 ± 1% cell viability. Similar results were obtained from the screening of *N*-(1′-ethyl-6-ferrocenyl-2-naphthoyl) amino acid and dipeptide esters **137**-**143**. Except for compound **138**, the rest of the derivatives show cell viability percentages lower than reference compound vincristine **129**. Compound **140** displays the greatest inhibition growth, with only 3 ± 1% cell viability; followed by compound **143** with 5 ± 1% cell viability. From all the *N*-(1′-alkyl-6-ferrocenyl-2-naphthoyl) amino acid and dipeptide esters **130**-**143**, compounds with the γ-aminobutyric ester moiety are generally the less active from the series.

Table 3.4. Cell viability percentage at 200 μM in SiHa human cervical carcinoma cells for *N*-(1′-methyl-6-ferrocenyl-2-naphthoyl) amino acid and dipeptide esters **130**-**136** and reference compound vincristine **129**.

Alkyl	Linker	Peptide ester	No.	% cell viability
CH_3-	Naphthoyl	GABA-OMe	**130**	22 ± 2
		GABA-OEt	**131**	40 ± 1
		Gly-Gly-OMe	**132**	4 ± 1
		Gly-Gly-OEt	**133**	30 ± 2
		Gly-L-Ala-OEt	**134**	2 ± 1
		Gly-D-Ala-OMe	**135**	10 ± 4
		Gly-D-Ala-OEt	**136**	19 ± 2
		Vincristine	**129**	42 ± 3

Table 3.5. Cell viability percentage at 200 μM in SiHa human cervical carcinoma cells for *N*-(1′-ethyl-6-ferrocenyl-2-naphthoyl) amino acid and dipeptide esters **137**-**143** and reference compound vincristine **129**.

Alkyl	Linker	Peptide ester	No.	% cell viability
CH_3-CH_2-	Naphthoyl	GABA-OMe	**137**	21 ± 3
		GABA-OEt	**138**	56 ± 1
		Gly-Gly-OMe	**139**	12 ± 2
		Gly-Gly-OEt	**140**	3 ± 1
		Gly-L-Ala-OEt	**141**	21 ± 2
		Gly-D-Ala-OMe	**142**	20 ± 1
		Gly-D-Ala-OEt	**143**	5 ± 1
		Vincristine	**129**	42 ± 3

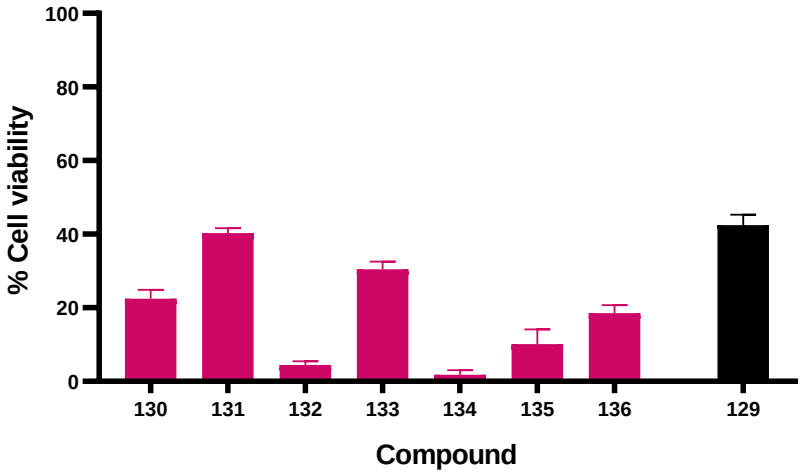

Figure 3.8. Cell viability percentage at 200 μM in SiHa human cervical carcinoma cells for *N*-(1′-methyl-6-ferrocenyl-2-naphthoyl) amino acid and dipeptide esters **130**-**136** and reference compound vincristine **129**. Data presented as an average of triplicate measurements ± S.D.

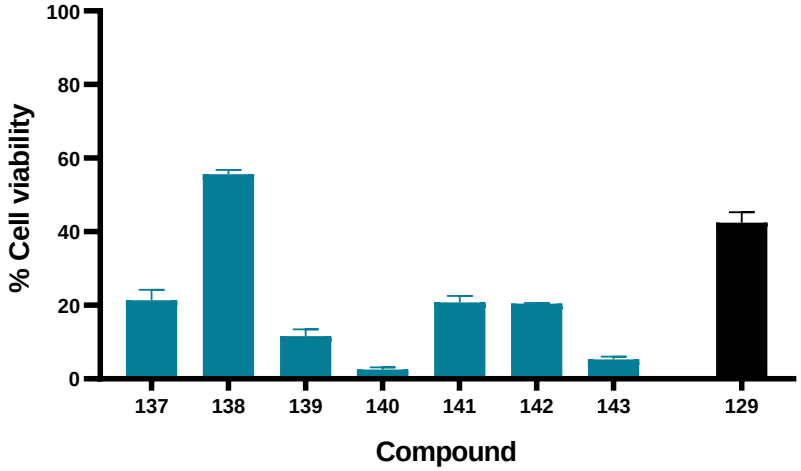

Figure 3.9. Cell viability percentage at 200 μM in SiHa human cervical carcinoma cells for *N*-(1′-ethyl-6-ferrocenyl-2-naphthoyl) amino acid and dipeptide esters **137**-**143** and reference compound vincristine **129**. Data presented as an average of triplicate measurements ± S.D.

3.4.2 *In vitro* evaluation in Chang cell line

The percentages of viability of Chang human liver cell line after exposure to derivatives **130**-**143** are shown in Table 3.6 and Figure 3.10 for *N*-(1′-methyl-6-ferrocenyl-2-naphthoyl) amino acid and dipeptide esters **130**-**136**, and in Table 3.7 and Figure 3.11 for *N*-(1′-ethyl-6-ferrocenyl-2-naphthoyl) amino acid and dipeptide esters **137**-**143**. From the screening of *N*-(1′-methyl-6-ferrocenyl-2-naphthoyl) amino acid and dipeptide esters **130**-**136**, it can be seen that most of the compounds show a strong growth inhibition, with cell viability values below 30%. However, compound **130** exhibited the lowest toxicity against Chang cell line, with a cell viability value of 47 ± 1%; followed by compound **131** with 45 ± 2% cell viability. Similar results were obtained from the screening of *N*-(1′-ethyl-6-ferrocenyl-2-naphthoyl) amino acid and dipeptide esters **137**-**143**. The lowest growth inhibition was shown by compounds **137**, **138** and **143**, with cell viability values of 51 ± 1%, 56 ± 1% and 41 ± 3%, respectively. The rest of these compounds were found highly toxic to Chang cell line, with cell viability values below 15%. Once again, the four compounds with the γ-aminobutyric ester moiety were the least toxic from all the *N*-(1′-alkyl-6-ferrocenyl-2-naphthoyl) amino acid and dipeptide esters **130**-**143**.

Table 3.6. Cell viability percentage at 200 μM in Chang human liver cells for *N*-(1′-methyl-6-ferrocenyl-2-naphthoyl) amino acid and dipeptide esters **130**-**136**.

Alkyl	Linker	Peptide ester	No.	% cell viability
CH_3-	Naphthoyl	GABA-OMe	**130**	47 ± 1
		GABA-OEt	**131**	45 ± 2
		Gly-Gly-OMe	**132**	4 ± 2
		Gly-Gly-OEt	**133**	27 ± 3
		Gly-L-Ala-OEt	**134**	1 ± 1
		Gly-D-Ala-OMe	**135**	10 ± 3
		Gly-D-Ala-OEt	**136**	24 ± 1

Table 3.7. Cell viability percentage at 200 μM in Chang human liver cells for *N*-(1′-ethyl-6-ferrocenyl-2-naphthoyl) amino acid and dipeptide esters **137**-**143**.

Alkyl	Linker	Peptide ester	No.	% cell viability
CH_3-CH_2-	Naphthoyl	GABA-OMe	**137**	51 ± 1
		GABA-OEt	**138**	56 ± 1
		Gly-Gly-OMe	**139**	10 ± 1
		Gly-Gly-OEt	**140**	1 ± 1
		Gly-L-Ala-OEt	**141**	4 ± 2
		Gly-D-Ala-OMe	**142**	12 ± 2
		Gly-D-Ala-OEt	**143**	41 ± 3

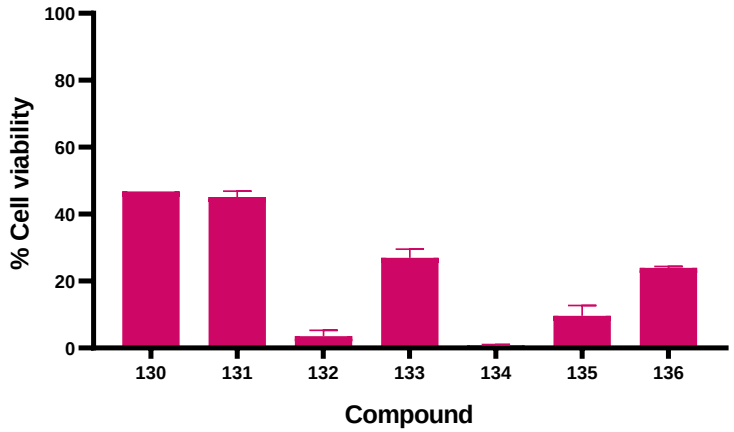

Figure 3.10. Cell viability percentage at 200 μM in Chang human liver cells for *N*-(1′-methyl-6-ferrocenyl-2-naphthoyl) amino acid and dipeptide esters **130**-**136**. Data presented as an average of triplicate measurements ± S.D.

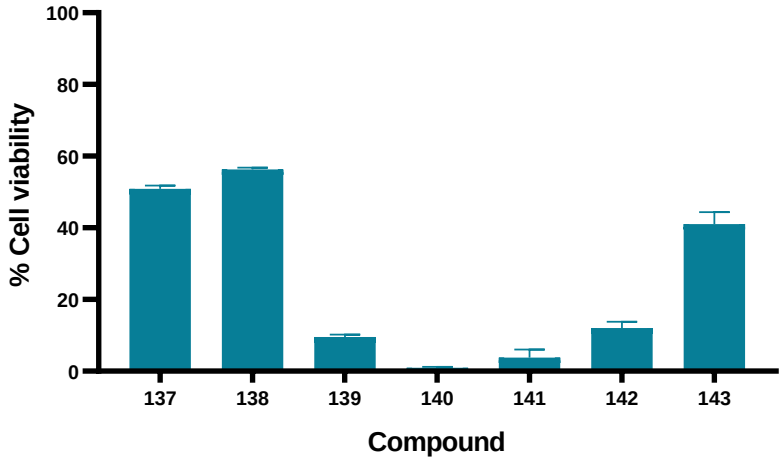

Figure 3.11. Cell viability percentage at 200 μM in Chang human liver cells for *N*-(1′-ethyl-6-ferrocenyl-2-naphthoyl) amino acid and dipeptide esters **137**-**143**. Data presented as an average of triplicate measurements ± S.D.

3.4.3 *In vitro* comparison study in both SiHa and Chang cell lines

A comparison of the percentages of viability in both SiHa human cervical carcinoma and Chang human liver cell lines after exposure to the *N*-(1′-alkyl-6-ferrocenyl-2-naphthoyl) amino acid and dipeptide esters **130**-**143** is shown in Table 3.8 and Figure 3.12.

Table 3.8. Comparison of cell viability percentage at 200 μM in SiHa and Chang cell lines for *N*-(1′-alkyl-6-ferrocenyl-2-naphthoyl) amino acid and dipeptide esters **130**-**143**.

Compound name	No.	% viability in SiHa	% viability in Chang
N-(1′-methyl-6-ferrocenyl-2-naphthoyl)-GABA-OMe	**130**	22 ± 2	47 ± 1
N-(1′-methyl-6-ferrocenyl-2-naphthoyl)-GABA-OEt	**131**	40 ± 1	45 ± 2
N-(1′-methyl-6-ferrocenyl-2-naphthoyl)-Gly-Gly-OMe	**132**	4 ± 1	4 ± 2
N-(1′-methyl-6-ferrocenyl-2-naphthoyl)-Gly-Gly-OEt	**133**	30 ± 2	27 ± 3
N-(1′-methyl-6-ferrocenyl-2-naphthoyl)-Gly-L-Ala-OEt	**134**	2 ± 1	1 ± 1
N-(1′-methyl-6-ferrocenyl-2-naphthoyl)-Gly-D-Ala-OMe	**135**	10 ± 4	10 ± 3
N-(1′-methyl-6-ferrocenyl-2-naphthoyl)-Gly-D-Ala-OEt	**136**	19 ± 2	24 ± 1
N-(1′-ethyl-6-ferrocenyl-2-naphthoyl)-GABA-OMe	**137**	21 ± 3	51 ± 1
N-(1′-ethyl-6-ferrocenyl-2-naphthoyl)-GABA-OEt	**138**	56 ± 1	56 ± 1
N-(1′-ethyl-6-ferrocenyl-2-naphthoyl)-Gly-Gly-OMe	**139**	12 ± 2	10 ± 1
N-(1′-ethyl-6-ferrocenyl-2-naphthoyl)-Gly-Gly-OEt	**140**	3 ± 1	1 ± 1
N-(1′-ethyl-6-ferrocenyl-2-naphthoyl)-Gly-L-Ala-OEt	**141**	21 ± 2	4 ± 2
N-(1′-ethyl-6-ferrocenyl-2-naphthoyl)-Gly-D-Ala-OMe	**142**	20 ± 1	12 ± 2
N-(1′-ethyl-6-ferrocenyl-2-naphthoyl)-Gly-D-Ala-OEt	**143**	5 ± 1	41 ± 3

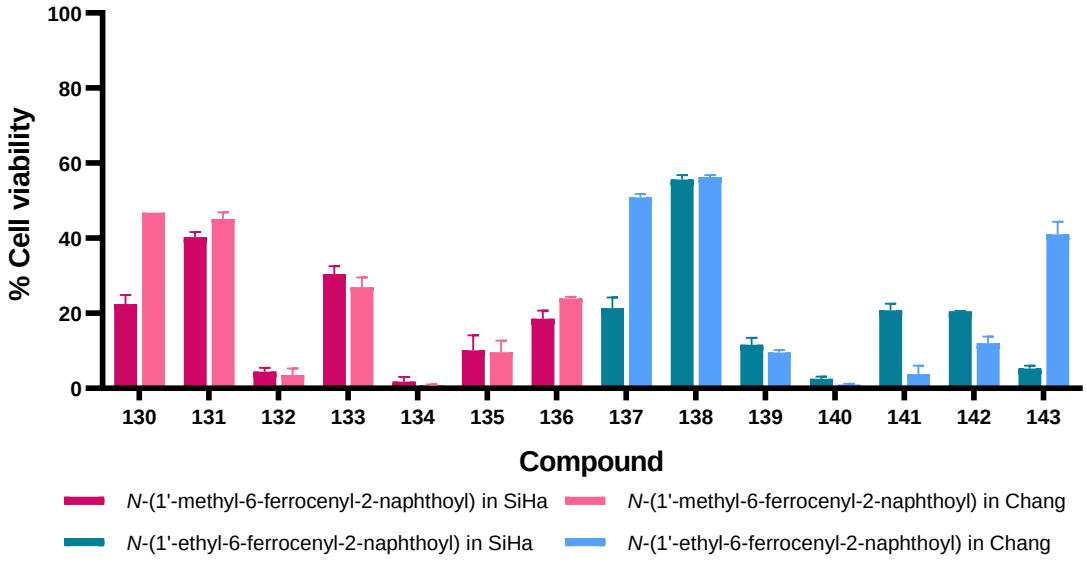

Figure 3.12. Comparison of cell viability percentage at 200 μM in SiHa and Chang cell lines for *N*-(1′-alkyl-6-ferrocenyl-2-naphthoyl) amino acid and dipeptide esters **130**-**143**. Data presented as an average of triplicate measurements ± S.D.

As observed for both alkyl series, compounds **130**, **131**, **137**, **138** and **143** showed the least toxicity against Chang human liver cell line, with cell viability values between 41-56%. From these derivatives, compound **138** did not seem to show a degree of selectivity between cancerous and non-cancerous cells, as its percentage of cell viability in SiHa human cervical carcinoma was roughly the same (56%). In the other hand, compounds **130**, **131**, **137** and 14**3** exhibited cell viability values between 5-40% against SiHa cell line, meaning that they inhibited more than 60% cell growth of cancer cells. Therefore, compounds **130**, **131**, **137** and **143** were selected for further analysis to determine their IC_{50} values.

3.4.4 IC_{50} determination

Further studies were conducted to determine the IC_{50} value of selected compounds **130**, **131**, **137** and **143** in SiHa human cervical carcinoma cell line, by screening of serial dilutions at concentrations ranging from 200 μM to 6.25 μM. The curves obtained are shown in Figure 3.13 (error bars from three independent experiments are too low to be shown). IC_{50} value of each compound were calculated and are enlisted in Table 3.9.

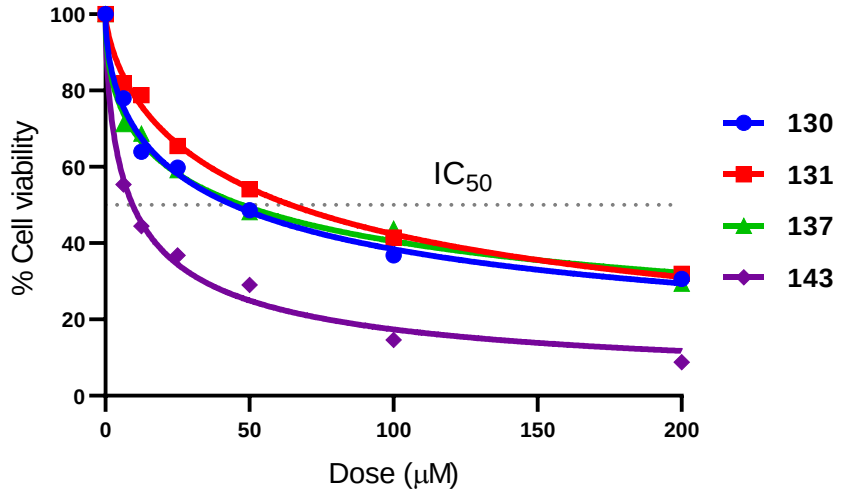

Figure 3.13. IC_{50} plot for selected compounds **130**, **131**, **137** and **143** in SiHa cell line.

Table 3.9. IC_{50} values for selected compounds **130**, **131**, **137** and **143** in SiHa cell line.

Compound name	No.	IC_{50} (μM)
N-(1′-methyl-6-ferrocenyl-2-naphthoyl)-GABA-OMe	**130**	50.83 ± 1.29
N-(1′-methyl-6-ferrocenyl-2-naphthoyl)-GABA-OEt	**131**	61.81 ± 2.52
N-(1′-ethyl-6-ferrocenyl-2-naphthoyl)-GABA-OMe	**137**	44.27 ± 2.89
N-(1′-ethyl-6-ferrocenyl-2-naphthoyl)-Gly-D-Ala-OEt	**143**	8.76 ± 0.98

As observed, all the selected *N*-(1′-alkyl-6-ferrocenyl-2-naphthoyl) amino acid and dipeptide derivatives inhibited the growth of SiHa human cervical carcinoma cells, and cytotoxicity is dependent on the concentration of the compounds tested. Compounds **130**, **131** and **137** display high IC_{50} values, between 44 and 62 μM. However, compound *N*-(1′-ethyl-6-ferrocenyl-2-naphthoyl)-glycine-D-alanine ethyl ester **143** was found to be the most active, with an IC_{50} value of 8.76 ± 0.98 μM; this result is better than the reported IC_{50} of cisplatin in the same cell line (19.5 ± 2.12 μM), which is a highly effective drug in treating cervical carcinoma.[274] These derivatives show strong inhibition in the growth of human cervical carcinoma cells (SiHa) whilst exhibiting less toxicity against human liver cells (Chang); these results suggest a degree of selectivity between cancerous and non-cancerous cells, hence these compounds are worthy to further analyze their application in cancer treatment.

3.5 *In vitro* study of *N*-(ferrocenylmethylamino acid)-fluorinated benzene carboxamides 144-154

The *in vitro* anticancer activity of a series of *N*-(ferrocenylmethylamino acid)-fluorinated benzene carboxamides **144**-**154** previously synthesized and characterized by Lu[195] was studied. These compounds follow the general structure of ferrocenyl carboxamides previously presented earlier, with variations in the amino acid or dipeptide chains as part of the SAR study of this type of derivatives (Figure 3.14).[195] The incorporation of fluorine atoms is a well-known strategy in drug-discovery research.[182] The structures of the *N*-(ferroceylmethylamino acid)-fluorinated benzene carboxamides **144**-**154** are presented in Figure 3.15. Screenings of each compound at a single dose of 10 μM in both SiHa human cervical carcinoma and Chang human liver cell lines were performed.

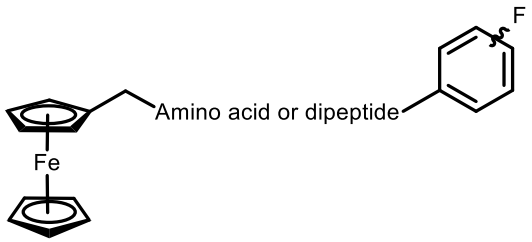

Figure 3.14. General structure of the *N*-(ferrocenylmethylamino acid)-fluorinated benzene carboxamides **144**-**154**.

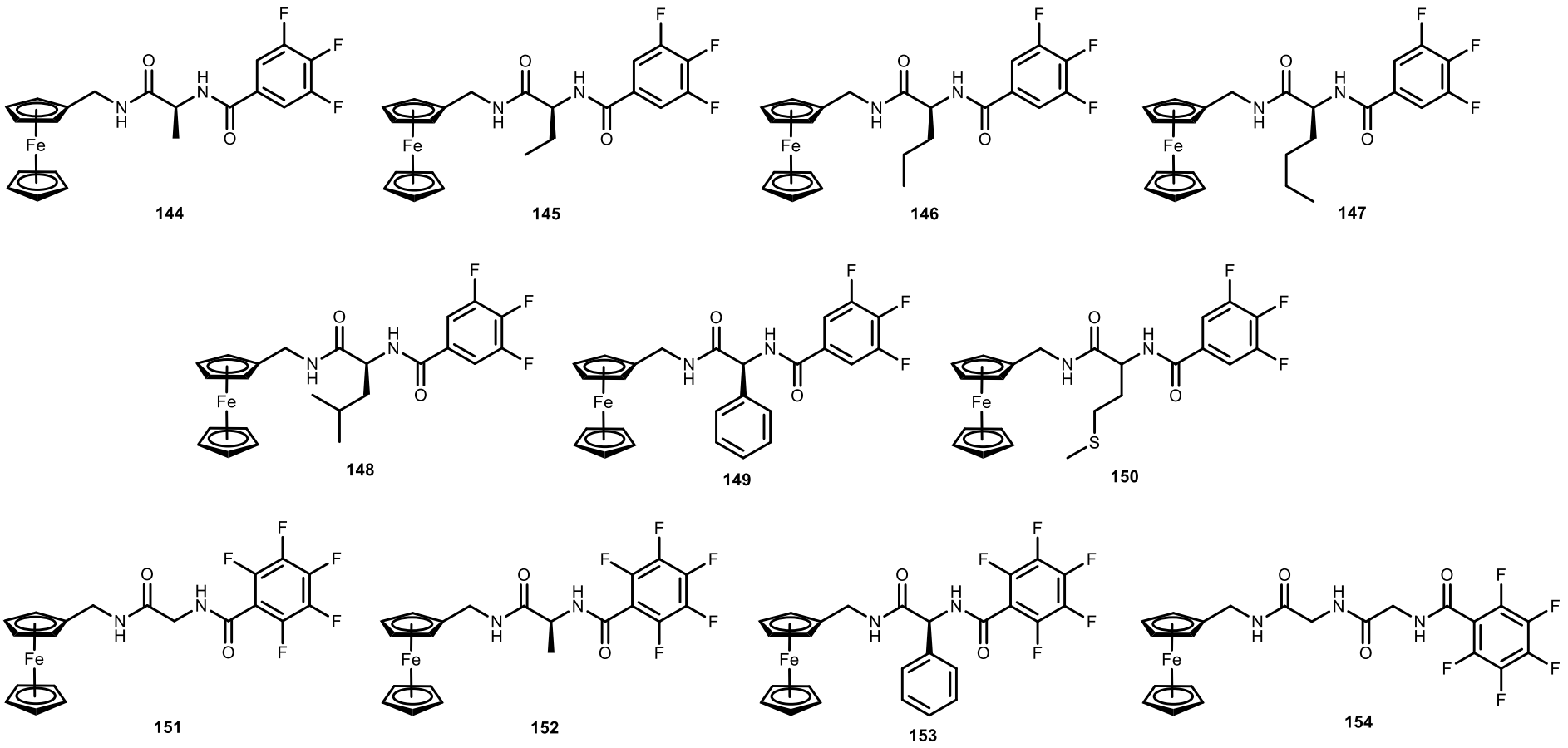

Figure 3.15. Structures of *N*-(ferrocenylmethylamino acid)-fluorinated benzene carboxamides **144**-**154**.

3.5.1 *In vitro* evaluation in SiHa cell line

The percentages of viability of SiHa human cervical carcinoma cell line after exposure to derivatives **144**-**154** and the reference compound vincristine **129** are shown in Table 3.10 and Figure 3.16. It can be observed that compounds **147**, **148** and **153** exhibited the strongest inhibition growth, with cell viability values of 56 ± 3%, 60 ± 1% and 40 ± 3%, respectively. However, they are not more active than reference compound vincristine **129** (33 ± 1%). The rest of the compounds did not show significant anti-proliferative effect, as they displayed cell viability values between 60-95%. For the tri-fluorinated compounds, the strongest inhibition in growth is observed with the amino acids having the longest alkyl chains (L-leucine and L-norleucine); whilst for the penta-fluorinated compounds, the aromatic amino acid L-(+)-α-phenylglycine appears as the most active.

Table 3.10. Cell viability percentage at 10 μM in SiHa human cervical carcinoma cells for *N*-(ferrocenylmethylamino acid)-fluorinated benzene carboxamides **144**-**154** and reference compound vincristine **129**.

Compound name	No.	% cell viability
N-(ferrocenylmethyl-L-alanine)-3,4,5-trifluorobenzene carboxamide	**144**	77 ± 1
N-(ferrocenylmethyl-L-2-aminobutyric acid)-3,4,5-trifluorobenzene carboxamide	**145**	66 ± 2
N-(ferrocenylmethyl-L-norvaline)-3,4,5-trifluorobenzene carboxamide	**146**	81 ± 2
N-(ferrocenylmethyl-L-norleucine)-3,4,5-trifluorobenzene carboxamide	**147**	56 ± 3
N-(ferrocenylmethyl-L-leucine)-3,4,5-trifluorobenzene carboxamide	**148**	60 ± 1
N-(ferrocenylmethyl-L-(+)-α-phenylglycine)-3,4,5-trifluorobenzene carboxamide	**149**	95 ± 2
N-(ferrocenylmethyl-L-methionine)-3,4,5-trifluorobenzene carboxamide	**150**	76 ± 2
N-(ferrocenylmethyl-glycine)-2,3,4,5,6-pentafluorobenzene carboxamide	**151**	67 ± 6
N-(ferrocenylmethyl-L-alanine)-2,3,4,5,6-pentafluorobenzene carboxamide	**152**	75 ± 4
N-(ferrocenylmethyl-L-(+)-α-phenylglycine)-2,3,4,5,6-pentafluorobenzene carboxamide	**153**	40 ± 3
N-(ferrocenylmethyl-glycine-glycine)–2,3,4,5,6-pentafluorobenzene carboxamide	**154**	71 ± 7
Vincristine	**129**	33 ± 1

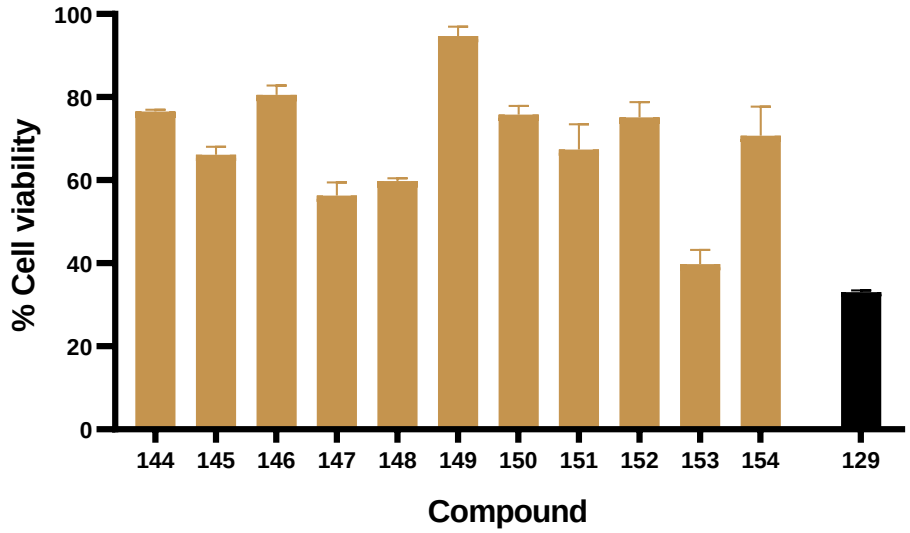

Figure 3.16. Cell viability percentage at 10 μM in SiHa human cervical carcinoma cells for *N*-(ferrocenylmethylamino acid)-fluorinated benzene carboxamides **144**-**154** and reference compound vincristine **129**. Data presented as an average of triplicate measurements ± S.D.

3.5.2 *In vitro* evaluation in Chang cell line

The percentages of viability of Chang human liver cell line after exposure to derivatives **144**-**154** are shown in Table 3.11 and Figure 3.17. As it can be seen, any compound showed a significant inhibition in the growth of Chang cells, as most derivatives tested showed cell viability values greater than 75%. These were excellent results as it means that the *N*-(ferrocenylmethylamino acid)-fluorinated benzene carboxamides **144**-**154** are only slightly cytotoxic to the non-cancerous cell line Chang. Compound **147** exhibited again the strongest anti-proliferative effect, with a cell viability value of 75%. Compounds **145** and **152** were found to be the least toxic, with 98% cell viability each. For the tri-fluorinated compounds, the strongest inhibition in growth is observed with the amino acid having the longest alkyl chain (L-norleucine); whilst for the penta-fluorinated compounds, the aromatic amino acid L-(+)-α-phenylglycine appears as the most active. This trend is the same as observed for SiHa cell line.

Table 3.11. Cell viability percentage at 10 μM in Chang human liver cells for *N*-(ferrocenylmethylamino acid)-fluorinated benzene carboxamides **144**-**154**.

Compound name	No.	% cell viability
N-(ferrocenylmethyl-L-alanine)-3,4,5-trifluorobenzene carboxamide	**144**	92 ± 7
N-(ferrocenylmethyl-L-2-aminobutyric acid)-3,4,5-trifluorobenzene carboxamide	**145**	98 ± 1
N-(ferrocenylmethyl-L-norvaline)-3,4,5-trifluorobenzene carboxamide	**146**	87 ± 3
N-(ferrocenylmethyl-L-norleucine)-3,4,5-trifluorobenzene carboxamide	**147**	75 ± 1
N-(ferrocenylmethyl-L-leucine)-3,4,5-trifluorobenzene carboxamide	**148**	96 ± 4
N-(ferrocenylmethyl-L-(+)-α-phenylglycine)-3,4,5-trifluorobenzene carboxamide	**149**	83 ± 1
N-(ferrocenylmethyl-L-methionine)-3,4,5-trifluorobenzene carboxamide	**150**	89 ± 4
N-(ferrocenylmethyl-glycine)-2,3,4,5,6-pentafluorobenzene carboxamide	**151**	93 ± 7
N-(ferrocenylmethyl-L-alanine)-2,3,4,5,6-pentafluorobenzene carboxamide	**152**	98 ± 1
N-(ferrocenylmethyl-L-(+)-α-phenylglycine)-2,3,4,5,6-pentafluorobenzene carboxamide	**153**	82 ± 1
N-(ferrocenylmethyl-glycine-glycine)–2,3,4,5,6-pentafluorobenzene carboxamide	**154**	94 ± 1

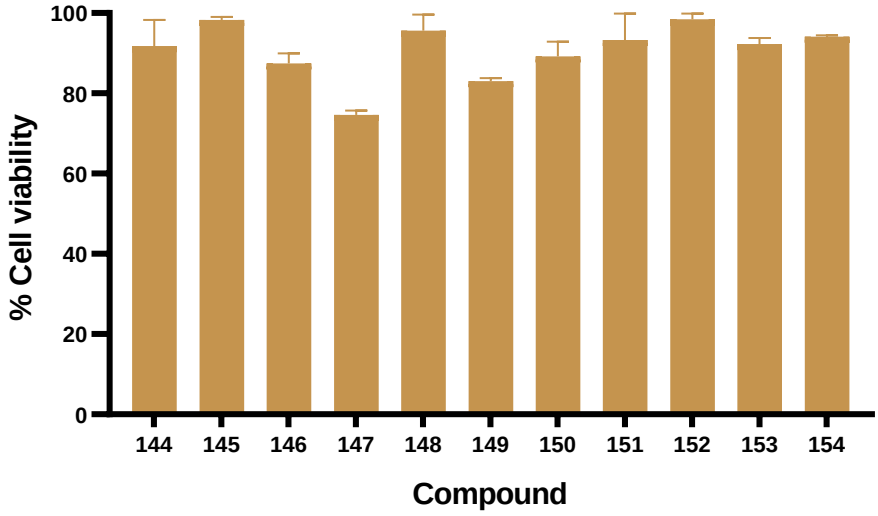

Figure 3.17. Cell viability percentage at 10 μM in Chang human liver cells for *N*-(ferrocenylmethylamino acid)-fluorinated benzene carboxamides **144**-**154**. Data presented as an average of triplicate measurements ± S.D.

3.5.3 *In vitro* comparison study in both SiHa and Chang cell lines

A comparison of the percentages of viability in both SiHa human cervical carcinoma and Chang human liver cell lines after exposure to the *N*-(ferrocenylmethylamino acid)-fluorinated benzene carboxamides **144**-**154** is shown in Table 3.12. As it can be observed, compounds **147**, **148** and **153** were the most active in SiHa cell line, inhibiting between 40-60% cell growth (56 ± 3%, 60 ± 1% and 40 ± 3%, respectively). In addition, these compounds showed limited toxicity towards Chang cell line, with only 5-25% cell inhibition (75 ± 1%, 96 ± 4% and 82 ± 1%, respectively). Therefore, compounds **147**, **148** and **153** were selected for further analysis to determine their IC_{50} values.

Table 3.12. Comparison of cell viability percentage at 10 μM in SiHa and Chang cell lines for *N*-(ferrocenylmethylamino acid)-fluorinated benzene carboxamides **144**-**154**.

Compound name	No.	% cell viability in SiHa	% cell viability in Chang
N-(ferrocenylmethyl-L-alanine)-3,4,5-trifluorobenzene carboxamide	**144**	77 ± 1	92 ± 7
N-(ferrocenylmethyl-L-2-aminobutyric acid)-3,4,5-trifluorobenzene carboxamide	**145**	66 ± 2	98 ± 1
N-(ferrocenylmethyl-L-norvaline)-3,4,5-trifluorobenzene carboxamide	**146**	81 ± 2	87 ± 3
N-(ferrocenylmethyl-L-norleucine)-3,4,5-trifluorobenzene carboxamide	**147**	56 ± 3	75 ± 1
N-(ferrocenylmethyl-L-leucine)-3,4,5-trifluorobenzene carboxamide	**148**	60 ± 1	96 ± 4
N-(ferrocenylmethyl-L-(+)-α-phenylglycine)-3,4,5-trifluorobenzene carboxamide	**149**	95 ± 2	83 ± 1
N-(ferrocenylmethyl-L-methionine)-3,4,5-trifluorobenzene carboxamide	**150**	76 ± 2	89 ± 4
N-(ferrocenylmethyl-glycine)-2,3,4,5,6-pentafluorobenzene carboxamide	**151**	67 ± 6	93 ± 7
N-(ferrocenylmethyl-L-alanine)-2,3,4,5,6-pentafluorobenzene carboxamide	**152**	75 ± 4	98 ± 1
N-(ferrocenylmethyl-L-(+)-α-phenylglycine)-2,3,4,5,6-pentafluorobenzene carboxamide	**153**	40 ± 3	82 ± 1
N-(ferrocenylmethyl-glycine-glycine)–2,3,4,5,6-pentafluorobenzene carboxamide	**154**	71 ± 7	94 ± 1

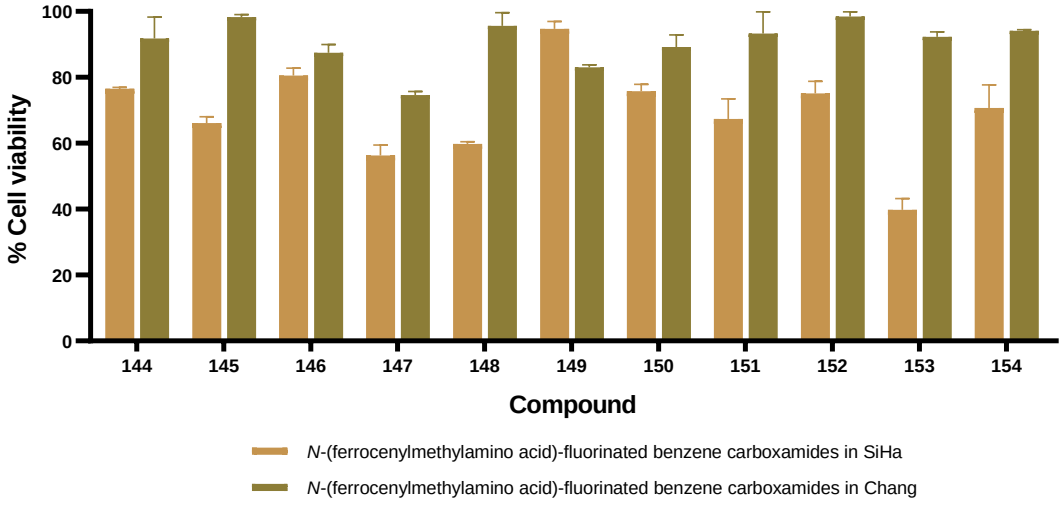

Figure 3.18. Comparison of cell viability percentage at 10 μM in SiHa and Chang cell lines for *N*-(ferrocenylmethylamino acid)-fluorinated benzene carboxamides **144**-**154**. Data presented as an average of triplicate measurements ± S.D.

3.5.4 IC_{50} determination

Further studies were conducted to determine the IC_{50} value of selected compounds **147**, **148** and **153** in both SiHa human cervical carcinoma and Chang human liver cell lines, by screening of serial dilutions at concentrations ranging from 40 μM to 1.25 μM. The curves obtained are shown in Figure 3.19A for SiHa cell line, and in Figure 3.19B for Chang cell line. Error bars represent the standard deviation from three independent experiments. From these plots, IC_{50} value of each compound was calculated and are enlisted in Table 3.13.

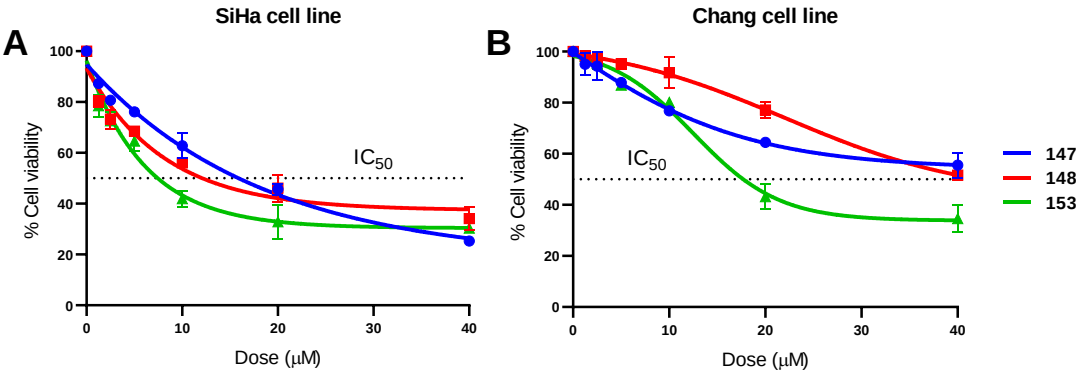

Figure 3.19. IC_{50} plot for selected compounds **147**, **148** and **153**. **A.** SiHa cell line. **B.** Chang cell line.

Table 3.13. IC_{50} values for selected compounds **147**, **148** and **153** in SiHa and Chang cell lines.

Compound name	No.	IC_{50} (μM) in SiHa cell line	IC_{50} (μM) in Chang cell line
N-(ferrocenylmethyl-L-norleucine)-3,4,5-trifluorobenzene carboxamide	**147**	17.47 ± 2.84	47.15 ± 3.53
N-(ferrocenylmethyl-L-leucine)-3,4,5-trifluorobenzene carboxamide	**148**	24.06 ± 5.15	42.17 ± 9.08
N-(ferrocenylmethyl-L-(+)-α-phenylglycine)-2,3,4,5,6-pentafluorobenzene carboxamide	**153**	8.18 ± 2.28	18.19 ± 3.02

The three selected *N*-(ferrocenylmethylamino acid)-fluorinated benzene carboxamides inhibited the growth of SiHa human cervical carcinoma cells, and cytotoxicity is dependent on the concentration of the compounds tested. At the same time, they show limited toxicity towards Chang human liver cells. Compounds **147** and **148** display IC_{50} values between 17-24 μM in SiHa cell line. Compound **153** was found to be the most active, with an IC_{50} value below 10 μM; this result is better than the reported IC_{50} of cisplatin in the same cell line (19.5 ± 2.12 μM), which is a highly effective drug in treating cervical carcinoma.[274] In addition, all three compounds exhibited a 2-fold increase in their IC_{50} for Chang cell line, with values between 18-47 μM. These results suggest that the *N*-(ferrocenylmethylamino acid)-fluorinated benzene carboxamides tested display a degree of selectivity between cancerous and non-cancerous cells, hence these compounds are worthy to further analyze their application in cancer treatment.

3.6 Structure-activity relationship of novel ferrocenyl derivatives

The *in vitro* anti-proliferative studies performed on the heterocyclic functionalised ferrocenyl derivatives **99**-**120**, *N*-(1′-alkyl-6-ferrocenyl-2-naphthoyl) amino acid and dipeptide esters **130**-**143** and *N*-(ferrocenylmethylamino acid)-fluorinated benzene carboxamides **144**-**154** can lead to the establishment of a SAR of these ferrocenyl compounds. The results obtained have shown a wide variety of activity in the SiHa human cervical carcinoma and Chang human liver cell lines.

The series of compounds tested consisted in two different ferrocenyl moieties: alkylated (methyl- and ethyl-) and non-alkylated ferrocene. In general, better activity was observed when the ferrocene unit was alkylated, with an average of 18% cell viability in SiHa cell line. Therefore, the alkyl group attached to the ferrocene core is playing an important role for a superior anti-proliferative effect, probably by decreasing the redox potential of this type of compounds and thereby making them easier to oxidise.[152]

Different conjugated linkers were used in the synthesis of the heterocyclic functionalised ferrocenyl derivatives **99**-**120**, such as naphthoyl, benzoyl and cinnamoyl. From these series, compounds with naphthalene spacer group are in general more effective at inhibiting cell proliferation than the corresponding benzoyl or cinnamoyl analogues. This observation is also confirmed with the *N*-(1′-alkyl-6-ferrocenyl-2-naphthoyl) amino acid and dipeptide esters **130**-**143**, as all these compounds contain a naphthalene ring as conjugated linker and they display strong anti-proliferative effect in the SiHa cell line compared with the rest of the compounds tested. Therefore, using a naphthoyl moiety as the spacer group generally improves the biological activity of the ferrocenyl derivatives. This enhancement may be due a better conjugation with the redox active ferrocene moiety, which would cause extended conjugation to the π-electrons of the Cp rings making initial oxidation of the iron centre easier.

In terms of orientation, the 6,2- and 3,2- positions were explored for naphthoyl derivatives, and *ortho*-, *meta*- and *para*- for benzoyl derivatives in the heterocyclic functionalised ferrocenyl derivatives **99**-**120**. With an average of 86% cell viability, the 6,2- series were the most active compounds compared with their analogues in other positions. In the other hand, *ortho*- derivatives displayed the weakest cell inhibition, with an average of 90% cell viability. It is probable that the steric hindrance present in the *ortho*- series compared with their analogues is affecting the biological activity for these derivatives.

The last approaches studied were: the innovative use of heterocycles (*N*-hydroxysuccinimide, benzylamine and cyclohexylamine), the classical amino acid and dipeptide esters, and fluorinated benzene carboxamides. In general, the *N*-(1′-alkyl-6-ferrocenyl-2-naphthoyl) amino acid and dipeptide esters displayed the highest anti-proliferative activity in SiHa cells; nevertheless, this effect was also observed against Chang cells. For example, compounds *N*-(1′-methyl-6-ferrocenyl-2-naphthoyl)-glycine-L-alanine ethyl ester **134** and *N*-(1′-ethyl-6-ferrocenyl-2-naphthoyl)-glycine-glycine ethyl ester **140** have been identified as the most potent derivatives in SiHa cell line, with growth inhibition percentages of 98% and 97%, respectively; unfortunately, this anti-proliferative effect was also observed in the Chang cell line, as these compounds inhibited 99% cell growth. For this reason, derivatives **134** and **140** cannot be considered for cancer treatment due to their high toxicity to human liver cells. From these series, compound **143** was found to be the most active, with an IC_{50} value of 8.76 ± 0.98 μM in SiHa cell line; this result is better than the reported IC_{50} of cisplatin in the same cell line (19.5 ± 2.12 μM), which is a highly effective drug in treating cervical carcinoma.[274]

Considering the activity in both cell lines, the replacement of the typical amino acid and dipeptide ester moieties by a heterocycle unit, like initially proposed as the main aim in this research project, was a positive approach in leading to a lower toxicity side effect to non-cancerous cells, although it also diminished the antineoplastic activity from strong to moderate. The most active novel heterocyclic functionalised ferrocenyl derivatives exhibited an average of 37% growth inhibition of SiHa cells, whilst only inhibiting an average of 20% cell growth in Chang cells. These percentages suggest an equivalent degree of selectivity compared to the least toxic *N*-(1′-alkyl-6-ferrocenyl-2-naphthoyl) amino acid and dipeptide esters, which display average growth inhibition percentages of 76% in SiHa and 68% in Chang. In general, the best activity was found when the heterocycle belongs to the NHS derivatives.

In summary, a moderate to high anti-proliferative effect against SiHa human cervical carcinoma cells and with low to moderate toxicity towards Chang human liver cells is achieved when (Figure 3.20):

(i) The ferrocene unit is alkylated.

(ii) A naphthalene ring is used as the spacer group.

(iii) The naphthalene linker is substituted in the 6,2- positions.

(iv) The final moiety is NHS-ester (moderate to SiHa, low to Chang) or Gly-D-Ala-OEt (high to SiHa, moderate to Chang).

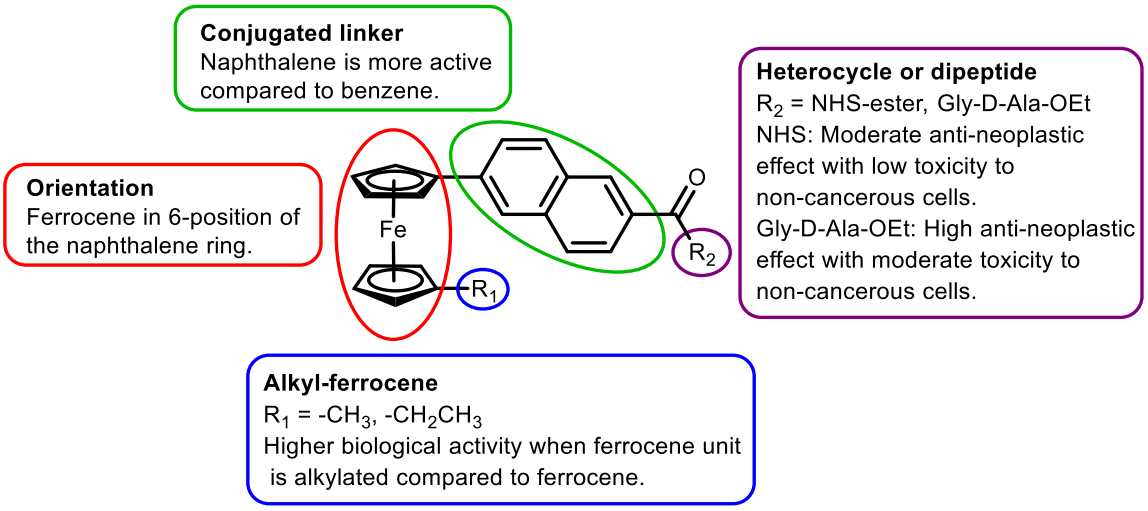

Figure 3.20. Structure-activity relationship for the ferrocenyl bioconjugates studied.

In relation to the *N*-(ferrocenylmethylamino acid)-fluorinated benzene carboxamides **144**-**154**, the incorporation of the fluorine moieties did not seem to be detrimental to the anti-proliferative effect. Despite compound **153**, all the rest of these fluorinated carboxamides do not inhibit more than 30% of SiHa cells. However, for the most active compounds, the following general trends were observed (Figure 3.21):

(i) Single amino acid chains were more active than the dipeptide chain.

(ii) Pentafluorinated derivatives were generally more active than trifluorinated compounds.

(iii) The highest inhibition in SiHa cell line was observed with the higher number of carbons in the chain attached to the carbon in the α position to the carbonyl of the amide group.

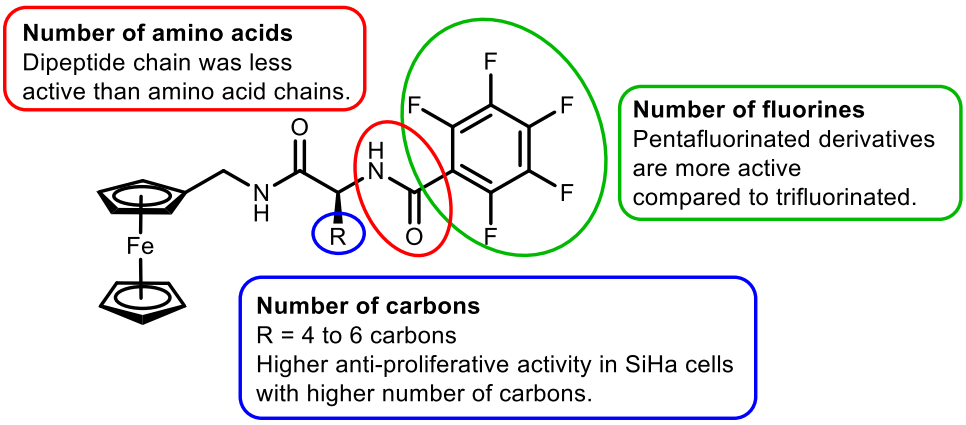

Figure 3.21. Structure-activity relationship for the ferrocenyl carboxamides studied.

3.7 Conclusions

As part of a further SAR study of ferrocenyl compounds, a series of novel heterocyclic functionalised ferrocenyl derivatives **99**-**120**, *N*-(1′-alkyl-6-ferrocenyl-2-naphthoyl) amino acid and dipeptide esters **130**-**143** and *N*-(ferrocenylmethylamino acid)-fluorinated benzene carboxamides **144**-**154** were evaluated for *in vitro* anti-proliferative effect in human cervical carcinoma (SiHa) and human liver (Chang) cell lines. Some of these ferrocenyl derivatives showed equivalent or better activity than the reference chemotherapeutic compound vincristine **129**. Compounds *N*-(1′-ethyl-6-ferrocenyl-2-naphthoyl)-glycine-D-Alanine ethyl ester **143** (IC_{50} = 8.76 ± 0.98 μM), *N*-(ferrocenylmethyl-L-norleucine)-3,4,5-trifluorobenzene carboxamide **147** (IC_{50} = 17.47 ± 2.84 μM) and *N*-(ferrocenylmethyl-L-(+)-α-phenylglycine)-2,3,4,5,6-pentafluorobenzene carboxamide **153** (IC_{50} = 8.18 ± 2.28 μM) have been identified as the most potent ferrocenyl derivatives in SiHa cell line, with moderate toxicity towards Chang cell line. These compounds display a better anticancer activity in SiHa cell line than cisplatin (IC_{50} = 19.5 ± 2.12 μM), which is a highly effective drug in treating cervical carcinoma.[274] For the ferrocenyl bioconjugates, it has been observed in this SAR study that a superior activity is observed when the ferrocene unit has been alkylated (-CH_3 or -CH_2CH_3). In addition, the use of a naphthalene ring substituted in the 6,2-positions enhances the anti-proliferative effect of the heterocyclic functionalized ferrocenyl derivatives relative to the 3,2-position or the benzoyl conjugated linker. Moreover, employing NHS-ester as the heterocycle has shown to be beneficial to the *in vitro* biological activity in SiHa cells with low toxicity to Chang cells, whilst the use of or Gly-D-Ala-OEt as the dipeptide moiety exhibits a high cell growth inhibition in SiHa cells with moderate toxicity to Chang cells. In relation to the ferrocenyl carboxamides, this SAR study showed that single amino acid chains were more active than the dipeptide chain tested. In addition, pentafluorinated derivatives were generally more active than trifluorinated compounds. In addition, the highest inhibition in SiHa cell line was observed with the higher number of carbons in the chain attached to the carbon in the α position to the carbonyl of the amide group, as L-(+)-α-phenylglycine, L-norleucine and L-leucine were more active than shorter amino acids such as L-alanine, L-2-aminobutyric acid or glycine.

3.8 Materials and methods

3.8.1 General information

Cell culture media, supplements, material, reactants and equipment used for all *in vitro* anti-proliferative analysis were kindly provided by Ingeniería Genética y Genómica laboratory from the School of Chemical Sciences at Universidad Autónoma de Nuevo León (Mexico), under the supervision of Dr. Mónica A. Ramírez-Cabrera and Dr. Eder Arredondo-Espinoza. The SiHa ATCC HTB-35 (human cervical carcinoma) and the Chang ATCC CCL-13 (normal human liver) cell lines were obtained from the American Type Culture Collection (ATCC). The WST-1 kit used to determine cell viability was obtained from Roche. Tips for automatic pipettors were obtained from Brand, and disposed after the first use. Filtration membranes of 0.22 μm were used and obtained from Millipore.

All cell culture work was carried out in a Thermo Fischer Scientific laminar flow hood. Before and after use, the laminar flow hood was cleaned with industrial disinfectants and 70% EtOH solution. Any items brought into the cabinet were also swabbed with 70% EtOH solution. Only one cell line was used in the laminar flow hood at a time; upon completion of work with any given cell line, the laminar flow hood was allowed to clear for 10 minutes before use in order to eliminate any possibility of cross-contamination between cell lines. Absorbance was read with a Biotek absorbance microplate reader model ELx800. All the *in vitro* evaluations were performed three times with three replicates of each. Results of the screenings are expressed as the percentage of cell viability ± standard deviation (relative to the negative controls). Standard deviations were calculated using data obtained from the three independent experiments.

3.8.2 Cell line culture and optical density determination

Cell lines SiHa (human cervical carcinoma) and Chang (normal human liver) were used for the evaluation of anti-proliferative activity *in vitro*. Cells were thawed and placed in culture flasks, adding 4 mL of EMEM with a supplement of 10% FBS and 1% Pen-Strep antibiotic. Flasks were incubated at 37 °C under a humified atmosphere of 95% O_2 and 5% CO_2 until grown as a monolayer culture; EMEM was changed every 3 days. Culture medium was discarded when 80% confluency was reached in all the surface. Cells were washed twice with 4 mL PBS solution; dead cells are deleted with other residues. Subsequently, 1 mL 0.25% trypsin-EDTA was added; cells were incubated at 37 °C for

less than 3 minutes; then trypsin was neutralised with 2 mL EMEM. Cells were centrifuged to remove medium with trypsin; after that, 3 mL EMEM were added. Cell pellet formed was re-suspended, and 20 μL suspension were taken to determine the cell concentration by counting cells using a Neubauer chamber with an inverted microscope. Once the cell concentration is obtained, a dilution from the suspension is made to obtain a 10 000 cells/100 μL cell concentration, which were placed in a 96-well plate. Plate is incubated at 37 °C under a humified atmosphere of 95% O_2 and 5% CO_2 for 24 h, until grown as a monolayer culture.[275]

3.8.3 Screening conditions

Preliminary screenings were performed due to the large volume of compounds to be evaluated. The number of compounds were reduced by exposing the cells with 10 μM of heterocyclic functionalised ferrocenyl derivatives **99**-**120** and *N*-(ferrocenylmethylamino acid)-fluorinated benzene carboxamides **144**-**154**, and 200 μM of *N*-(1′-alkyl-6-ferrocenyl-2-naphthoyl) amino acid and dipeptide esters **130**-**143**. All screenings were done in triplicate. Selected compounds were chosen for IC_{50} analysis depending on the percentage of cell viability exhibited in both cell lines. They were further screened with serial dilutions in different ranges of concentrations: from 200 μM to 6.25 μM for compounds **130**, **131**, **137** and **143**; and from 40 μM to 1.25 μM for compounds **147**, **148** and **153**.

3.8.4 Preparation of the compounds to be evaluated (dilutions)

Organometallic complexes are not normally soluble in water; still, *in vitro* experiments can be carried out with a percentage of alcohol and/or DMSO. A stock solution of each sample was prepared in a suitable solvent (DMSO, H_2O or EtOH). Diluted solutions of the test samples were prepared at a 2x final concentration by adding the cell culture medium with a calculated amount of the stock solution.

3.8.5 Cell exposure to compounds

10 000 cells/well were seeded in 96-well plates, and incubated at 37 °C under a humified atmosphere of 95% O_2 and 5% CO_2 for 24 h until grown as a monolayer culture. 100 μL aliquot of each diluted solution was added to each well of the plate. A positive (vincristine

129 for SiHa cell line or Triton X-100 for Chang cell line), negative (cell with medium) and blank (empty wells) controls were included. The plate was gently agitated and then incubated at 37 °C under a humified atmosphere of 95% O_2 and 5% CO_2 for 24 h. Assessment of cell survival in the presence of the test sample was then determined by the WST-1 assay.[275,276] To determine the IC_{50} values, same procedure as before was followed but employing serial dilutions in different ranges of concentrations: from 200 μM to 6.25 μM for compounds **130**, **131**, **137** and **143**; and from 40 μM to 1.25 μM for compounds **147**, **148** and **153**.

3.8.6 Proliferation evaluation via WST-1 assay

Proliferation percentage was measured using a WST-1 assay. After incubation time, medium was removed, and wells are washed twice with 100 μL PBS. Then 100 μL EMEM with 5% WST-1 were added, and a first reading of optical density at 450 nm was performed immediately in the Absorbance Microplate Reader; this result is recorded as *t* = 0. Plate was incubated again under the conditions already mentioned, and optical density was read again at one and two hours after (*t* = 1 and *t* = 2).[267,275,276]

3.8.7 Percentage of cell viability calculation

The percentage of cell viability can be determined using the absorbances obtained, where the absorbance of the negative control is considered a 100% of viability and 0% cytotoxicity. The average absorbance of the blank control is subtracted from the average absorbances of all the readings; this is to minimise any possible optical deviation due to the plate itself. Then, the average absorbance of the desired compounds is multiplied times 100 and divided by the average absorbance of the negative control; thus, the cell viability percentage can be obtained according to the concentration of the compounds. Standard deviations were calculated using data obtained from three independent experiments.

CHAPTER 4

4 DNA studies of novel heterocyclic functionalised ferrocenyl derivatives

My contribution to Chapter 4 was the investigation of the binding affinity of the novel heterocyclic functionalised ferrocenyl derivatives **99**-**120** to DNA, following a number of high throughput assays already established within Dr. Andrew Kellett's group under the supervision of Nicolò Fantoni. Suitable candidates from this study were selected, and I studied their capability to induce oxidative DNA damage in the presence of added oxidant and reductant; their starting materials were also analysed for comparison. These experiments were carried out at Nano Research Facilities and National Institute for Cellular Biotechnology – Dublin City University (Dublin, Ireland), under the supervision of Dr. Andrew Kellett.

4.1 Introduction

The determination of the drug-DNA interaction is an important part in the rational design of promising metallodrug candidates. DNA is generally accepted as the ultimate target of anti-cancer metallodrugs, which induce blocking of replication, transcription and, ultimately, cell division.[277,278] Understanding the interaction of small molecules with DNA (where and how the molecule binds to DNA) is vital because this process frequently includes conformational changes to the DNA structure. There are two modes of small molecules binding to DNA, which can be also present as a combination:[279,280]

(i) covalent binding, which yields permanent changes to DNA through formation of adducts (for example, cisplatin **15**); it tends to occur at preferred sites following an initial non-specific binding event; and

(ii) non-covalent binding, where the interaction drug-DNA is reversible but result in cytotoxic effects by temporarily altering DNA structure and therefore DNA function; it is dependent on the equilibrium constant of the drug-DNA site association.

A considerable number of assays have been developed to explore the metallodrug-DNA interactions. A range of molecular methods currently employed by the Kellett group[281] include:

(i) direct methods, such as X-ray crystallography, NMR spectroscopy, mass spectrometry and viscosity; or

(ii) indirect methods, like competitive inhibition experiments, fluorescence and absorbance spectroscopy, circular dichroism and electrophoresis-based techniques.

For this research work, an indirect fluorometric assay and electrophoretic-based techniques were chosen for studying the interaction of the novel heterocyclic functionalised ferrocenyl derivatives **99**-**120** with DNA. Competitive fluorescent displacement was used as the indirect fluorometric assay. The DNA oxidative damage was evaluated with an electrophoretic-based method, followed by the study of the ROS responsible for such damage using the same technique.

4.1.1 Indirect fluorometric assay

Different fluorogenic organic molecules with high affinity and binding selectivity to nucleic acids have been used to investigate the indirect DNA binding affinity of metallodrugs. One of the most common fluorophores used for this purpose is the red fluorescent 3,8-diamino-5-ethyl-6-phenylphenanthridinium bromide **155**, also known as ethidium bromide (EtBr, Figure 4.1).[281]

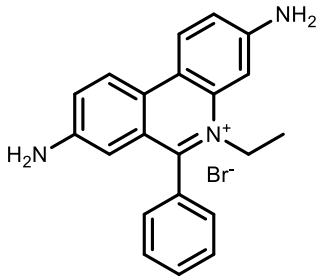

Ethidium bromide
155

Figure 4.1. Structure of ethidium bromide, EtBr **155**.

As with most DNA intercalators, it is a planar heteroaromatic compound with extended π-backbones, which allows easy infiltration into the DNA backbone followed by van der Waals interactions between base pairs.[282] EtBr **155** has low fluorescence in solution but become highly fluorescent once bound to DNA; therefore, this photophysical property can be used to indirectly determine the ability of metallodrugs to bind DNA over diminution of fluorescence intensity.[281]

4.1.2 Electrophoretic-based technique

Gel electrophoresis is a common analytical method to analyse, separate and purify nucleic acid samples. This technique takes advantage of the innate negative charge of DNA, as it consists in the movement of DNA through a solid-phase sieve-like medium (such as agarose or polyacrylamide) under the influence of an electric potential difference; DNA then moves in this electric field from the cathode to the anode, as an anion. The rate of DNA migration through the medium depends on different factors, including the length of the DNA sequence and its conformation. Therefore, long DNA fragments move slower than shorter fragments as they undergo greater resistance when moving through the gel.[278,281]

This assay is particularly useful to study plasmid DNA vectors isolated from bacteria, which are generally found in a supercoiled (SC) state. The treatment of SC plasmid DNA by damaging agents, such as metallodrugs, generates open-circular (OC) and linear (L) isoforms. SC DNA moves easily through the gel due to its compacted form and small mass-to-charge ratio. These supercoils are released when plasmid becomes nicked on a single strand, leading to the subsequent formation of OC DNA which suffers more resistance in the medium because of its larger size. Finally, L DNA is formed as a result of double strand breaks; this form undergoes less resistance than OC DNA through the gel (Figure 4.2). Therefore, plasmid DNA can be used to identify DNA damage induced by the metallodrug, and the rate of interconversion between DNA isoforms assessed by band densitometry.[281]

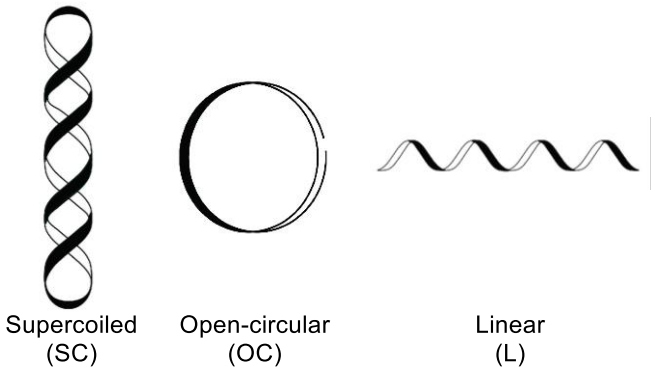

Figure 4.2. Representation of supercoiled (SC), open-circular (OC) and linear (L) DNA isoforms.

4.2 DNA binding studies

The competitive EtBr displacement assay is an indirect titration technique used to determine the apparent binding constants (K_{app}) of non-fluorescent DNA-binding ligands and complexes.[281] The pioneers with the introduction of a fluorescence assay based on the binding of EtBr to nucleic acids were Le Pecq and Paoletti in 1967. When EtBr binds in the intercalated state there is a ~25 fold fluorescence enhancement as a result of the hydrophobic environment surrounding the EtBr molecule.[283]

However, the first report on the use of EtBr as an intercalator to determine drug-DNA binding constants was proposed by Morgan *et al.* in 1979, with an assay performed in rectangular quartz cuvettes.[284] In recent years, Kellett *et al.* have modified this experiment to now be performed in 96-well plates, allowing a highly efficient drug-DNA

binding analysis.[285] This new procedure includes treating DNA (10 mM) with an excess of the intercalating EtBr (12.6 mM) in order to saturate all available binding sites, and therefore exhibiting strong fluorescence. If the drug can displace the EtBr from the DNA, then a reduction in the fluorescence is observed (Figure 4.3).

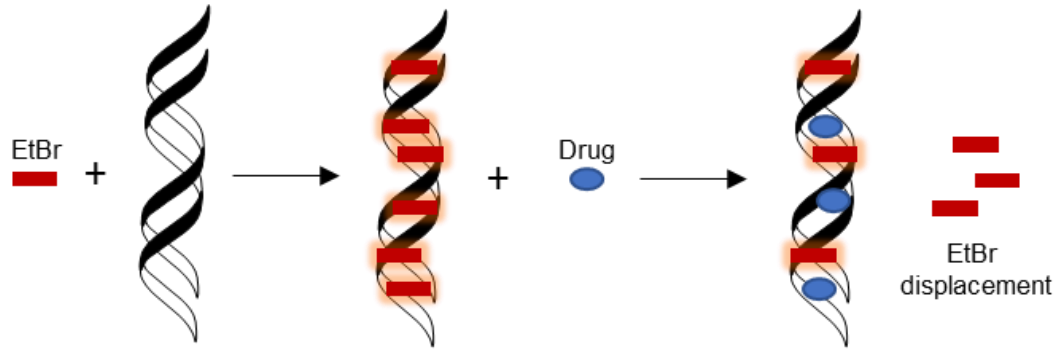

Figure 4.3. Representation of the EtBr competitive displacement assay.

This quantitative titration assay is then used to determine the C_{50} value, which corresponds to the amount of test drug required to induce a 50% decrease in the fluorescence of the EtBr. Drug concentrations are measured in triplicate, and the apparent binding constants are calculated using the formula:

$$K_{\text{app}} = \frac{K_{\text{e}} \times 12.6}{\text{C}_{50}}$$

where K_e = 8.8 × 10^6 M·bp^{-1} (apparent binding constant on ctDNA).

This is a reproducible method which can be applied to series of structurally related compounds, as in the case of the novel heterocyclic functionalised ferrocenyl derivatives **99**-**120**, in order to rank the binding affinity of these compounds over a defined concentration range.[285,286]

4.2.1 Fluorescence of compounds 99-120

An important limitation of the competitive fluorescent displacement method is the dependence of a fluorogenic reporter. Therefore, the quenching of the reporter by the metallodrug must be examined prior to analysis.[281] For this reason, stock solutions of the novel heterocyclic functionalised ferrocenyl derivatives **99**-**120** in CH_3CN were first analysed for fluorescence. Fortunately, none of the compounds evaluated showed significant fluorescence that could interfere with the EtBr displacement analysis.

4.2.2 Buffer selection

The feature of solubility in aqueous media is a much desired, if not crucial, attribute to any drug system requiring administration by intravenous or intraperitoneal techniques, such as anticancer drugs. The lack of water-solubility of these drugs often prove dose-limiting in chemotherapy, and many promising anticancer agents may never reach the clinical testing phase unless suitable ways can be found to make them water-soluble.[287–289] The EtBr displacement assay was initially performed according to the protocol outlined by Kellett *et al*., which involves the use of aqueous HEPES (pH = 7.0) as the buffer for the preparation of the samples to be tested.[281,285,286] However, it was observed that some stock solutions of the novel heterocyclic functionalised ferrocenyl derivatives **99**-**120** in CH_3CN crashed out when HEPES buffer was added. The poor solubility in aqueous media is a known drawback of ferrocenyl derivatives.[288–290] To overcome this limitation, buffers at different pH were tried as enlisted in Table 4.1. As expected, the best choice was found to be acetate buffer at pH = 5; this may be due to the fact that amines become protonated in low pH and hence solubility improves.

Table 4.1. Buffers tried for solubilisation of compounds **99**-**120**.

Trial	Buffer	pH
1	HEPES	7.0
2	PBS	6.0
3	Acetate	6.0
4	Phosphate	6.0
5	Acetate	5.0

4.2.3 Preliminary screening for 3 h

A preliminary EtBr displacement assay of all novel heterocyclic functionalised ferrocenyl derivatives **99**-**120** with ctDNA was performed in a range of concentrations between 1-700 μM in acetate buffer (pH=5), where fluorescence was recorded at 1, 2 and 3 h incubation times. The aim of this analysis was to identify the compounds that can reach the C_{50}, which is the concentration required to reduce 50 % fluorescence of EtBr on ctDNA. From this screening, it was observed that some derivatives did not quench 50% fluorescence of EtBr on ctDNA during the 3 h of incubation even at the highest concentration tested, as shown in Figure 4.4A for compound **106**; these derivatives were disregarded. Only compounds **104**, **110**-**112**, **114** and **120** were observed to quench ~50% or higher fluorescence of EtBr on ctDNA, as shown in Figure 4.4B for compound **111**; and thus only these compounds were selected for further analysis.

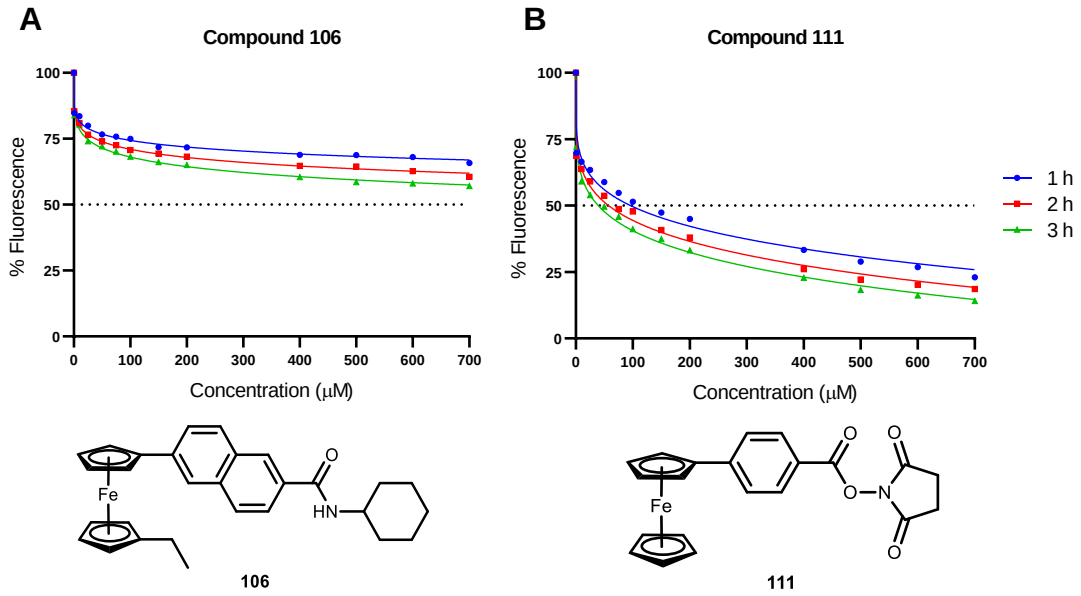

Figure 4.4. Comparison of fluorescence analysis after EtBr displacement assay. Data presented as an average of triplicate measurements. **A.** Compound **106**; **B.** Compound **111**.

4.2.4 EtBr displacement assay for 12 h

To further characterise the binding kinetics, EtBr displacement assays of selected compounds **104**, **110**-**112**, **114** and **120** with ctDNA were performed in triplicate, with a range of concentrations between 1-750 μM. Fluorescence was read every hour during 12 h incubation. The C_{50} of compounds reducing 50% fluorescence of EtBr on ctDNA was calculated using a sigmoidal model in GraphPad Prism 8. The C_{50} value was then used to calculate the apparent binding constant (K_{app}) every hour using the formula presented earlier. From the selected derivatives, only the K_{app} values of compounds **104**, **110** and **111** were calculated at different incubation times, as they were the only derivatives that reached C_{50}. As it can be observed in Figure 4.5, compound **111** was the only one quenching 50% fluorescence at the first hour of incubation; compound **104** did it after 6 h and compound **110** only until 11 hours. Therefore, compound **111** showed the best interaction with DNA, with K_{app} values between 4.2×10^5 and 2.2×10^6 M bp^{-1} which suggest a strong bind of **111** to ctDNA, and are comparable or higher than the reported K_{app} of some other ferrocenyl derivatives, which laid in the range of 3.9×10^3 to 5.6×10^5 M bp^{-1}.[291–295]

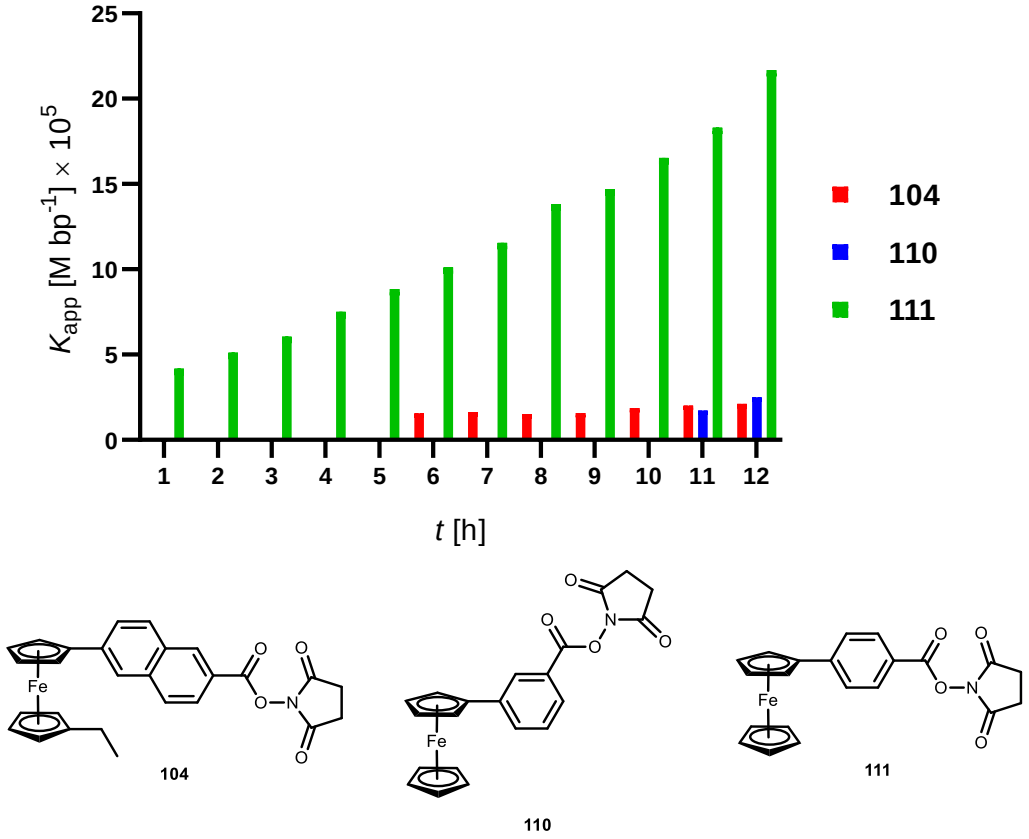

Figure 4.5. Time course K_{app} values of selected compounds **104**, **110** and **111**.

4.3 DNA damage studies

It is known that DNA damage plays a key role in many biological processes such as ageing, mutagenesis and carcinogenesis, due to the susceptibility of cellular DNA to experience different forms of damage from endogenous (enzymatic or spontaneous metabolic conversions) and exogenous (genotoxic agents including ionizing radiation, redox metal ion overload, therapeutic metallodrug exposure) sources. These factors can cause direct or indirect damage to nucleotides, and therefore leading to important biological consequences such as replication errors in genetic code and oxidative DNA base lesions. There are two main mechanisms for DNA damage: hydrolytic and oxidative. Hydrolytic agents involve the cleavage of the phosphate backbone, which can be enzymatically repaired by DNA ligases; whilst oxidative mechanisms cause the production of free radicals with subsequent DNA cleavage by oxidative attack to a range of C-H positions of the deoxyribose moiety.[260,281,296]

The presence/absence of exogenous oxidant and reductant agents have been identified as a factor for oxidative DNA damage. Because DNA is sensitive to ROS radicals, redox-active metal complexes in the presence of oxidant or reductant are then able to induce oxidative DNA damage.[281,296] This approach was used to study the capability of the novel heterocyclic functionalised ferrocenyl derivatives to induce oxidative DNA damage in the presence of H_2O_2 (oxidising agent) and sodium L-ascorbate (reducing agent). Based on the results of previous binding studies, the main interest was focused on compounds **104** and **111** because they were the best compounds on reaching the C_{50} in the EtBr displacement assay. Ferrocene **61**, ethyl ferrocene **62** and compound **103** were also included in some experiments as controls for comparison.

4.3.1 Control analysis of drug-DNA interaction

The interaction of pUC19 supercoiled DNA with compounds **104** or **111** was studied in a range of concentrations between 50-700 μM. The solutions were incubated at 37 °C for 24 h and analysed using standard agarose gel electrophoresis (Figure 4.6). As observed, compounds **104** and **111** do not exhibit damage of the DNA as only the SC DNA band is observed even at high concentrations. This suggests that these compounds are unreactive with DNA alone and require exogenous activation by reductant or oxidant to produce ROS.

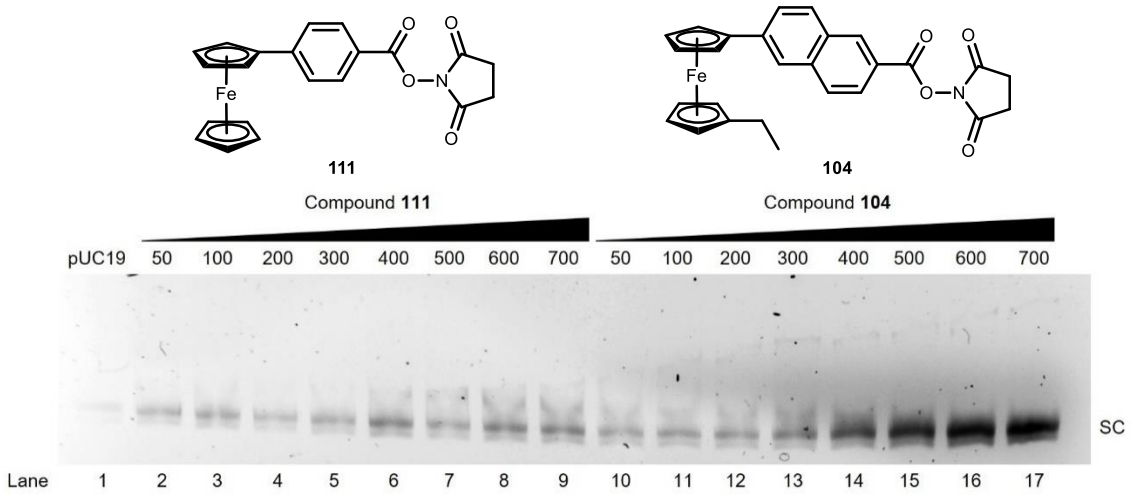

Figure 4.6. Agarose gel electrophoresis of pUC19 supercoiled DNA (400 ng) incubated at 37 °C for 24 h with increasing concentrations of compounds **111** (lanes 2-9) and **104** (lanes 10-17). Lane 1 = pUC19 untreated control.

4.3.2 Analysis of drug-DNA interaction with added oxidant and reductant agents for 6 h

The interaction of pUC19 supercoiled DNA with compound **111** in the presence of a reductant (sodium L-ascorbate) and an oxidant (H_2O_2) -both of which are natively found in the cellular environment- was studied in a range of concentrations between 50-700 μM. The solutions were incubated at 37 °C for 6 h and analysed using standard agarose gel electrophoresis (Figure 4.7). It can be observed that compound **111** induced damage of pUC19 supercoiled DNA in the presence of added oxidant/reductant. In the presence of sodium L-ascorbate, the degradation process is seen immediately at 50 μM, as OC band is observed (lane 2); the intensity in the band of SC DNA is decreasing as OC DNA is being produced; however, no L DNA is observed even at the highest concentration of 700 μM (lane 6). The higher activity was found in the presence of H_2O_2, as all SC DNA has been converted into OC DNA form at 500 μM (lane 10) and complete degradation of DNA is identified at 700 μM (lane 11).

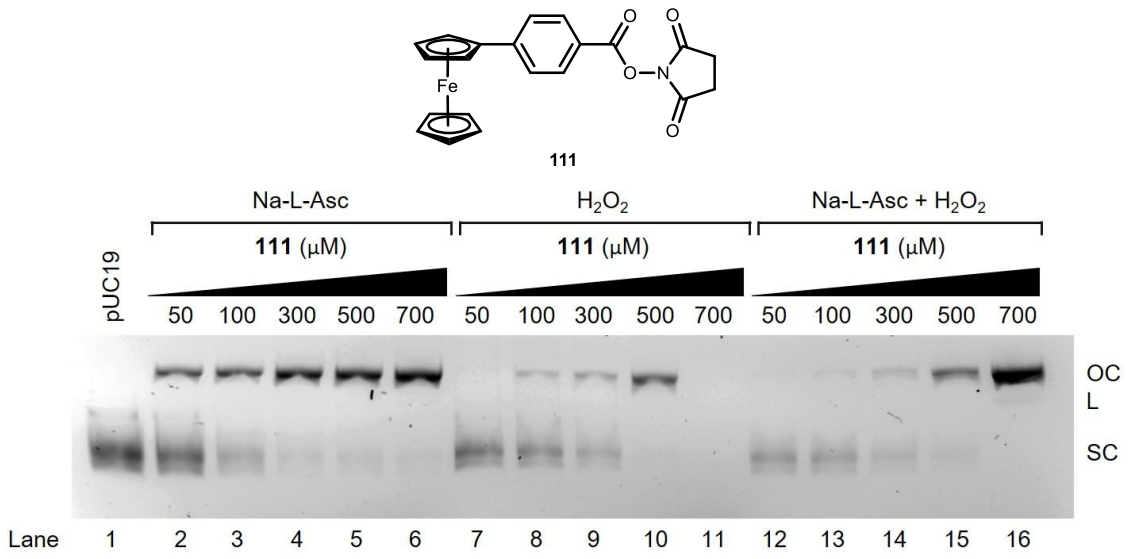

Figure 4.7. Agarose gel electrophoresis of pUC19 supercoiled DNA (400 ng) incubated at 37 °C for 6 h with increasing concentrations of compound **111** and in the presence of 1 mM sodium ascorbate (lanes 2-6), 1 mM H_2O_2 (lanes 7-11) and 1 mM sodium ascorbate + 1 mM H_2O_2 (lanes 12-16). Lane 1 = pUC19 untreated control.

4.3.3 Analysis of drug-DNA interaction with oxidant and reductant agents for 12 h

The previous investigation with 6 h incubation was used as a preliminary analysis to determine the optimal conditions for studying the drug-DNA interaction in the presence of oxidant/reductant agents; however, no L DNA form was identified, and in some cases even complete degradation of DNA was observed. Given that anti-proliferative studies were performed at 24 h, it was decided to repeat the analysis with a longer incubation time (12 h), and therefore reducing the range of concentrations as a greater degradation is expected with longer exposure of DNA to the metallodrug. In addition, a control of pUC19 supercoiled DNA with 1 mM sodium ascorbate only was included as a control, due to the observation of OC band immediately in the first concentration tested in the previous preliminary screening (Figure 4.7, lane 2); this is to confirm that sodium ascorbate is not inducing DNA damage by itself.

The interaction of pUC19 supercoiled DNA with compounds **111**, **104**, **103** or ferrocene **61** (Figure 4.8) under the presence of a reductant (sodium L-ascorbate) and an oxidant (H_2O_2) was studied in a range of concentrations between 10-500 μM. The solutions were incubated at 37 °C for 12 h and analysed using standard agarose gel electrophoresis (Figure 4.9).

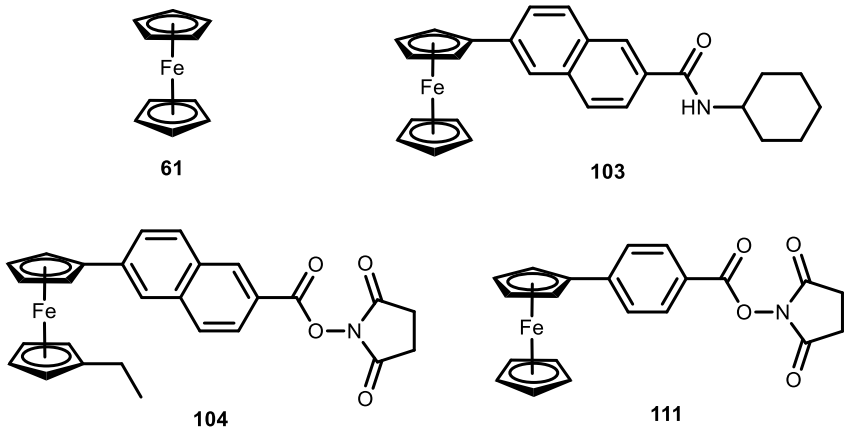

Figure 4.8. Compounds selected for DNA damage studies.

In all cases, the degradation process is seen immediately at 10 μM, as the OC band is observed in the lane 2 of all the gels. In addition, it can be confirmed that the DNA damage induced by sodium L-ascorbate itself is minimal, as only a light OC band is observed in the control (lane A20).

For compound **111** (Figure 4.9A) in the presence of sodium L-ascorbate, the intensity in the band of SC DNA is decreasing as OC DNA is being produced (lanes 2-10); SC DNA is completely converted into OC form at a concentration of 500 μM and only a light band of L DNA is observed (lane 10). Once again, the best results were achieved in the presence of H_2O_2, as all SC DNA has been converted into OC DNA form at 150 μM (lane 15), a small amount of L DNA is observed at 200 μM (lane 16) and complete degradation of DNA is seen at 300 μM and above (lanes 17-19).

For compound **104** (Figure 4.9B) in the presence of sodium L-ascorbate, the SC band is observed through all the concentrations tested, hence the total transition to OC form was not completed and therefore no L DNA was observed either (lanes 2-10). Just as in the previous compound analysed, the higher activity was found in the presence of H_2O_2, as total absence of SC DNA is observed at 150 μM in conjunction with a strong band for OC and a light band of L forms (lane 15). The intensity of OC band is decreased, and L DNA form is more evident at 200 μM (lane 16). Finally, complete degradation of DNA is observed at 300 μM and above (lanes 17-19), which is exactly the same range as previous compound.

Compound **103** (Figure 4.9C) was included in this study to confirm that the structure of compounds tested is crucial for DNA damage. Unlike compounds **111** and **104**, which both are NHS-ester derivatives, compound **103** belongs to the cyclohexylamine series (Figure 4.8). This was found to be detrimental for DNA damage, as the SC band is observed through all the concentrations tested in both sodium L-ascorbate and H_2O_2 experiments, hence the total transition to OC form was not completed and therefore no L DNA was observed either (lanes 2-19). This confirms that the NHS-ester moiety is playing a key role for DNA damage.

The study of ferrocene **61** (Figure 4.9D) was used as a control to check if the structural moieties attached to the novel ferrocenyl heterocyclic functionalised derivatives synthesised during the present research work have a considerable impact on their biological activity. Indeed, the presence of SC DNA is observed through all the concentrations tested in both sodium L-ascorbate and H_2O_2 assays, therefore the total transition to OC form was not accomplished and hence no L DNA was observed either in any case (lanes 2-19). This confirms that ferrocene **61** itself is not capable to complete the degradation of SC DNA within the range of concentrations tested, unlike compounds **111** and **104** which even completed a total degradation of DNA in the presence of H_2O_2 at 300 μM and above concentrations.

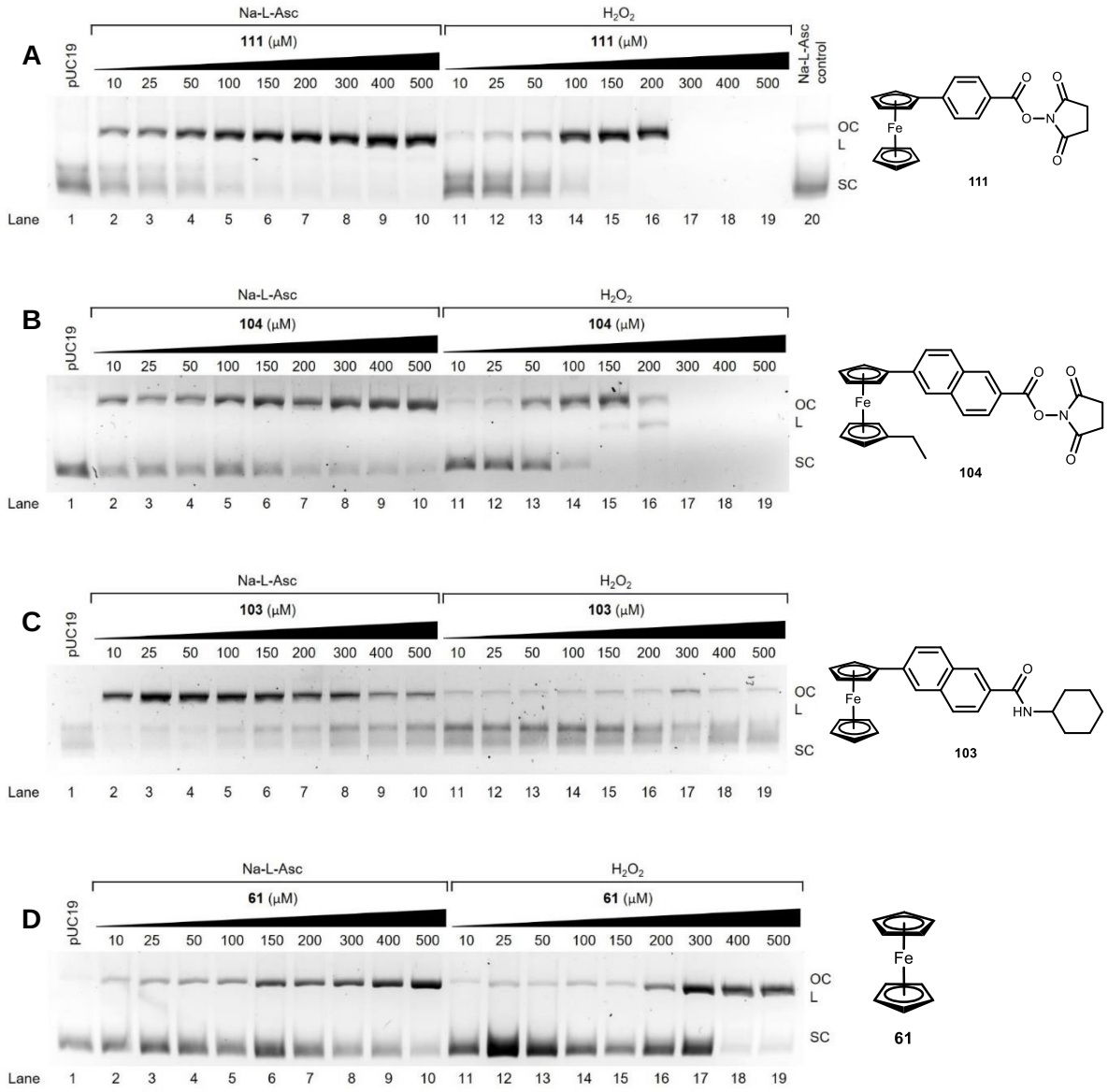

Figure 4.9. Agarose gel electrophoresis of pUC19 supercoiled DNA (400 ng) incubated at 37 °C for 12 h with increasing concentrations of **A)** compound **111**, **B)** compound **104, C)** compound **103** and **D)** ferrocene **61**, and in the presence of 1 mM sodium ascorbate (lanes 2-10) and 1 mM H_2O_2 (lanes 11-19). Lane 1 = pUC19 untreated control; lane 20 = pUC19 + 1 mM sodium ascorbate control.

4.4 Study and identification of ROS

4.4.1 Introduction

Oxygen radical generation is an unavoidable consequence of aerobic processes, and has been related to several pathological conditions, such as cancer, cardiovascular diseases, ageing and neurodegenerative diseases.[297,298] The sequential reduction of molecular oxygen can produce reactive intermediates such as superoxide anion ($O_2^{\bullet -}$) and hydrogen peroxide (H_2O_2), starting a cascade of redox reactions leading to the formation of hydroxyl radicals ($^{\bullet}OH$) and metal-oxo radical species through Fenton-like chemistry (Scheme 4.1).[299] It is important to point out that the superoxide anion is quite unreactive with DNA alone, but in the presence of biologically relevant transition metals such as iron(III) and copper(II), a one electron redox reaction starts the production of these ROS, like in Scheme 1.2 showed earlier in Chapter 1 for bleomycin **30**.

$$O_2 + e^- \rightarrow O_2^{\bullet -} \text{ (superoxide)}$$
$$O_2^{\bullet -} + H_2O \rightarrow HO_2^{\bullet} + OH^- \text{ (hydroperoxyl radical)}$$
$$HO_2^{\bullet} + e^- + H \rightarrow H_2O_2 \text{ (hydrogen peroxide)}$$
$$H_2O_2 + e^- \rightarrow OH^- + {}^{\bullet}OH \text{ (hydroxyl radical)}$$

Scheme 4.1. Generation of ROS by the reduction of molecular oxygen.

Reactive oxygen species (ROS) responsible for the oxidative DNA damage induced by compounds **104**, **111** and ferrocene **61** in the presence of H_2O_2 were investigated using supercoiled plasmid DNA with a selection of ROS-specific antioxidants and stabilisers, as shown in Table 4.2.[281] Ethyl ferrocene **62** was included in this study in order to have a better comparison with compound **104**, as this derivative contains the ethyl ferrocene moiety instead of ferrocene.

Table 4.2. Selected free radical scavengers[a] and intracellular antioxidants[b].

Scavenger	Radical species			
	$O_2^{\bullet -}$	$^{\bullet}OH$	$^1O_2$	H_2O_2
Tiron[a,b]	✓			
D-mannitol[b]		✓		
L-histidine[a]			✓	
KI[a]				✓

4.4.2 Results

The interaction of pUC19 supercoiled DNA with ferrocene **61**, compound **111**, ethyl ferrocene **62** or compound **104** under the presence of an oxidant (H_2O_2) and ROS scavengers was studied in a range of concentrations between 50-300 μM. The solutions were incubated at 37 °C for 12 h and analysed using standard agarose gel electrophoresis (Figure 4.10).

Control experiments (lanes 2-6) are in excellent agreement with those observed previously in Figure 4.9. Ferrocene **61** in the presence of H_2O_2 (Figure 4.10A) do not complete the transition from SC to OC DNA, as both bands are observed through all the concentrations tested (lanes 2-6), just as seen before in Figure 4.9D (lanes 11-19). For compounds **111** and **104** in the presence of H_2O_2 (Figure 4.10B and Figure 4.10D, respectively), all SC DNA has been transformed into OC and L forms at 150 μM (lane 4), the same concentration observed in lane 15 of Figure 4.9A and Figure 4.9B, respectively. However, it is evident again that compound **104** is more active than compound **111**, because the intensity of the OC band at 150 μM in the latter derivative is stronger and only a light band for L DNA is observed, whilst the L band in the first derivative is clearer. At 200 μM, compound **104** exhibits a total degradation of DNA, with no bands observed for any DNA form (Figure 4.10D, lane 5); whilst some remnants of OC and L DNA are still observed for compound **111** at the same concentration (Figure 4.10B, lane 5).

The control of ethyl ferrocene **62** in the presence of H_2O_2 (Figure 4.10C) shows OC and L DNA at 300 μM (lane 6) with no SC DNA left; this suggest that this compound induce a superior DNA oxidative damage than its analogue ferrocene **61**. This observation is consistent with the comparison between compounds **104** and **111**, where compound containing the ethyl ferrocene moiety (**104**) is more active than compound containing the ferrocene moiety (**111**). These results suggest that the alkyl group in the ferrocenyl moiety is playing an important role on the redox process.

Results in all the gels suggest that $O_2^{\bullet -}$ is the most prevalent radical species involved in strand scission, as the presence of tiron considerably impedes cleavage activity of all derivatives (lanes 7-11). In addition, $^1O_2$ is also present for derivatives with ferrocenyl moiety, as added L-histidine was also found to delay cleavage activity of ferrocene **61** and compound **111**. It was observed that the presence of the H_2O_2 scavenger, KI, inhibits DNA cleavage of tested derivatives (lanes 22-26); this observation is consistent with previous results, as the oxidant H_2O_2 was found to be essential for the complexes to start the DNA oxidative damage.

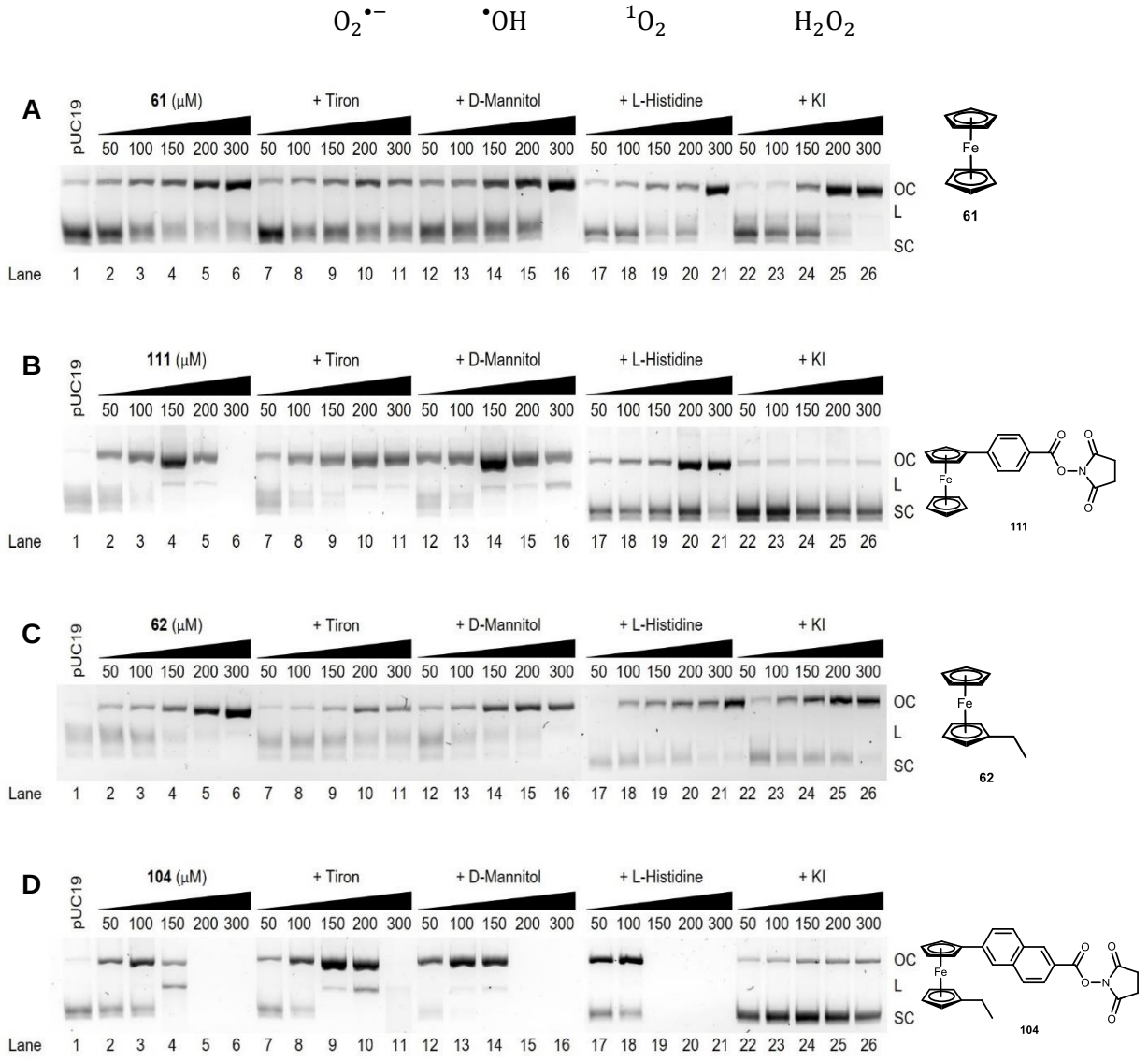

Figure 4.10. Agarose gel electrophoresis of pUC19 supercoiled DNA (400 ng) incubated at 37 °C for 12 h with increasing concentrations of **A)** ferrocene **61**, **B)** compound **111, C)** ethyl ferrocene **62** and **D)** compound **104**, and in the presence of 1 mM H_2O_2. Lane 1 = pUC19 untreated control; lanes 2-6: metal complex only; lanes 7-11: complex + 10 mM tiron; lanes 12-16: complex + 10 mM D-mannitol; lanes 17-21: complex + 10 mM L-histidine; and lanes 22-26: complex + 10 mM KI.

4.5 Conclusions

The interaction of the novel heterocyclic functionalised ferrocenyl derivatives **99**-**120** with DNA was investigated through an indirect fluorometric assay. Results from the competitive fluorescent displacement assay with EtBr show that not all derivatives reach the C_{50}, which is the concentration required to reduce by 50 % fluorescence of EtBr on ctDNA. The C_{50} values obtained are needed to calculate the apparent binding constant (K_{app}) of each complex to ctDNA. The best results were obtained from compounds **104**, **110** and **111**, which all are NHS-ester derivatives; this suggest that the NHS ring is playing an important role on the intercalation activity of complexes to DNA. Compound **111** reached the C_{50} after 1 h incubation, compound **104** did it after 6 h and compound **110** only until 11 hours. Therefore, compound **111** showed the best interaction with DNA, with K_{app} values between 4.2×10^{5} - 2.2×10^{6} M bp^{-1} which suggest a strong binding of **111** to ctDNA, and are comparable or higher than the reported K_{app} of some other ferrocenyl derivatives, which laid in the range of 3.9×10^{3} - 5.6×10^{5} M bp^{-1}.[291–295]

In the absence of an added oxidant, compounds **104** and **111** do not exhibit DNA damage, as only the SC DNA band is observed over an extended concentration range (50-700 μM). This result suggests that the ferrocenyl derivatives require an exogenous oxidant to release the active Fe species that catalyses the ROS generation at the DNA interface. To further study this oxidative pathway, a variety of ROS specific scavengers including 4,5-dihydroxy-1,3-benzenedisulfonic acid (tiron), D-mannitol, L-histidine and KI were employed to probe the role of superoxide ($O_2^{\bullet-}$), the hydroxyl radical ($^{\bullet}OH$), singlet oxygen ($^1O_2$), hydrogen peroxide (H_2O_2) or a combination thereof. For this study, compounds **104** and **111** and their corresponding ferrocenyl moieties (ethyl ferrocene **62** and ferrocene **61**, respectively) were tested. In all cases, pre-incubation with tiron significantly impeded the DNA damage, hence suggesting that superoxide ($O_2^{\bullet-}$) is the most prevalent radical species involved in the cleavage mechanism of these compounds. In addition, singlet oxygen ($^1O_2$) is also present for derivatives with ferrocenyl moiety, as added L-histidine was also found to delay cleavage activity of ferrocene **61** and compound **111**. In these experiments, delayed onset of OC DNA formation, inhibition of L DNA and protection of SC DNA were observed. It was also evident that compounds containing alkylated ferrocene (**104** and **62**) are more active than their corresponding ferrocenyl analogues (**111** and **61**); this observation suggest that the alkyl group is important in decreasing the redox potential of these compounds.

4.6 Materials and methods

4.6.1 DNA binding studies

The competitive ethidium bromide displacement assay was conducted using a similar procedure to the reported by Kellett *et al*.[300] Briefly, a working solution was prepared containing 20 μM UltraPure calf thymus DNA (ctDNA, Invitrogen 15633-019, ε_{260}=12,824 $M \cdot bp^{-1} \cdot cm^{-1}$), 25.2 μM EtBr and 40 mM NaCl in 50 mM acetate buffer (pH = 5). Serial aliquots of ferrocenyl derivative were added to working solutions in a 96-well plate. The volume of each well was adjusted to 100 μL such that the final concentration of ctDNA and EtBr were 10 and 12.6 μM, respectively. The plate was incubated at room temperature (≈20 °C) before being analysed using a Bio-Tek synergy HT multi-mode microplate reader with excitation and emission wavelengths of 530 and 590 nm, respectively. The plates were analysed hourly for 3 h.

From the panel of derivatives tested, only compounds observed to quench ~50% or higher fluorescence of EtBr on ctDNA during the 3 h analysis were selected for further characterise the binding kinetics. The same procedure as above was followed, with each drug concentration measured in triplicate. The plates were analysed hourly for 12 h. Apparent binding constants (K_{app}) were calculated using the formula:

$$K_{\mathrm{app}} = \frac{K_{\mathrm{e}} \times 12.6}{\mathrm{C}_{50}}$$

where K_e = 8.8 × 10^6 $M \cdot bp^{-1}$ (apparent binding constant on ctDNA).

4.6.2 Gel electrophoresis experiments on pUC19 DNA

4.6.2.1 DNA cleavage in the presence of an added reductant/oxidant

Reactions were carried out according to the literature procedure by Kellett *et al*.[301] Stock solutions of the compounds to be tested were initially prepared in CH_3CN, and further dilutions were prepared in 80 mM HEPES buffer (Fisher) at pH 7.2. Supercoiled pUC19 plasmid DNA (400 ng) was exposed to increasing concentrations of each test compound in the presence of 25 mM NaCl and 1 mM of sodium L-ascorbate or H_2O_2. Reaction mixtures were vortexed and incubated at 37 °C for 12 h. The 6X loading dye (Fermentas) containing 10 mM tris(hydroxymethyl)aminomethane-HCl (pH 7.6), 0.03% bromophenol blue, 0.03% xylene cyanole FF, 60% glycerol and 60 mM EDTA was added to each

sample before loading onto a 1.2% agarose gel containing 4 μL of SYBR safe DNA gel stain (Invitrogen). Electrophoresis was completed at 70 V for 12 h in 1X Tris−acetate−EDTA buffer (Millipore) and photographed using a UV transilluminator.

4.6.2.2 DNA cleavage in the presence of ROS scavengers

The assay was carried out according to the method recently reported by Kellett *et al*.[302] Briefly, in a final volume of 20 μL, 80 mM HEPES, 25 mM NaCl, 1 mM H_2O_2 and 400 ng of pUC19 DNA were treated with varying drug concentrations (50, 100, 150, 200 and 300 μM) in the presence of 10 mM of the following ROS scavengers: 4,5-dihydroxy-1,3-benzenedisulfonic acid (Tiron), D-Mannitol, L-Histidine and KI. The reactions mixtures were vortexed and incubated at 37 °C for 12 h, and gel electrophoresis was carried out as previously stated.

General conclusions

In recent years, Kenny *et al.* have reported the antineoplastic activity of several series of ferrocenyl bioconjugates, researching the SAR by modifying the three key moieties of their molecules: a ferrocenyl redox-active centre, an aromatic conjugated linker and an amino acid or dipeptide ester chain.[181,183–195] The aim of this work was to continue the exploration of the SAR in these type of compounds in order to identify potential candidates for biological studies with increased activity and solubility. The amino acid or dipeptide ester chain moiety offers an excellent option for introducing diversity into this series of ferrocenyl derivatives. It has been reported that the biological activity decreases when the length of the peptide chain is extended to tri- or tetrapeptides;[187] hence, longer chains were not an option for SAR analysis. As previous research indicated that antineoplastic activity is higher when small α-amino acids are used[197], the coupling of short amino cyclic molecules such as aminopyridine, benzylamine or cyclohexylamine was considered as an interesting approach to yield an innovative variety for ferrocenyl derivatives other than amino acids.

A series of novel heterocyclic functionalised ferrocenyl derivatives **99**-**120** were prepared using EDC/NHS coupling protocol, a procedure similar to that used for the synthesis of the previous ferrocenyl dipeptide esters in Dr. Peter Kenny's research group.[181,183–195] These compounds were characterised by a range of spectroscopic techniques including ^{1}H NMR, ^{13}C NMR, DEPT-135, COSY, HSQC, HMBC, IR, UV-Vis and MS. All compounds gave spectroscopic and analytical data in accordance with their expected structures, except for the coupling reaction with 4-aminopyridine **96** where the unusual NHS-esters were obtained; this was confirmed with mass spectrometry and X-ray crystallography studies. A change of the coupling protocol is suggested as future work, as an attempt to obtain the ferrocenyl 4-aminopyridine derivatives; this can involve the use of a base stronger than triethylamine, which was used as part of the EDC/NHS protocol.

The *in vitro* antiproliferative activity of these novel compounds **99**-**120**, and a series of *N*-(1′-alkyl-6-ferrocenyl-2-naphthoyl) amino acid and dipeptide esters **130**-**143** and *N*-(ferrocenylmethylamino acid)-fluorinated benzene carboxamides **144**-**154**

previously synthesised by Lu[195], was evaluated in human cervical carcinoma (SiHa) and human liver (Chang) cell lines. Some of these ferrocenyl derivatives showed equivalent or better activity than the reference chemotherapeutic compound vincristine **129**. The SAR study of the ferrocenyl bioconjugates **99**-**120** and **130**-**143** showed that: (i) superior activity is observed when the ferrocene unit is alkylated (-CH_3 or -CH_2CH_3); (ii) a naphthalene ring substituted in the 6,2-positions enhances the anti-proliferative effect of the heterocyclic functionalized ferrocenyl derivatives relative to the 3,2-position or the benzoyl conjugated linker; and (iii) NHS-ester as the heterocycle displays moderate biological activity in SiHa cells with low toxicity to Chang cells, whilst Gly-D-Ala-OEt as the dipeptide moiety exhibits a high cell growth inhibition in SiHa cells with moderate toxicity to Chang cells. In relation to the ferrocenyl carboxamides, this SAR study showed that: (i) single amino acid chains were more active than the dipeptide chain tested; (ii) pentafluorinated derivatives were generally more active than trifluorinated compounds; and (iii) the highest inhibition in SiHa cell line was observed with the higher number of carbons in the chain attached to the carbon in the α position to the carbonyl of the amide group, as L-(+)-α-phenylglycine, L-norleucine and L-leucine were more active than shorter amino acids such as L-alanine, L-2-aminobutyric acid or glycine. Due to the large number of derivatives, only compounds showing stronger anti-proliferative effects on SiHa cell line with less toxicity against Chang cells were then selected for further determination of IC_{50} value, which corresponds to the concentration of the drug required for 50% inhibition of cell growth. Compounds *N*-(1′-ethyl-6-ferrocenyl-2-naphthoyl)-glycine-D-Alanine ethyl ester **143** (IC_{50} = 8.76 ± 0.98 μM), *N*-(ferrocenylmethyl-L-norleucine)-3,4,5-trifluorobenzene carboxamide **147** (IC_{50} = 17.47 ± 2.84 μM) and *N*-(ferrocenylmethyl-L-(+)-α-phenylglycine)-2,3,4,5,6-pentafluorobenzene carboxamide **153** (IC_{50} = 8.18 ± 2.28 μM) have been identified as the most potent ferrocenyl derivatives in SiHa cell line, with moderate toxicity towards Chang cell line. These compounds display a better anticancer activity in SiHa cell line than cisplatin (IC_{50} = 19.5 ± 2.12 μM), which is a highly effective drug in treating cervical carcinoma.[274] These results suggest that ferrocenyl complexes are promising anticancer agents worthy of future therapeutic analysis. For future SAR work, a combination of the unusual NHS-ester and Gly-D-Ala represents an interesting approach, in order to investigate if the high inhibition to SiHa cells from the dipeptide moiety is maintained along with the low toxicity to Chang cells from the NHS-ester moiety. In addition, the use of other cancerous cell lines is strongly recommended.

The interaction of the novel heterocyclic functionalised ferrocenyl derivatives **99**-**120** with DNA was investigated via the competitive fluorescent displacement assay with EtBr. Results showed that not all derivatives reach the C_{50}, which is the concentration required to reduce by 50 % fluorescence of EtBr on ctDNA. The C_{50} values obtained are needed to calculate the apparent binding constant (K_{app}) of each complex to ctDNA. The best results were obtained from compounds **104**, **110** and **111**, which all are NHS-ester derivatives; this suggest that the NHS ring is playing an important role on the binding activity of complexes to DNA. Compound **111** showed the best interaction with DNA, with K_{app} values between 4.2×10^5 - 2.2×10^6 M bp^{-1} which suggest a strong binding of **111** to ctDNA, and are comparable or higher than the reported K_{app} of some other ferrocenyl derivatives, which laid in the range of 3.9×10^3 - 5.6×10^5 M bp^{-1}.[291–295] A further investigation into the specific mode of binding of these ferrocenyl complexes with DNA is suggested, which can be achieved by exploring the non-covalent modes by which metal complexes bind to DNA, such as intercalation, insertion, groove binding, and phosphate clamp.[281]

In the absence of an added oxidant, no DNA cleavage was observed with compounds **104** and **111** over an extended concentration range (50-700 μM); this suggested that the ferrocenyl derivatives required an exogenous oxidant to start the ROS generation at the DNA interface. To further study this oxidative pathway, compounds **104** and **111** and their corresponding ferrocenyl moieties (ethyl ferrocene **62** and ferrocene **61**, respectively) were tested with a variety of ROS specific scavengers including 4,5-dihydroxy-1,3-benzenedisulfonic acid (tiron), D-mannitol, L-histidine and KI, which were employed to probe the role of superoxide ($O_2^{\bullet-}$), hydroxyl radical ($^{\bullet}OH$), singlet oxygen ($^1O_2$) and hydrogen peroxide (H_2O_2), respectively (or a combination thereof). In these experiments, delayed onset of OC DNA formation, inhibition of L DNA and protection of SC DNA were observed. In all cases, pre-incubation with tiron significantly impeded the DNA damage, hence suggesting that superoxide ($O_2^{\bullet-}$) is the most prevalent radical species involved in the cleavage mechanism of these compounds. In addition, singlet oxygen ($^1O_2$) is also present for derivatives with ferrocenyl moiety, as added L-histidine was also found to delay cleavage activity of ferrocene **61** and compound **111**. It was also evident that compounds containing alkylated ferrocene (**104** and **62**) are more active than their corresponding ferrocenyl analogues (**111** and **61**); this observation suggest that the alkyl group in the ferrocenyl moiety is playing an important role on the redox process.

Appendix

A. Supplementary X-ray data for 2,5-dioxopyrrolidin-1-yl 2 ferrocenylbenzoate (compound 109)

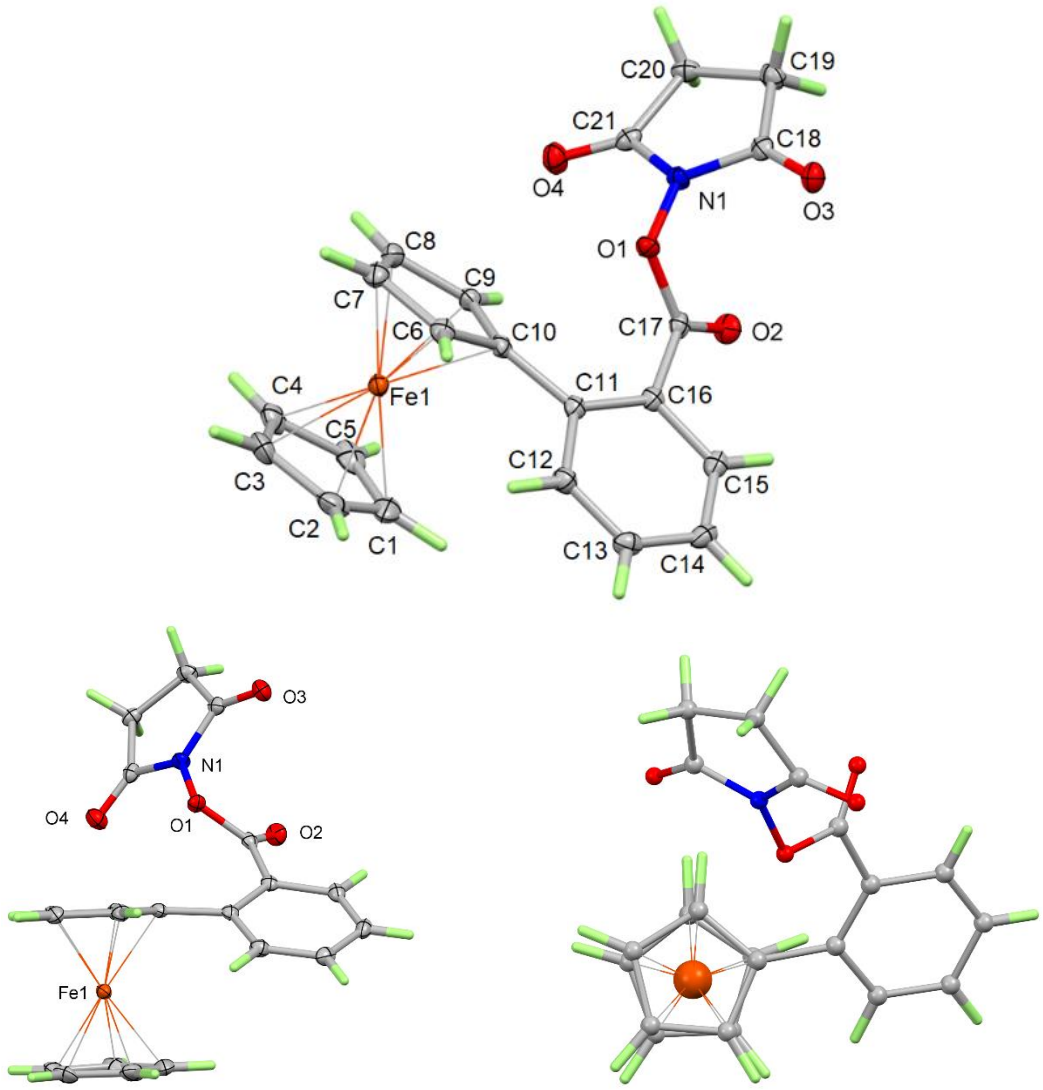

a. Crystal data

$C_{21}H_{17}FeNO_4$	$F(000)$ = 832
M_r = 403.21	D_x = 1.582 Mg m^{-3}
Monoclinic, $P2_1/c$	Cu $K\alpha$ radiation, λ = 1.54184 Å
a = 20.1605 (3) Å	Cell parameters from 5985 reflections
b = 7.4716 (1) Å	θ = 4.5–74.5°
c = 11.4251 (2) Å	m = 7.39 mm^{-1}
b = 100.428 (1)°	T = 100 K
V = 1692.55 (5) Å^3	Block, orange
Z = 4	0.25 × 0.10 × 0.09 mm

b. Data collection

XtaLAB Synergy, Dualflex, AtlasS2 diffractometer	3326 independent reflections
Radiation source: micro-focus sealed X-ray tube, PhotonJet (Cu) X-ray Source	3173 reflections with $I > 2s(I)$
Mirror monochromator	R_{int} = 0.019
Detector resolution: 5.2923 pixels mm^{-1}	θ_{max} = 74.7°, θ_{min} = 4.5°
ω scans	h = -24→22
Absorption correction: gaussian *CrysAlis PRO* 1.171.40.21a (Rigaku Oxford Diffraction, 2018) Numerical absorption correction based on gaussian integration over a multifaceted crystal model Empirical absorption correction using spherical harmonics, implemented in SCALE3 ABSPACK scaling algorithm.	k = -9→7
T_{min} = 0.369, T_{max} = 0.929	l = -12→14
10221 measured reflections	

c. Refinement

Refinement on F^2	Primary atom site location: dual
Least-squares matrix: full	Secondary atom site location: difference Fourier map
$R[F^2 > 2\sigma(F^2)]$ = 0.024	Hydrogen site location: inferred from neighbouring sites
$wR(F^2)$ = 0.060	H-atom parameters constrained
S = 1.03	$w = 1/[s^2(F_o^2) + (0.0299P)^2 + 0.8255P]$ where $P = (F_o^2 + 2F_c^2)/3$
3326 reflections	$(\Delta/\sigma)_{max} < 0.001$
244 parameters	$\Delta\rho_{max}$ = 0.26 e $Å^{-3}$
0 restraints	$\Delta\rho_{min}$ = -0.30 e $Å^{-3}$

d. Computing details

Data collection: *CrysAlis PRO* 1.171.40.21a[245]; cell refinement: *CrysAlis PRO* 1.171.40.21a[245]; data reduction: *CrysAlis PRO* 1.171.40.21a[245]; program(s) used to solve structure: SHELXT[248]; program(s) used to refine structure: *SHELXL2018*/3[303]; molecular graphics: *Mercury*[304]; software used to prepare material for publication: Olex2[247], *publCIF*[305].

e. Geometric parameters (Å, °)

Fe1—C1	2.0404 (16)	O3—C18	1.2078 (17)	C9—C10	1.433 (2)
Fe1—C2	2.0461 (16)	O4—C21	1.2015 (18)	C10—C11	1.4792 (18)
Fe1—C3	2.0499 (15)	N1—C18	1.3860 (18)	C11—C12	1.405 (2)
Fe1—C4	2.0422 (15)	N1—C21	1.3966 (18)	C11—C16	1.405 (2)
Fe1—C5	2.0361 (16)	C1—C2	1.418 (3)	C12—C13	1.383 (2)
Fe1—C6	2.0506 (14)	C1—C5	1.421 (3)	C13—C14	1.391 (2)
Fe1—C7	2.0461 (15)	C2—C3	1.424 (2)	C14—C15	1.379 (2)
Fe1—C8	2.0366 (15)	C3—C4	1.419 (2)	C15—C16	1.4065 (19)
Fe1—C9	2.0359 (15)	C4—C5	1.423 (2)	C16—C17	1.484 (2)
Fe1—C10	2.0517 (13)	C6—C7	1.422 (2)	C18—C19	1.505 (2)
O1—N1	1.3880 (15)	C6—C10	1.436 (2)	C19—C20	1.534 (2)
O1—C17	1.3958 (17)	C7—C8	1.425 (2)	C20—C21	1.506 (2)
O2—C17	1.1955 (18)	C8—C9	1.427 (2)		

C1—Fe1—C2	40.62 (8)	C8—Fe1—C10	68.96 (5)	C7—C8—Fe1	69.93 (8)
C1—Fe1—C3	68.47 (7)	C9—Fe1—C1	118.52 (7)	C7—C8—C9	108.23 (12)
C1—Fe1—C4	68.63 (6)	C9—Fe1—C2	154.84 (7)	C9—C8—Fe1	69.47 (8)
C1—Fe1—C6	126.81 (6)	C9—Fe1—C3	161.29 (6)	C8—C9—Fe1	69.52 (8)
C1—Fe1—C7	164.57 (7)	C9—Fe1—C4	123.11 (6)	C8—C9—C10	108.08 (13)
C1—Fe1—C10	107.14 (6)	C9—Fe1—C5	104.74 (6)	C10—C9—Fe1	70.07 (8)
C2—Fe1—C3	40.68 (6)	C9—Fe1—C6	68.88 (6)	C6—C10—Fe1	69.47 (8)
C2—Fe1—C6	110.08 (6)	C9—Fe1—C7	68.94 (6)	C6—C10—C11	123.61 (13)
C2—Fe1—C7	127.69 (7)	C9—Fe1—C8	41.01 (6)	C9—C10—Fe1	68.89 (8)
C2—Fe1—C10	121.39 (6)	C9—Fe1—C10	41.04 (6)	C9—C10—C6	107.34 (12)
C3—Fe1—C6	122.53 (6)	N1—O1—C17	111.14 (10)	C9—C10—C11	128.82 (13)
C3—Fe1—C10	157.09 (6)	O1—N1—C21	122.37 (11)	C11—C10—Fe1	122.68 (10)
C4—Fe1—C2	68.42 (7)	C18—N1—O1	120.80 (11)	C12—C11—C10	117.51 (12)
C4—Fe1—C3	40.57 (7)	C18—N1—C21	116.77 (12)	C12—C11—C16	117.30 (13)
C4—Fe1—C6	156.12 (6)	C2—C1—Fe1	69.91 (9)	C16—C11—C10	125.14 (13)
C4—Fe1—C7	120.11 (6)	C2—C1—C5	107.93 (14)	C13—C12—C11	122.06 (14)
C4—Fe1—C10	160.77 (6)	C5—C1—Fe1	69.44 (9)	C12—C13—C14	119.90 (14)
C5—Fe1—C1	40.79 (7)	C1—C2—Fe1	69.47 (9)	C15—C14—C13	119.60 (13)
C5—Fe1—C2	68.44 (7)	C1—C2—C3	108.11 (15)	C14—C15—C16	120.75 (13)
C5—Fe1—C3	68.46 (7)	C3—C2—Fe1	69.80 (9)	C11—C16—C15	120.33 (13)
C5—Fe1—C4	40.84 (6)	C2—C3—Fe1	69.52 (9)	C11—C16—C17	126.73 (12)

C5—Fe1—C6	162.61 (6)	C4—C3—Fe1	69.42 (8)	C15—C16—C17	112.94 (12)
C5—Fe1—C7	153.88 (7)	C4—C3—C2	107.92 (14)	O1—C17—C16	112.16 (11)
C5—Fe1—C8	117.87 (7)	C3—C4—Fe1	70.01 (9)	O2—C17—O1	121.68 (13)
C5—Fe1—C10	123.83 (6)	C3—C4—C5	107.96 (14)	O2—C17—C16	125.98 (13)
C6—Fe1—C10	40.97 (6)	C5—C4—Fe1	69.35 (8)	O3—C18—N1	124.01 (13)
C7—Fe1—C3	109.05 (6)	C1—C5—Fe1	69.77 (9)	O3—C18—C19	130.06 (13)
C7—Fe1—C6	40.63 (6)	C1—C5—C4	108.07 (15)	N1—C18—C19	105.93 (11)
C7—Fe1—C10	68.87 (6)	C4—C5—Fe1	69.81 (9)	C18—C19—C20	105.71 (11)
C8—Fe1—C1	153.15 (7)	C7—C6—Fe1	69.52 (8)	C21—C20—C19	106.49 (12)
C8—Fe1—C2	163.81 (7)	C7—C6—C10	108.34 (13)	O4—C21—N1	125.17 (14)
C8—Fe1—C3	125.35 (6)	C10—C6—Fe1	69.56 (8)	O4—C21—C20	129.75 (13)
C8—Fe1—C4	105.88 (6)	C6—C7—Fe1	69.85 (8)	N1—C21—C20	105.08 (12)
C8—Fe1—C6	68.61 (6)	C6—C7—C8	108.01 (13)		
C8—Fe1—C7	40.85 (6)	C8—C7—Fe1	69.21 (8)		

REFERENCES

(1) Cancer http://www.who.int/mediacentre/factsheets/fs297/en/ (accessed Jul 9, 2017).

(2) What Is Cancer? https://www.cancer.gov/about-cancer/understanding/what-is-cancer (accessed Jul 9, 2017).

(3) Hanahan, D.; Weinberg, R. A. The Hallmarks of Cancer. *Cell* **2000**, *100* (1), 57–70.

(4) Chiang, A. C.; Massagué, J. Molecular Basis of Metastasis. *N. Engl. J. Med.* **2008**, *359* (26), 2814–2823.

(5) Cancer by Type https://www.cancerquest.org/patients/cancer-type (accessed Jul 9, 2017).

(6) NCI Dictionary of Cancer Terms https://www.cancer.gov/publications/dictionaries/cancer-terms (accessed Jul 9, 2017).

(7) Classical Hodgkin lymphoma https://www.lymphomas.org.uk/about-lymphoma/types/hodgkin-lymphoma/classical-hodgkin-lymphoma (accessed Jul 9, 2017).

(8) Fact Sheets by Cancer http://globocan.iarc.fr/Pages/fact_sheets_cancer.aspx (accessed Jul 9, 2017).

(9) Brandan, M. E.; Villaseñor, Y. Detección Del Cáncer de Mama: Estado de La Mamografía En México. *Cancerología* **2006**, *1* (3), 147–162.

(10) Gruijl, F. R. D. UV Radiation, DNA Damage, Mutations and Skin Cancer. In *Environmental UV Radiation: Impact on Ecosystems and Human Health and Predictive Models*; Nato Science Series: IV: Earth and Environmental Sciences; Springer, Dordrecht, 2006; Vol. 57, pp 249–258.

(11) What Causes Cancer? https://www.cancer.org/cancer/cancer-causes.html (accessed Jul 10, 2017).

(12) O'Reilly, K. M. A.; Mclaughlin, A. M.; Beckett, W. S.; Sime, P. J. Asbestos-Related Lung Disease. *Am. Fam. Physician* **2007**, *75* (5), 683–688.

(13) Lin, C.-K.; Chang, Y.-Y.; Wang, J.-D.; Lee, L. J.-H. Increased Standardised Incidence Ratio of Malignant Pleural Mesothelioma in Taiwanese Asbestos Workers: A 29-Year Retrospective Cohort Study. *BioMed Res. Int.* **2015**, *2015*.

(14) Bartsch, H.; Malaveille, C.; Friesen, M.; Kadlubar, F. F.; Vineis, P. Black (Air-Cured) and Blond (Flue-Cured) Tobacco Cancer Risk IV: Molecular Dosimetry Studies Implicate Aromatic Amines as Bladder Carcinogens. *Eur. J. Cancer* **1993**, *29* (8), 1199–1207.

(15) Hecht, S. S. Tobacco Smoke Carcinogens and Lung Cancer. *JNCI J. Natl. Cancer Inst.* **1999**, *91* (14), 1194–1210.

(16) Chen, C.-J.; Chen, C. W.; Wu, M.-M.; Kuo, T.-L. Cancer Potential in Liver, Lung, Bladder and Kidney Due to Ingested Inorganic Arsenic in Drinking Water. *Br. J. Cancer* **1992**, *66* (5), 888–892.

(17) Smith, A. H.; Hopenhayn-Rich, C.; Bates, M. N.; Goeden, H. M.; Hertz-Picciotto, I.; Duggan, H. M.; Wood, R.; Kosnett, M. J.; Smith, M. T. Cancer Risks from Arsenic in Drinking Water. *Environ. Health Perspect.* **1992**, *97*, 259–267.

(18) Serrano, A.; Hernández, M. C.; De la Garza Salazar, J.; Herrera, L. A. Helicobacter Pylori y Cáncer Gástrico. *Cancerología* **2009**, *4*, 193–204.

(19) Koskela, P.; Anttila, T.; Bjørge, T.; Brunsvig, A.; Dillner, J.; Hakama, M.; Hakulinen, T.; Jellum, E.; Lehtinen, M.; Lenner, P.; et al. Chlamydia Trachomatis Infection as a Risk Factor for Invasive Cervical Cancer. *Int. J. Cancer* **2000**, *85* (1), 35–39.

(20) Borrell Palanca, A.; Queipo Zaragozá, J. A.; Beltrán Meseguer, J. F.; Chicote Pérez, F.; Escoms Trullenque, F.; Pastor Sempere, F. Infección Vesical Por Esquistosoma: Una Causa Inhabitual de Hematuria. *Actas Urol. Esp.* **2008**, *32* (2), 253–255.
(21) Sripa, B.; Brindley, P. J.; Mulvenna, J.; Laha, T.; Smout, M. J.; Mairiang, E.; Bethony, J. M.; Loukas, A. The Tumorigenic Liver Fluke Opisthorchis Viverrini – Multiple Pathways to Cancer. *Trends Parasitol.* **2012**, *28* (10), 395–407.
(22) McLaughlin-Drubin, M. E.; Munger, K. Viruses Associated with Human Cancer. *Biochim. Biophys. Acta* **2008**, *1782* (3), 127–150.
(23) Patel, P.; Hanson, D. L.; Sullivan, P. S.; Novak, R. M.; Moorman, A. C.; Tong, T. C.; Holmberg, S. D.; Brooks, J. T.; for the Adult and Adolescent Spectrum of Disease Project and HIV Outpatient Study Investigators. Incidence of Types of Cancer among HIV-Infected Persons Compared with the General Population in the United States, 1992–2003. *Ann. Intern. Med.* **2008**, *148* (10), 728.
(24) Silverberg, M. J.; Chao, C.; Leyden, W. A.; Xu, L.; Tang, B.; Horberg, M. A.; Klein, D.; Quesenberry, C. P.; Towner, W. J.; Abrams, D. I. HIV Infection and the Risk of Cancers with and without a Known Infectious Cause. *AIDS Lond. Engl.* **2009**, *23* (17), 2337–2345.
(25) Gopal, S.; Achenbach, C. J.; Yanik, E. L.; Dittmer, D. P.; Eron, J. J.; Engels, E. A. Moving Forward in HIV-Associated Cancer. *J. Clin. Oncol.* **2014**, *32* (9), 876–880.
(26) Lizcano, M.; Carrillo, A.; Contreras, A. Infección Por Virus Del Papiloma Humano: Epidemiología, Historia Natural y Carcinogénesis. *Cancerología* **2009**, *4*, 205–216.
(27) Chaturvedi, A. K.; Engels, E. A.; Anderson, W. F.; Gillison, M. L. Incidence Trends for Human Papillomavirus-Related and -Unrelated Oral Squamous Cell Carcinomas in the United States. *J. Clin. Oncol. Off. J. Am. Soc. Clin. Oncol.* **2008**, *26* (4), 612–619.
(28) Reynales Londoño, J. Infección Por Virus Del Papiloma Humano y Cáncer de Cuello Uterino. *Med. Bogotá* **2012**, *34* (4), 323–346.
(29) Bartosch, B. Hepatitis B and C Viruses and Hepatocellular Carcinoma. *Viruses* **2010**, *2* (8), 1504–1509.
(30) Alavian, S. M.; Haghbin, H. Relative Importance of Hepatitis B and C Viruses in Hepatocellular Carcinoma in EMRO Countries and the Middle East: A Systematic Review. *Hepat. Mon.* **2016**, *16* (3).
(31) Perz, J. F.; Armstrong, G. L.; Farrington, L. A.; Hutin, Y. J. F.; Bell, B. P. The Contributions of Hepatitis B Virus and Hepatitis C Virus Infections to Cirrhosis and Primary Liver Cancer Worldwide. *J. Hepatol.* **2006**, *45* (4), 529–538.
(32) Martínez de Merlo, E. M.; Pérez Díaz, C. Influencia de La Edad En El Desarrollo Del Cáncer. How Age Can Influence on Cancer Development. *RECVET Rev. Electrónica Clínica Vet.* **2007**, *2*, 1–4.
(33) Wakelee, H. A.; Chang, E. T.; Gomez, S. L.; Keegan, T. H.; Feskanich, D.; Clarke, C. A.; Holmberg, L.; Yong, L. C.; Kolonel, L. N.; Gould, M. K.; et al. Lung Cancer Incidence in Never Smokers. *J. Clin. Oncol.* **2007**, *25* (5), 472–478.
(34) Granados García, M.; Herrera Gómez, Á. *Manual de oncología. Procedimientos médico quirúrgicos*, 4th ed.; Instituto Nacional de Cancerología (México); McGraw-Hill: México, 2010.
(35) La muerte celular: necrosis y apoptosis http://ocw.unican.es/ciencias-de-la-salud/biogerontologia/materiales-de-clase-1/capitulo-5.-bases-celulares-del-envejecimiento/5.4-la-muerte-celular-necrosis-y-adoptosis (accessed Jul 13, 2017).
(36) Khan Academy http://es.khanacademy.org (accessed Jul 13, 2017).

(37) Mecanismos de muerte celular: apoptosis y necrosis. http://www.anestesia.org.ar/search/articulos_completos/1/1/284/c.php (accessed Jul 13, 2017).
(38) Citotoxicidad celular http://inmunologia-online.tripod.com/tema14/etexto14.htm (accessed Jul 13, 2017).
(39) Katzung, B. *Basic & Clinical Pharmacology*, 9th ed.; McGraw Hill Professional, 2004.
(40) Cómo se usa la cirugía contra el cáncer https://www.cancer.org/es/tratamiento/tratamientos-y-efectos-secundarios/tipos-de-tratamiento/cirugia/como-se-usa-la-cirugia-contra-el-cancer.html (accessed Jul 15, 2017).
(41) La cirugía como tratamiento contra el cáncer http://www.infocancer.org.mx/la-ciruga-como-tratamiento-contra-el-cncer-con906i0.html (accessed Jul 15, 2017).
(42) Conceptos básicos de la radioterapia https://www.cancer.org/es/tratamiento/tratamientos-y-efectos-secundarios/tipos-de-tratamiento/radioterapia/conceptos-basicos.html (accessed Jul 15, 2017).
(43) Granados, M.; Luna, K.; Campos, E.; Lavin, A. Cáncer de La Laringe: Nuevas Tendencias. *Cancerología* **2007**, *2*, 55–66.
(44) Petrelli, N. J.; Winer, E. P.; Brahmer, J.; Dubey, S.; Smith, S.; Thomas, C.; Vahdat, L. T.; Obel, J.; Vogelzang, N.; Markman, M.; et al. Clinical Cancer Advances 2009: Major Research Advances in Cancer Treatment, Prevention, and Screening—A Report From the American Society of Clinical Oncology. *J. Clin. Oncol.* **2009**, *27* (35), 6052–6069.
(45) Atta-ur-Rahman; Choudhary, M. I. *Frontiers in Anti-Cancer Drug Discovery: Volume 9*; Bentham Science Publishers, 2018.
(46) Perales, M.-A.; Abutalib, S. A.; Bollard, C. *Cell and Gene Therapies*; Springer, 2018.
(47) Stella, V.; Borchardt, R.; Hageman, M.; Oliyai, R.; Maag, H.; Tilley, J. *Prodrugs: Challenges and Rewards*; Springer Science & Business Media, 2007.
(48) Wang, J.; Shen, W.-C.; Zaro, J. L. *Antibody-Drug Conjugates: The 21st Century Magic Bullets for Cancer*; Springer, 2015.
(49) Jr, K. J. O.; Hurvitz, S. A. *Antibody-Drug Conjugates: Fundamentals, Drug Development, and Clinical Outcomes to Target Cancer*; John Wiley & Sons, 2016.
(50) Palekar-Shanbhag, P.; Jog, S. V.; Chogale, M. M.; Gaikwad, S. S. Theranostics for Cancer Therapy. *Curr. Drug Deliv.* **2013**, *10* (3), 357–362.
(51) Chen, X.; Wong, S. *Cancer Theranostics*; Academic Press, 2014.
(52) Cómo la quimioterapia es usada para tratar el cáncer https://www.cancer.org/es/tratamiento/tratamientos-y-efectos-secundarios/tipos-de-tratamiento/quimioterapia/como-la-quimioterapia-es-usada-para-tratar-el-cancer.html (accessed Jul 15, 2017).
(53) Tratamientos http://www.infocancer.org.mx/tratamientos-con454i0.html (accessed Jul 15, 2017).
(54) Kaye, S. B. New Antimetabolites in Cancer Chemotherapy and Their Clinical Impact. *Br. J. Cancer* **1998**, *78* (Suppl 3), 1–7.
(55) Parker, W. B.; Secrist, J. A.; Waud, W. R. Purine Nucleoside Antimetabolites in Development for the Treatment of Cancer. *Curr. Opin. Investig. Drugs Lond. Engl. 2000* **2004**, *5* (6), 592–596.
(56) Skubisz, M. M.; Tong, S. The Evolution of Methotrexate as a Treatment for Ectopic Pregnancy and Gestational Trophoblastic Neoplasia: A Review. *ISRN Obstet. Gynecol.* **2012**, *2012*.

(57) Wu, J.; Jiao, S. Expression of HENTl and ERCC1 Genes in Tumor Tissues Non-Small Cell Lung Cancer. *Asian Pac. J. Trop. Med.* **2013**, *6* (11), 908–911.
(58) Rowinsky, E. K.; Donehower, R. C. The Clinical Pharmacology and Use of Antimicrotubule Agents in Cancer Chemotherapeutics. *Pharmacol. Ther.* **1991**, *52* (1), 35–84.
(59) Vincristine Sulfate Monograph https://www.drugs.com/monograph/vincristine-sulfate.html (accessed Jul 18, 2017).
(60) Paclitaxel Monograph https://www.drugs.com/monograph/paclitaxel.html (accessed Jul 18, 2017).
(61) Kingston, D. G. I. The Chemistry of Taxol. *Pharmacol. Ther.* **1991**, *52* (1), 1–34.
(62) Band Horwitz, S. Mechanism of Action of Taxol. *Trends Pharmacol. Sci.* **1992**, *13*, 134–136.
(63) Checchi, P. M.; Nettles, J. H.; Zhou, J.; Snyder, J. P.; Joshi, H. C. Microtubule-Interacting Drugs for Cancer Treatment. *Trends Pharmacol. Sci.* **2003**, *24* (7), 361–365.
(64) Keglevich, P.; Hazai, L.; Kalaus, G.; Szántay, C. Modifications on the Basic Skeletons of Vinblastine and Vincristine. *Molecules* **2012**, *17* (5), 5893–5914.
(65) Glosario: Genotóxico https://www.greenfacts.org/es/glosario/ghi/genotoxico-genotoxicidad.htm (accessed Jul 16, 2017).
(66) Peters, W. P.; Shpall, E. J.; Jones, R. B.; Olsen, G. A.; Bast, R. C.; Gockerman, J. P.; Moore, J. O. High-Dose Combination Alkylating Agents with Bone Marrow Support as Initial Treatment for Metastatic Breast Cancer. *J. Clin. Oncol.* **1988**, *6* (9), 1368–1376.
(67) Kobayashi, H.; Man, S.; Graham, C. H.; Kapitain, S. J.; Teicher, B. A.; Kerbel, R. S. Acquired Multicellular-Mediated Resistance to Alkylating Agents in Cancer. *Proc. Natl. Acad. Sci.* **1993**, *90* (8), 3294–3298.
(68) Hawkins, M. M.; Kinnier Wilson, L. M.; Burton, H. S.; Potok, M. H. N.; Winter, D. L.; Marsden, H. B.; Stovall, M. A. Radiotherapy, Alkylating Agents, and Risk of Bone Cancer After Childhood Cancer. *J. Natl. Cancer Inst.* **1996**, *88* (5), 270–278.
(69) Bensinger, W. I.; Schiffman, K. S.; Holmberg, L.; Appelbaum, F. R.; Maziarz, R.; Montgomery, P.; Ellis, E.; Rivkin, S.; Weiden, P.; Lilleby, K.; et al. High-Dose Busulfan, Melphalan, Thiotepa and Peripheral Blood Stem Cell Infusion for the Treatment of Metastatic Breast Cancer. *Bone Marrow Transplant.* **1997**, *19* (12), 1183–1189.
(70) Fukuoka, M.; Furuse, K.; Saijo, N.; Nishiwaki, Y.; Ikegami, H.; Tamura, T.; Shimoyama, M.; Suemasu, K. Randomized Trial of Cyclophosphamide, Doxorubicin, and Vincristine Versus Cisplatin and Etoposide Versus Alternation of These Regimens in Small-Cell Lung Cancer. *JNCI J. Natl. Cancer Inst.* **1991**, *83* (12), 855–861.
(71) Roth, B. J.; Johnson, D. H.; Einhorn, L. H.; Schacter, L. P.; Cherng, N. C.; Cohen, H. J.; Crawford, J.; Randolph, J. A.; Goodlow, J. L.; Broun, G. O. Randomized Study of Cyclophosphamide, Doxorubicin, and Vincristine versus Etoposide and Cisplatin versus Alternation of These Two Regimens in Extensive Small-Cell Lung Cancer: A Phase III Trial of the Southeastern Cancer Study Group. *J. Clin. Oncol. Off. J. Am. Soc. Clin. Oncol.* **1992**, *10* (2), 282–291.
(72) Noda, K.; Nishiwaki, Y.; Kawahara, M.; Negoro, S.; Sugiura, T.; Yokoyama, A.; Fukuoka, M.; Mori, K.; Watanabe, K.; Tamura, T.; et al. Irinotecan plus Cisplatin Compared with Etoposide plus Cisplatin for Extensive Small-Cell Lung Cancer. *N. Engl. J. Med.* **2002**, *346* (2), 85–91.

(73) Price, B. A.; Peters, N. H. Treatment of Metastatic Testicular Tumours with Bleomycin, Etoposide, Cisplatin and Vincristine (BEPV). *J. R. Soc. Med.* **1992**, *85* (11), 674–678.
(74) Verschraegen, C. F.; Levy, T.; Kudelka, A. P.; Llerena, E.; Ende, K.; Freedman, R. S.; Edwards, C. L.; Hord, M.; Steger, M.; Kaplan, A. L.; et al. Phase II Study of Irinotecan in Prior Chemotherapy-Treated Squamous Cell Carcinoma of the Cervix. *J. Clin. Oncol. Off. J. Am. Soc. Clin. Oncol.* **1997**, *15* (2), 625–631.
(75) Lord, C. J.; Ashworth, A. Targeted Therapy for Cancer Using PARP Inhibitors. *Curr. Opin. Pharmacol.* **2008**, *8* (4), 363–369.
(76) Murai, J.; Huang, S. N.; Das, B. B.; Renaud, A.; Zhang, Y.; Doroshow, J. H.; Ji, J.; Takeda, S.; Pommier, Y. Trapping of PARP1 and PARP2 by Clinical PARP Inhibitors. *Cancer Res.* **2012**, *72* (21), 5588–5599.
(77) Lord, C. J.; Ashworth, A. PARP Inhibitors: Synthetic Lethality in the Clinic. *Science* **2017**, *355* (6330), 1152–1158.
(78) Wa, D. DNA-Intercalating Ligands as Anti-Cancer Drugs: Prospects for Future Design. *Anticancer. Drug Des.* **1989**, *4* (4), 241–263.
(79) Doxorubicin Hydrochloride Monograph https://www.drugs.com/monograph/doxorubicin-hydrochloride.html (accessed Jul 18, 2017).
(80) Ogura, M. Adriamycin (doxorubicin). *Gan To Kagaku Ryoho* **2001**, *28* (10), 1331–1338.
(81) Sonpavde, G.; Ansari, R.; Walker, P.; Sciortino, D. F.; Gabrys, G. T.; Murdock, A.; Gonin, R.; Einhorn, L. H. Phase II Study of Doxorubicin and Paclitaxel as Second-Line Chemotherapy of Small-Cell Lung Cancer: A Hoosier Oncology Group Trial. *Am. J. Clin. Oncol.* **2000**, *23* (1), 68–70.
(82) Bc, B. DNA Intercalating Anti-Tumour Agents. *Anticancer. Drug Des.* **1991**, *6* (1), 1–35.
(83) About side effects of chemotherapy http://www.cancerresearchuk.org/about-cancer/cancer-in-general/treatment/chemotherapy/side-effects/about#collapse-202823 (accessed Jul 20, 2017).
(84) Love, R. R.; Leventhal, H.; Easterling, D. V.; Nerenz, D. R. Side Effects and Emotional Distress during Cancer Chemotherapy. *Cancer* **1989**, *63* (3), 604–612.
(85) Chemotherapy Side Effects https://www.cancer.org/treatment/treatments-and-side-effects/treatment-types/chemotherapy/chemotherapy-side-effects.html (accessed Jul 20, 2017).
(86) Brydøy, M.; Fosså, S. D.; Dahl, O.; Bjøro, T. Gonadal Dysfunction and Fertility Problems in Cancer Survivors. *Acta Oncol.* **2007**, *46* (4), 480–489.
(87) Chabner, B. A.; Longo, D. L. *Cancer Chemotherapy and Biotherapy: Principles and Practice*; Lippincott Williams & Wilkins, 2010.
(88) Giaccone, G.; Pinedo, H. M. Drug Resistance. *The Oncologist* **1996**, *1* (1 & 2), 82–87.
(89) Lippert, T. H.; Ruoff, H.-J.; Volm, M. Intrinsic and Acquired Drug Resistance in Malignant Tumors. The Main Reason for Therapeutic Failure. *Arzneimittelforschung.* **2008**, *58* (6), 261–264.
(90) Housman, G.; Byler, S.; Heerboth, S.; Lapinska, K.; Longacre, M.; Snyder, N.; Sarkar, S. Drug Resistance in Cancer: An Overview. *Cancers* **2014**, *6* (3), 1769–1792.
(91) Mitra, A.; Mishra, L.; Li, S. EMT, CTCs and CSCs in Tumor Relapse and Drug-Resistance. *Oncotarget* **2015**, *6* (13), 10697–10711.
(92) Shibue, T.; Weinberg, R. A. EMT, CSCs, and Drug Resistance: The Mechanistic Link and Clinical Implications. *Nat. Rev. Clin. Oncol.* **2017**, *14* (10), 611–629.

(93) Thomas, G. *Medicinal Chemistry: An Introduction*, 2nd. edition.; John Wiley & Sons, 2011.
(94) Gianferrara, T.; Bratsos, I.; Alessio, E. A Categorization of Metal Anticancer Compounds Based on Their Mode of Action. *Dalton Trans.* **2009**, No. 37, 7588–7598.
(95) Peyrone, M. Ueber Die Einwirkung Des Ammoniaks Auf Platinchlorür. *Justus Liebigs Ann. Chem.* **1844**, *51* (1), 1–29.
(96) Kauffman, G. B.; Pentimalli, R.; Doldi, S.; Hall, M. D. Michele Peyrone (1813-1883), Discoverer of Cisplatin. *Platin. Met. Rev.* **2010**, *54* (4), 250–256.
(97) Rosenberg, B.; VanCamp, L.; Trosko, J. E.; Mansour, V. H. Platinum Compounds: A New Class of Potent Antitumour Agents. *Nature* **1969**, *222* (5191), 385–386.
(98) Patrick, G. L. *An Introduction to Medicinal Chemistry*; Oxford University Press, 2005.
(99) Wang, D.; Lippard, S. J. Cellular Processing of Platinum Anticancer Drugs. *Nat. Rev. Drug Discov.* **2005**, *4* (4), 307–320.
(100) Romero-Canelón, I.; Sadler, P. J. Next-Generation Metal Anticancer Complexes: Multitargeting via Redox Modulation. *Inorg. Chem.* **2013**, *52* (21), 12276–12291.
(101) Neault, J. F.; Tajmir-Riahi, H. A. Interaction of Cisplatin with Human Serum Albumin. Drug Binding Mode and Protein Secondary Structure. *Biochim. Biophys. Acta* **1998**, *1384* (1), 153–159.
(102) Fuertes, M. A.; Alonso, C.; Pérez, José. M. Biochemical Modulation of Cisplatin Mechanisms of Action: Enhancement of Antitumor Activity and Circumvention of Drug Resistance. *Chem. Rev.* **2003**, *103* (3), 645–662.
(103) Arnesano, F.; Natile, G. Mechanistic Insight into the Cellular Uptake and Processing of Cisplatin 30 Years after Its Approval by FDA. *Coord. Chem. Rev.* **2009**, *253* (15), 2070–2081.
(104) Boer, D. R.; Canals, A.; Coll, M. DNA-Binding Drugs Caught in Action: The Latest 3D Pictures of Drug-DNA Complexes. *Dalton Trans. Camb. Engl. 2003* **2009**, No. 3, 399–414.
(105) Kelland, L. The Resurgence of Platinum-Based Cancer Chemotherapy. *Nat. Rev. Cancer* **2007**, *7* (8), 573–584.
(106) Avendaño, C.; Menéndez, J. C. *Medicinal Chemistry of Anticancer Drugs*; Elsevier, 2015.
(107) Fischer, J.; Ganellin, C. R. *Analogue-Based Drug Discovery*; John Wiley & Sons, 2006.
(108) Sledge, G. W. Cisplatin and Platinum Analogues in Breast Cancer. *Semin. Oncol.* **1992**, *19* (1), 78–82.
(109) Chaney, S. G.; Vaisman, A. Specificity of Platinum-DNA Adduct Repair. *J. Inorg. Biochem.* **1999**, *77* (1–2), 71–81.
(110) Shen, D.-W.; Pouliot, L. M.; Hall, M. D.; Gottesman, M. M. Cisplatin Resistance: A Cellular Self-Defense Mechanism Resulting from Multiple Epigenetic and Genetic Changes. *Pharmacol. Rev.* **2012**, *64* (3), 706–721.
(111) Galluzzi, L.; Senovilla, L.; Vitale, I.; Michels, J.; Martins, I.; Kepp, O.; Castedo, M.; Kroemer, G. Molecular Mechanisms of Cisplatin Resistance. *Oncogene* **2012**, *31* (15), 1869–1883.
(112) Bertrand, B.; Doulain, P.-E.; Goze, C.; Bodio, E. Development of Trackable Metal-Based Drugs: New Generation of Therapeutic Agents. *Dalton Trans.* **2016**, *45* (33), 13005–13011.
(113) Hartinger, C. G.; Dyson, P. J. Bioorganometallic Chemistry--from Teaching Paradigms to Medicinal Applications. *Chem. Soc. Rev.* **2009**, *38* (2), 391–401.

(114) Pigeon, P.; Top, S.; Vessières, A.; Huché, M.; Görmen, M.; Arbi, M. E.; Plamont, M.-A.; McGlinchey, M. J.; Jaouen, G. A New Series of Ferrocifen Derivatives, Bearing Two Aminoalkyl Chains, with Strong Antiproliferative Effects on Breast Cancer Cells. *New J. Chem.* **2011**, *35* (10), 2212–2218.
(115) Yan, Y. K.; Melchart, M.; Habtemariam, A.; Sadler, P. J. Organometallic Chemistry, Biology and Medicine: Ruthenium Arene Anticancer Complexes. *Chem. Commun. Camb. Engl.* **2005**, No. 38, 4764–4776.
(116) Komeda, S.; Casini, A. Next-Generation Anticancer Metallodrugs. *Curr. Top. Med. Chem.* **2012**, *12* (3), 219–235.
(117) Murray, J. H.; Harding, M. M. Organometallic Anticancer Agents: The Effect of the Central Metal and Halide Ligands on the Interaction of Metallocene Dihalides Cp2MX2 with Nucleic Acid Constituents. *J. Med. Chem.* **1994**, *37* (13), 1936–1941.
(118) Gómez-Ruiz, S.; Maksimović-Ivanić, D.; Mijatović, S.; Kaluđerović, G. N. On the Discovery, Biological Effects, and Use of Cisplatin and Metallocenes in Anticancer Chemotherapy. *Bioinorg. Chem. Appl.* **2012**, *2012*, 1–14.
(119) Motswainyana, W. M.; Ajibade, P. A. Anticancer Activities of Mononuclear Ruthenium(II) Coordination Complexes https://www.hindawi.com/journals/ac/2015/859730/ (accessed Feb 7, 2019).
(120) Köpf-Maier, P.; Köpf, H. Non-Platinum Group Metal Antitumor Agents. History, Current Status, and Perspectives. *Chem. Rev.* **1987**, *87* (5), 1137–1152.
(121) Neuse, E. W. Macromolecular Ferrocene Compounds as Cancer Drug Models. *J. Inorg. Organomet. Polym. Mater.* **2005**, *15* (1), 3–31.
(122) Köpf, H.; Köpf-Maier, P. Titanocene Dichloride—The First Metallocene with Cancerostatic Activity. *Angew. Chem. Int. Ed. Engl.* **1979**, *18* (6), 477–478.
(123) Lümmen, G.; Sperling, H.; Luboldt, H.; Otto, T.; Rübben, H. Phase II Trial of Titanocene Dichloride in Advanced Renal-Cell Carcinoma. *Cancer Chemother. Pharmacol.* **1998**, *42* (5), 415–417.
(124) Kröger, N.; Kleeberg, U. R.; Mross, K.; Edler, L.; Hossfeld, D. K. Phase II Clinical Trial of Titanocene Dichloride in Patients with Metastatic Breast Cancer. *Oncol. Res. Treat.* **2000**, *23* (1), 60–62.
(125) Tacke, M.; Allen, L. T.; Cuffe, L.; Gallagher, W. M.; Lou, Y.; Mendoza, O.; Müller-Bunz, H.; Rehmann, F.-J. K.; Sweeney, N. Novel Titanocene Anti-Cancer Drugs Derived from Fulvenes and Titanium Dichloride. *J. Organomet. Chem.* **2004**, *689* (13), 2242–2249.
(126) Rehmann, F.-J. K.; Rous, A. J.; Mendoza, O.; Sweeney, N. J.; Strohfeldt, K.; Gallagher, W. M.; Tacke, M. A Trimethoxyphenyl Substituted Ansa-Titanocene: A Possible Anti-Cancer Drug. *Polyhedron* **2005**, *24* (11), 1250–1255.
(127) Sweeney, N. J.; Mendoza, O.; Müller-Bunz, H.; Pampillón, C.; Rehmann, F.-J. K.; Strohfeldt, K.; Tacke, M. Novel Benzyl Substituted Titanocene Anti-Cancer Drugs. *J. Organomet. Chem.* **2005**, *690* (21), 4537–4544.
(128) Valadares, M. C.; Ramos, A. L.; Rehmann, F.-J. K.; Sweeney, N. J.; Strohfeldt, K.; Tacke, M.; Queiroz, M. L. S. Antitumour Activity of [1,2-Di(Cyclopentadienyl)-1,2-Di(p-N,N-Dimethylaminophenyl)-Ethanediyl] Titanium Dichloride in Xenografted Ehrlich's Ascites Tumour. *Eur. J. Pharmacol.* **2006**, *534* (1–3), 264–270.
(129) Pampillón, C.; Claffey, J.; Hogan, M.; Tacke, M. Novel Achiral Titanocene Anti-Cancer Drugs Synthesised from Bis-N,N-Dimethylamino Fulvene and Lithiated Heterocyclic Compounds. *Biometals Int. J. Role Met. Ions Biol. Biochem. Med.* **2008**, *21* (2), 197–204.
(130) Strohfeldt, K.; Tacke, M. Bioorganometallic Fulvene-Derived Titanocene Anti-Cancer Drugs. *Chem. Soc. Rev.* **2008**, *37* (6), 1174–1187.

(131) Hogan, M.; Claffey, J.; Fitzpatrick, E.; Hickey, T.; Pampillón, C.; Tacke, M. Synthesis and Cytotoxicity Studies of Titanocene C Analogues https://www.hindawi.com/journals/mbd/2008/754358/ (accessed Feb 7, 2019).
(132) Olszewski, U.; Claffey, J.; Hogan, M.; Tacke, M.; Zeillinger, R.; Bednarski, P. J.; Hamilton, G. Anticancer Activity and Mode of Action of Titanocene C. *Invest. New Drugs* **2011**, *29* (4), 607–614.
(133) Monti-Bragadin, C.; Ramani, L.; Samer, L.; Mestroni, G.; Zassinovich, G. Effects of Cis-Dichlorodiammineplatinum (II) and Related Transition Metal Complexes on Escherichia Coli. *Antimicrob. Agents Chemother.* **1975**, *7* (6), 825–827.
(134) Durig, J. R.; Danneman, J.; Behnke, W. D.; Mercer, E. E. The Induction of Filamentous Growth in Escherichia Coli by Ruthenium and Palladium Complexes. *Chem. Biol. Interact.* **1976**, *13* (3), 287–294.
(135) Giraldi, T.; Sava, G.; Bertoli, G.; Mestroni, G.; Zassinovich, G. Antitumor Action of Two Rhodium and Ruthenium Complexes in Comparison with Cis-Diamminedichloroplatinum(II). *Cancer Res.* **1977**, *37* (8 Part 1), 2662–2666.
(136) Clarke, M. J. Oncological Implications of the Chemistry of Ruthenium. *Met. Ions Biol. Syst.* **1980**, *11*, 231–283.
(137) Clarke, M. J.; Bitler, S.; Rennert, D.; Buchbinder, M.; Kelman, A. D. Reduction and Subsequent Binding of Ruthenium Ions Catalyzed by Subcellular Components. *J. Inorg. Biochem.* **1980**, *12* (1), 79–87.
(138) Baulieu, E.; Forman, D. T.; Ingelman-Sundberg, M.; Jaenicke, L.; Kellen, J. A.; Nagai, Y.; Springer, G. F.; Träger, L.; Will-Shahab, L.; Wittliff, J. L. *Ruthenium and Other Non-Platinum Metal Complexes in Cancer Chemotherapy*; Springer Science & Business Media, 2013.
(139) Sava, G.; Pacor, S.; Mestroni, G.; Alessio, E. Na[Trans-RuCl4(DMSO)Im], a Metal Complex of Ruthenium with Antimetastatic Properties. *Clin. Exp. Metastasis* **1992**, *10* (4).
(140) Frausin, F.; Scarcia, V.; Cocchietto, M.; Furlani, A.; Serli, B.; Alessio, E.; Sava, G. Free Exchange across Cells, and Echistatin-Sensitive Membrane Target for the Metastasis Inhibitor NAMI-A (Imidazolium Trans-Imidazole Dimethyl Sulfoxide Tetrachlororuthenate) on KB Tumor Cells. *J. Pharmacol. Exp. Ther.* **2004**, *313* (1), 227–233.
(141) Sava, G.; Frausin, F.; Cocchietto, M.; Vita, F.; Podda, E.; Spessotto, P.; Furlani, A.; Scarcia, V.; Zabucchi, G. Actin-Dependent Tumour Cell Adhesion after Short-Term Exposure to the Antimetastasis Ruthenium Complex NAMI-A. *Eur. J. Cancer* **2004**, *40* (9), 1383–1396.
(142) Antonarakis, E. S.; Emadi, A. Ruthenium-Based Chemotherapeutics: Are They Ready for Prime Time? *Cancer Chemother. Pharmacol.* **2010**, *66* (1), 1–9.
(143) Trondl, R.; Heffeter, P.; R. Kowol, C.; A. Jakupec, M.; Berger, W.; K. Keppler, B. NKP-1339, the First Ruthenium-Based Anticancer Drug on the Edge to Clinical Application. *Chem. Sci.* **2014**, *5* (8), 2925–2932.
(144) Bergamo, A.; Gaiddon, C.; Schellens, J. H. M.; Beijnen, J. H.; Sava, G. Approaching Tumour Therapy beyond Platinum Drugs: Status of the Art and Perspectives of Ruthenium Drug Candidates. *J. Inorg. Biochem.* **2012**, *106* (1), 90–99.
(145) Gransbury, G. K.; Kappen, P.; Glover, C. J.; Hughes, J. N.; Levina, A.; Lay, P. A.; Musgrave, I. F.; Harris, H. H. Comparison of KP1019 and NAMI-A in Tumour-Mimetic Environments. *Met. Integr. Biometal Sci.* **2016**, *8* (8), 762–773.
(146) Sigel, A.; Sigel, H.; Freisinger, E.; Sigel, R. K. O. *Metallo-Drugs: Development and Action of Anticancer Agents*; Walter de Gruyter GmbH & Co KG, 2018.

(147) Ciambellotti, S.; Pratesi, A.; Severi, M.; Ferraro, G.; Alessio, E.; Merlino, A.; Messori, L. The NAMI A - Human Ferritin System: A Biophysical Characterization. *Dalton Trans. Camb. Engl. 2003* **2018**, *47* (33), 11429–11437.
(148) Jaouen, G.; Metzler-Nolte, N. *Medicinal Organometallic Chemistry*; Springer, 2010.
(149) Kealy, T. J.; Pauson, P. L. A New Type of Organo-Iron Compound. *Nature* **1951**, *168* (4285), 1039–1040.
(150) Miller, S. A.; Tebboth, J. A.; Tremaine, J. F. Dicyclopentadienyliron. *J. Chem. Soc.* **1952**, 632–635.
(151) Wilkinson, G.; Rosenblum, M.; Whiting, M. C.; Woodward, R. B. THE STRUCTURE OF IRON BIS-CYCLOPENTADIENYL. *J. Am. Chem. Soc.* **1952**, *74* (8), 2125–2126.
(152) Long, N. J. *Metallocenes: An Introduction to Sandwich Complexes*; Wiley, 1998.
(153) Hillard, E. A.; Jaouen, G. Bioorganometallics: Future Trends in Drug Discovery, Analytical Chemistry, and Catalysis. *Organometallics* **2011**, *30* (1), 20–27.
(154) Chohan, Z. H. Antibacterial and Antifungal Ferrocene Incorporated Dithiothione and Dithioketone Compounds. *Appl. Organomet. Chem.* **2006**, *20* (2), 112–116.
(155) Biot, C.; Glorian, G.; Maciejewski, L. A.; Brocard, J. S.; Domarle, O.; Blampain, G.; Millet, P.; Georges, A. J.; Abessolo, H.; Dive, D.; et al. Synthesis and Antimalarial Activity in Vitro and in Vivo of a New Ferrocene−Chloroquine Analogue. *J. Med. Chem.* **1997**, *40* (23), 3715–3718.
(156) Dive, D.; Biot, C. Ferrocene Conjugates of Chloroquine and Other Antimalarials: The Development of Ferroquine, a New Antimalarial. *ChemMedChem* **2008**, *3* (3), 383–391.
(157) Domarle, O.; Blampain, G.; Agnaniet, H.; Nzadiyabi, T.; Lebibi, J.; Brocard, J.; Maciejewski, L.; Biot, C.; Georges, A. J.; Millet, P. In Vitro Antimalarial Activity of a New Organometallic Analog, Ferrocene-Chloroquine. *Antimicrob. Agents Chemother.* **1998**, *42* (3), 540–544.
(158) da Silva, C. H. T. P.; Ponte, G. D.; Neto, A. F.; Taft, C. A. Rational Design of Novel Diketoacid-Containing Ferrocene Inhibitors of HIV-1 Integrase. *Bioorganic Chem.* **2005**, *33* (4), 274–284.
(159) Fouda, M. F. R.; Abd-Elzaher, M. M.; Abdelsamaia, R. A.; Labib, A. A. On the Medicinal Chemistry of Ferrocene. *Appl. Organomet. Chem.* **2007**, *21* (8), 613–625.
(160) Abd-Elzaher, M. M.; Ali, I. A. I. Preparation, Characterization and Biological Studies of Some Novel Ferrocenyl Compounds. *Appl. Organomet. Chem.* **2006**, *20* (2), 107–111.
(161) Ward, S. G.; Taylor, R. C.; Köpf-Maier, P.; Köpf, H.; Balzarini, J.; De Clercq, E. Assessment of the in Vitro Broad-Spectrum Antiviral Activity of Some Selected Antitumor Metallocene and Metallocenium Complexes. *Appl. Organomet. Chem.* **1989**, *3* (6), 491–497.
(162) Runqiu, H.; Qingmin, W. Synthesis, Spectroscopy and Biological Activity of Novel Acylhydrazines Containing Ferrocenyl Moiety. *J. Organomet. Chem.* **2001**, *637*, 94–98.
(163) Souza, N. B. de; Aguiar, A. C. C.; Oliveira, A. C. de; Top, S.; Pigeon, P.; Jaouen, G.; Goulart, M. O. F.; Krettli, A. U. Antiplasmodial Activity of Iron(II) and Ruthenium(II) Organometallic Complexes against Plasmodium Falciparum Blood Parasites. *Mem. Inst. Oswaldo Cruz* **2015**, *110* (8), 981–988.
(164) Biot, C.; Nosten, F.; Fraisse, L.; Ter-Minassian, D.; Khalife, J.; Dive, D. The Antimalarial Ferroquine: From Bench to Clinic. *Parasite* **2011**, *18* (3), 207–214.

(165) Köpf-Maier, P.; Köpf, H.; Neuse, E. W. Ferrocenium Salts—The First Antineoplastic Iron Compounds. *Angew. Chem. Int. Ed. Engl.* **1984**, *23* (6), 456–457.
(166) Köpf-Maier, P.; Köpf, H.; Neuse, E. W. Ferricenium Complexes: A New Type of Water-Soluble Antitumor Agent. *J. Cancer Res. Clin. Oncol.* **1984**, *108* (3), 336–340.
(167) Osella, D.; Ferrali, M.; Zanello, P.; Laschi, F.; Fontani, M.; Nervi, C.; Cavigiolio, G. On the Mechanism of the Antitumor Activity of Ferrocenium Derivatives. *Inorganica Chim. Acta* **2000**, *306* (1), 42–48.
(168) Morantes, C. Y. A.-. Cytotoxicity and Reactive Oxygen Species Generated by Ferrocenium and Ferrocene on MCF7 and MCF10A Cell Lines. *J. Cancer Sci. Ther.* **2012**, *04* (09).
(169) Tabbì, G.; Cassino, C.; Cavigiolio, G.; Colangelo, D.; Ghiglia, A.; Viano, I.; Osella, D. Water Stability and Cytotoxic Activity Relationship of a Series of Ferrocenium Derivatives. ESR Insights on the Radical Production during the Degradation Process. *J. Med. Chem.* **2002**, *45* (26), 5786–5796.
(170) Osella, D.; Mahboobi, H.; Colangelo, D.; Cavigiolio, G.; Vessières, A.; Jaouen, G. FACS Analysis of Oxidative Stress Induced on Tumour Cells by SERMs. *Inorganica Chim. Acta* **2005**, *358* (6), 1993–1998.
(171) Drug Approval Package: Bleomycin NDA #064084 https://www.accessdata.fda.gov/drugsatfda_docs/anda/96/064084_bleomycin-sulfate_toc.cfm (accessed Feb 10, 2019).
(172) Kowalski, K.; Zakrzewski, J.; Long, N. J.; Suwaki, N.; Mann, D. J.; White, A. J. P. Synthesis, Structure and Assessment of the Cytotoxic Properties of 2,5-Dimethylazaferrocenyl Phosphonates. *Dalton Trans.* **2006**, No. 4, 571–576.
(173) Kowalski, K.; Suwaki, N.; Zakrzewski, J.; White, A. J. P.; Long, N. J.; Mann, D. J. In Vitro DNA Scission Activity of Heterometallocenes. *Dalton Trans.* **2007**, *0* (7), 743–748.
(174) Top, S.; Tang, J.; Vessières, A.; Carrez, D.; Provot, C.; Jaouen, G. Ferrocenyl Hydroxytamoxifen: A Prototype for a New Range of Oestradiol Receptor Site-Directed Cytotoxics. *Chem. Commun.* **1996**, No. 8, 955–956.
(175) Top, S.; Dauer, B.; Vaissermann, J.; Jaouen, G. Facile Route to Ferrocifen, 1-[4-(2-Dimethylaminoethoxy)]-1-(Phenyl-2-Ferrocenyl-but-1-Ene), First Organometallic Analogue of Tamoxifen, by the McMurry Reaction. *J. Organomet. Chem.* **1997**, *541* (1–2), 355–361.
(176) Top, S.; Vessières, A.; Cabestaing, C.; Laios, I.; Leclercq, G.; Provot, C.; Jaouen, G. Studies on Organometallic Selective Estrogen Receptor Modulators. (SERMs) Dual Activity in the Hydroxy-Ferrocifen Series. *J. Organomet. Chem.* **2001**, *637*, 500–506.
(177) Top, S.; Vessières, A.; Leclercq, G.; Quivy, J.; Tang, J.; Vaissermann, J.; Huché, M.; Jaouen, G. Synthesis, Biochemical Properties and Molecular Modelling Studies of Organometallic Specific Estrogen Receptor Modulators (SERMs), the Ferrocifens and Hydroxyferrocifens: Evidence for an Antiproliferative Effect of Hydroxyferrocifens on Both Hormone-Dependent and Hormone-Independent Breast Cancer Cell Lines. *Chem. – Eur. J.* **2003**, *9* (21), 5223–5236.
(178) Jaouen, G.; Top, S.; Vessieres, A.; Leclercq, G.; McGlinchey, M. J. The First Organometallic Selective Estrogen Receptor Modulators (SERMs) and Their Relevance to Breast Cancer. *Curr. Med. Chem.* **2004**, *11* (18), 2505–2517.
(179) Plażuk, D.; Vessières, A.; Hillard, E. A.; Buriez, O.; Labbé, E.; Pigeon, P.; Plamont, M.-A.; Amatore, C.; Zakrzewski, J.; Jaouen, G. A [3]Ferrocenophane Polyphenol

Showing a Remarkable Antiproliferative Activity on Breast and Prostate Cancer Cell Lines. *J. Med. Chem.* **2009**, *52* (15), 4964–4967.

(180) Görmen, M.; Plażuk, D.; Pigeon, P.; Hillard, E. A.; Plamont, M.-A.; Top, S.; Vessières, A.; Jaouen, G. Comparative Toxicity of [3]Ferrocenophane and Ferrocene Moieties on Breast Cancer Cells. *Tetrahedron Lett.* **2010**, *51* (1), 118–120.

(181) Kelly, P. N.; Prêtre, A.; Devoy, S.; O'Rielly, I.; Devery, R.; Goel, A.; Gallagher, J. F.; Lough, A. J.; Kenny, P. T. M. Synthesis, Structural Characterisation and Biological Activity of Novel N-(Ferrocenylmethyl)Benzene-Carboxamide Derivatives. *J. Organomet. Chem.* **2007**, *692* (6), 1327–1331.

(182) Böhm, H.-J.; Banner, D.; Bendels, S.; Kansy, M.; Kuhn, B.; Müller, K.; Obst-Sander, U.; Stahl, M. Fluorine in Medicinal Chemistry. *ChemBioChem* **2004**, *5* (5), 637–643.

(183) Corry, A. J.; Goel, A.; Alley, S. R.; Kelly, P. N.; O'Sullivan, D.; Savage, D.; Kenny, P. T. M. *N-ortho*-Ferrocenyl Benzoyl Dipeptide Esters: Synthesis, Structural Characterization and in Vitro Anti-Cancer Activity of N-{ortho-(Ferrocenyl)Benzoyl}-Glycine-L-Alanine Ethyl Ester and N-{ortho-(Ferrocenyl)Benzoyl}-L-Alanine-Glycine Ethyl Ester. *J. Organomet. Chem.* **2007**, *692* (6), 1405–1410.

(184) Goel, A.; Savage, D.; Alley, S. R.; Kelly, P. N.; O'Sullivan, D.; Mueller-Bunz, H.; Kenny, P. T. M. The Synthesis and Structural Characterization of Novel N-Meta-Ferrocenyl Benzoyl Dipeptide Esters: The X-Ray Crystal Structure and in Vitro Anti-Cancer Activity of N-{meta-Ferrocenyl)Benzoyl}-l-Alanine-Glycine Ethyl Ester. *J. Organomet. Chem.* **2007**, *692* (6), 1292–1299.

(185) Corry, A. J.; O'Donovan, N.; Mooney, Á.; O'Sullivan, D.; Rai, D. K.; Kenny, P. T. M. Synthesis, Structural Characterization, in Vitro Anti-Proliferative Effect and Cell Cycle Analysis of N-(Ferrocenyl)Benzoyl Dipeptide Esters. *J. Organomet. Chem.* **2009**, *694* (6), 880–885.

(186) Mooney, Á.; Corry, A. J.; O'Sullivan, D.; Rai, D. K.; Kenny, P. T. M. The Synthesis, Structural Characterization and in Vitro Anti-Cancer Activity of Novel N-(3-Ferrocenyl-2-Naphthoyl) Dipeptide Ethyl Esters and Novel N-(6-Ferrocenyl-2-Naphthoyl) Dipeptide Ethyl Esters. *J. Organomet. Chem.* **2009**, *694* (6), 886–894.

(187) Corry, A. J.; Mooney, Á.; O'Sullivan, D.; Kenny, P. T. M. Synthesis, Characterization and in Vitro Anti-Cancer Activity of N-(Ferrocenyl)Benzoyl Tri- and Tetrapeptide Esters. *Inorganica Chim. Acta* **2009**, *362* (9), 2957–2961.

(188) Mooney, Á.; Corry, A. J.; Ruairc, C. N.; Mahgoub, T.; O'Sullivan, D.; O'Donovan, N.; Crown, J.; Varughese, S.; Draper, S. M.; Rai, D. K.; et al. Synthesis, Characterisation and Biological Evaluation of N-(Ferrocenyl)Naphthoyl Amino Acid Esters as Anticancer Agents. *Dalton Trans.* **2010**, *39* (35), 8228–8239.

(189) Mooney, Á.; Tiedt, R.; Mahgoub, T.; O'Donovan, N.; Crown, J.; White, B.; Kenny, P. T. M. Structure–Activity Relationship and Mode of Action of N-(6-Ferrocenyl-2-Naphthoyl) Dipeptide Ethyl Esters: Novel Organometallic Anticancer Compounds. *J. Med. Chem.* **2012**, *55* (11), 5455–5466.

(190) Butler, W. E.; Kelly, P. N.; Harry, A. G.; Tiedt, R.; White, B.; Devery, R.; Kenny, P. T. M. The Synthesis, Structural Characterization and Biological Evaluation of N-(Ferrocenylmethyl Amino Acid) Fluorinated Benzene-Carboxamide Derivatives as Potential Anticancer Agents. *Appl. Organomet. Chem.* **2013**, *27* (6), 361–365.

(191) Butler, W. E. Synthesis, Characterisation and Biological Evaluation of N-Ferrocenylmethyl Amino Acid Benzene Carboxamide Derivatives and N-Ferrocenyl Benzoyl Amino Alkane Derivatives as Anti-Cancer Agents. PhD thesis, Dublin City University, Dublin, Ireland, 2012.

(192) Harry, A. G.; Murphy, J.; Butler, W. E.; Tiedt, R.; Mooney, Á.; Manton, J. C.; Pryce, M. T.; O'Donovan, N.; Walsh, N.; Crown, J.; et al. The Synthesis, Structural Characterization and in Vitro Anti-Cancer Activity of Novel N-{6-(Ferrocenyl) Ethynyl-2-Naphthoyl} Amino Acid and Dipeptide Ethyl Esters. *J. Organomet. Chem.* **2013**, *734*, 86–92.
(193) Harry, A. G.; Butler, W. E.; Manton, J. C.; Pryce, M. T.; O'Donovan, N.; Crown, J.; Rai, D. K.; Kenny, P. T. M. The Synthesis, Structural Characterization and in Vitro Anti-Cancer Activity of Novel 1-Alkyl-1′-N-Para-(Ferrocenyl) Benzoyl Dipeptide Esters. *J. Organomet. Chem.* **2014**, *757*, 28–35.
(194) Tiedt, R. Synthesis, Characterisation and Biological Evaluation of Novel N-Ferrocenyl Amino Acid and Dipeptide Derivatives as Potential Anticancer Agents. PhD thesis, Dublin City University, Dublin, Ireland, 2014.
(195) Lu, L. Novel Ferrocenyl Peptide Bioconjugates as Anti-Cancer Agents. PhD thesis, Dublin City University, Dublin, Ireland, 2018.
(196) Wani, W. A.; Baig, U.; Shreaz, S.; Shiekh, R. A.; Iqbal, P. F.; Jameel, E.; Ahmad, A.; Mohd-Setapar, S. H.; Mushtaque, M.; Hun, L. T. Recent Advances in Iron Complexes as Potential Anticancer Agents. *New J. Chem.* **2016**, *40* (2), 1063–1090.
(197) Mooney, Á. Synthesis, Characterisation and Biological Evaluation of Novel N-Ferrocenyl Naphthoyl Amino Acid and Dipeptide Derivatives as Potential Anti-Cancer Agents. PhD thesis, Dublin City University, Dublin, Ireland, 2010.
(198) Beagley, P.; Blackie, M. A. L.; Chibale, K.; Clarkson, C.; Moss, J. R.; Smith, P. J. Synthesis and Antimalarial Activity in Vitro of New Ruthenocene–Chloroquine Analogues. *J. Chem. Soc. Dalton Trans.* **2002**, 4426–4433.
(199) Pigeon, P.; Top, S.; Vessières, A.; Huché, Michel; Hillard, E. A.; Salomon, E.; Jaouen, G. Selective Estrogen Receptor Modulators in the Ruthenocene Series. Synthesis and Biological Behavior. *J. Med. Chem.* **2005**, *48* (8), 2814–2821.
(200) Carboxylic acids https://s10.lite.msu.edu/res/msu/botonl/b_online/library/newton/Chy251_253/Lectures/CarboxylicAcids/CarboxylicAcids.html (accessed Aug 12, 2017).
(201) Reaction between acyl chlorides and alcohols - addition / elimination http://www.chemguide.co.uk/mechanisms/addelim/alcohol.html (accessed Aug 12, 2017).
(202) Carey, F. A.; Sundberg, R. J. *Advanced Organic Chemistry*; Springer Science & Business Media, 2000.
(203) Jones, J. *Amino Acid and Peptide Synthesis*; Oxford University Press, 2002.
(204) Valeur, E.; Bradley, M. Amide Bond Formation: Beyond the Myth of Coupling Reagents. *Chem. Soc. Rev.* **2009**, *38* (2), 606–631.
(205) Montalbetti, C. A. G. N.; Falque, V. Amide Bond Formation and Peptide Coupling. *Tetrahedron* **2005**, *61* (46), 10827–10852.
(206) Bodanszky, M. *Principles of Peptide Synthesis*; Springer Science & Business Media, 2012.
(207) Fischer, M. J. E. Amine Coupling through EDC/NHS: A Practical Approach. *Methods Mol. Biol.* **2010**, *627*, 55–73.
(208) Greenberg, A. *The Amide Linkage: Structural Significance in Chemistry, Biochemistry, and Materials Science*; John Wiley & Sons, 2002.
(209) Abraham, R. J.; Byrne, J. J.; Griffiths, L.; Perez, M. 1H Chemical Shifts in NMR: Part 23, the Effect of Dimethyl Sulphoxide versus Chloroform Solvent on 1H Chemical Shifts. *Magn. Reson. Chem.* **2006**, *44* (5), 491–509.
(210) Cremer, D.; Binkley, J. S.; Pople, J. A. Molecular Orbital Theory of the Electronic Structure of Organic Compounds. 25. Conformations of Methyl- and Fluoro-

Substituted Cyclopentanes and Cyclohexanes. *J. Am. Chem. Soc.* **1976**, *98* (22), 6836–6839.
(211) Kao, P. N.; Turner, P. H. Conformational Study of Cyclohexanecarboxaldehyde by Microwave Spectroscopy. *J. Am. Chem. Soc.* **1979**, *101* (16), 4497–4499.
(212) Wiberg, K. B. Conformational Studies in the Cyclohexane Series. 3. The Dihalocyclohexanes. *J. Org. Chem.* **1999**, *64* (17), 6387–6393.
(213) Taddei, F.; Kleinpeter, E. The Anomeric Effect in Substituted Cyclohexanes. I. The Role of Hyperconjugative Interactions and Steric Effect in Monosubstituted Cyclohexanes. *J. Mol. Struct. THEOCHEM* **2004**, *683* (1), 29–41.
(214) Tomé, L. I. N.; Rosado, M. T. S.; Ermelinda, M.; Eusébio, S.; Redinha, J. S. Molecular Structure of Mono- and 1,2-Aminoderivatives of Cyclohexane: Steric Strain Effects as Determining Factors. *J. Mol. Struct. THEOCHEM* **2007**, *804* (1–3), 65–74.
(215) Sánchez-Viesca, F.; Gómez, R. Electric Hindrance and Dipole Moments in 2-Aminopyridine Nitration. *Am. J. Chem.* **2015**, *5* (1), 19–22.
(216) Gasparro, F. P.; Kolodny, N. H. NMR Determination of the Rotational Barrier in N,N-Dimethylacetamide. A Physical Chemistry Experiment. *J. Chem. Educ.* **1977**, *54* (4), 258.
(217) Bruch, M. *NMR Spectroscopy Techniques, Second Edition*; CRC Press, 1996.
(218) Batta, G.; Kövér, K.; Jr, C. S. *Methods for Structure Elucidation by High-Resolution NMR: Applications to Organic Molecules of Moderate Molecular Weight*; Elsevier, 1997.
(219) Imoto, K. *Multifunctional Molecular Magnets Based on Octacyanidometalates*; Springer, 2017.
(220) Albert, A.; Goldacre, R.; Phillips, J. 455. The Strength of Heterocyclic Bases. *J. Chem. Soc. Resumed* **1948**, 2240.
(221) Clayden, J.; Greeves, N.; Warren, S. *Organic Chemistry*; OUP Oxford, 2012.
(222) Katritzky, A. R.; Boulton, A. J. *Advances in Heterocyclic Chemistry*; Academic Press, 2014.
(223) Wilson, J. G.; Bottomley, W. The Reaction of Methyl Propiolate with 2-aminopyridines. *J. Heterocycl. Chem.* **1967**, *4* (3), 360–364.
(224) Kondo, T.; Kotachi, S.; Ogino, S.; Watanabe, Y. Ruthenium Complex-Catalyzed Novel and Facile Synthesis of Imidazo[1,2-a]Pyridines from 2-Aminopyridines and Vicinal-Diols. *Chem. Lett.* **1993**, *22* (8), 1317–1320.
(225) Breteche, A.; Duflos, M.; Dassonville, A.; Nourrisson, M.-R.; Brelet, J.; Le Baut, G.; Grimaud, N.; Petit, J.-Y. New N -Pyridinyl(Methyl)-Indole-2- and 3-(Alkyl)Carboxamides and Derivatives Acting as Systemic and Topical Inflammation Inhibitors. *J. Enzyme Inhib. Med. Chem.* **2002**, *17* (6), 415–424.
(226) Larock, R. C.; Wang, Y.; Dong, X.; Yao, T. Synthesis of C-5 Substituted Nucleosides via Palladium-Catalyzed Coupling of Dienes and Amines. *Tetrahedron* **2005**, *61* (48), 11427–11439.
(227) González, I.; Mosquera, J.; Guerrero, C.; Rodríguez, R.; Cruces, J. Selective Monomethylation of Anilines by $Cu(OAc)_2$ -Promoted Cross-Coupling with $MeB(OH)_2$. *Org. Lett.* **2009**, *11* (8), 1677–1680.
(228) Ueda, S.; Nagasawa, H. Facile Synthesis of 1,2,4-Triazoles via a Copper-Catalyzed Tandem Addition−Oxidative Cyclization. *J. Am. Chem. Soc.* **2009**, *131* (42), 15080–15081.
(229) Larrosa, M.; Guerrero, C.; Rodríguez, R.; Cruces, J. Selective Copper-Promoted Cross-Coupling of Aromatic Amines with Alkyl Boronic Acids. *Synlett* **2010**, *2010* (14), 2101–2105.

(230) Tursky, M.; Lorentz-Petersen, L. L. R.; Olsen, L. B.; Madsen, R. Iridium- and Ruthenium-Catalysed Synthesis of 2,3-Disubstituted Indoles from Anilines and Vicinal Diols. *Org. Biomol. Chem.* **2010**, *8* (24), 5576.
(231) Mojarradi, H. Coupling of Substances Containing a Primary Amine to Hyaluronan via Carbodiimide-Mediated Amidation, Uppsala Universitet, 2011.
(232) Sankari Devi, E.; Alanthadka, A.; Tamilselvi, A.; Nagarajan, S.; Sridharan, V.; Maheswari, C. U. Metal-Free Oxidative Amidation of Aldehydes with Aminopyridines Employing Aqueous Hydrogen Peroxide. *Org. Biomol. Chem.* **2016**, *14* (35), 8228–8231.
(233) Li, Z.; Gelbaum, C.; Fisk, J. S.; Holden, B.; Jaganathan, A.; Whiteker, G. T.; Pollet, P.; Liotta, C. L. Aqueous Suzuki Coupling Reactions of Basic Nitrogen-Containing Substrates in the Absence of Added Base and Ligand: Observation of High Yields under Acidic Conditions. *J. Org. Chem.* **2016**, *81* (18), 8520–8529.
(234) Khadra, A.; Mayer, S.; Organ, M. G. Pd-PEPPSI-IPentCl: A Useful Catalyst for the Coupling of 2-Aminopyridine Derivatives. *Chem. – Eur. J.* **2017**, *23* (13), 3206–3212.
(235) Leonard, M. *Intermediate Organic Chemistry*; Lulu.com, 2014.
(236) Jacobsen, N. E. *NMR Spectroscopy Explained: Simplified Theory, Applications and Examples for Organic Chemistry and Structural Biology*; John Wiley & Sons, 2007.
(237) Pavia, D. L.; Lampman, G. M.; Kriz, G. S.; Vyvyan, J. A. *Introduction to Spectroscopy*; Cengage Learning, 2014.
(238) Williams, D. H.; Fleming, I. *Spectroscopic Methods in Organic Chemistry*; McGraw-Hill, 2008.
(239) Hart, H.; Hadad, C. M.; Craine, L. E.; Hart, D. J. *Organic Chemistry: A Short Course*; Cengage Learning, 2011.
(240) Smith, B. C. *Infrared Spectral Interpretation: A Systematic Approach*; CRC Press, 1998.
(241) Silverstein, R. M.; Webster, F. X.; Kiemle, D. J.; Bryce, D. L. *Spectrometric Identification of Organic Compounds*; John Wiley & Sons, 2014.
(242) Scheinmann, F. *An Introduction to Spectroscopic Methods for the Identification of Organic Compounds: Mass Spectrometry, Ultraviolet Spectroscopy, Electron Spin Resonance Spectroscopy, Nuclear Magnetic Resonance Spectroscopy (Recent Developments), Use of Various Spectral Methods Together, and Documentation of Molecular Spectra*; Elsevier, 2013.
(243) Wepplo, P. *The Language of Organic Chemistry*; CurvedArrowPress: United States of America, 2006.
(244) Reactions of Aromatic Compounds - Examples of Ar-SE Reaction http://www.chemgapedia.de/vsengine/vlu/vsc/en/ch/12/oc/vlu_organik/aromaten/reaktionen/ar_se_beispiele.vlu/Page/vsc/en/ch/12/oc/aromaten/reaktionen/ar_se/azokupplung/azokupplung.vscml.html (accessed Aug 11, 2017).
(245) *Rigaku Oxford Diffraction, CrysAlisPro Software System*; Rigaku Corporation: Oxford, UK, 2018.
(246) Hübschle, C. B.; Sheldrick, G. M.; Dittrich, B. ShelXle: A Qt Graphical User Interface for SHELXL. *J. Appl. Crystallogr.* **2011**, *44* (6), 1281–1284.
(247) Dolomanov, O. V.; Bourhis, L. J.; Gildea, R. J.; Howard, J. a. K.; Puschmann, H. OLEX2: A Complete Structure Solution, Refinement and Analysis Program. *J. Appl. Crystallogr.* **2009**, *42* (2), 339–341.
(248) Sheldrick, G. M. SHELXT – Integrated Space-Group and Crystal-Structure Determination. *Acta Crystallogr. Sect. Found. Adv.* **2015**, *71* (1), 3–8.

(249) Corry, A. J. Novel Ferrocenyl Benzoyl Peptide Esters as Anti-Cancer Agents and Ferrocenoyl Self Assembled Monolayers as Anion Sensors. PhD thesis, Dublin City University, 2009.
(250) N-(5-amino-1-naphthyl)acetamide http://www.molmall.net/product/10784 (accessed Aug 13, 2017).
(251) Ryan, J. A. *Introduction to Animal Cell Culture Technical Bulletin*; CLS-AN-042-REV1; Corning Life Sciences: New York, 2008.
(252) Paul, J. *Cell and Tissue Culture*; Williams and Wilkins, 1961.
(253) Harrison, R. G. The Croonian Lecture: On the Origin and Development of the Nervous System Studied by the Methods of Experimental Embryology. *Proc. R. Soc. Lond. B Biol. Sci.* **1935**, *118* (808), 155–196.
(254) Freshney, R. I. *Culture of Animal Cells: A Manual of Basic Technique and Specialized Applications*; John Wiley & Sons, 2015.
(255) Aslantürk, Ö. S. In Vitro Cytotoxicity and Cell Viability Assays: Principles, Advantages, and Disadvantages. *Genotoxicity - Predict. Risk Our Actual World* **2017**.
(256) Ishiyama, M.; Tominaga, H.; Shiga, M.; Sasamoto, K.; Ohkura, Y.; Ueno, K. A Combined Assay of Cell Vability and in Vitro Cytotoxicity with a Highly Water-Soluble Tetrazolium Salt, Neutral Red and Crystal Violet. *Biol. Pharm. Bull.* **1996**, *19* (11), 1518–1520.
(257) Davey, J.; Lord, J. M. *Essential Cell Biology: Cell Structure*; OUP Oxford, 2003; Vol. 1.
(258) Clynes, M. *Animal Cell Culture Techniques*; Springer Science & Business Media, 2012.
(259) Boyd, J. W.; Neubig, R. R. *Cellular Signal Transduction in Toxicology and Pharmacology: Data Collection, Analysis, and Interpretation*; John Wiley & Sons, 2019.
(260) El-Gewely, M. R. *Biotechnology Annual Review*; Elsevier, 2005.
(261) Borenfreund, E.; Puerner, J. A. A Simple Quantitative Procedure Using Monolayer Cultures for Cytotoxicity Assays (HTD/NR-90). *J. Tissue Cult. Methods* **1985**, *9* (1), 7–9.
(262) Barile, F. A. *Introduction to In Vitro CytotoxicologyMechanisms and Methods*; CRC Press, 1994.
(263) McGaw, L. J.; Elgorashi, E. E.; Eloff, J. N. 8 - Cytotoxicity of African Medicinal Plants Against Normal Animal and Human Cells. In *Toxicological Survey of African Medicinal Plants*; Kuete, V., Ed.; Elsevier, 2014; pp 181–233.
(264) Roche Diagnostics. *Cell Proliferation Reagent WST-1*; 11 644 807 001; Germany, 2006.
(265) Yin, L.-M.; Wei, Y.; Wang, Y.; Xu, Y.-D.; Yang, Y.-Q. Long Term and Standard Incubations of WST-1 Reagent Reflect the Same Inhibitory Trend of Cell Viability in Rat Airway Smooth Muscle Cells. *Int. J. Med. Sci.* **2013**, *10* (1), 68–72.
(266) CytoScan™ - WST-1 Cell Proliferation Assay http://sambomed.co.kr/renewal/bbs/board.php?bo_table=products&wr_id=1996&sca=G-Biosciences (accessed Aug 14, 2017).
(267) Favela Hernández, J. M. de J. Aislamiento y Caracterización de Los Compuestos Antibacterianos y Antituberculosos de Larrea Tridentata, Determinación de Su Toxicidad y Mecanismo de Acción Del Compuesto Más Activo. PhD thesis, Universidad Autónoma de Nuevo León, Mexico, 2012.
(268) Torres, R.; Modak, B.; Urzúa, A.; Delle Monache, F.; Damonte, E.; Pujol, C. A. Propiedades Antivirales de Compuestos Naturales y Semi-Sintéticos de La Resina de Heliotropium Filifolium. *Bol. Soc. Chil. Quím.* **2002**, *47* (3), 259–263.

(269) Casaroli Marano, R. P. Guión de Prácticas de Biología Celular. *Universitat de Barcelona*. 2005.
(270) BioVision, Inc. Ready-to-use Cell Proliferation Colorimetric Reagent, WST-1 http://www.biovision.com/ready-to-use-cell-proliferation-colorimetric-reagent-wst-1.html (accessed Aug 14, 2017).
(271) Ngamwongsatit, P.; Banada, P. P.; Panbangred, W.; Bhunia, A. K. WST-1-Based Cell Cytotoxicity Assay as a Substitute for MTT-Based Assay for Rapid Detection of Toxigenic Bacillus Species Using CHO Cell Line. *J. Microbiol. Methods* **2008**, *73* (3), 211–215.
(272) Ngai, K.-C.; Yeung, C.-Y.; Leung, C.-S. Difference in Susceptibilities of Different Cell Lines to Bilirubin Damage. *J. Paediatr. Child Health* **2000**, *36* (1), 51–55.
(273) Gao, Q.; Wang, X.-Y.; Zhou, J.; Fan, J. Cell Line Misidentification: The Case of the Chang Liver Cell Line. *Hepatology* **2011**, *54* (5), 1889–1889.
(274) Hafiza, W. A. G. W. N.; Latifah, S. Y. Potential Implications of GRP58 Expression and Susceptibility of Cervical Cancer to Cisplatin and Thymoquinone-Based Therapy. *OncoTargets Ther.* **2014**, *7*, 1375–1387.
(275) Ramírez Cabrera, M. A. Evaluación de la cinética de distribución y toxicidad de las nanopartículas de plata. PhD thesis, Universidad Autónoma de Nuevo León, Mexico, 2010.
(276) Espinoza Arredondo, E. U. Síntesis de Porfirinas y Metaloporfirinas No Simétricas Funcionalizadas Con L-Glutamato y Evaluación de Sus Propiedades Fotodinámicas y Anticancerígenas. PhD thesis, Universidad Autónoma de Nuevo León, Mexico, 2014.
(277) Jakupec, M. A.; Galanski, M.; Keppler, B. K. Tumour-Inhibiting Platinum Complexes—State of the Art and Future Perspectives. In *Reviews of Physiology, Biochemistry and Pharmacology*; Reviews of Physiology, Biochemistry and Pharmacology; Springer Berlin Heidelberg: Berlin, Heidelberg, 2003; pp 1–53.
(278) Timerbaev, A. R.; Hartinger, C. G.; Keppler, B. K. Metallodrug Research and Analysis Using Capillary Electrophoresis. *TrAC Trends Anal. Chem.* **2006**, *25* (9), 868–875.
(279) Sherman, S. E.; Lippard, S. J. Structural Aspects of Platinum Anticancer Drug Interactions with DNA. *Chem. Rev.* **1987**, *87* (5), 1153–1181.
(280) Hamilton, P. L.; Arya, D. P. Natural Product DNA Major Groove Binders. *Nat. Prod. Rep.* **2012**, *29* (2), 134–143.
(281) Kellett, A.; Molphy, Z.; Slator, C.; McKee, V.; Farrell, N. P. Molecular Methods for Assessment of Non-Covalent Metallodrug–DNA Interactions. *Chem. Soc. Rev.* **2019**, *48* (4), 971–988.
(282) Waring, M. J. *DNA-Targeting Molecules as Therapeutic Agents*; Royal Society of Chemistry, 2018.
(283) Lepecq, J.-B.; Paoletti, C. A Fluorescent Complex between Ethidium Bromide and Nucleic Acids: Physical—Chemical Characterization. *J. Mol. Biol.* **1967**, *27* (1), 87–106.
(284) Morgan, A. R.; Lee, J. S.; Pulleyblank, D. E.; Murray, N. L.; Evans, D. H. Review: Ethidium Fluorescence Assays. Part 1. Physicochemical Studies. *Nucleic Acids Res.* **1979**, *7* (3), 547–569.
(285) Prisecaru, A.; Molphy, Z.; Kipping, R. G.; Peterson, E. J.; Qu, Y.; Kellett, A.; Farrell, N. P. The Phosphate Clamp: Sequence Selective Nucleic Acid Binding Profiles and Conformational Induction of Endonuclease Inhibition by Cationic Triplatin Complexes. *Nucleic Acids Res.* **2014**, *42* (22), 13474–13487.

(286) Molphy, Z.; Prisecaru, A.; Slator, C.; Barron, N.; McCann, M.; Colleran, J.; Chandran, D.; Gathergood, N.; Kellett, A. Copper Phenanthrene Oxidative Chemical Nucleases. *Inorg. Chem.* **2014**, *53* (10), 5392–5404.
(287) Swarts, J. C.; Neuse, E. W.; Lamprecht, G. J. Synthesis and Characterization of Water-Soluble Polyaspartamide-Ferrocene Conjugates for Biomedical Applications. *J. Inorg. Organomet. Polym.* **1994**, *4* (2), 143–153.
(288) Swarts, J. C.; Swarts, D. M.; Maree, D. M.; Neuse, E. W.; La, C. M.; Van, J. L. Polyaspartamides as Water-Soluble Drug Carriers. Part 1: Antineoplastic Activity of Ferrocene-Containing Polyaspartamide Conjugates. *Anticancer Res.* **2001**, *21* (3B), 2033–2037.
(289) Fourie, E.; Erasmus, E.; Swarts, J. C.; Jakob, A.; Lang, H.; Joone, G. K.; Rensburg, C. E. J. V. Cytotoxicity of Ferrocenyl–Ethynyl Phosphine Metal Complexes of Gold and Platinum. *Anticancer Res.* **2011**, *31* (3), 825–829.
(290) Buriez, O.; Heldt, J. M.; Labbé, E.; Vessières, A.; Jaouen, G.; Amatore, C. Reactivity and Antiproliferative Activity of Ferrocenyl–Tamoxifen Adducts with Cyclodextrins against Hormone-Independent Breast-Cancer Cell Lines. *Chem. – Eur. J.* **2008**, *14* (27), 8195–8203.
(291) Shah, A.; Zaheer, M.; Qureshi, R.; Akhter, Z.; Faizan Nazar, M. Voltammetric and Spectroscopic Investigations of 4-Nitrophenylferrocene Interacting with DNA. *Spectrochim. Acta. A. Mol. Biomol. Spectrosc.* **2010**, *75* (3), 1082–1087.
(292) Krishnamoorthy, P.; Sathyadevi, P.; Butorac, R. R.; Cowley, A. H.; Bhuvanesh, N. S. P.; Dharmaraj, N. Copper(i) and Nickel(Ii) Complexes with 1 : 1 vs. 1 : 2 Coordination of Ferrocenyl Hydrazone Ligands: Do the Geometry and Composition of Complexes Affect DNA Binding/Cleavage, Protein Binding, Antioxidant and Cytotoxic Activities? *Dalton Trans.* **2012**, *41* (15), 4423.
(293) Asghar, F.; Badshah, A.; Shah, A.; Rauf, M. K.; Ali, M. I.; Tahir, M. N.; Nosheen, E.; Zia-ur-Rehman; Qureshi, R. Synthesis, Characterization and DNA Binding Studies of Organoantimony(V) Ferrocenyl Benzoates. *J. Organomet. Chem.* **2012**, *717*, 1–8.
(294) Zhao, X.-L.; Han, M.-J.; Zhang, A.-G.; Wang, K.-Z. DNA- and RNA-Binding and Enhanced DNA-Photocleavage Properties of a Ferrocenyl-Containing Ruthenium(II) Complex. *J. Inorg. Biochem.* **2012**, *107* (1), 104–110.
(295) Gul, R.; Khan, A.; Badshah, A.; Rauf, M. K.; Shah, A.; Zia-ur-Rehman; Bano, A.; Naz, R.; Tahir, M. N. New Supramolecular Ferrocenyl Phenylguanidines as Potent Antimicrobial and DNA-Binding Agents. *J. Coord. Chem.* **2013**, *66* (11), 1959–1973.
(296) Pitié, M.; Pratviel, G. Activation of DNA Carbon−Hydrogen Bonds by Metal Complexes. *Chem. Rev.* **2010**, *110* (2), 1018–1059.
(297) Shigenaga, M. K.; Hagen, T. M.; Ames, B. N. Oxidative Damage and Mitochondrial Decay in Aging. *Proc. Natl. Acad. Sci.* **1994**, *91* (23), 10771.
(298) Cooke, M. S.; Evans, M. D. 8-Oxo-Deoxyguanosine: Reduce, Reuse, Recycle? *Proc. Natl. Acad. Sci.* **2007**, *104* (34), 13535.
(299) Kellett, A.; Howe, O.; O'Connor, M.; McCann, M.; Creaven, B. S.; McClean, S.; Foltyn-Arfa Kia, A.; Casey, A.; Devereux, M. Radical-Induced DNA Damage by Cytotoxic Square-Planar Copper(II) Complexes Incorporating o-Phthalate and 1,10-Phenanthroline or 2,2′-Dipyridyl. *Free Radic. Biol. Med.* **2012**, *53* (3), 564–576.
(300) McCann, M.; McGinley, J.; Ni, K.; O'Connor, M.; Kavanagh, K.; McKee, V.; Colleran, J.; Devereux, M.; Gathergood, N.; Barron, N.; et al. A New Phenanthroline–Oxazine Ligand: Synthesis, Coordination Chemistry and Atypical DNA Binding Interaction. *Chem. Commun.* **2013**, *49* (23), 2341.

(301) Prisecaru, A.; Devereux, M.; Barron, N.; McCann, M.; Colleran, J.; Casey, A.; McKee, V.; Kellett, A. Potent Oxidative DNA Cleavage by the Di-Copper Cytotoxin: [Cu2(μ-Terephthalate)(1,10-Phen)4]2+. *Chem. Commun.* **2012**, *48* (55), 6906.
(302) Slator, C.; Molphy, Z.; McKee, V.; Long, C.; Brown, T.; Kellett, A. Di-Copper Metallodrugs Promote NCI-60 Chemotherapy via Singlet Oxygen and Superoxide Production with Tandem TA/TA and AT/AT Oligonucleotide Discrimination. *Nucleic Acids Res.* **2018**, *46* (6), 2733–2750.
(303) Sheldrick, G. M. Crystal Structure Refinement with SHELXL. *Acta Crystallogr. Sect. C Struct. Chem.* **2015**, *71* (1), 3–8.
(304) Macrae, C. F.; Edgington, P. R.; McCabe, P.; Pidcock, E.; Shields, G. P.; Taylor, R.; Towler, M.; Streek, J. van de. Mercury: Visualization and Analysis of Crystal Structures. *J. Appl. Crystallogr.* **2006**, *39* (3), 453–457.
(305) Westrip, S. P. PublCIF: Software for Editing, Validating and Formatting Crystallographic Information Files. *J. Appl. Crystallogr.* **2010**, *43* (4), 920–925.